NASA
CR
3590
c.1

TECH LIBRARY KAFB, NM
0062139

NASA Contractor Report 3590

Interpretation Methodology and Analysis of In-Flight Lightning Data

LOAN COPY: RETURN TO
AFWL TECHNICAL LIBRARY
KIRTLAND AFB, N.M.

Terence Rudolph and Rodney A. Perala

CONTRACT NAS1-16489
OCTOBER 1982

NASA

TECH LIBRARY KAFB, NM
0062139

NASA Contractor Report 3590

Interpretation Methodology and Analysis of In-Flight Lightning Data

Terence Rudolph and Rodney A. Perala
Electro Magnetic Applications, Inc.
Denver, Colorado

Prepared by Electro Magnetic Applications, Inc.
for Research Triangle Institute for
NASA Langley Research Center
under Contract NAS1-16489

National Aeronautics
and Space Administration

**Scientific and Technical
Information Branch**

1982

TABLE OF CONTENTS

CHAPTER	TITLE	
1	INTRODUCTION	1
2	REVIEW OF EXISTING DATA	3
	2.1 Background	3
	2.2 Terminology	5
	2.3 D-Dot Data	5
	2.4 B-Dot Data	10
	2.5 I-Dot Data	10
	2.6 Boom Current and Field Mill Measurements	10
	2.7 Qualitative Data Interpretation	14
	2.8 Summary of 1980 Data	34
3	INTERPRETATION APPROACH	35
4	MODEL VALIDATION	45
5	INTERPRETATION OF LEMP DATA	54
6	INTERPRETATION OF DIRECT STRIKE DATA	62
	6.1 Background	62
	6.2 Analysis of Flight 80-018 (Figure 6.3)	66
	6.3 Flight 80-019 (Figure 6.4)	66
	6.4 Flight 80-036 (Figure 6.5)	75
	6.5 Flight 80-038, Run 6 (Figure 6.6)	75
	6.6 Flight 80-038, Run 4 (Figure 6.7)	75
	6.7 Discussion of Other Waveforms	83
7	NONLINEAR EFFECTS	85
	7.1 Background	85
	7.2 Air Conductivity Modeling	86
	7.3 Application of the Air Conductivity Model	88
	7.4 Improvements in Air Conductivity Modeling	94
8	UNIQUENESS	97
9	PRELIMINARY INTERPRETATION METHODOLOGY	100
	9.1 Background	100
	9.2 Approach	100
10	SUGGESTIONS FOR THE IN-FLIGHT TEST PROGRAM	105
	10.1 Background	105
	10.2 More Sensor Points	105
	10.3 Truly Simultaneous Measurements	106
	10.4 Actual Field Measurements	106
	10.5 Variety in Flight Altitudes	108
	10.6 Faster Sampling Rate for I-dot Sensors	108

TABLE OF CONTENTS (Concluded)

CHAPTER	TITLE	
	10.7 Addition of a Wing or Tail Boom	108
11	CONCLUSION AND SUMMARY	109
12	REFERENCES	110
APPENDIX A	. . . . .	112

LIST OF FIGURES

FIGURE	TITLE	
2.1	D-Dot Record which Shows no Late-Time Charging of Aircraft (Flight 80-019)	7
2.2	D-Dot Record Showing Late-Time Charging of Aircraft (Flight 80-018)	8
2.3	Typical B-Dot Record for Direct Strike (Flight 80-038)	11
2.4	Typical B-Dot Record for Nearby Lightning (Flight 81-045)	12
2.5	Typical I-Dot Record. Note 6 MHz Resonance (Flight 80-038)	13
2.6	Electric Field and Current Measured on Flight 81-043	15
2.7	History of Approach of Initial Lightning Charge	17
2.8	Electric Field Expected at Nose of Aircraft due to Initial Attachment of Lightning Charge to the Nose	18
2.9	Example of Data Record which may be Due to Initial Attachment to Nose of the Aircraft (Flight 80-038)	19
2.10	Electric Field Expected at Nose of Aircraft due to Initial Attachment of Lightning Charge to the Rear	20
2.11	Example of Data Record which may be due to Initial Attachment to Rear of the Aircraft (Flight 80-036)	21
2.12	Electric Field Expected at the Nose due to Subsequent Leader Interaction with the Aircraft	23
2.13	Example of Data Record which may be due to Subsequent Leader Interaction with Aircraft (Flight 80-019)	24
2.14	Electric Field Expected at Nose to the K-Change Interaction with Aircraft	25
2.15	Example of Data Record which may be due to K-Change Interaction with Aircraft (Flight 80-019)	26
2.16	Electric Field Expected at Nose due to Exit of Leader from the Aircraft	27
2.17	Example of Data Record which may be due to Exit of Leader from Aircraft (Flight 80-038)	29
2.18	Overview of D-Dot for Flight 80-019	30
2.19	First K-Change in True History of Flight 80-019	30
2.20	A Subsequent Leader from Flight 80-019	31
2.21	Subsequent K-Change and Leader from Flight 80-019	32
2.22	Subsequent K-Change from Flight 80-019	33
2.23	Subsequent Leader from Flight 80-019	33

LIST OF FIGURES (Cont'd)

FIGURE	TITLE	
3.1	The Discretizing Mesh for the One-Dimensional (1D) Maxwell's Equation Problem [13]	37
3.2	Finite Difference Equations in Rectangular Coordinates Set Up with Externally Supplied E-Fields [13]	40
3.3	Block Model of F106	42
3.4	F106 With Dimensions and Sensor Locations	43
4.1	Apparatus for Aircraft Lightning Modeling	46
4.2	Magnetic Field Measured at a Radial Distance of 6 Inches and 60 Inches from Airplane	47
4.3	Measured Response of Displacement Current Derivative Sensor	48
4.4	Measured Response of Magnetic Field Derivative Sensor	49
4.5	Comparison of Measured and Predicted Response of Magnetic Field Derivative Sensor	51
4.6	Comparison of Measured and Predicted Displacement Current Derivative Sensor	52
5.1	Example of D-Dot Record without Significant Structure (Flight 80-023)	55
5.2	Example of B-Dot Record Showing Significant Structure (Flight 80-023)	55
5.3	LEMP D-dot Record Showing Aircraft Resonances (Flight 81-026)	56
5.4	Monopolar D-Dot Record Showing Weak Aircraft Resonances (Flight 81-026)	58
5.5	Monopolar B-Dot Record Probably Caused by Slow Rise Time LEMP (Flight 81-026)	58
6.1	Example of Monopolar D-Dot Response of Aircraft (Flight 80-019)	64
6.2	D-Dot Record Showing no Significant Structure (Flight 80-029)	67
6.3	D-Dot Record from Flight 80-018	68
6.4	D-Dot Record from Flight 80-019	69
6.5	D-Dot Record from Flight 80-036	70
6.6	D-Dot Record from Flight 80-038	71
6.7	D-Dot Record from Flight 80-038, Run 4	72

LIST OF FIGURES (Concluded)

FIGURE	TITLE	
6.8	Overlay of Figure 6.3 and Numerical Prediction (Flight 80-018)	73
6.9	Injected Current Waveform for Prediction of Figure 6.8	74
6.10	Overlay of Figure 6.4 and Numerical Prediction (Flight 80-019)	76
6.11	Injected Current Waveform for Prediction of Figure 6.10	77
6.12	Overlay of Figure 6.5 and Numerical Prediction (Flight 80-036)	78
6.13	Injected Current Waveform for Prediction of Figure 6.12	79
6.14	Overlay of Figure 6.6 and Numerical Prediction (Flight 80-038)	80
6.15	Injected Current Waveform for Prediction of Figure 6.14	81
6.16	Overlay of Figure 6.7 and Numerical Prediction (Flight 80-038)	81
6.17	Injected Current Waveform for Prediction of Figure 6.16	82
7.1	D-Dot Data Record Showing Possible Initial Leader Attachment to Nose of Aircraft (Flight 80-038)	87
7.2	Rod-Plane Gap Arrangement for Experiment of Collins and Meek [23]	91
7.3	Field Variation at Rod and Plane	91
7.4	Predicted Field Variation at Rod	92
7.5	Predicted Field Variation at Plate	93
9.1	D-Dot Measurement from Flight 80-019	102
9.2	Effect of Rise Time on Predicted Response	103
10.1	Field Waveforms which will Give Identical Derivative Responses	107

LIST OF TABLES

TABLE	TITLE	
2.1	1980 Direct Strike Data Summary	4
2.2	1981 Lightning Data Summary	6
2.3	Summary of Maximum Observed Values for the 1980 Data Set	34
7.1	Air Chemistry Coefficient Formulas [19]	89

CHAPTER 1

INTRODUCTION

The electromagnetic interaction of lightning with aircraft has received an increasing amount of interest in recent years for several reasons. The first reason has to do with the knowledge of the environment. Recent studies by Uman [1], Baum [2] and others [3] have shown that the frequency content of lightning waveforms has significant amplitude in the aircraft resonance region, which is in sharp contrast to previous understanding of the lightning environment [4].

A second set of reasons has to do with aircraft technology. New and existing aircraft are being made out of advanced composite materials because their advantageous strength to weight ratios when compared to metals. These composites do not offer as much electromagnetic shielding as do metals. In addition, modern aircraft are being equipped with low-level semiconductor circuitry which have critical roles in functions such as stores management and fly-by-wire systems. Therefore, a great concern arises for preventing upset of these critical digital systems.

Because of these reasons, it is necessary to understand the electromagnetic aspects of the lightning/aircraft interaction event. A major requirement for understanding this event is to have actual in-flight data. Therefore, in recent years NASA has attempted to obtain such data by instrumenting an F106B aircraft and penetrating thunderstorms with the intent of being struck by lightning. Valuable data have been obtained and published [5-8]. However, the data is not readily interpretable. That is to say, one cannot determine from a casual inspection of the data what physical processes actually occurred during the interaction event. In fact, it appears that understanding of this data requires considerable numerical analysis and perhaps advancement in the state-of-the-art in understanding the nonlinear aspects of the interaction events.

The general objective of this reported work, therefore, is to understand this interaction. Specifically, the following questions have been addressed:

1. What were the lightnings which caused the responses which were measured on the F106B [6-8]? This is the inverse problem usually posed in electromagnetic interaction. The usual problem is, that, given the source, determine the response. In the present case, the problem is, given the response, determine the source.

2. Can a methodology be developed which can be used to take in-flight data from any aircraft (not only the F106B) and extend it to other aircraft ? During the process of answering the first question, a methodology to do this for other aircraft becomes evident. The goal here is to be able to interpret and extend data taken on any aircraft test program.

In this report, the existing data is first reviewed and discussed in Chapter 2. The method of interpreting this data is given in Chapter 3, and the model used for this is validated in Chapter 4. Interpretation of nearby lightning data is presented in Chapter 5, and the direct stroke data interpretation is given in Chapter 6. In Chapter 7 nonlinear effects are discussed. The problems associated with finding unique solutions are described in Chapter 8, and in Chapter 9 is outlined the preliminary interpretation methodology. Suggestions for the inflight test program are made in Chapter 10.

Conclusions are given in Chapter 11. It has been found that the lightning data can be inverted to determine lightning channel currents. Most of the data can be explained by current rise times of less than 100 nanoseconds with amplitudes on the order of one kiloamp. Nonlinear effects need to be addressed in more detail, and more thought has to be put into the problems associated with uniqueness.

CHAPTER 2

REVIEW OF EXISTING DATA

2.1 Background

During the summer seasons of 1980 and 1981 NASA has flown an instrumented F106B research aircraft into thunderstorms in an effort to collect electromagnetic lightning data from both direct strikes to the aircraft and lightning electromagnetic pulses (LEMP) from nearby strikes. The majority of the data acquired [7,9,10] is in the form of records of time derivatives of fields and currents as a function of time. The actual measurements made were of the time derivative of the current flowing on the pitot boom at the nose of the aircraft, I-dot; the time derivative of the displacement current at a forward position underneath the fuselage, D-dot; and the time derivative of the magnetic flux on the fuselage just above the right wing, B-dot. The orientation of B for this last sensor is such as to correspond to a current flowing axially along the fuselage. In addition to these time derivative measurements, one of the 1981 flights obtained measurements from a current sensor on the pitot boom and on an electric field mill.

During the 1980 season there were ten direct strikes to the aircraft for which recordings were made. These strikes resulted in twenty data records, seven D-dot, eight B-dot, and five I-dot. There were two flights for which nearby lightning was measured resulting in five total records of which three were D-dot and two B-dot. This information is summarized in Table 2.1. There were again ten direct strikes to the aircraft reported in 1981, but recordings were made for only three of these because of problems caused by undetected failure of an attenuator. Six records were acquired from these three strikes, five of these being B-dot and the other a direct measure of the current on the boom. Twenty-one records were made of nearby lightning, of which ten were D-dot and eleven B-dot. Fourteen of these twenty-one records were made when the sensor sensitivity was increased in an effort to measure the excitation of the aircraft by free-field illumination.

Table 2.1 1980 Direct Strike Data Summary [9]

DATE	FLIGHT NO.	NO. STRIKES (COMMENTS)	$\dot{D}$ FWD (A)	$\dot{B}$ LONG (A)	$\dot{I}$ (B)	$\dot{D}$ R. WING (B)
6-17	80-018	1 (BOOM)	1	0	0	0
	80-019	2 (BOOM)	1	0 *	0 **	0
7-22	80-023	0 (NEARBY)	3	1	***	0
8-12	80-029	1 (CANOPY)	1	3	***	0
8-15	80-030	0	0	1	***	0
9-1	80-036	1 (NOSE)	1	1	***	0
9-3	80-038	5 (BOOM)	3	4	5	0

(A) EXPANDED BIOMATION DIGITAL TRANSIENT RECORDER 10 ns/SAMPLE
(B) RCA ADVISER 62 6-MHz B.W. ANALOG RECORDER (100 ns STEP RESPONSE)
* X 10 GAIN CHANGE ** X 100 GAIN CHANGE
*** BOOM NOT INVOLVED DATA NOT EXPECTED

The information for the 1981 season is summarized in Table 2.2.

2.2 Terminology

Because all of the F106 lightning measurements were made at a relatively high altitude ($\sim$ 5 km), the type of lightning seen was cloud lightning, rather than cloud to ground discharges. Cloud lightning takes place between positive and negative charge centers and is believed to consist of a continuously propagating leader which generates five or six weak return strokes which are called K-changes [1]. The K-changes occur as the leader intercepts regions of charge opposite to its own. In this report the terms "stepped leader" and "dart leader" will be retained for initial and subsequent leaders, respectively, and "K-change" will be used for the process which corresponds to a return stroke in a cloud to cloud or intracloud discharge. In addition the term "flash" will be applied to the entire lightning event, because "stroke" is reserved for cloud to ground lightning in the literature.

2.3 D-Dot Data

There are some definite classifications that can be made in the D-dot measurements. The direct strike records almost invariably show peak amplitudes of from fifteen to twenty-five amps per square meter and have structure which is characteristic of aircraft resonances. The one exception to this is flight 80-029 in which the strike was to the canopy of the aircraft. (All other strikes were to the nose or boom.) For direct strikes D-dot is indicative of a charging rate on the forward part of the aircraft, so similar peak D-dot amplitudes imply a similar charging rate which in turn implies a similar current waveform attaching to the nose of the aircraft, at least for the beginning of the interaction event. At later times two behaviors are seen. Some of the records show D-dot going to zero as would be expected if the lightning charge had passed through the aircraft and exited from another extremity, leaving a net charge on the nose, which corresponds to a normal electric field of about 100 KV/m. An example is shown in Figure 2.1. Others, however, show D-dot approaching a constant nonzero value at late time and staying there for several microseconds before abruptly dropping to zero. Figure 2.2 is an example of this behavior and

Table 2.2 1981 Lightning Data Summary [10]

DATE	FLIGHT NO.	NO. STRIKES	$\dot{D}_F$ (SENSOR LOCATION 2)	$\dot{B}_L$ (SENSOR LOCATION 6)	I (SENSOR LOCATION 1)
7-1	81-026	0	10(1)	4(2)	0
8-6	81-041	0(NEARBY)	-	2	0
8-11	81-042	1	-	1	0
8-16	81-043	1(BOOM)	-	1	1(3)
		1	-	3	0
9-8	81-045	0(NEARBY)	0	5	0

(1) Recorder sensitivity increased 40dB

(2) Recorder sensitivity increased 20dB

(3) Recorded by Boeing data logger

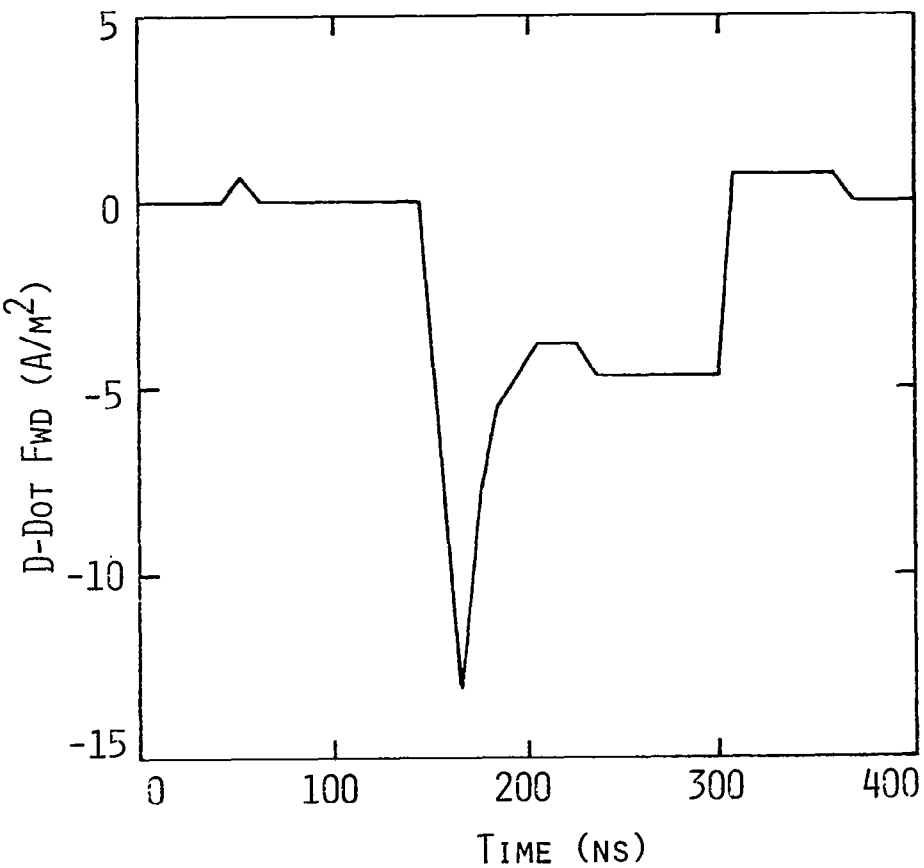

Figure 2.1 D-Dot Record Which Shows No Late-Time Charging of the Aircraft (Flight 80-019)

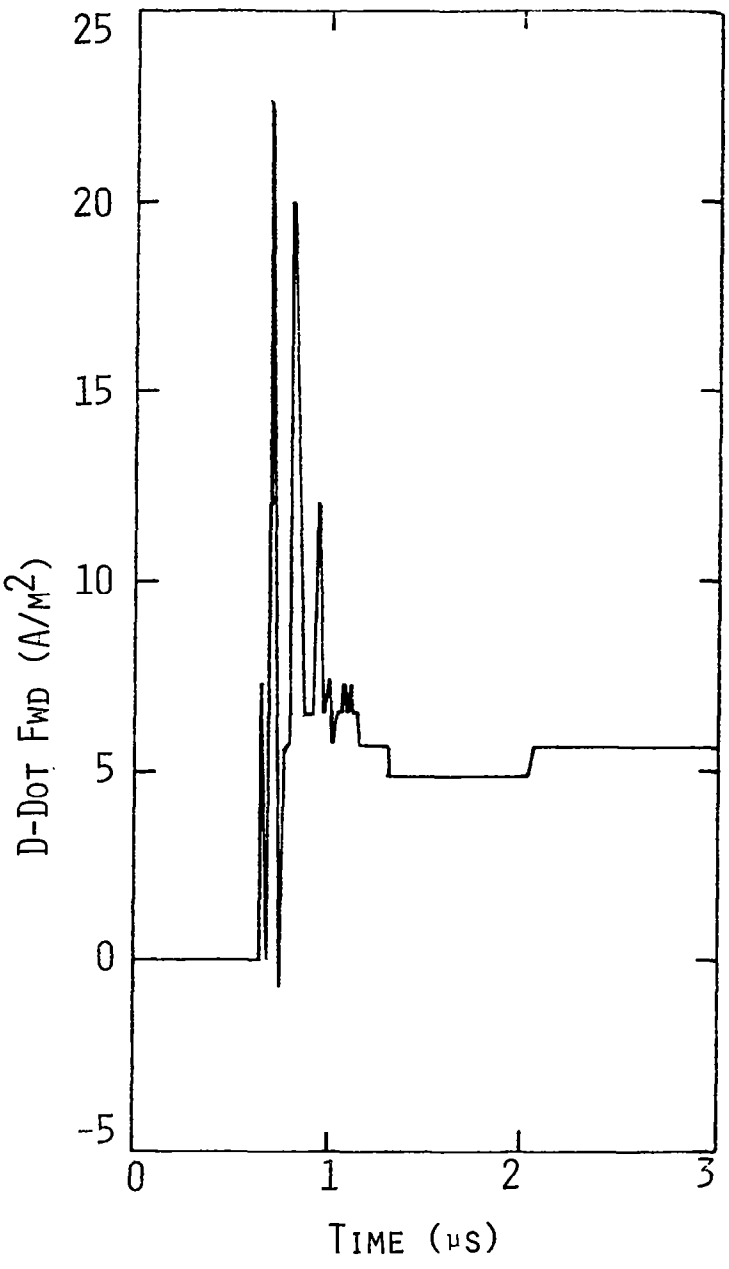

FIGURE 2.2 D-DOT RECORD SHOWING LATE-TIME CHARGING OF THE AIRCRAFT (FLIGHT No. 80-013)

shows a net normal electric field of about 2.4 MV/m. This is characteristic of lightning current entering the aircraft at one point and continuing to charge up the aircraft, as if an exit point were not available. The two types of D-dot records could be interpreted as dart and stepped leader behavior, because the dart type leader will charge the aircraft through a previously established current channel, whereas the stepped leader also charges the aircraft but must then forge its own continuing channel by air breakdown processes before exiting the aircraft. The long tail on these D-dot records may be formed as the electric field builds to air breakdown level somewhere on the aircraft. The early time structure of these D-dot records are indicative of aircraft resonances. Thus there is a relatively high spectral content in the aircraft resonance regions, up to about 10 MHz. This implies risetimes of the incident current pulses of less than 100 nanoseconds. Of course one must keep in mind the inherent selection effect of time derivative measurements. A fast pulse is much more likely to be above the threshold of the recorder than a slow one.

The presence of suspected stepped and dart leader pulses in the D-dot records prompts one to ask whether there are any K-change records. This in turn leads one to question what a K-change record would look like. First of all it should be of opposite polarity from the leader that preceded it, since the net charge which built up on the plane is being drawn off. A slower rise time in the K-change pulse would also lead to less structure and a longer duration, at least when compared with the dart leader. The slower rise time would also give a smaller amplitude in the record. There is some evidence of K-changes in the data. This evidence will be examined in more detail when flight 80-019 is discussed later in this chapter.

The D-dot records from nearby lightning are almost entirely from flight 81-026 for which the sensitivity of the D-dot instrumentation was increased by 40 db. Because for nearby lightning no net charge flows onto the aircraft, any D-dot measured is indicative of a polarization of the aircraft. This polarization should give a much lower level of D-dot than that from a direct strike, and that is found to be the case. Peak D-dot amplitudes are down by about a factor of 100 from direct strike records. Less

structure is seen in the records also, because the increased sensitivity has allowed slower rise time pulses with less high frequency content to be recorded. It is more difficult with these records to determine the actual form of the source lightning, because of the increased number of variables, i.e. direction of the lightning, distance, orientation, amplitudes, etc.

2.4 B-dot Data

B-dot data collected over the two thunderstorm seasons are less easily classified. Both direct strike and LEMP records show a similar structure with a few cycles of the major aircraft resonance, and those from direct strikes tend to have a somewhat longer duration. These direct data also tend to have larger peak amplitudes, ranging up to about 900 Tesla/second in the measurements. The LEMP peak amplitudes are less than 200 Tesla/second. Typical examples of direct strike and LEMP B-dots are shown in Figures 2.3 and 2.4 respectively. The B-dot numbers normally indicate no significant net current density (total time integral is approximately zero).

2.5 I-Dot Data

I-dot data is of course seen only for direct strikes, and records were produced by only one flight in 1980, 80-038. The I-dot analog tape recorder bandpass characteristics [6] act as a 6 MHz filter for these records, an example of which is shown in Figure 2.5. While in principle the unfolding of the true response from the filtered data is possible if one knows the filter characteristics, in reality numerical inaccuracies pose serious difficulties because of the low signal to noise ratio of the higher frequency data. One then should not attempt to use the I-dot records to infer information regarding the high frequency content of lightning.

2.6 Boom Current and Field Mill Measurements

Two other types of measurements were made on flight 81-043. For this flight, an attached stroke was of sufficient size to trigger a boom current sensor. A field mill for measuring the electric field on the aircraft was also operating for this strike. The records

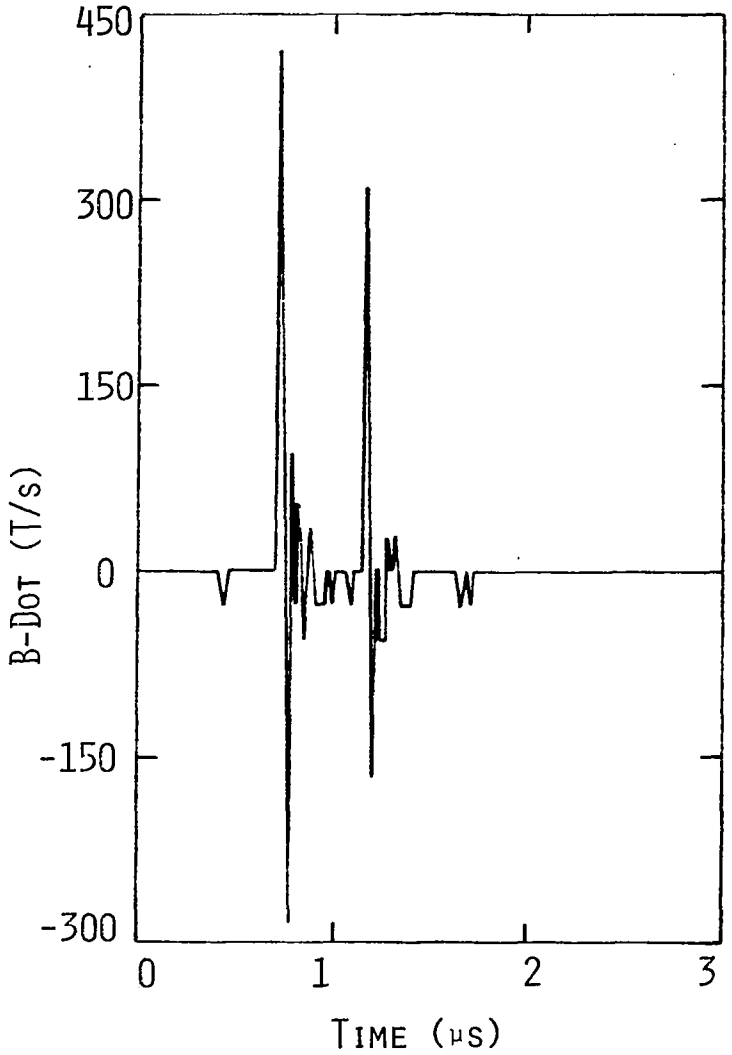

FIGURE 2.3 TYPICAL B-DOT RECORD FOR DIRECT STRIKE (FLIGHT 80-038)

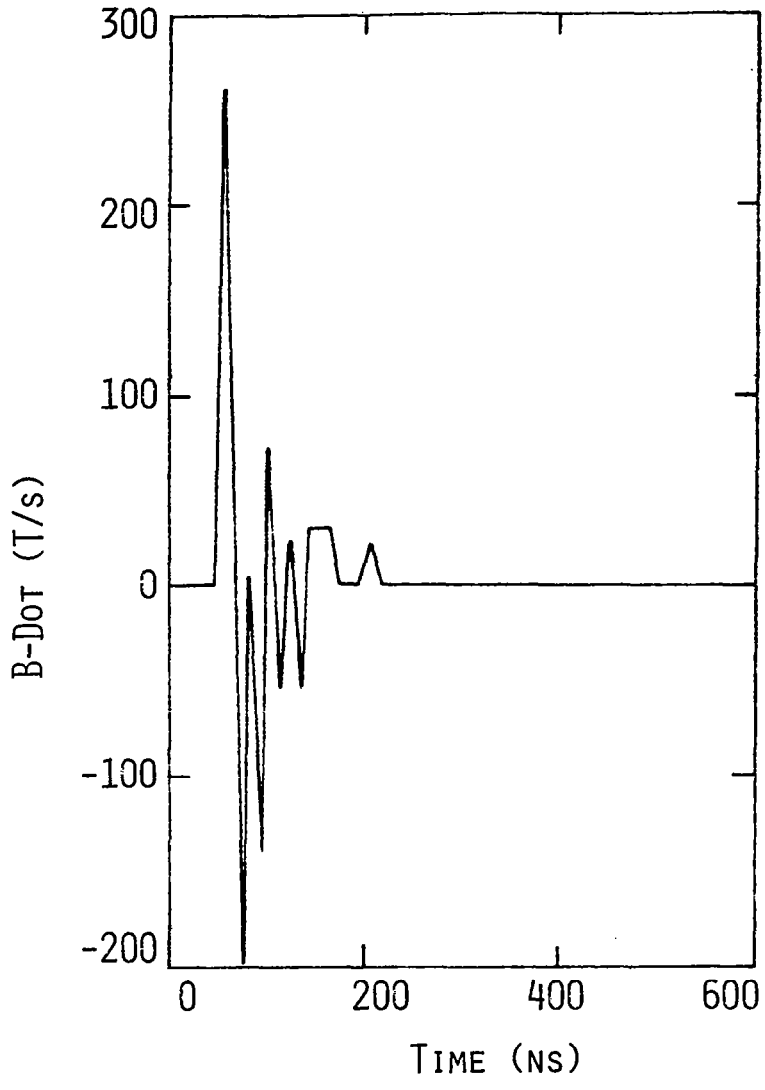

FIGURE 2.4 TYPICAL B-DOT RECORD FOR NEARBY LIGHTNING (FLIGHT 81-045)

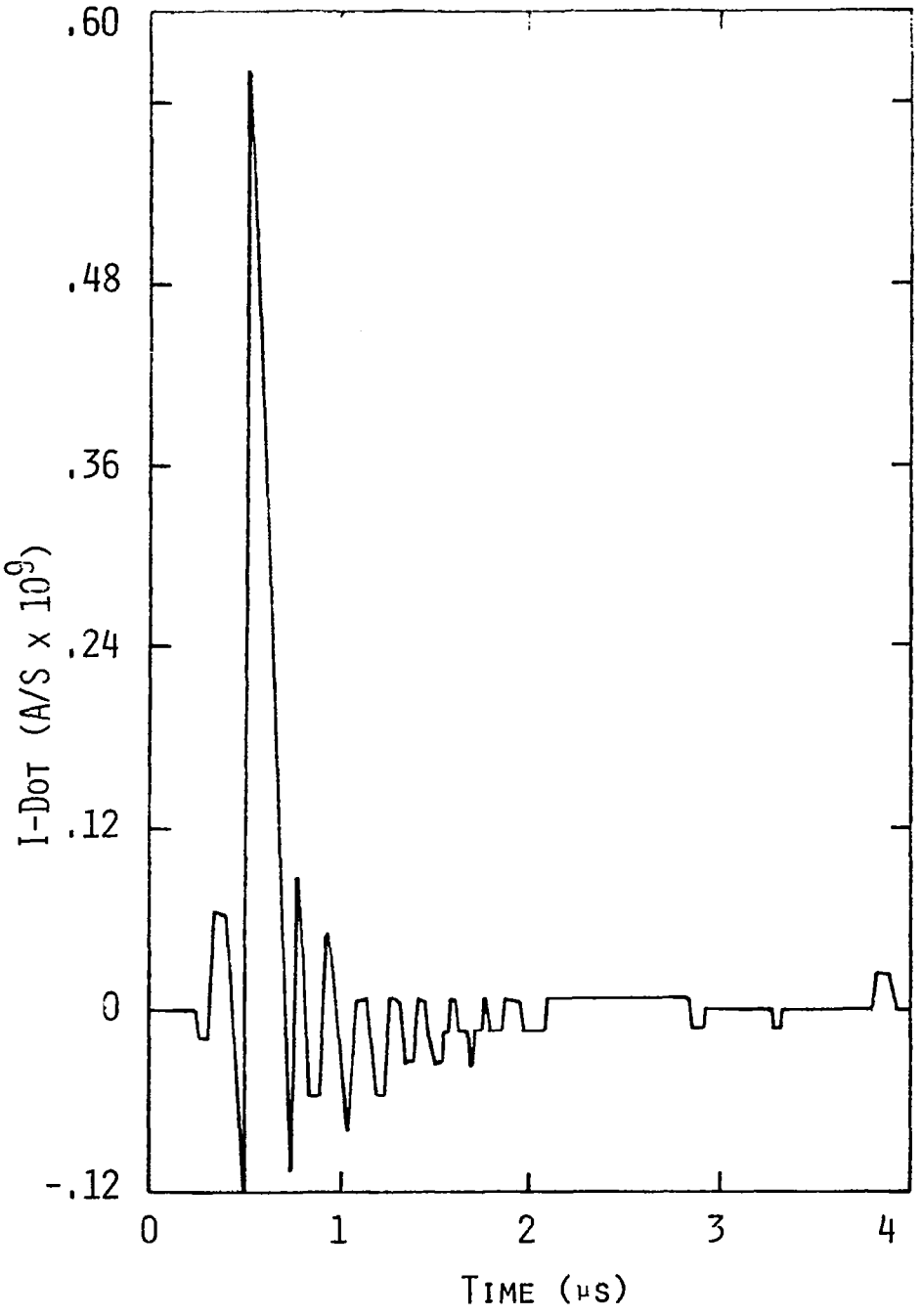

Figure 2.5 Typical I-Dot Record. Note the 6 MHz Resonance (Flight 80-038)

produced are on a much longer time scale than the time derivative data and are shown in Figure 2.6. These types of measurements are important for two reasons. First, they will record lightning events with less high frequency content than the derivative records. A slowly changing waveform which does not trigger the derivative instrumentation may still eventually grow large enough to be recorded by the field mill and current sensor. Second, simultaneous field and derivative data provide a constant of integration for the derivatives. That is, if the derivative data are integrated in time, there is an unknown integration constant that must be added because the derivative instrumentation did not trigger until some time after the actual beginning of the lightning pulse. Another way of saying this is that the direct field measurements (if they have sufficiently fast time resolution) will determine whether the lightning pulses have slow leading or trailing edges which might be missed with derivative measurements.

2.7 Qualitative Data Interpretation

Consider now some gedanken models of what the data records should look like, if one assumes a very simple lightning model. The following discussion will refer to direct strikes only, although some aspects will also apply to nearby lightning. The discussion will also center on the expected D-dot response of the aircraft, because this allows an easier differentiation between the different types of phenomena seen in a lightning flash.

The first case to consider is the approach of a stepped leader toward the nose of the aircraft. Assume that the leader is negatively charged. (For a positive leader simply reverse all the signs.) The sequence of events is portrayed in Figure 2.7. The aircraft initially has no net charge, but as the leader approaches, the aircraft polarizes to produce a net positive charge near the nose and a net negative charge near the tail. This is shown in Figure 2.7(a) and (b). As the leader approaches the plane a positively charged streamer starts out from the nose to meet the leader charge, shown in Figure 2.7(c). The charge on the aircraft continues to polarize as the streamer forms. Eventually the leader and the streamer meet (Figure 2.7(d)), and negative charge flows quickly onto

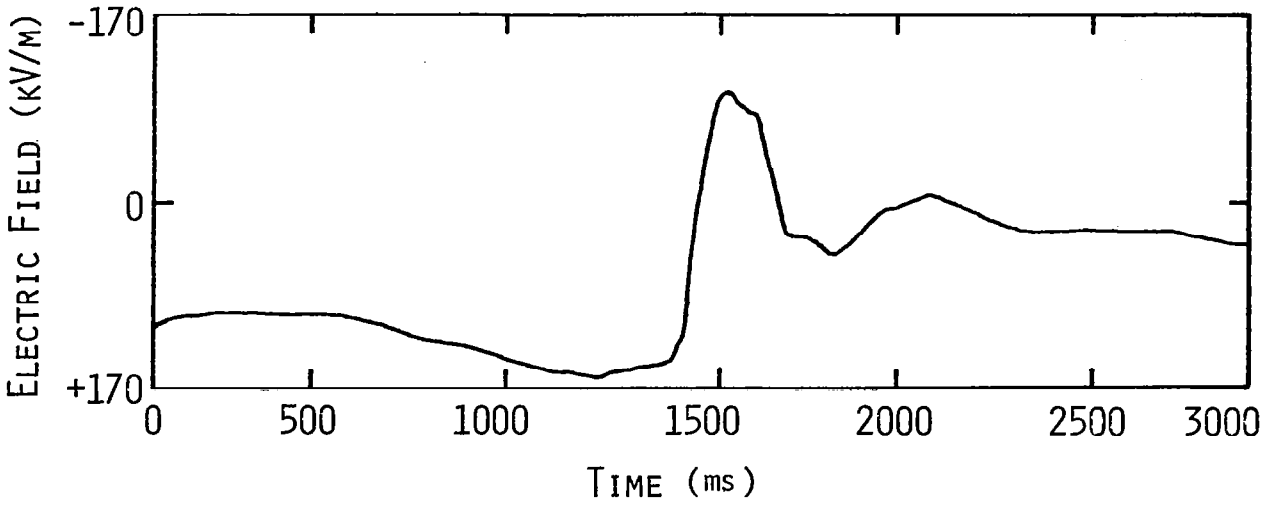

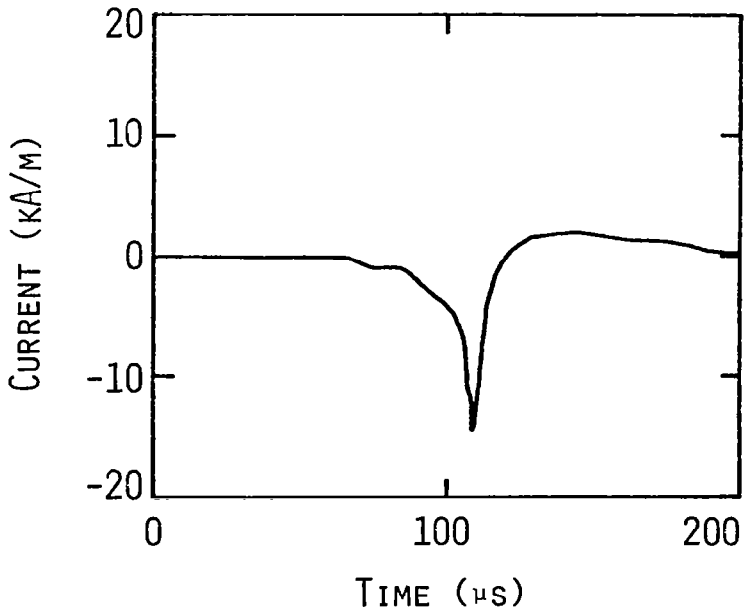

FIGURE 2.6 ELECTRIC FIELD AND CURRENT MEASURED ON FLIGHT 81-043

the aircraft, in Figure 2.7(e). This reverses the sign of the electric field at the nose of the aircraft and gives the aircraft a net negative charge. The negative charge from the leader continues to build on the aircraft until the electric field gets large enough at some point to cause air breakdown. Then a streamer forms from that point and the lightning channel continues, as in Figure 2.7(f). The process in (f) may take a long time to occur depending on the size of the plane and the magnitude of the leader charge. Or it may not occur at all, if the leader is small enough.

Next consider what this implies about the D-dot behavior of the aircraft. In Figure 2.8 is shown the general form of the electric field expected at the nose along with its derivative. The electric field starts positive as the polarization and initial streamer form. It then switches sign as the charge from the leader flows onto the aircraft, and stays at some negative value because the aircraft is now part of the negatively charged leader channel. If one remembers that the curves in Figure 2.8 show only a general behavior, and compares these with Figure 2.9, which is a D-dot record from flight 80-038, one observes that the overall structure is very much the same, and differences can be accounted for by the presence of aircraft resonances.

Next consider the approach of a stepped leader from the rear of an aircraft. The only change from the first scenario is that the initial polarization of the aircraft is opposite. Now negative charge accumulates on the nose. The new electric field waveform and its derivative are shown in Figure 2.10. Now compare this to Figure 2.11, which is the D-dot record from flight 80-036. Again, the overall similarities are striking. This is not meant to suggest that the scenarios presented here are the only possible explanations for the data records in Figures 2.9 and 2.11. In fact Figure 2.11 has been closely duplicated using a relatively simple injected current at the nose of the aircraft. This injected current case will be discussed more fully in Chapter 6, but it serves here to illustrate the difficulty of determining a driving source from a single response on the aircraft. There may be many possible sources which give the same response at that single point. This uniqueness problem is taken up in more detail in Chapter 8.

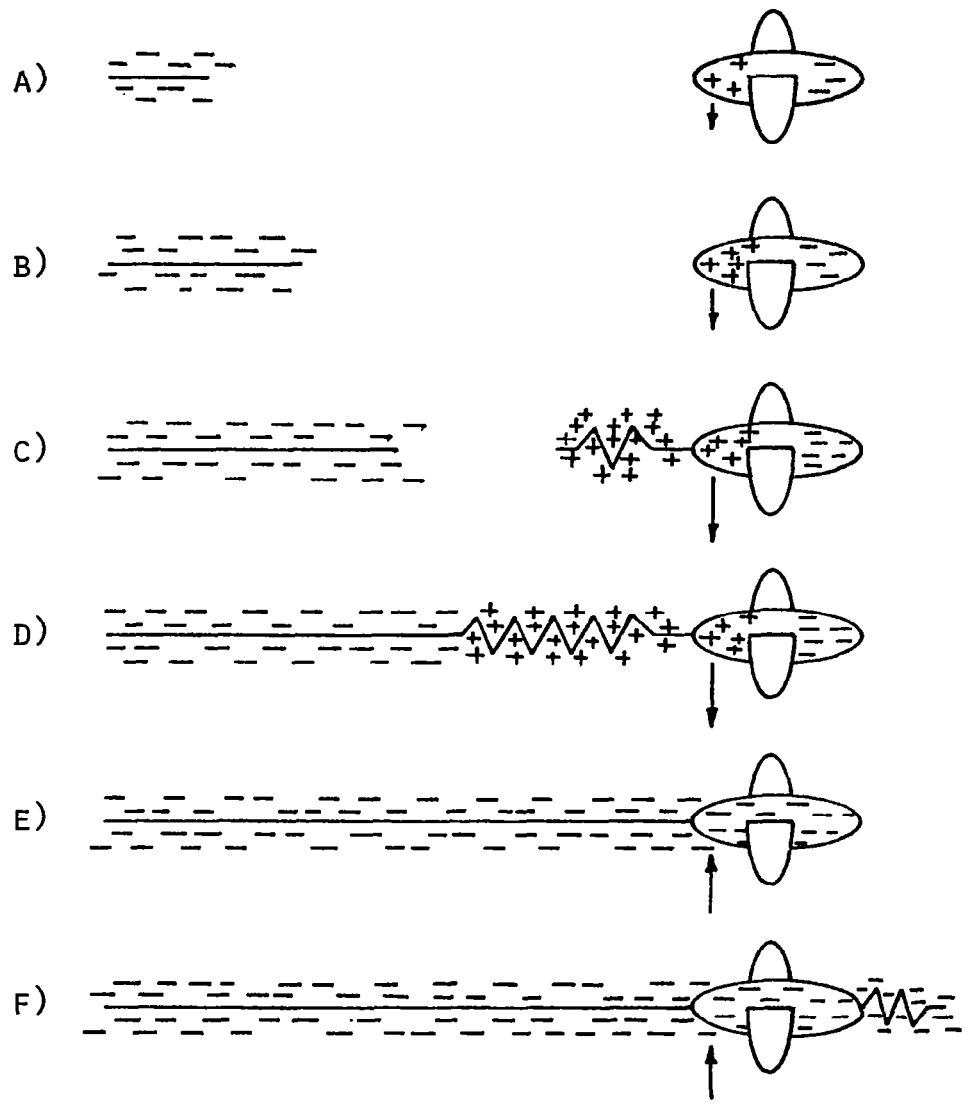

FIGURE 2.7 A-F HISTORY OF APPROACH OF INITIAL LIGHTNING CHARGE (ARROW REPRESENTS ELECTRIC FIELD)

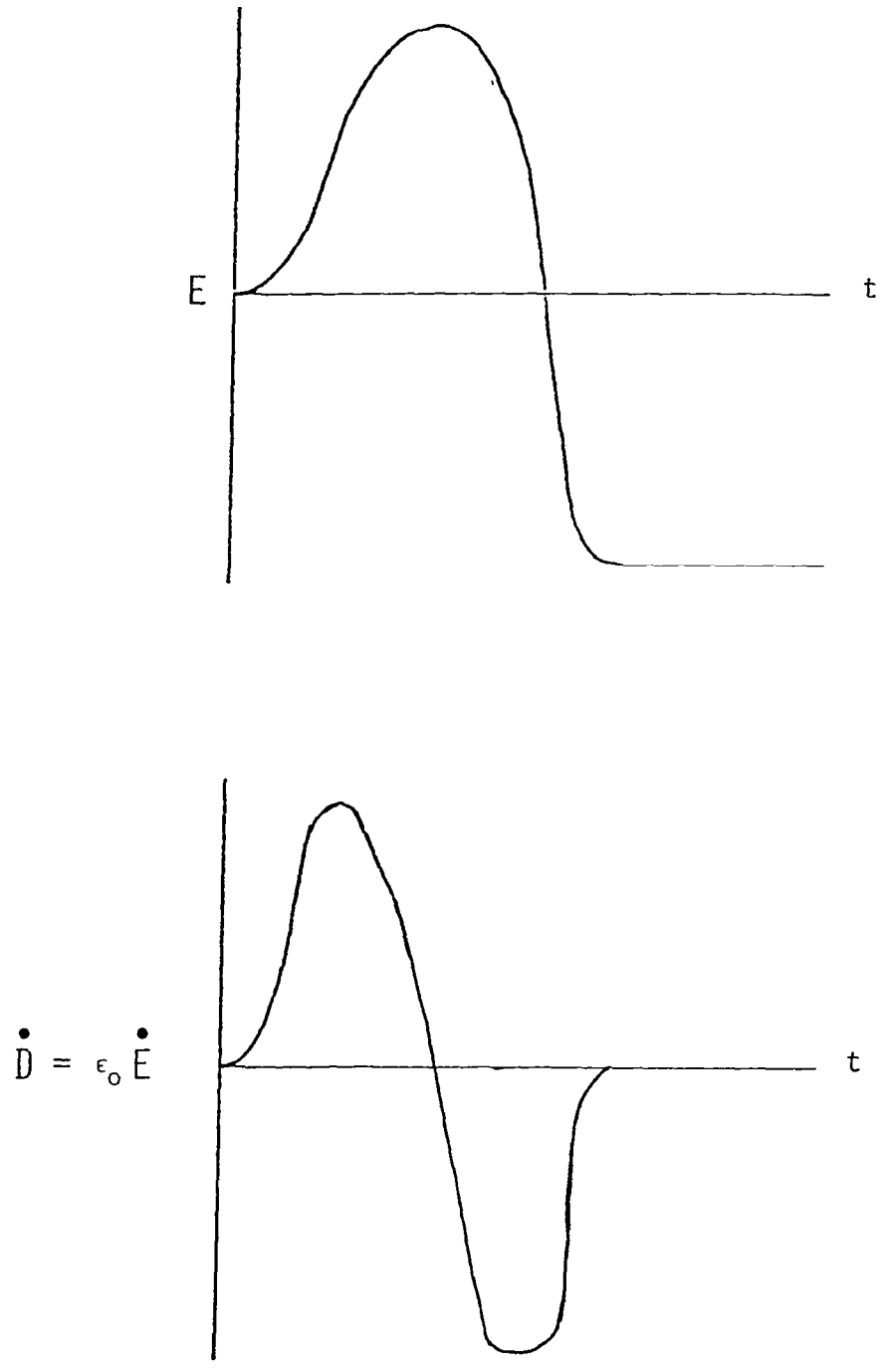

FIGURE 2.8 ELECTRIC FIELD EXPECTED AT NOSE OF AIRCRAFT DUE TO INITIAL ATTACHMENT OF LIGHTNING CHARGE TO THE NOSE

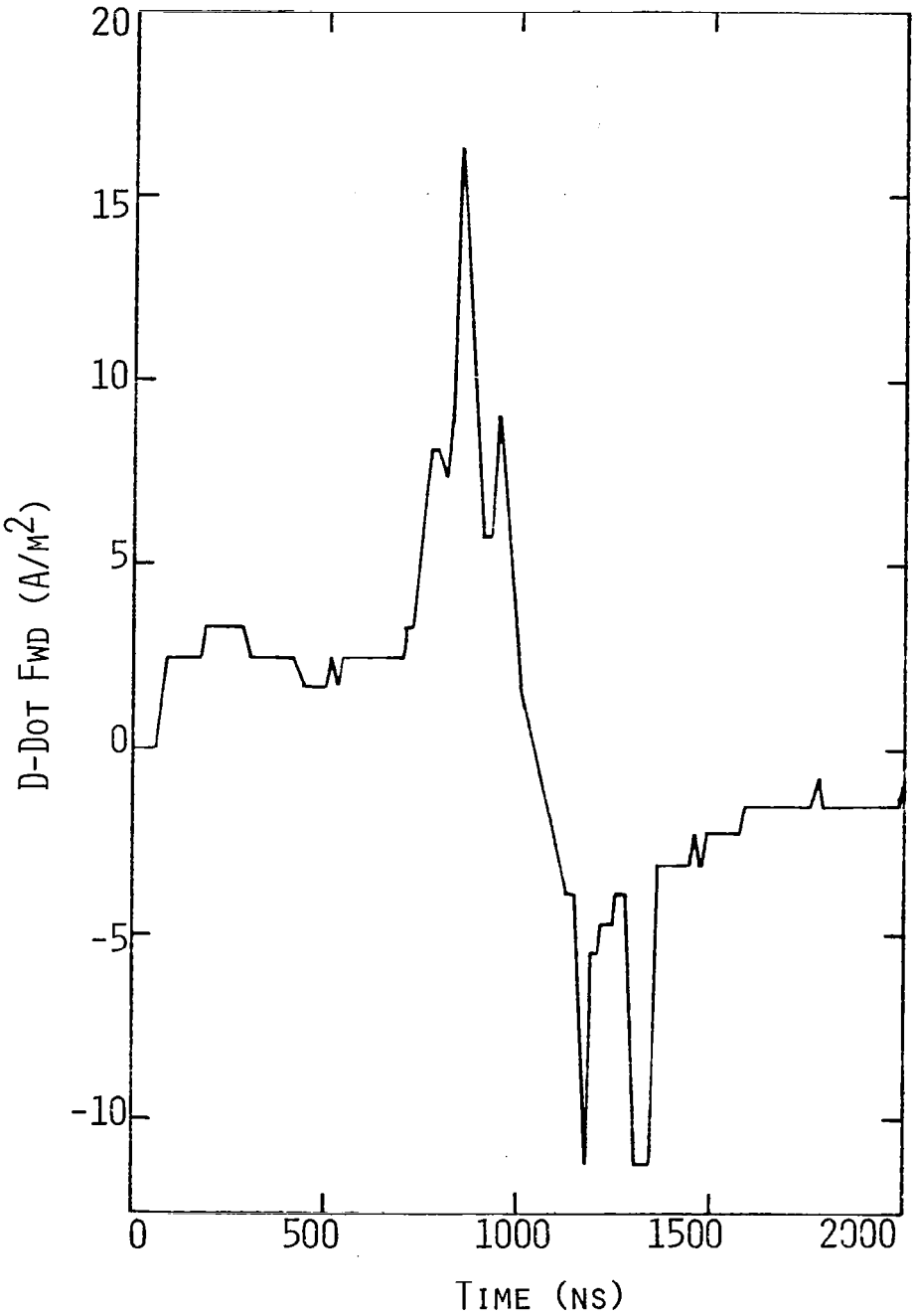

FIGURE 2.9 EXAMPLE OF DATA RECORD WHICH MAY BE DUE TO INITIAL ATTACHMENT TO THE NOSE OF THE AIRCRAFT (FLIGHT 80-038)

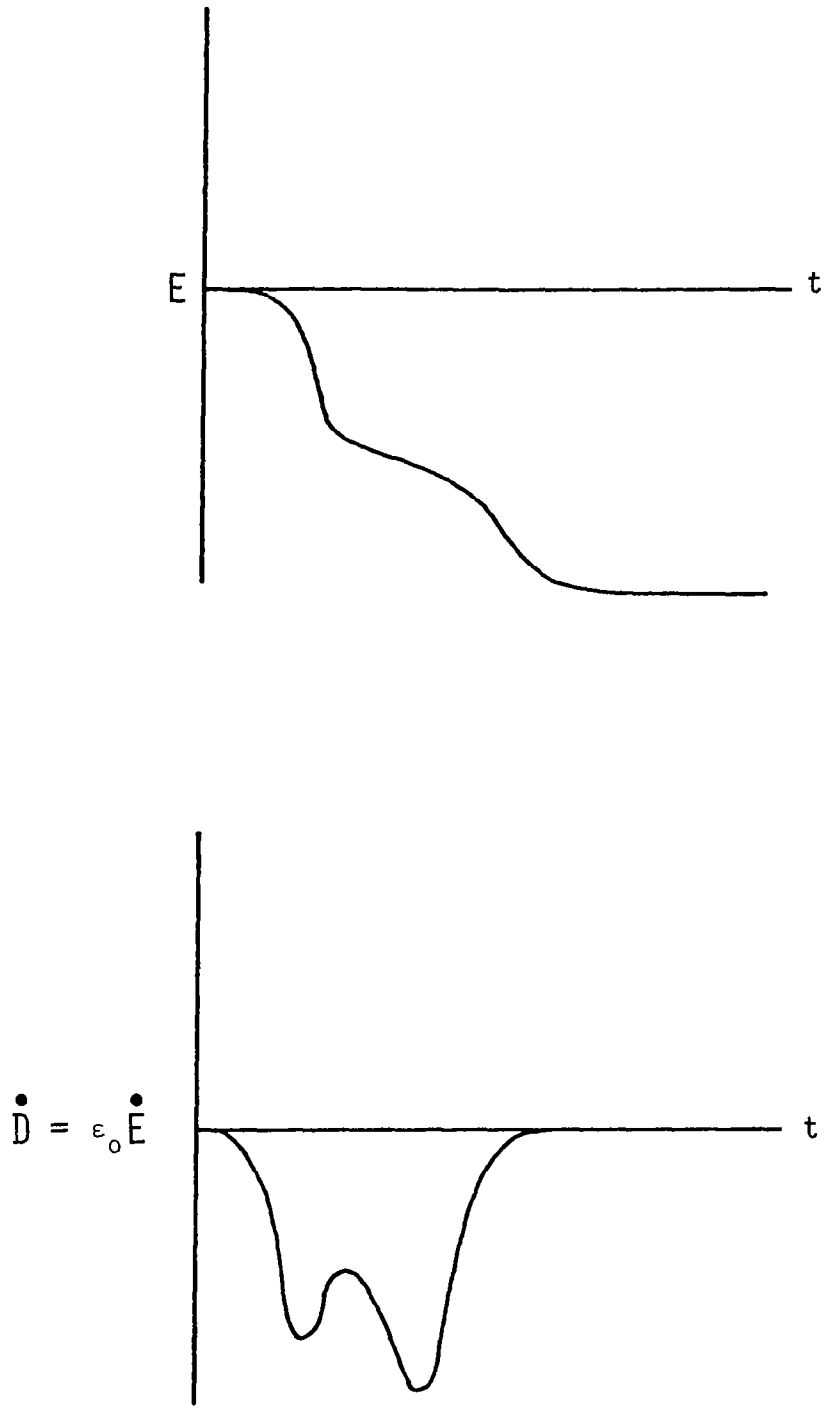

FIGURE 2.10 ELECTRIC FIELD EXPECTED AT NOSE OF AIRCRAFT DUE TO INITIAL ATTACHMENT OF LIGHTNING CHARGE TO THE REAR

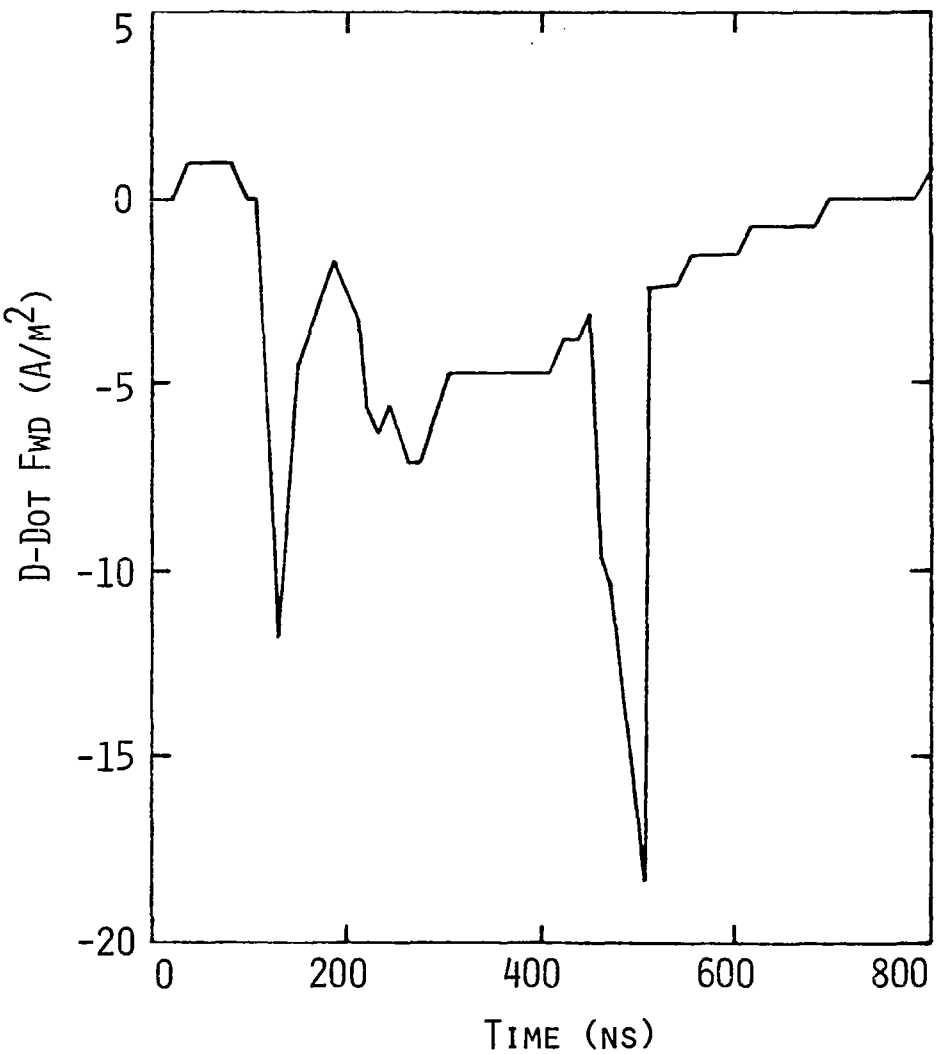

FIGURE 2.11 EXAMPLE OF DATA RECORD WHICH MAY BE DUE TO INITITAL ATTACHMENT TO REAR OF THE AIRCRAFT (FLIGHT 80-036)

Next consider the general behavior of the dart leader. It will be assumed that this is an accumulation of negative charge which propagates along a previously established lightning channel. The aircraft is initially negatively charged due to its being part of the channel formed by the passage of a previous leader or K-change. As the charge from the dart leader flows onto the plane it becomes more negatively charged. The expected behavior of the electric field and its derivative is shown in Figure 2.12. Compare this with Figure 2.13, a D-dot record from flight 80-019. The basic structures are again very similar.

Another lightning phenomenon to be considered is the K-change. The simple model for this is similar to that of the dart leader, except that instead of depositing negative charge on the aircraft, the K-change sweeps the charge off. The expected field behavior is shown in Figure 2.14. The important thing to recognize about this figure is the opposite polarity of the D-dot graph. A measured D-dot response from flight 80-019 is offered for comparison in Figure 2.15.

The one direct interaction phenomenon yet to be treated is that of the exit of the stepped leader from the aircraft. After the stepped leader attaches to the plane, a net negative charge accumulates until the electric field at some point on the plane becomes large enough to cause air breakdown. At that time negative charge flows off the plane and the stepped leader continues on its way. The exit of the leader from the aircraft is, as in the case of attachment, a nonlinear process. The expected field and derivative behavior is shown in Figure 2.16. The form of the derivative data in Figure 2.16 is not qualitatively different from the K-change behavior of Figure 2.14. There are some differences, however. The exiting leader waveform should show a slow buildup of negative field before the positive spike. It may be, though, that this buildup is too slow to be recorded by the derivative instrumentation. Also, if the air breakdown occurs rapidly enough, aircraft resonances could be excited which would not be seen for a slower K-change event. Actual field measurements would be helpful here in differentiating between the two phenomena, because the exiting leader would leave a significant negative charge on the aircraft, while the K-change would leave very little net charge behind. As a possible

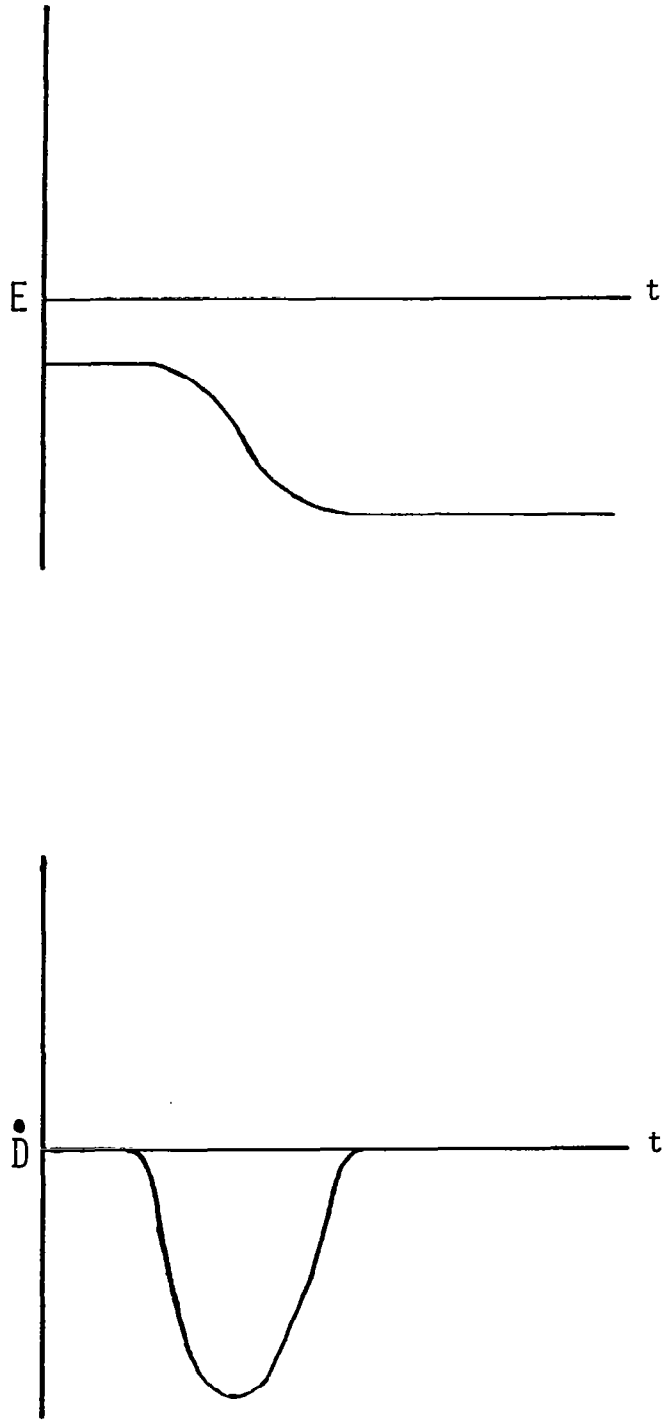

FIGURE 2.12 ELECTRIC FIELD EXPECTED AT THE NOSE DUE TO SUBSEQUENT LEADER INTERACTION WITH THE AIRCRAFT

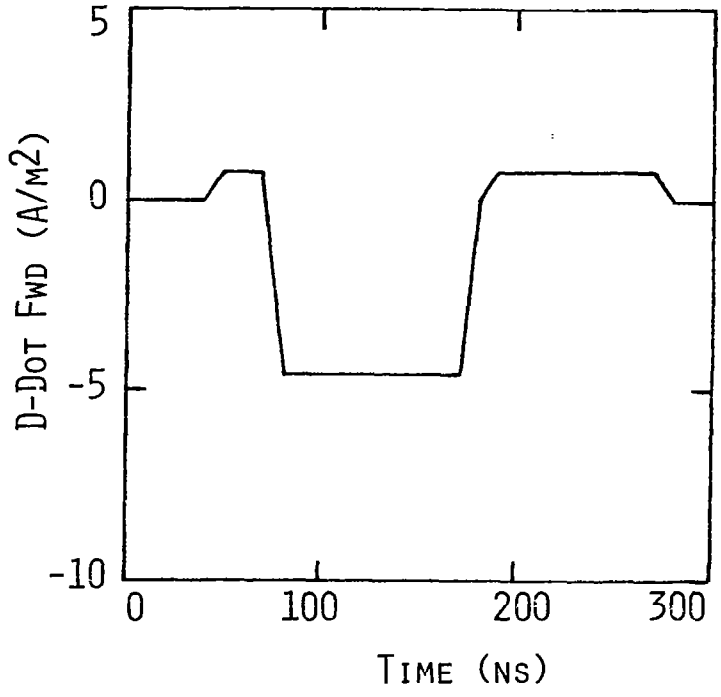

Figure 2.13 Example of Data Record Which May be Due to Subsequent Leader Interaction with the Aircraft (Flight 80-019)

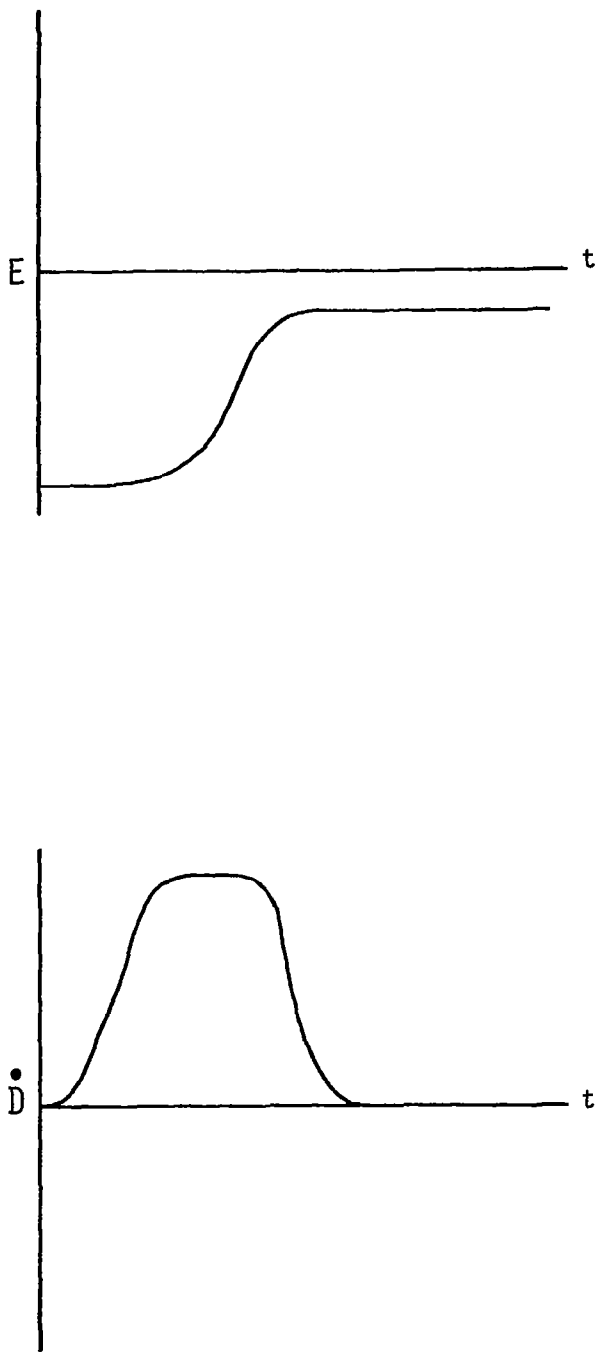

FIGURE 2.14 ELECTRIC FIELD EXPECTED AT NOSE DUE TO K-CHANGE INTERACTION WITH AIRCRAFT

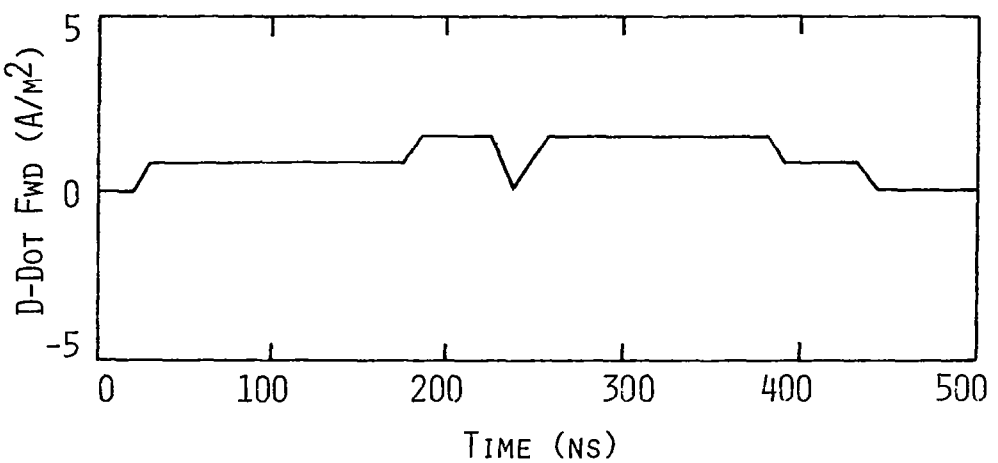

Figure 2.15 Example of Data Record Which May be Due to K-Change Interaction with the Aircraft (Flight 80-019)

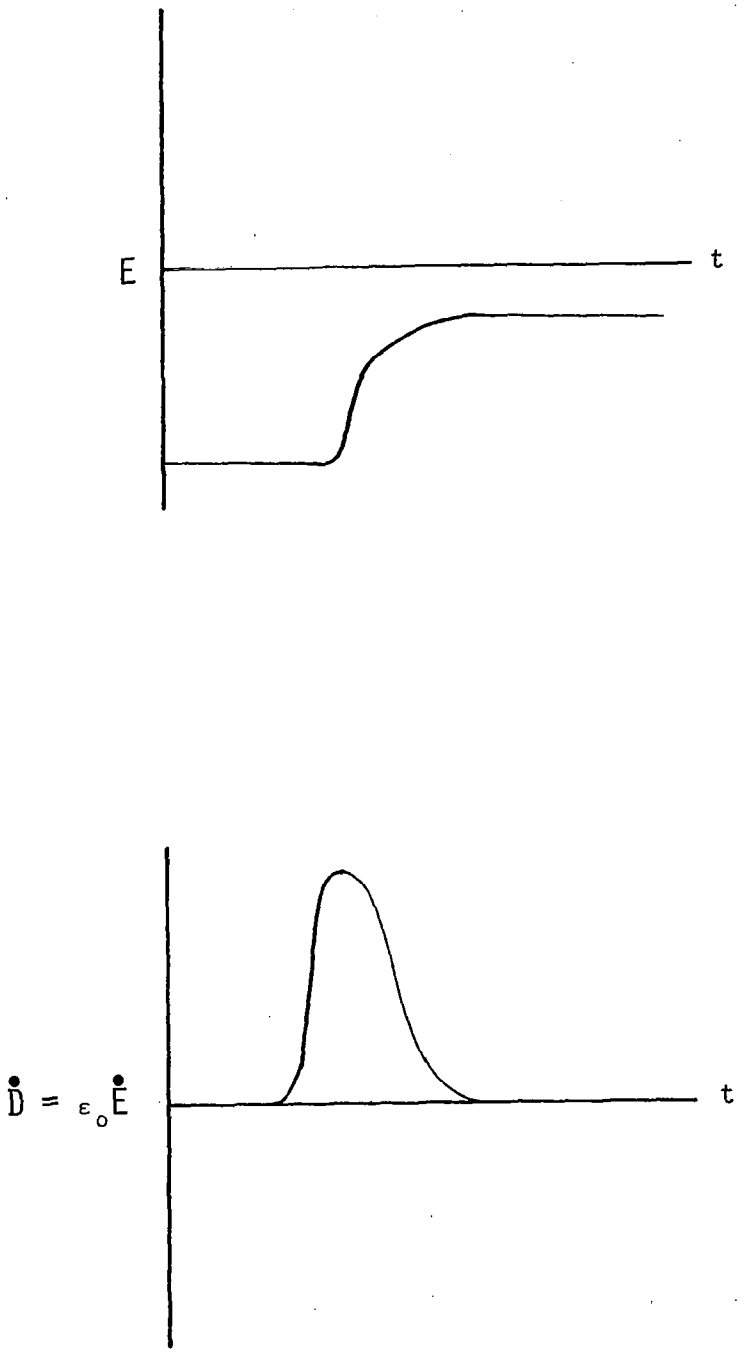

FIGURE 2.16 ELECTRIC FIELD EXPECTED AT NOSE DUE TO EXIT OF LEADER FROM THE AIRCRAFT

example of an exiting leader waveform from the measured data, consider Figure 2.17, which is a D-dot record from flight 80-038.

The scenarios considered in the discussion just completed have all assumed negatively charged leaders and positive return strokes, which may be the most common situation. However, positive leaders and negative K-changes also do occur. Figures for the general behavior of the fields for this case can easily be constructed by simply changing the signs on the figures for the cases considered. The time scale is likely to be different for the positive leader case, but the gross behavior of the fields should be unchanged.

It is useful to conclude this discussion by examining the D-dot records of flight 80-019 in some detail. Figure 2.18 gives an overview of the D-dot data collected on that flight, and Figures 2.19 to 2.23 are expanded versions of the spikes shown in Figure 2.18. If one accepts the simple models discussed above the chronology of events can be explained. The assumptions must be made that an initial stepped leader did not trigger the D-dot sensor, so no record of this event exists. Then, however, Figure 2.19 represents a K-change. The next figure can be explained as a dart leader pulse, as is shown in Chapter 6. Figure 2.21 follows with a subsequent K-change and another dart leader pulse. Then Figure 2.22 represents the next K-change and the sequence ends with a final dart leader in Figure 2.23. All the waveforms are consistent with the gedanken models developed earlier. Even the timing between the leaders and the subsequent K-changes is consistent. Two cyles of leader and K-change appear in the sequence. The time between the first leader and K-change is about 84 μsec, and between the second two is about 85 μsec. If one assumes average dart leader and K-change propagation velocities this implies that the charge center to which the dart leader was going, and from which the K-change originated, was approximately 165 meters from the plane. This evidence together with the waveshapes seen in the records suggests that the data of flight 80-019 represents a multiple flash lightning event, of which only a portion was captured by the instrumentation system.

To conclude this section, possible nonlinearities in the data will be considered. First of all it should be made clear that nonlinear physical

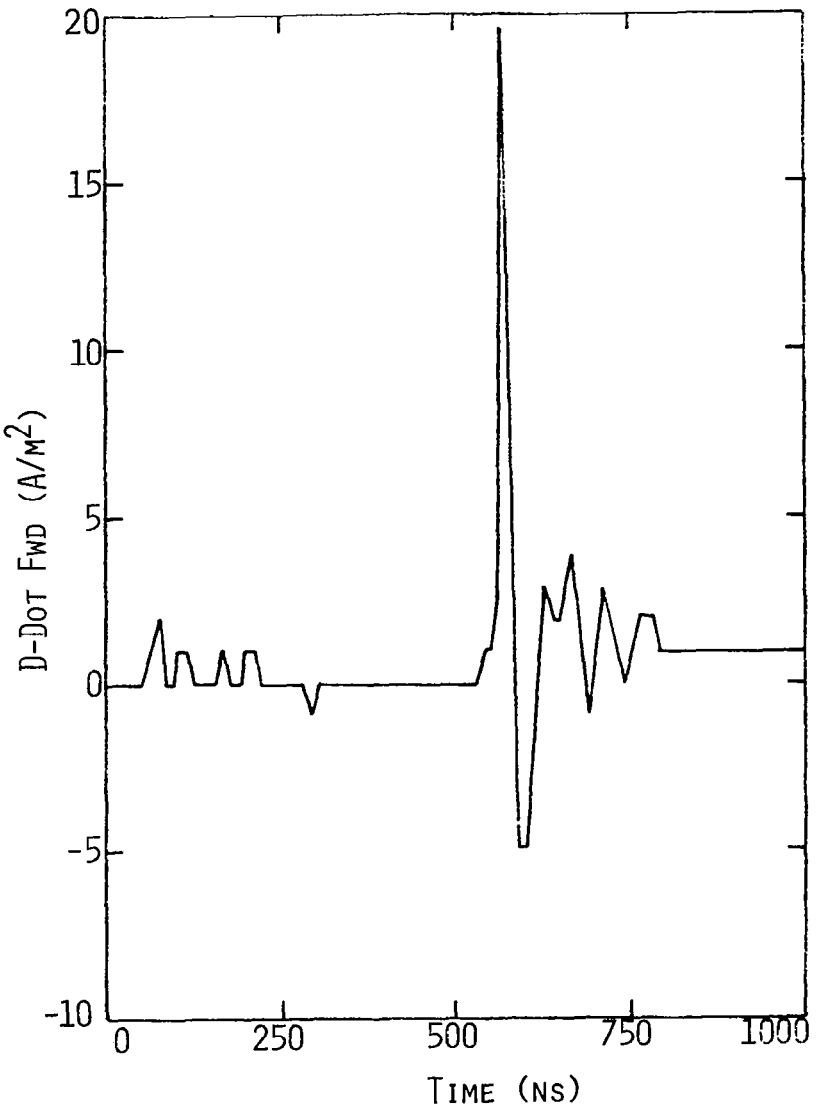

Figure 2.17 Example of Data Record Which May be Due to Exit of Leader From the Aircraft (Flight 80-038)

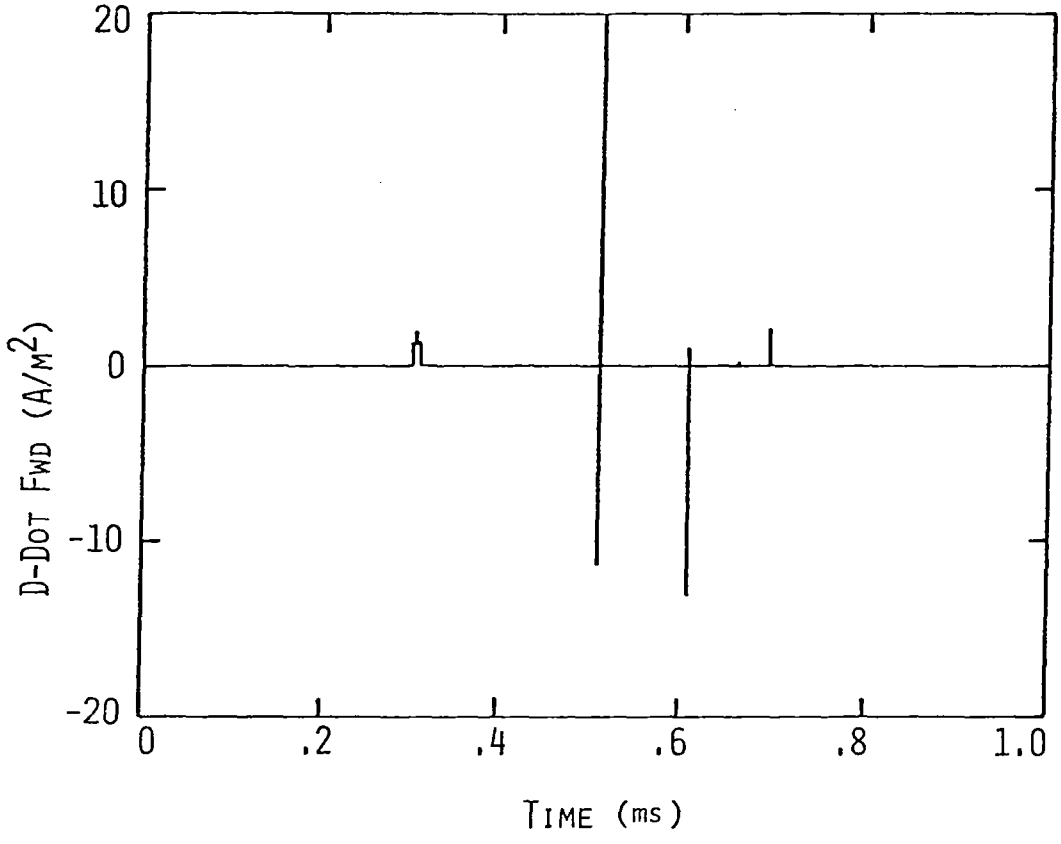

Figure 2.18 Overview of D-Dot for Flight 80-019

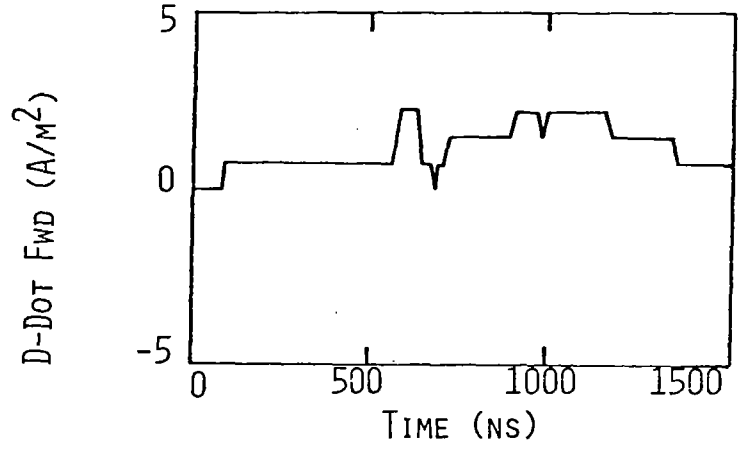

Figure 2.19 First K-Change in the History of Flight 80-019

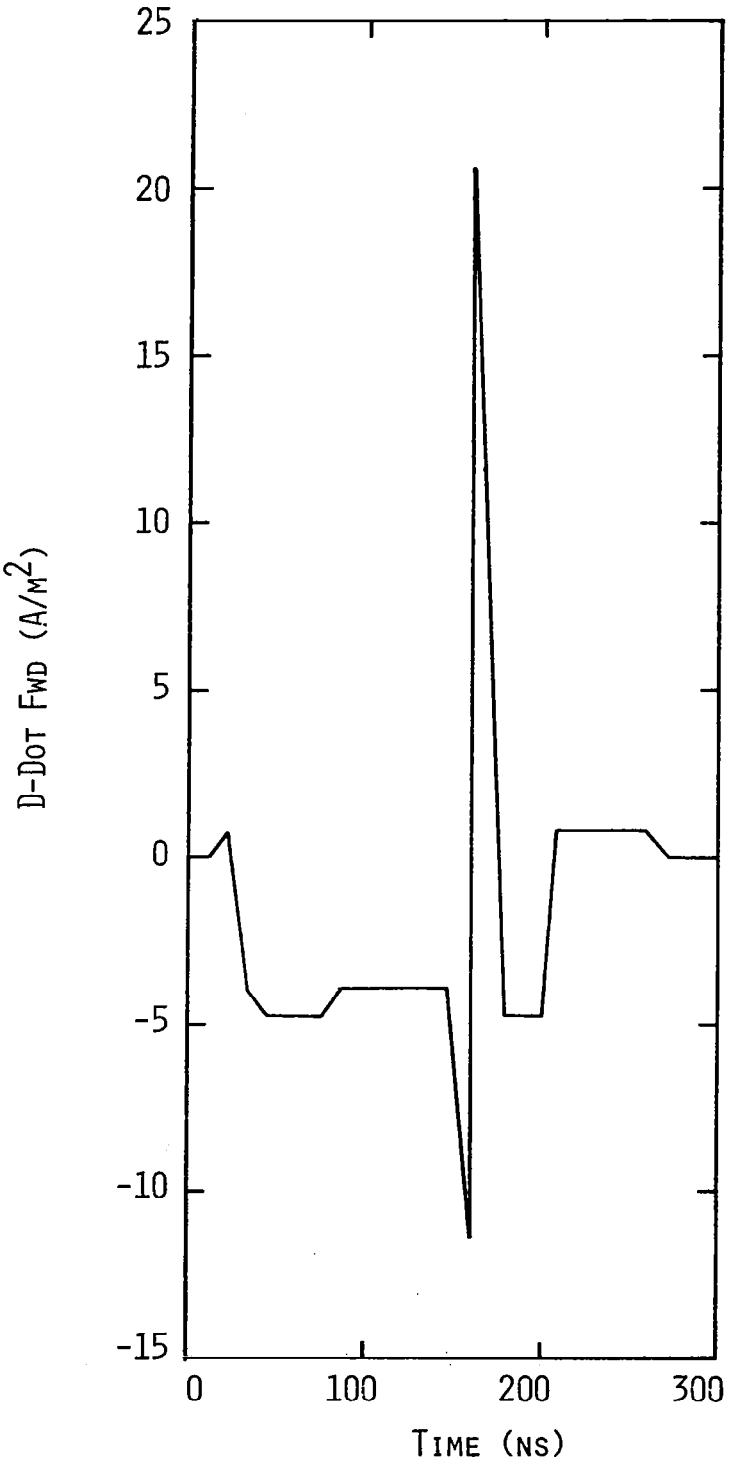

FIGURE 2.20 A SUBSEQUENT LEADER FROM FLIGHT 80-019

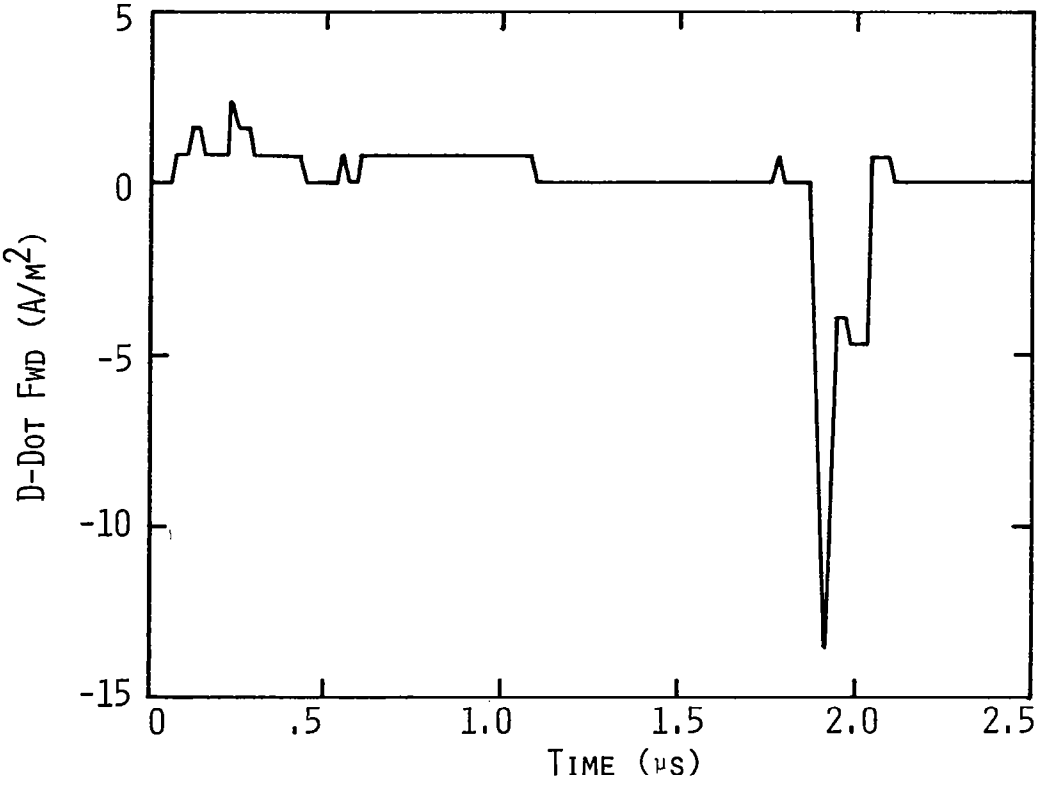

Figure 2.21 Subsequent K-Change and Leader from Flight 80-019

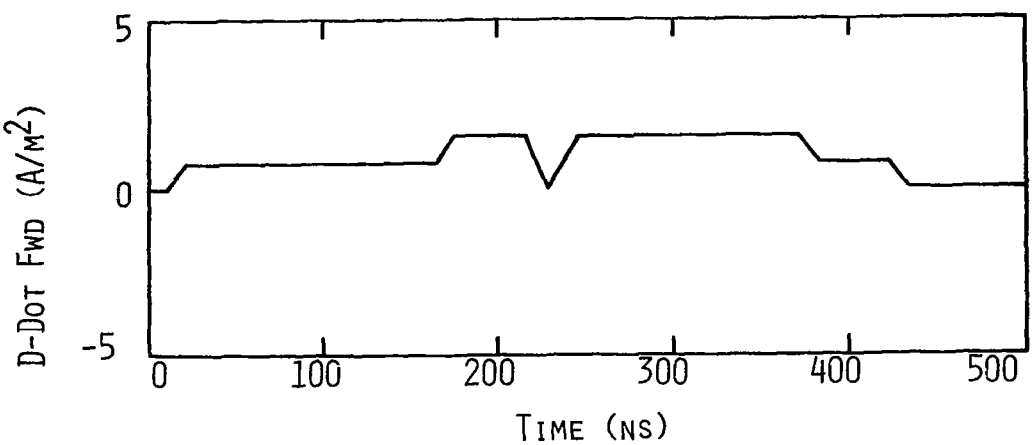

Figure 2.22 Subsequent K-Change from Flight 80-019

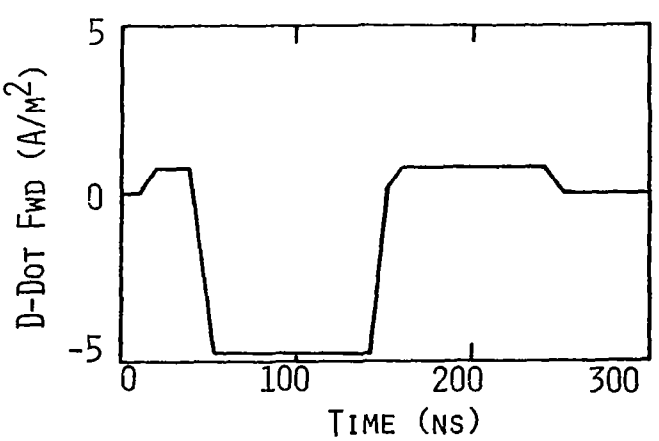

Figure 2.23 Subsequent Leader From Flight 80-019

processes are taking place all during the lightning event, so the real question here is which processes require nonlinear modeling. It would appear that dart leader and K-change phenomena, for which an established conducting channel already exists, can be modeled linearly. Also the aircraft's interaction with nearby lightning is linear and can be easily modeled using free-field illumination. Stepped leader interaction and the actual attachment process will require nonlinear modeling. The initial polarization of the aircraft by the approaching leader charge and streamer formation are easiest to model nonlinearly. By guessing at the nonlinear magnitudes and forcing these processes in a linear model, it is possible to do the nonlinear problem in a linear fashion, but accuracy will certainly suffer. What must be forced to occur in a linear computer code would occur naturally in a nonlinear code giving results which would be more satisfying and credible.

2.8 Summary of 1980 Data

The 1980 data was reviewed to identify maximum observed values, which are summarized in Table 2.3. These values were obtained by inspection and approximate graphical integration of the derivative data.

Table 2.3 Summary of Maximum Observed Values for the 1980 Data Set.

$\frac{\partial E}{\partial t}$:	2.4×10^{12} V/m/s
E :	2.4×10^{6} V/m
$\frac{\partial H}{\partial t}$:	7×10^{8} A/m/sec
H :	16 A/m
$\frac{\partial I}{\partial t}$:	(Band limited) 6×10^{8} A/sec
I :	110 A

CHAPTER 3

INTERPRETATION APPROACH

The major tool used for analyzing the response of the F106 aircraft to lightning is the computer code T3DFD, standing for time domain three dimensional finite difference code. The code solves Maxwell's equations in three dimensions, and is capable of modeling complex geometries, space and time varying permittivity, permeability, and air conductivity. It is also possible to model sources in various ways. For this study, free field illumination using Huygen's sources [11] and direct current injection onto the aircraft were the two sources employed. The current injection technique was used to model direct strikes and the free field technique was used for nearby lightning.

The finite differencing of Maxwell's equations in the manner used by T3DFD was first suggested by Yee [12]. A basic understanding of the method can be obtained by considering a simple one-dimensional problem: the computation of the field in a radially inhomogenous media, $\sigma = \sigma(r)$, $\varepsilon = \varepsilon(r)$, with axial current sources, $J_z = J_z(r)$ [13].

The field everywhere must satisfy Maxwell's equations:

$$\nabla \times \vec{E} = -\mu \frac{\partial \vec{H}}{\partial t} , \tag{3.1}$$

and

$$\nabla \times \vec{H} = \vec{J} + \sigma \vec{E} + \varepsilon \frac{\partial \vec{E}}{\partial t} , \tag{3.2}$$

where common definitions in MKS units are used. Because there is no ϕ or z dependence, (3.1) and (3.2) reduce to

$$\frac{\partial E_z}{\partial r} = -\mu \frac{\partial H_\phi}{\partial t}, \tag{3.3}$$

$$\frac{1}{r}\left(\frac{\partial (rH_\phi)}{\partial r}\right) = J_z + \sigma E_z + \varepsilon \frac{\partial E_z}{\partial t}. \tag{3.4}$$

The solution proceeds by replacing each derivative by its finite difference approximation. The differenced form of (3.3) is:

$$\mu\left(\frac{H_\phi(r,t + 1/2\ \Delta t) - H_\phi(r,t - 1/2\ \Delta t)}{\Delta t}\right) = \frac{E_z(r + 1/2\ \Delta r,t) - E_z(r - 1/2\ \Delta r,t)}{\Delta r}$$

Central differencing has been used in (3.5), that is, derivatives at "r" or "t" are approximated by differences centered at these points. This results in smaller discretization error than that which results from one-sided differences [13]. One can also observe that in (3.5) E_z and H_ϕ are never required at the same space or time point. By using averages, (3.4) can be made to have the same characteristic:

$$\varepsilon(r)\left(\frac{E_z(r,t + 1/2\ \Delta t) - E_z(r,t - 1/2\ \Delta t)}{\Delta t}\right) + \sigma(r)\left(\frac{E_z(r,t, + 1/2\ \Delta t) + E_z(r,t - 1/2\ \Delta t)}{2}\right) =$$

$$-J_z(r,t) + \frac{1}{r}\left(\frac{(r + 1/2\ \Delta r)\, H_\phi\ (r + 1/2\ \Delta r,t)\ - (r - 1/2\ \Delta r)\ H_\phi\ (r-1/2\ \Delta r,t)}{\Delta r}\right) \tag{3.6}$$

Here rH_ϕ is differenced as one variable. Since $H_\phi \sim 1/r$ for small r the function rH_ϕ is more slowly varying than H_ϕ alone, and so, more computational accuracy can be expected. Then the r-t continuum can be discretized with 2 superimposed meshes (Figure 3.1) in which the differences needed in (3.5) and (3.6) are easily identified. To simplify the notation, let

$$E_z^{\,n}(j) \equiv E_z\left(r(j),\ t_E(n)\right) \equiv E_z\left((j-1/2)\ \Delta r,\ (n-1/2)\Delta t\right), \tag{3.7}$$

$$H_\phi^{\,n}(j) \equiv H_o\left(r_o(j),\ t_H(n)\right) \equiv H_\phi\left((j-1)\Delta r,\ (n-1)\ \Delta t,\right) \tag{3.8}$$

where n = 1,2 ---- and j = 1,2 ---- $(j_{can} + 1)$ and j_{can} is the number of locations for which finite difference calculations will be made.

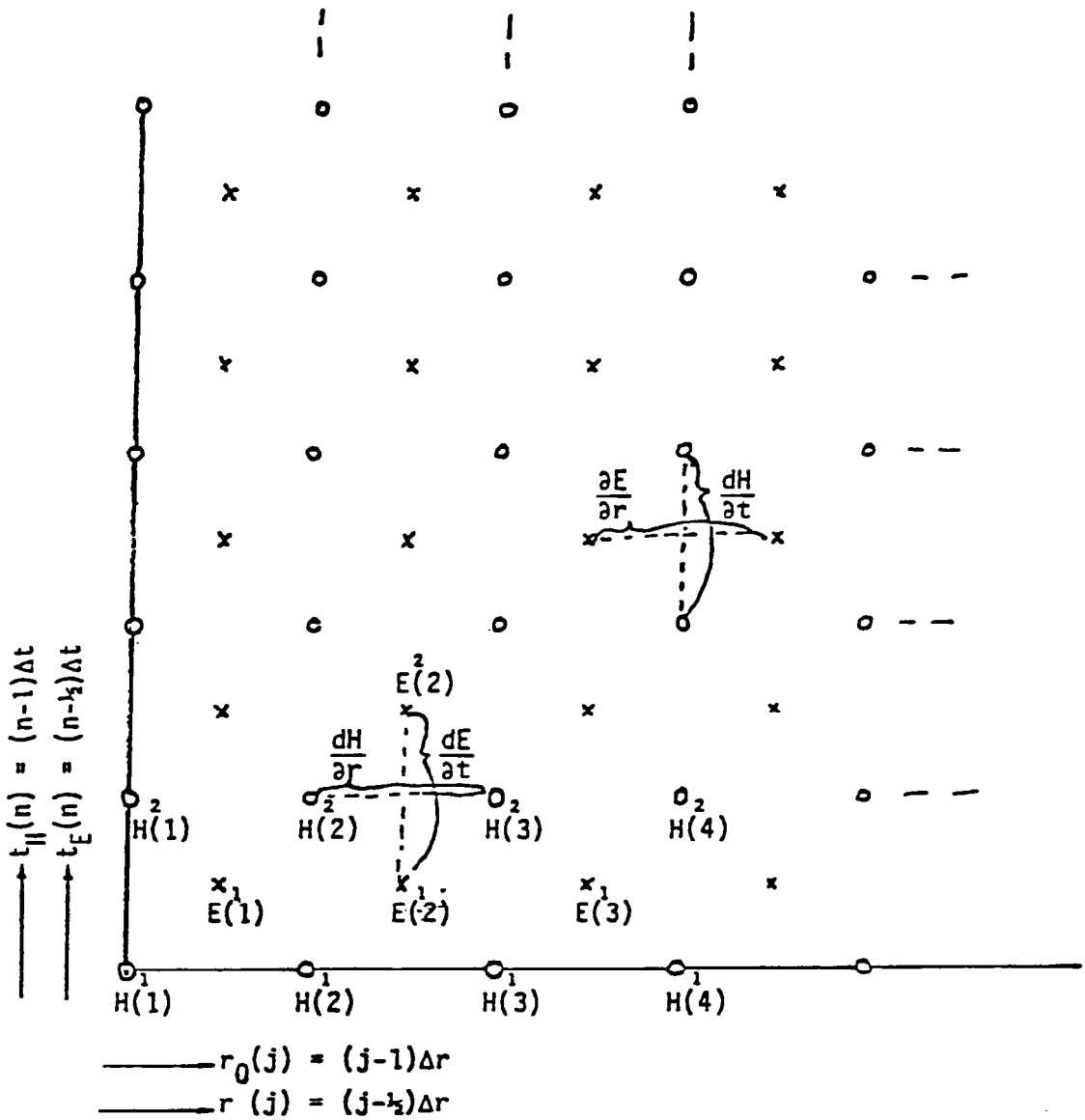

FIGURE 3.1 THE DISCRETIZING MESH FOR THE ONE-DIMENSIONAL (1D) MAXWELL'S EQUATIONS PROBLEM [13]

From here on the notation $j\varepsilon\,[1,\ j_{can}+1]$ will be used to mean $j = 1,2,3\text{---}(j_{can}+1)$. With this notation, (3.5) and (3.6) become

$$\mu\left(\frac{H_\phi^{n+1}(j+1)-H_\phi^{n}(j+1)}{\Delta t}\right)=\frac{E_z^{n}(j+1)-E_z^{n}(j)}{\Delta r} \tag{3.9}$$

and

$$\begin{aligned}\varepsilon\ r(j)\ \left(\frac{E_z^{n+1}(j)-E_z^{n}(j)}{\Delta t}\right)+\sigma(r(j))\ \left(\frac{E_z^{n+1}(j)+E_z^{n}(j)}{2}\right)\\ =-J_z\Big(\ r(j),t_H(n+1)\Big)+\frac{1}{r(j)}\left(\frac{r_o(j+1)\ H_\phi^{n+1}(j+1)-r_o(j)\ H_\phi^{n+1}(j)}{\Delta r}\right)\end{aligned} \tag{3.10}$$

Rearranging (3.9) and (3.10),

$$H_\phi^{n+1}(j+1)=H_\phi^{n}(j+1)+\frac{\Delta t}{\mu\Delta r}\Big(E_z^{n}(j+1)-E_z^{n}(j)\Big), \qquad j\varepsilon[1,j_{can}-1] \tag{3.11}$$

and

$$\begin{aligned}B(j)\cdot E_z^{n+1}(j)=A(j)\cdot E_z^{n}(j)-J_z\Big(\ r(j),t_H(n+1)\Big)\\ +\frac{1}{r(j)\Delta r}\Big[r_o(j+1)\ H_\phi^{n+1}(j+1)\\ -r_o(j)\ H_\phi^{n+1}(j)\Big],\qquad j\varepsilon[1,j_{can}]\end{aligned} \tag{3.12}$$

where

$$A(j)=\left(\frac{\varepsilon\Big(\ r(j)\Big)}{\Delta t}-\frac{\sigma\Big(\ r(j)\Big)}{2}\right)$$

and

$$B(j) = \left(\frac{\varepsilon\left[r(j) \right]}{\Delta t} + \frac{\sigma\left[r(j) \right]}{2} \right) \tag{3.13}$$

Equations (3.11) and (3.12) are the basic ingredients of the time-explicit finite-difference approach. In (3.11) the magnetic field at a new time is computed from the electric field at an earlier time. In (3.12) the electric field at a new time is computed from the current sources and the magnetic field at an earlier time. By cycling between (3.11) and (3.12) the solution "marches" from initial conditions at $t = 0$ to the distribution at any time of interest.

The development of 2D finite difference equations is exactly analogous to the development of the one-dimensional (1D) equations and is not given here. It can, however, be found in Merewether and Fisher [13]. In Figure 3.2, the essential equations needed to program 3D problems in rectangular coordinates are provided. Also given are illustrations showing how E and H field grids are interwoven and a list of the field quantities on the edge of the problem space that must be provided. Because there are six field components to be evaluated at a larger number of space points, the computer resource requirements for 3D problems are much larger than those needed for 1D problems.

A close examination of Equations (3.11) and (3.12) will reveal that not all of the magnetic field grid points can be calculated by the finite difference scheme. The spatial boundary, which consists of tangential H fields, needs a special method of calculation, called a radiation boundary condition. This involves estimating the field that would be expected on the boundary from the fields inside the boundary. Many such conditions have been developed, and all make some assumption about the character of the radiation approaching the boundary. The version of T3DFD used in this study uses a variation on the method of Mur [14], in which it is assumed the radiation consists of plane waves propagating outward along the rectangular coordinate axes. This method has the advantage of stability for at least several thousand time steps, whereas

Assumptions: None

Maxwell's Equations

$$-u\frac{\partial H_x}{\partial t} = \left(\frac{\partial E_z}{\partial y} - \frac{\partial E_y}{\partial z}\right) \qquad H_x^n(i,j,k) = H_x(x(i),y_0(j),z_0(k),t_H(n))$$

$$-u\frac{\partial H_y}{\partial t} = \left(\frac{\partial E_x}{\partial z} - \frac{\partial E_z}{\partial x}\right) \qquad H_y^n(i,j,k) = H_y(x_0(i),y(j),z_0(k),t_H(n))$$

$$-u\frac{\partial H_z}{\partial t} = \left(\frac{\partial E_y}{\partial x} - \frac{\partial E_x}{\partial y}\right) \qquad H_z^n(i,j,k) = H_z(x_0(i),y_0(j),z(k),t_H(n))$$

$$\epsilon\frac{\partial E_x}{\partial t} + \sigma E_x = \left(\frac{\partial H_z}{\partial y} - \frac{\partial H_y}{\partial z}\right) - j_x \qquad E_x^n(i,j,k) = E_x(x_0(i),y(j),z(k),t_E(n))$$

$$\epsilon\frac{\partial E_y}{\partial t} + \sigma E_y = \left(\frac{\partial H_x}{\partial z} - \frac{\partial H_z}{\partial x}\right) - j_y \qquad E_y^n(i,j,k) = E_y(x(i),y_0(j),z(k),t_E(n))$$

$$\epsilon\frac{\partial E_z}{\partial t} + \sigma E_z = \left(\frac{\partial H_y}{\partial x} - \frac{\partial H_x}{\partial y}\right) - j_z \qquad E_z^n(i,j,k) = E_z(x(i),y(j),z_0(k),t_E(n))$$

$$x_0(i) = (i-1)\Delta x \;,\; y_0(j) = (j-1)\Delta y \;,\; z_0(k) = (k-1)\Delta z \;,\; t_H(n) = (n-1)\Delta t$$

$$x(i) =)i-1/2)\Delta x \;,\; y(j) = (j-1/2)\Delta y \;,\; z(j) = (k-1/2)\Delta z \;,\; t_E(n) = (n-1/2)\Delta t$$

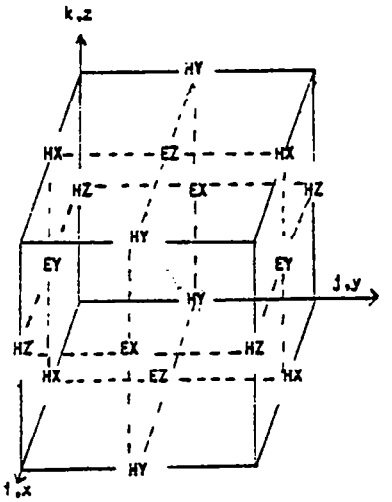

Finite Difference Equations (non-uniform grid allowed)

$$H_x^{n+1}(i,j+1,k+1) = H_x^n(i,j+1,k+1) - \frac{\Delta t}{u}\left(\frac{E_z^n(i,j+1,k+1) - E_z^n(i,j,k+1)}{y(j+1) - y(j)}\right) + \frac{\Delta t}{u}\left(\frac{E_y^n(i,j+1,k+1) - E_y^n(i,j+1,k)}{z(k+1) - z(k)}\right) \quad \begin{cases} i\epsilon[1,i_{can}] \\ j\epsilon[1,j_{can}-1] \\ k\epsilon[1,k_{can}-1] \end{cases}$$

$$H_y^{n+1}(i+1,j,k+1) = H_y^n(i+1,j,k+1) - \frac{\Delta t}{u}\left(\frac{E_x^n(i+1,j,k+1) - E_x^n(i+1,j,k)}{z(k+1) - z(k)}\right) + \frac{\Delta t}{u}\left(\frac{E_z^n(i+1,j,k+1) - E_z^n(i,j,k+1)}{x(i+1) - x(i)}\right) \quad \begin{cases} i\epsilon[1,i_{can}-1] \\ j\epsilon[1,j_{can}] \\ k\epsilon[1,k_{can}-1] \end{cases}$$

$$H_z^{n+1}(i+1,j+1,k) = H_z^n(i+1,j+1,k) - \frac{\Delta t}{u}\left(\frac{E_y^n(i+1,j+1,k) - E_y^n(i,j+1,k)}{x(i+1) - x(i)}\right) + \frac{\Delta t}{u}\left(\frac{E_x^n(i+1,j+1,k) - E_x^n(i+1,j,k)}{y(j+1) - y(j)}\right) \quad \begin{cases} i\epsilon[1,i_{can}-1] \\ j\epsilon[1,j_{can}-1] \\ k\epsilon[1,k_{can}] \end{cases}$$

$$B\cdot E_x^{n+1}(i,j,k) = A\cdot E_x^n(i,j,k) - j_x + \left(\frac{H_z^{n+1}(i,j+1,k) - H_z^{n+1}(i,j,k)}{y_0(j+1) - y_0(j)}\right) - \left(\frac{H_y^{n+1}(i,j,k+1) - H_y^{n+1}(i,j,k)}{z_0(k+1) - z_0(k)}\right) \quad \begin{cases} i\epsilon[1,i_{can}] \\ j\epsilon[1,j_{can}] \\ k\epsilon[1,k_{can}] \end{cases}$$

$$B\cdot E_y^{n+1}(i,j,k) = A\cdot E_y^n(i,j,k) - j_y + \left(\frac{H_x^{n+1}(i,j,k+1) - H_x^{n+1}(i,j,k)}{z_0(k+1) - z_0(k)}\right) - \left(\frac{H_z^{n+1}(i+1,j,k) - H_z^{n+1}(i,j,k)}{x_0(i+1) - x_0(i)}\right) \quad \begin{cases} i\epsilon[1,i_{can}] \\ j\epsilon[1,j_{can}] \\ k\epsilon[1,k_{can}] \end{cases}$$

$$B\cdot E_z^{n+1}(i,j,k) = A\cdot E_z^n(i,j,k) - j_z + \left(\frac{H_y^{n+1}(i+1,j,k) - H_y^{n+1}(i,j,k)}{x_0(i+1) - x_0(i)}\right) - \left(\frac{H_x^{n+1}(i,j+1,k) - H_x^{n+1}(i,j,k)}{y_0(j+1) - y_0(j)}\right) \quad \begin{cases} i\epsilon[1,i_{can}] \\ j\epsilon[1,j_{can}] \\ k\epsilon[1,k_{can}] \end{cases}$$

where

$$A = \left(\frac{\epsilon}{\Delta t} - \frac{\sigma}{2}\right) \;,\; B = \left(\frac{\epsilon}{\Delta t} + \frac{\sigma}{2}\right) \;,\; j_x = j_x(t_H(n+1)) \;,\; j_y = j_y(t_H(n+1)) \;,\; j_z = j_z(t_H(n+1))$$

all evaluated at desired E component location

Externally supplied values are tangential electric fields on outer surface of problem space:

$$H_x^n(i,j,1) \;,\; H_y^n(i,j,1) \;,\; H_x^n(i,j,k_{can}+1) \;,\; H_y^n(i,j,k_{can}+1) \qquad \text{all } i\epsilon[1,i_{can}] \;,\; j\epsilon[1,j_{can}]$$

$$H_x^n(i,1,k) \;,\; H_z^n(i,1,k) \;,\; H_x^n(i,j_{can}+1,k) \;,\; H_z^n(i,j_{can}+1,k) \qquad \text{all } i\epsilon[1,i_{can}] \;,\; k\epsilon[1,k_{can}]$$

$$H_y^n(1,j,k) \;,\; H_z^n(1,j,k) \;,\; H_y^n(i_{can}+1,j,k) \;,\; H_z^n(i_{can}+1,j,k) \qquad \text{all } j\epsilon[1,j_{can}] \;,\; k\epsilon[1,k_{can}]$$

FIGURE 3.2 FINITE DIFFERENCE EQUATIONS IN RECTANGULAR COORDINATES SET UP WITH EXTERNALLY SUPPLIED E-FIELDS [13]

some other methods can generate numerical noise which will cause instability in T3DFD after only several hundred time steps.

The insertion of the F106 aircraft into T3DFD is accomplished by means of a subroutine which zeros all electric field grid points which are spatially within the aircraft. This technique strictly requires that the aircraft skin be perfectly conducting and a solid enclosure with no openings to the outside. Of course the real F106 does not conform to these requirements, but the technique is a good approximation when the skin is metallic and only the external response of the aircraft is desired. A block model of the F106, which is what the aircraft looks like to the T3DFD code, is shown in Figure 3.3.

Three views of the F106, top, side, and front, are shown in Figure 3.4 along with dimensions. The approximate locations of the three time derivative sensors used in 1980 and 1981 are also indicated. The I-dot sensor, measuring the time derivative of the current, is located on the boom of the aircraft. The measured output from this sensor was used as a guide in determining the current flowing onto the aircraft from a direct lightning strike. I-dot could not be predicted by T3DFD because of the way current was numerically injected onto the F106 (I-dot is prescribed, not calculated). The D-dot sensor measuring the time derivative of the displacement current was located on the forward part and underneath the fuselage. The B-dot sensor measuring the time derivative of magnetic flux was located on the right side of the fuselage just above the right wing.

It should be noted that the technique of finite differencing used by T3DFD establishes a limit on how much spatial resolution can be achieved. The grid spacing chosen tends to be a compromise between the desired fine resolution and computer limitations. The F106 was gridded so that resolution in the length of the aircraft was one meter, and in the other two rectangular directions it was one-half meter. This spatial resolution limit means that the sensor locations in the numerical code could be as much as a half

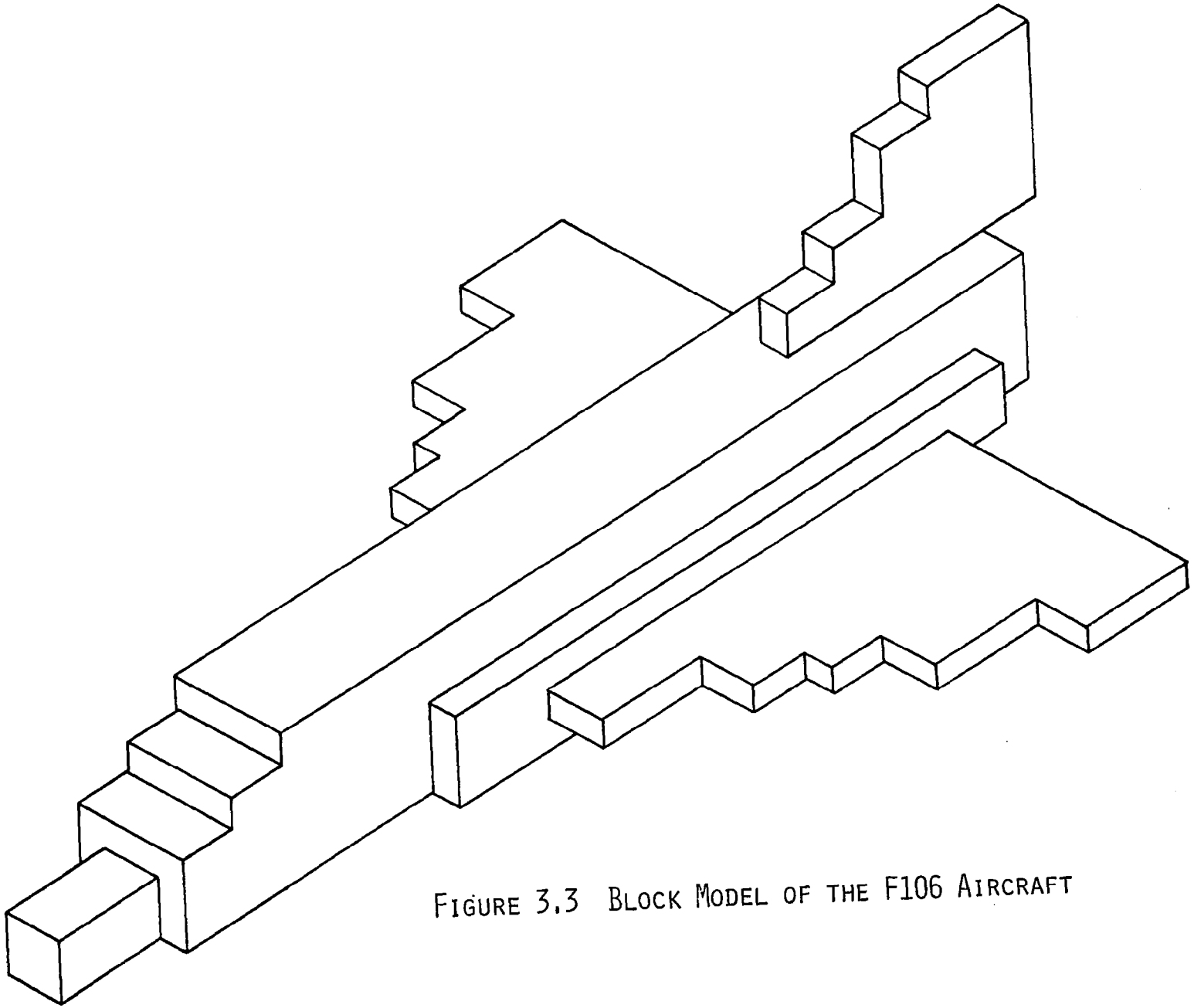

FIGURE 3.3 BLOCK MODEL OF THE F106 AIRCRAFT

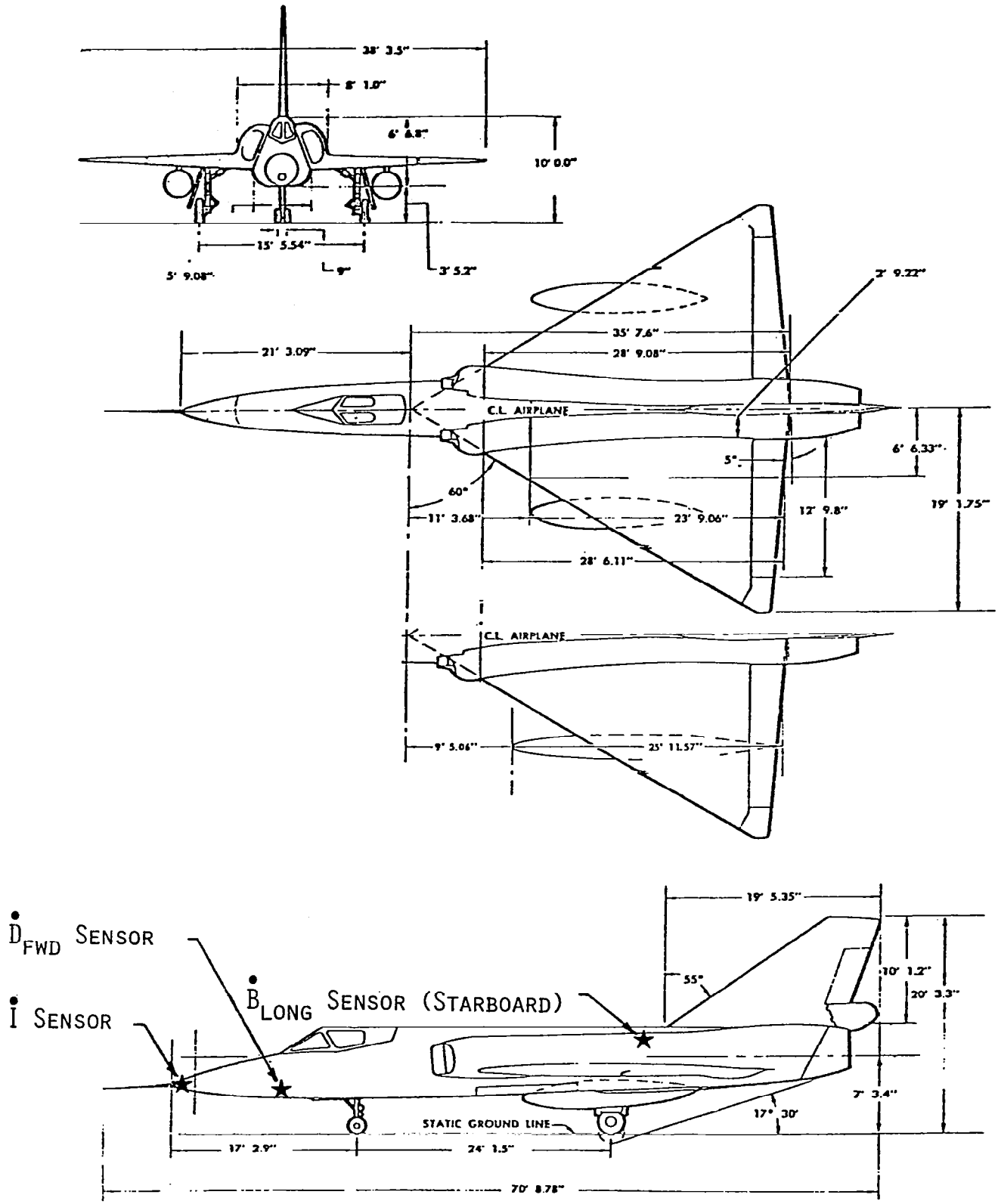

FIGURE 3.4 DIMENSIONS AND SENSOR LOCATIONS FOR F106

meter displaced from their real positions. An example of this is the numerical D-dot sensor. The real sensor is placed symmetrically with respect to left and right on the underside of the fuselage. Finite difference restrictions require that the numerical sensor be displaced by one-fourth meter either to the left or right of this position. This will result in some disagreement when symmetry arguments are compared with numerical predictions. This affects only the LEMP data interpretation for certain cases of angle of incidence and polarization which are given on Page 112. Also T3DFD actually calculates average fields, with the averaging done over the lattice cell centered on the field grid point, so the space over which T3DFD calculates an aircraft response is likely to be somewhat larger than that for the real sensor.

The spatial grid size chosen for finite differencing imposes a limit on the size of the time step through the Courant condition. This is expressed analytically in Equation (3.14).

$$\Delta t < \frac{1}{c}\left(\frac{1}{\Delta x^2} + \frac{1}{\Delta y^2} + \frac{1}{\Delta z^2}\right)^{-1/2}. \qquad (3.14)$$

Δx, Δy, and Δz represent the grid spacing along the coordinate axes and c is the speed of light. Equation (3.14) is simply a requirement that the numerical speed of propagation be greater than the actual physical speed. The spatial grid chosen for the F106 requires that the time step be less than 1.11 nanoseconds. The actual time step used was one nanosecond, and this represents the time resolution of the code.

CHAPTER 4

MODEL VALIDATION

To check the accuracy of the finite difference model of the F106 a comparison was made between the code's predicted response and the measurements of the scale model current injection test of Trost, et al. [15], performed at Texas Tech. The experimental arrangement was as shown in Figure 4.1. The setup is designed to simulate the interaction of an attached lightning strike with the aircraft. A scale model of the F106 was suspended by wires, representing a lightning channel, and external electric and magnetic field time derivative responses were measured. Also circumferential B-dot was measured halfway up the lower wire in an effort to determine the current actually injected onto the model. B from this latter measurement is shown in Figure 4.2. Figures 4.3 and 4.4 present the measured electric and magnetic field responses on the model.

Figure 4.2, from which the injected current was deduced, needs further explanation. The measurement was taken at a point 5 feet from the nose of the model, and 6 inches from the wire, so the B field in the plot is an indication of the current at that point in the wire, which is not the same as the injected current. That this is true can be seen from the waveform of the B field, which shows a second peak approximately ten nanoseconds after the first peak. The 10 nanosecond period corresponds to the travel time of the signal from the measuring point to the model and back, indicating that the second peak in Figure 4.2 is a reflection from the model travelling back along the wire. A reflection occurs at the injection point of the model because of the mismatch of impedances there. The model presents a lower impedance to the current than the wire does, and hence, more current is injected onto the model than is flowing in the wire. This results in the reflected wave seen in the second peak of the plot. The conclusion of all this is that the actual injected current must be determined from the sum of the two peaks, and not by the waveform of

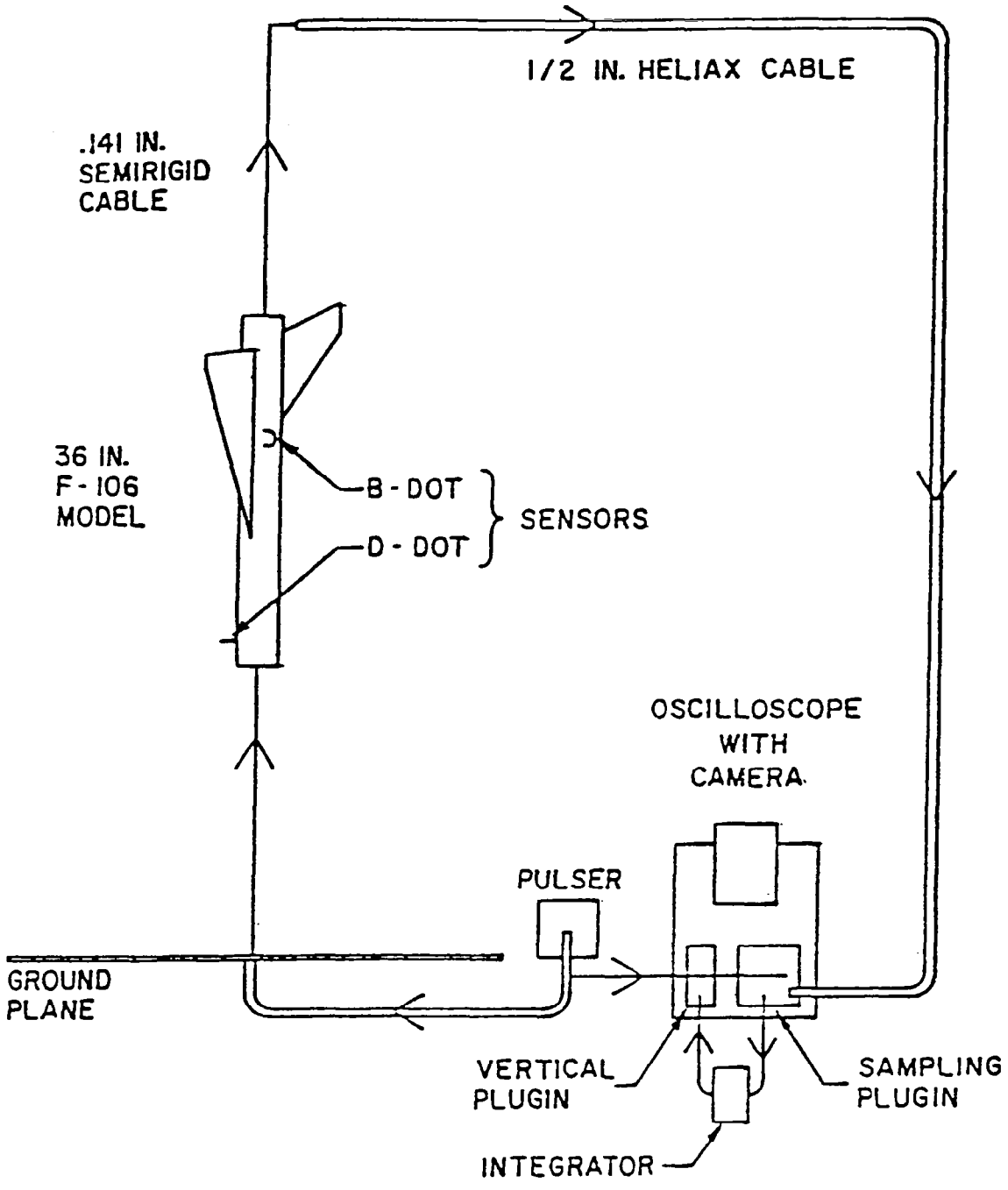

FIGURE 4.1 APPARATUS FOR AIRCRAFT-LIGHTNING MODELING [15]

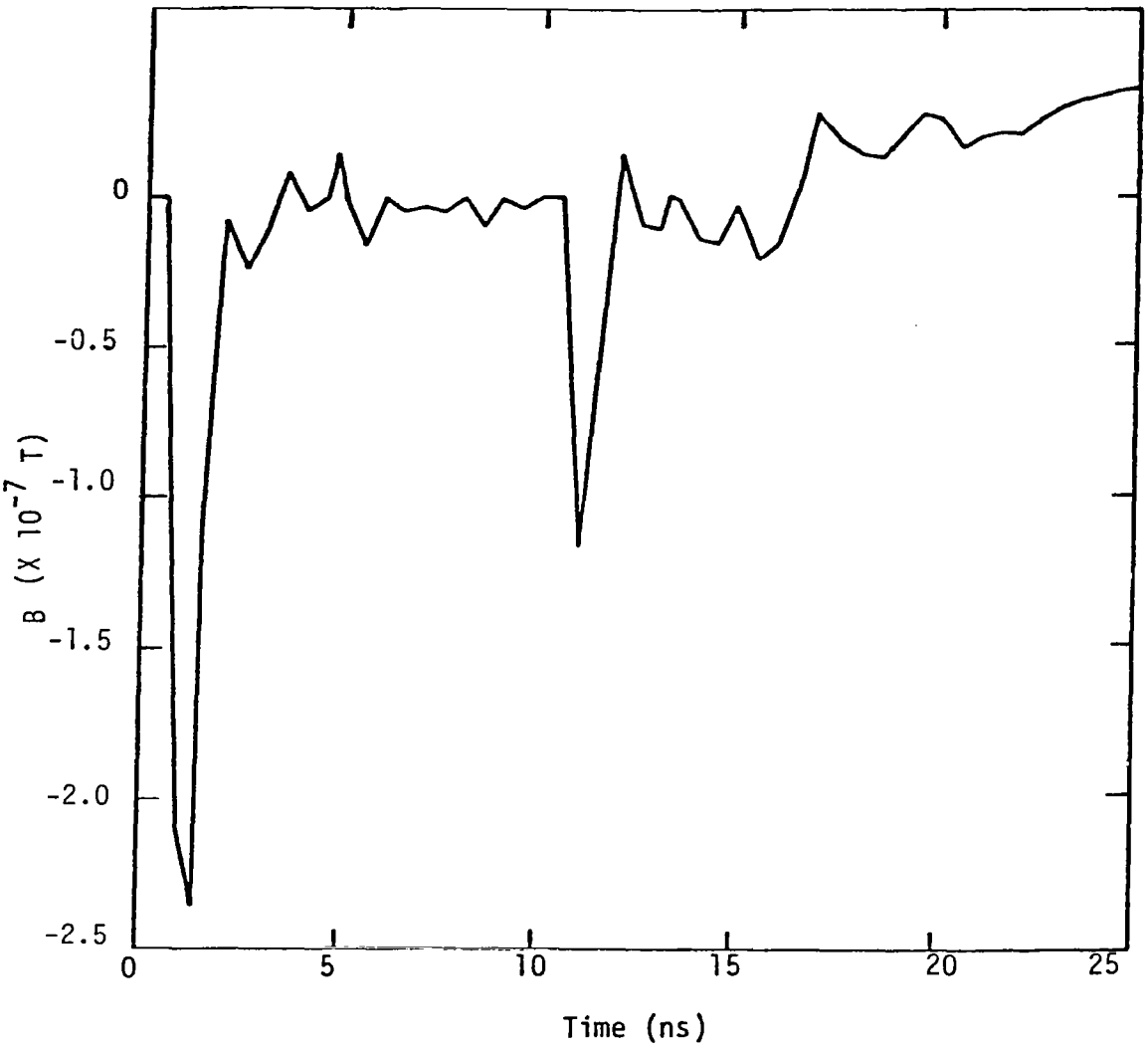

FIGURE 4.2 MAGNETIC FIELD MEASURED AT A RADIAL DISTANCE OF 6 INCHES AND AN AXIAL DISTANCE OF 60 INCHES FROM AIRPLANE [15]

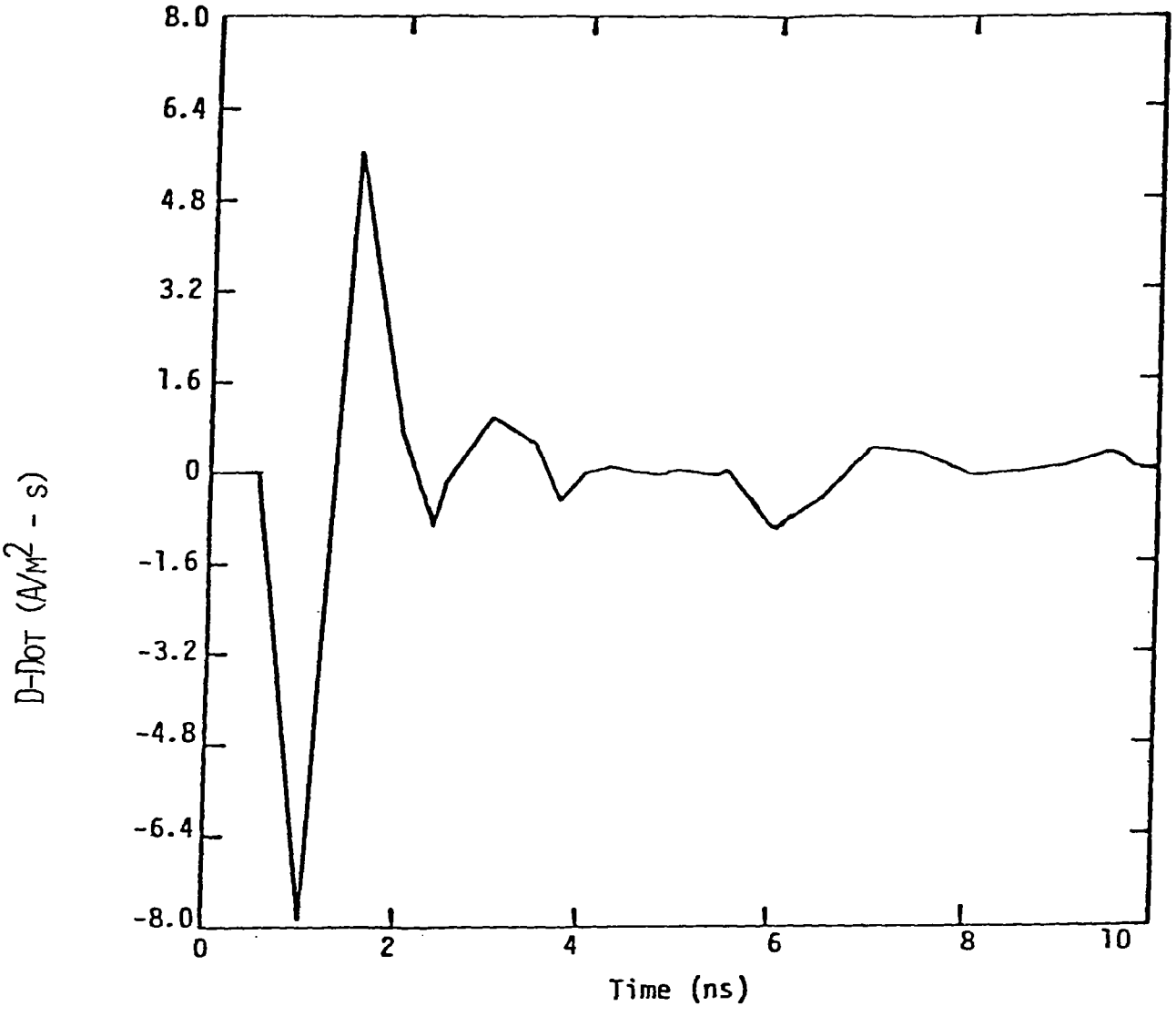

FIGURE 4.3 MEASURED RESPONSE OF DISPLACEMENT CURRENT DERIVATIVE SENSOR [15]

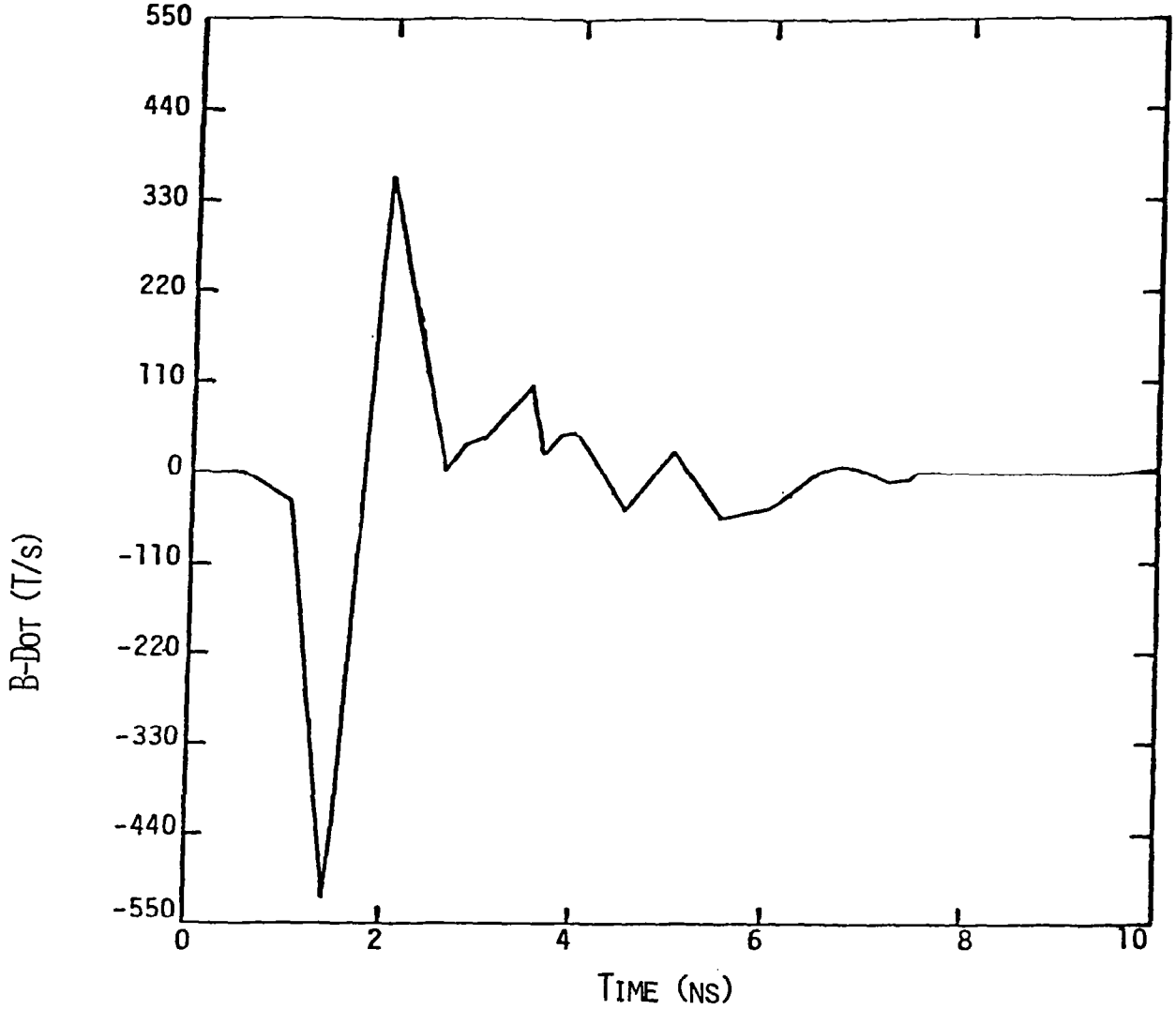

Figure 4.4 Measured Response of Magnetic Field Derivative Sensor [15]

Figure 4.2 as it stands. For the validation studies the injected current was deduced by shifting the maximum of the second pulse of Figure 4.2 to the time position of the first maximum and then summing point by point.

A difficulty which arose in the analysis was in how to accurately determine the injected current from the magnetic field measurement. The most obvious way is to assume the simple expression $B(t) = \mu_0 I(t)/2\pi r$, where r is the perpendicular distance of the measurement point from the wire. But this is really a magnetostatic assumption and at least requires that the pulse width be much greater than the signal travel time from the wire to the measuring point. In the present case the pulse width is about .75 nanoseconds and the travel time is .5 nanoseconds, so the requirement is not satisfied. In order to solve the problem more accurately, an integral expression can be derived for the current in terms of the magnetic field [11]. This expression is complex in the present case, and it would have required a significant amount of time to unfold the true current from the measured field. It was determined that the cost in time was not justified and the decision was made to use the simple formula $B(t) = \mu_0 I(t)/2\pi r$, even though it may not be as accurate as one would like. The accuracy of the finite difference model could still be checked, although the injected current could be somewhat inaccurate, and exact matching with measured responses could no longer be expected.

In order to compare directly the measured scale model responses to the predicted computer model responses, it was necessary to scale the injected current. There was a factor of 18.8 in size between the scale model and the full size F106 in the finite difference code, and scaling was needed to preserve frequency characteristics between the two models. A discussion of the proper way to perform this scaling is given in [16].

The results of the validation tests are shown in Figures 4.5 and 4.6. Figure 4.5 overlays the measured and predicted responses for the B-dot sensor, and Figure 4.6 does the same for the D-dot sensor. The agreement is quite good despite the uncertainty in the injected current, probably indicating that the simple minded method for calculating I(t) was not too much in error. In any case the close agreement obtained between the

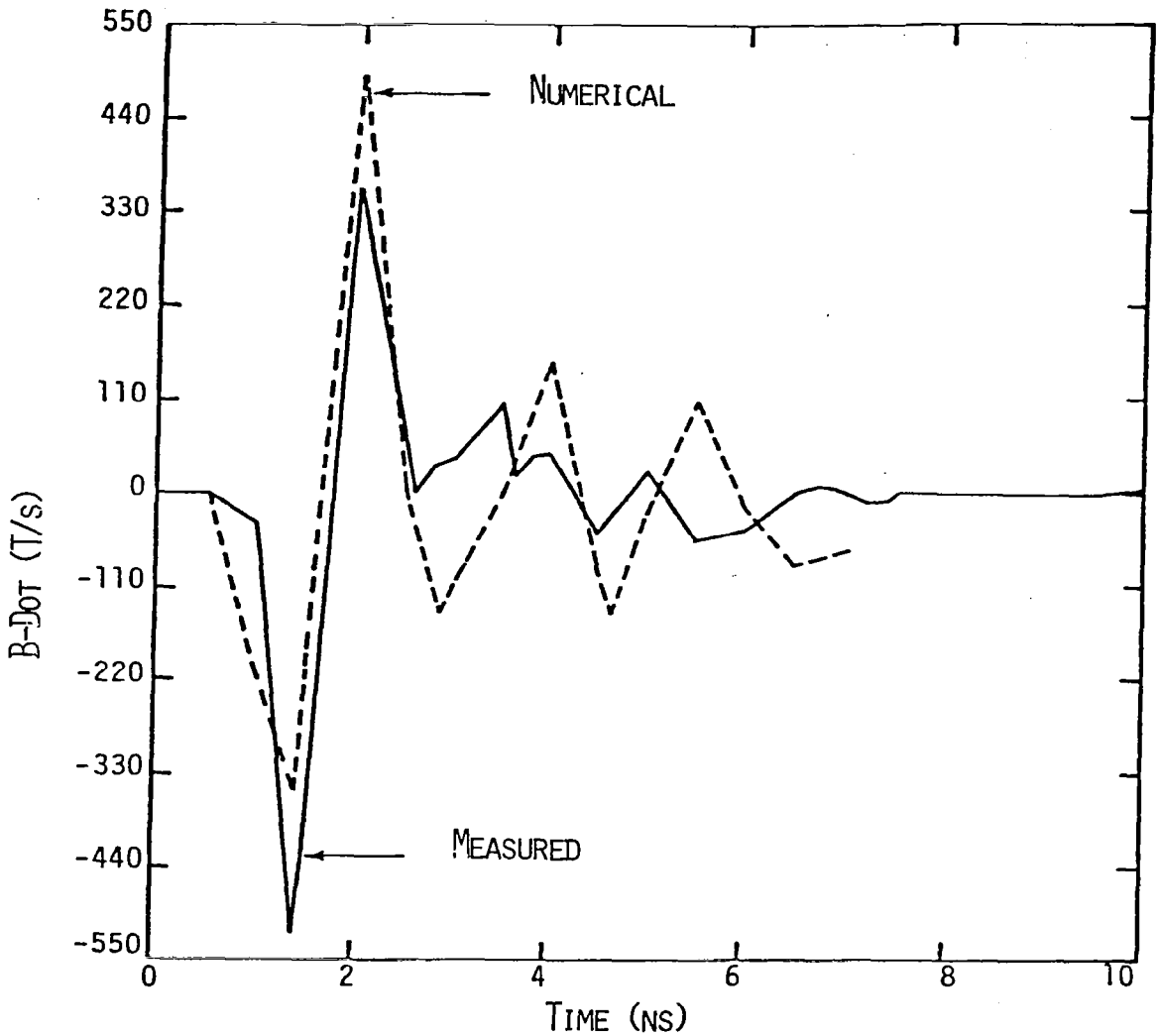

FIGURE 4.5 COMPARISON OF MEASURED AND PREDICTED RESPONSE OF MAGNETIC FIELD DERIVATIVE SENSOR

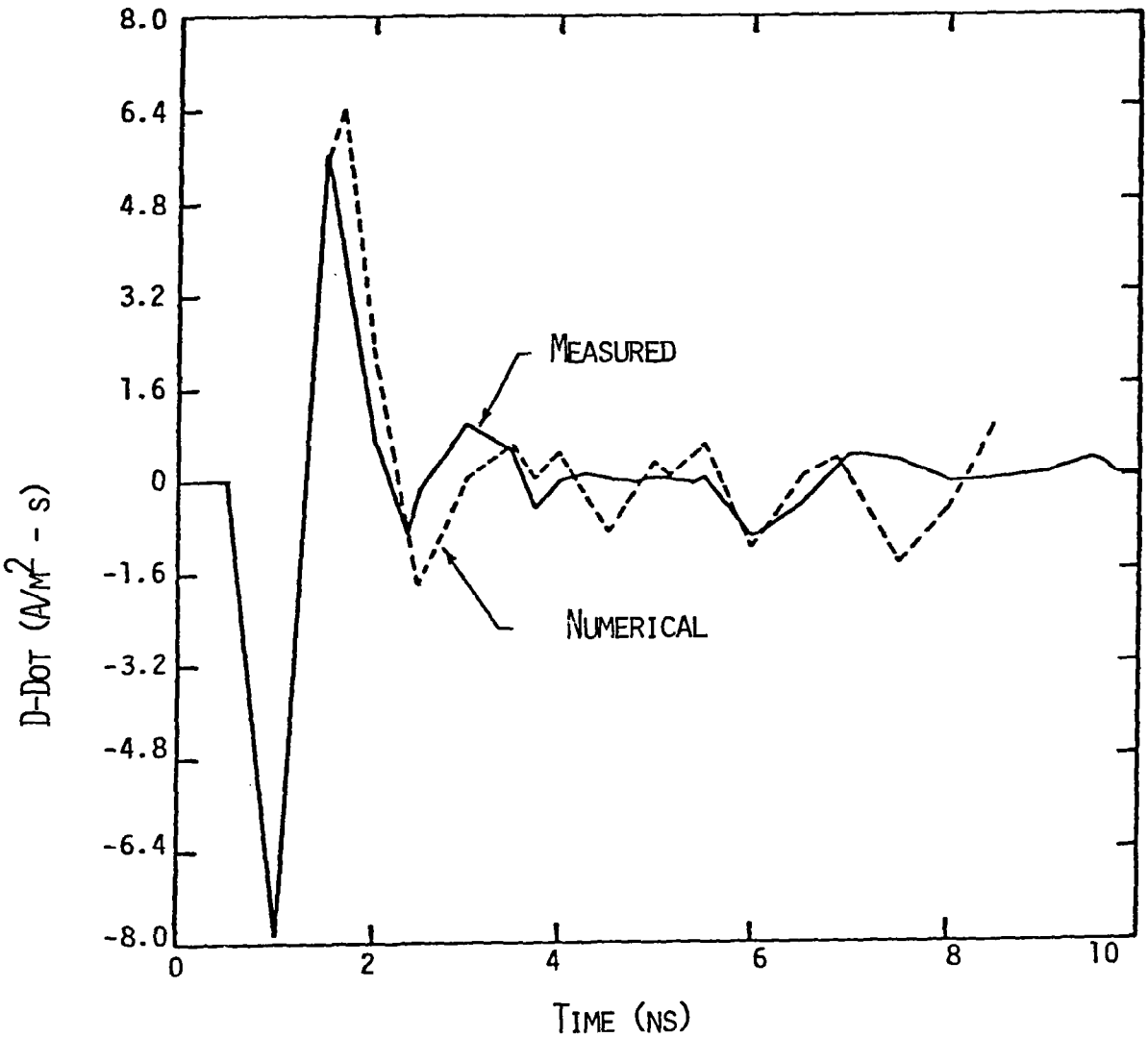

Figure 4.6 Comparison of Measured and Predicted Displacement Current Derivative Sensor

predicted and measured values gives sufficient confidence that the finite difference model of the F106 can be used to accurately predict the aircraft's response to direct lightning strikes. It should be pointed out that differences in the derivative values are more difficult to observe in integrated waveforms.

CHAPTER 5

INTERPRETATION OF LEMP DATA

The 1980-81 lightning data contain several records which are attributable to LEMP from nearby lightning. All records obtained from flight numbers 80-023 and 80-030 of the 1980 data set, and flight numbers 81-026, 81-041, and 81-045 from the 1981 flights are caused by LEMP. That no direct strike was involved in these flights was determined from pilot comments and the absence of fresh pit marks on the aircraft.

For the 1980 flights the LEMP data consist of three D-dot records and two B-dot records. The D-dot records are of limited usefulness, because they are a series of small spikes without structure having amplitude very near the sensitivity limit of the instrumentation. Record 3 of flight 80-023 is shown in Figure 5.1 as an example. The B-dot records from 1980 do show structure because of aircraft resonances. Record 1 of flight 80-023 is offered in Figure 5.2. The B-dot records are bipolar and less than a microsecond in duration. This indicates a fast rise time event, both because of the duration and the excitation of aircraft resonances.

With the exception of flight 81-026, the 1981 LEMP data are similar to that of 1980. Excluding 81-026, there were seven B-dot records obtained and no D-dot records. This is consistent with the triggering level on the D-dot sensor being too high to record LEMP interaction. The B-dot records again show much structure, with duration and amplitude comparable within a factor of two to the 1980 data. For LEMP analysis, however, the really interesting flight was 81-026. In this flight the D-dot recorder sensitivity was increased 40 db and the B-dot recorder sensitivity increased 20 db. This was done in a deliberate attempt to measure free-field aircraft excitation. The attempt was highly successful in that ten D-dot and four B-dot records were obtained for this single flight. Two of the D-dot records, 8 and 10, show a bipolar character and structure which is characteristic of aircraft resonances. Record 8 is offered as an example in Figure 5.3.

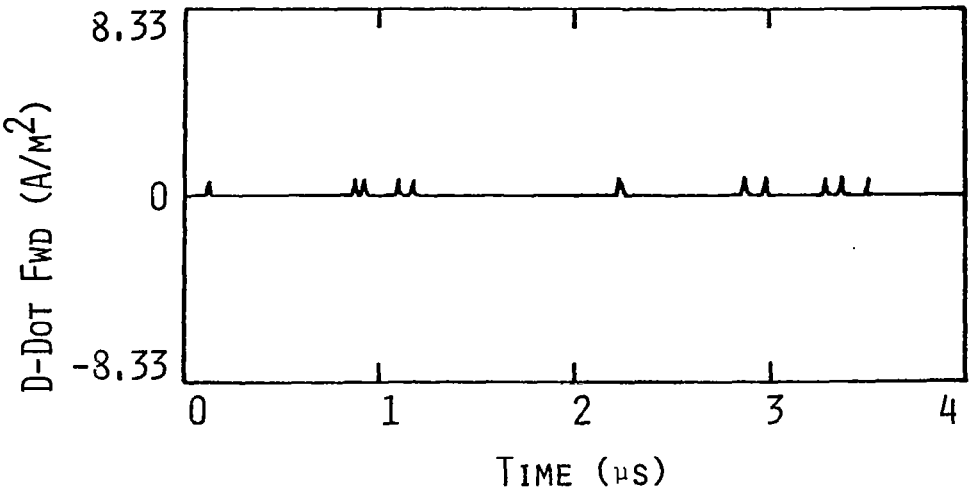

Figure 5.1 Example of D-Dot Record Without Significant Structure (Flight 80-023)

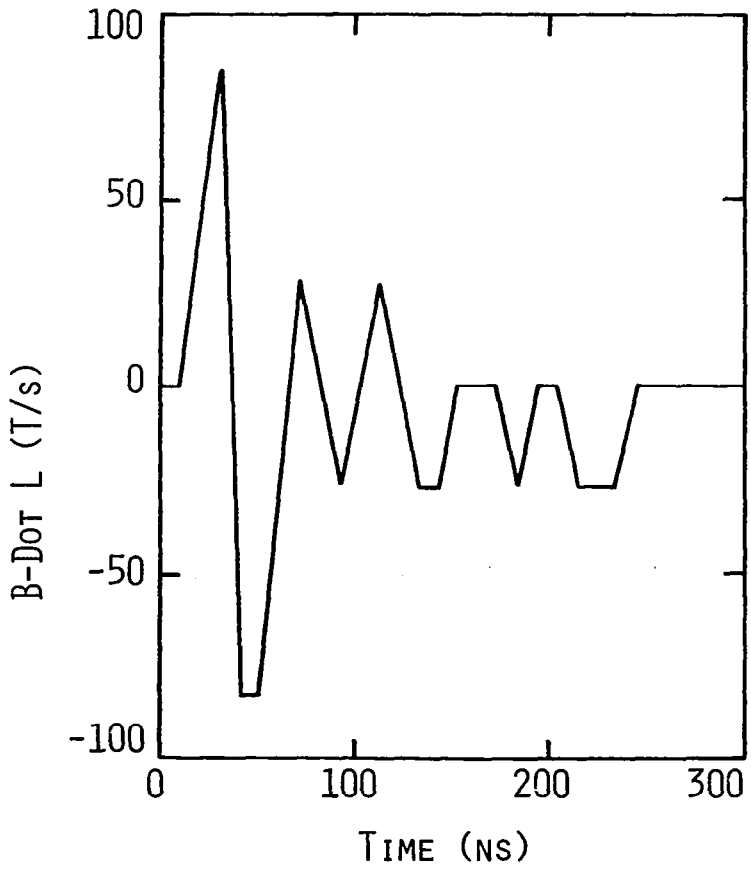

Figure 5.2 Example of B-Dot Record Showing Significant Structure (Flight 80-023)

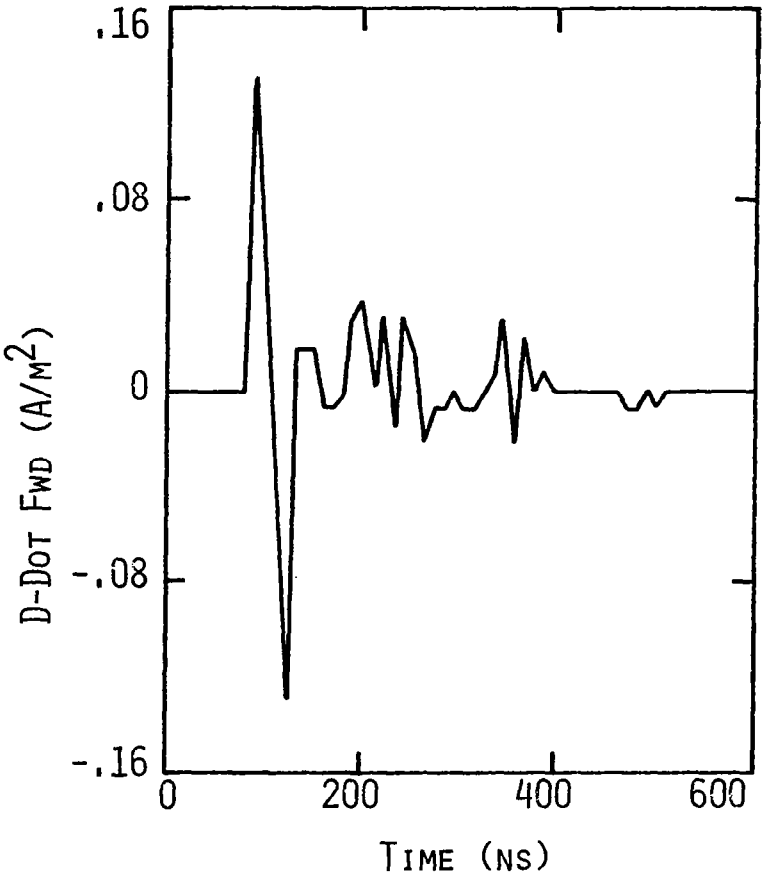

Figure 5.3 LEMP D-Dot Record Showing Aircraft Resonances (Flight 81-026)

This indicates LEMP with enough spectral content in its structure to excite these resonances. The other eight D-dot records, with Figure 5.4 as an example, are monopolar and of longer duration. Aircraft resonances are weakly represented, if at all. This type of record indicates a LEMP with less spectral content, or equivalently, a much slower rise time. One should also note that none of the D-dot waveforms acquired on flight 81-026 would have triggered the D-dot sensor without the increased sensitivity.

Three of the four B-dot records from flight 81-026 are similar to the other LEMP B-dot records. The exception is record 9, which shows a monopolar character and longer duration than is usual for a B-dot record. It is also of much smaller amplitude. The record is shown in Figure 5.5. It is likely to be caused by a pulse of slower rise time compared to the other B-dot records. Note also that this record would have been very uninteresting without the increased sensitivity of the sensor.

The abundance of LEMP data from flight 81-026 indicates that a selection effect is present when running the aircraft instrumentation at the reduced sensitivity. To avoid biasing any conclusions from the data it is necessary to determine which pulses the sensor system is selecting. This is easy to do by considering the nature of the time derivatives on which the instrumentation triggers. Large time derivatives are produced either by field changes in very short times or large field changes in longer times. The first corresponds to short rise time pulses and the second to very intense fields, i.e.; sources which must be quite near the sensors. Hence the instrumentation system at the reduced sensitivity level selects lightning which is very close or has a very fast rise time. This conclusion is supported by the records from flight 81-026 which lack aircraft resonance characteristics. The increased sensitivity has allowed the measurement of pulses with slower rise time and less spectral content. The selection effect inherent in the instrumentation system should be kept firmly in mind when making any generalization from the recorded data to all LEMP.

The approach that was taken to interpret the measured LEMP data was to perform a parameter study of plane wave illumination of the aircraft using the T3DFD finite difference code. This was done because there is no information on angle of incidence, polarization, or the location, size,

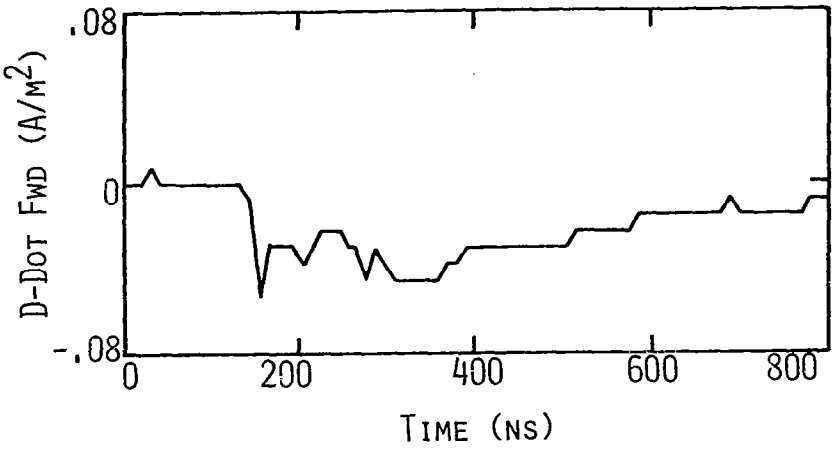

Figure 5.4 Monopolar D-Dot Record Showing Weak Aircraft Resonance (Flight 81-026)

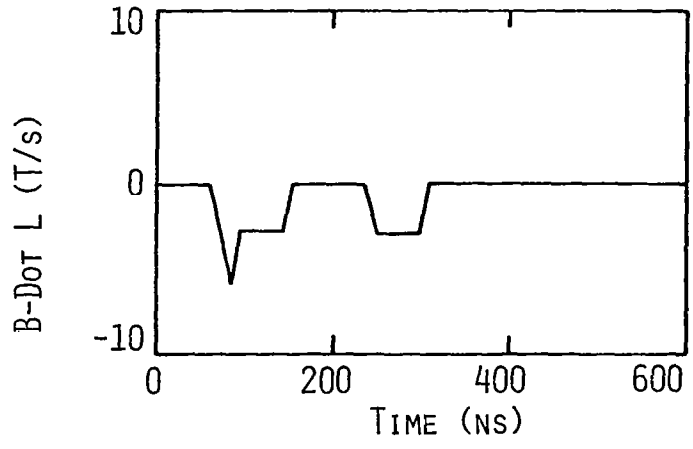

Figure 5.5 Monopolar B-Dot Record Probably Caused by Slow Rise Time LEMP (Flight 81-026)

or strength of the lightning source. The parameters varied in the study were the direction from which the plane wave illuminated the aircraft, the polarization of the wave, and the rise time of the wave. There were six different directions of illumination - right and left sides, top and bottom, front and back. For each illumination direction two orthogonal electric field polarizations were used, one chosen to be along the axis of the fuselage and the other perpendicular to it, if possible. Of course for front and back illumination this was not possible. For that case vertical and horizontal polarizations were used. For each direction of illumination and polarization a series of four plane waves with different rise times was used. The rise time referred to is the time from zero to peak of a step change of 1000 volts/meter amplitude with a sine-squared leading edge. The four rise times used were 20, 40, 100 and 200 nanoseconds. The step function waveshape was used for all runs as the simplest possible model of the lightning pulse. This removed any possible complications from structure within the plane wave and allowed for simpler interpretation of the results.

Variation of the parameters listed resulted in 48 separate computer runs, the output of which was the appropriate field and its time derivative at each of the aircraft sensor positions as a function of time. This could then be compared directly with the measured data records. A summary of the results of the parameter study is presented in Appendix A.

When comparing the results of the parameter study with measured aircraft responses, a few things should be remembered. First of all the parameter study is idealized in several ways. Only plane waves were allowed, whereas nearby lightning may have more of a cylindrical wave character. The waves in the parameter study propagated along coordinate axes with convenient horizontal and vertical polarizations. The actual angles of incidence and polarization are unknown and are probably not one of the orthogonal cases considered. Finally, real LEMP is likely to have more structure in the waveshape than has been allowed in the study. Keeping the caveats in mind then, one should not expect exact matches between the results of the parameter study and measured data. The figures of Appendix A can be used only as a general guide to the lightning pulse which interacted

with the aircraft in any given record.

Application of the results of the parameter study to the measured data does allow one to make some general statements about the pulse that illuminated the aircraft. As an example consider flight 80-023, record 1, (Figure 5.2), where B-dot amplitudes of about 80 Tesla/second are recorded. For this same event D-dot was less than or of the order of 1 Amp/m^2, because no simultaneous D-dot data was recorded. Suppose one selects the Figure A.2(d) to match the waveshape of Figure 5.2. An amplitude of approximately 9 kV/m is required to match the peak amplitudes properly. Now consider Figure A.2(b), which is the D-dot prediction for the same incident wave. This figure then predicts a D-dot response of about 5 Amp/m^2 which would easily trigger the D-dot instrumentation. But the D-dot channel did not trigger, so one must look elsewhere for the correct excitation waveform. Consider next Figure A.10(d) which requires an incident amplitude of about 1 kV/m to give the measured B-dot peaks. Figure A.10(b) then predicts a peak D-dot of about 1.5 Amp/m^2 which is below the threshold of detection. This case then may be a more likely candidate for the incident wave, even though the predicted wave shapes are somewhat different. This difference may be accounted for by the many simplifying assumptions used in the parameter study.

With the exception of the records of flight 81-026, the measured LEMP data can all be explained by plane waves of amplitude between 1 and 5 kV/m and rise times of less than 100 nanoseconds (the latter is because of the observed resonances in the measured data). This conclusion comes from a comparison of the data records with the responses predicted by the parameter study. Comparing peak B-dot amplitudes with upper limits on D-dot amplitude indicates that incident electric fields must be largely horizontal. The amplitudes imply relatively weak or distant lightning, probably the former because of the selection effect discussed earlier. This is consistent with cloud flashes rather than cloud to ground strikes. It is also consistent with currents measured for direct strikes to the aircraft, where only relatively small currents, on the order of a few kiloamps, are seen.

For flight 81-026 the increased instrumentation sensitivity allowed much smaller LEMP to be recorded. These records are about a factor of ten smaller than any of the others and are indicative of incident electric fields from 100 to 500 V/m. The monopolar D-dot records are a separate case entirely for which the parameter study does not apply. These monopolar D-dot records imply much longer rise times in the incident pulse, probably greater than 200 nanoseconds, because no aircraft resonances are seen. The records of flight 81-026 are from more distant lightning than for the other flights and include a wider spectrum of rise times.

A few comments about uniqueness are in order here. That is, if one can match a measured aircraft response with a case in the parameter study, it does not mean that the LEMP that hit the aircraft has been determined uniquely. There are many other incident directions, polarizations, and waveshapes that could produce the same single response. Without truly simultaneous measurements from different points on the aircraft any incident pulse which gives the correct response must be regarded as a solution to the problem, rather than the solution. Simultaneous measurements do not completely eliminate the uniqueness difficulty, but do greatly reduce the range of possible answers. In the absence of simultaneous measurements one is not completely helpless, however, in deciding between possible solutions. Occam's razor can be applied, meaning solutions which conform to what is already known about lightning can be chosen over outlandish waveshapes that produce desired responses, but are far from accepted lightning shapes. The LEMP parameter study took this into account by choosing the simple step function waveshapes described earlier. Real LEMP will deviate from this to some extent but probably not enough to alter the results of the study significantly.

CHAPTER 6

INTERPRETATION OF DIRECT STRIKE DATA

6.1 Background

The test flights of 1980 and 1981 have produced data on 13 direct strikes to the aircraft. Of these 13, 10 occurred in 1980 and three in 1981. The 1980 data consist of seven D-dot records and eight B-dot records. There were also five strikes for which I-dot was recorded on the nose boom of the aircraft. In the 1981 direct strike data, there are no D-dot records, five B-dot, and one case for which the current was directly recorded on the nose boom. Of the 13 direct strikes, 12 were attachments to the nose or nose boom. The one exception was an attachment to the canopy. The D-dot record for this strike shows no structure, and it is likely that the instrumentation just barely triggered. Therefore, no analysis was possible for the strike.

The analysis for the strikes which do show structure was concentrated on the D-dot records. These records show much more variation in structure than the B-dot records, and for this reason are more likely to allow one to differentiate between different lightning phenomena. A D-dot record is, in a sense, closer to the physics of the problem, because its integral, the normal electric field, is indicative of the excess charge at the measuring point. The determination of where this charge is on the plane, and where it is going, is essentially the heart of the problem. A B-dot record, on the other hand, must be integrated to give one component of the current at the sensor point. While this information is useful, it is somewhat less useful than D-dot data, which directly shows the movement of charge on the aircraft. The I-dot records would be very useful if they were not greatly filtered by the 6 MHz bandpass of the analog recorder. The filtering distorts the waveform of the entering current and the data records can be used only as a guide for the actual amplitude of the current.

It should be understood that there is necessarily some ambiguity in the time derivative measurements. This can best be explained through the use of an example. Consider the D-dot waveform in Figure 6.1. It shows a positive D-dot which implies that the electric field at the sensor point is becoming more positive with time. But there are still two possibilities associated with this increasingly positive electric field. The first is that the electric field started at near zero at the beginning of the record and as positive charge accumulated around the sensor it became large and positive. This could happen for example, if a positively charged leader attached to the nose of the plane. The second possibility is that the plane was already negatively charged. For this case the electric field at the sensor at the beginning of the record would have been large and negative. The positive D-dot would then correspond to the removal of negative charge from around the sensor, decreasing the large negative field to near zero. This would occur, for example, when a positive K-change interacted with the aircraft. So the record of Figure 6.1 can be explained as either the addition of excess positive charge to the plane or the removal of excess negative charge. To resolve the ambiguity it may be necessary to make actual field measurements to determine whether the plane has a net charge local to the sensor at the start of a derivative record.

There is another difficulty with the direct strike data which is related to the entry and exit points of a lightning strike. These points are determined by pilot comments and physical examination of the aircraft [18]. The question must be asked, however, regarding what it is that is entering and exiting. To clarify the question one needs to consider the complete history of a lightning interaction with an aircraft. Assume the initial stepped leader approaches the plane from the front, attaches to the nose, and exits from the tail. Eventually the leader reaches a center of opposite charge, and a K-change starts back along the channel created by the leader. It reaches the plane and <u>enters</u> on the tail and <u>exits</u> from the nose. Subsequent leaders and K-changes follow this same pattern. So the definition of entry and exit points varies depending on whether a leader or a K-change is meant.

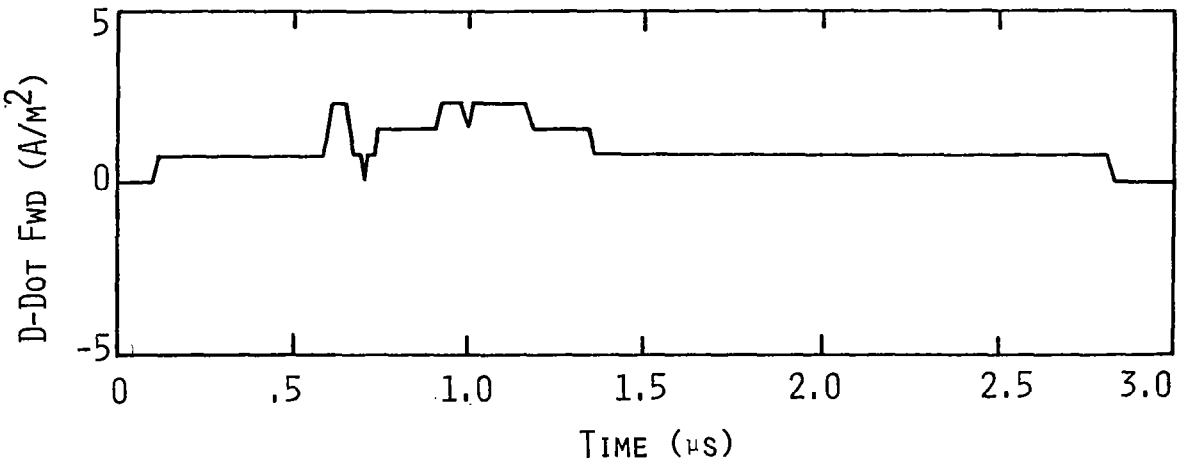

Figure 6.1 Example of Monpolar D-Dot Response of Aircraft (Flight 80-019)

The situation becomes more complicated when multiple entry and exit points are involved. For example, a leader may attach at the nose but exit from the tail and a wing tip. The K-change which follows may then enter through one or both of the leader's exits. The amplitude of the K-change current will generally be different for the two entry points, and the time of entry will also vary, because of differing path lengths. The difference in time of entry may be only a few nanoseconds, but this can make a significant difference in the response seen on the aircraft, and must be considered.

In summary, the distinction between entry points and exit points is somewhat unclear, so in the present analysis they were put on an equal footing. That is, they were regarded as simple attachment points, and currents were allowed either to flow on or off the aircraft there. Currents were injected at nominal exit points as well as entry points in the effort to determine what may have caused a given aircraft response.

One last difficulty in the analysis of the direct strikes that needs to be mentioned is the problem of uniqueness of the derived lightning sources. If a source is found which produces the correct response, it is necessary to determine if that source is unique. In general, the answer is yes only if the response is correct at all points in space, not at a single sensor point. This point is discussed in more detail in Chapter 8, so here it will simply be stated that the response at a single point on the plane cannot uniquely determine the characteristics of the lightning strike which caused it. Mathematically there will be an infinity of possible sources. The requirements that these sources be physically possible, their exit/entry points correspond to those actually observed, and that they conform in a general sense to what is already known about lightning, reduce the infinity to some smaller number, but by no means insure uniqueness. Although no finite number of sensor points can guarantee mathematical uniqueness, two or more <u>simultaneous</u> measurements would increase confidence in a derived source to a high level.

As mentioned earlier the actual analysis of the direct strike records concentrated on D-dot measurements. Of these a subset was chosen to exclude records which were at the lower limit of the sensors' sensitivity.

Hence records such as D-dot for flight 80-029 shown in Figure 6.2 were not considered because of lack of structure. D-dot records which were analyzed in detail are presented in Figures 6.3 to 6.7.

6.2 Analysis of Flight 80-018 (Figure 6.3)

This record shows an increasingly positive electric field which, as noted previously, probably indicates a positively charged leader or positive K-change. There is a long, constant slope tail lasting for about 3-1/2 microseconds, which implies a long, slow positiye charging of the aircraft or a long, slow negative discharge. The abrupt drop to zero at the end of the tail suggests a nonlinear effect. Pilot comments and aircraft examination indicate that the lightning strike attached to the nose of the aircraft and exited from the tail and the left wing tip. The approach of the strike was described as being relatively slow, so it was probably a leader which attached to the nose. Any K-change would then have entered at the two points on the rear of the plane and exited through the nose. A successful approximation to the early part of the waveform of Figure 6.3 was obtained by using the leader model. A current was injected at the nominal entry point having a step function character with a sine-squared leading edge of rise time 44.4 nanoseconds. (A method for arriving at this number is described in Chapter 9.) There was no exit point for the current in the model, and the absence or presence of one made little difference in the result. An overlay of the model prediction with the measured response is shown in Figure 6.8. The injected current waveform is shown in Figure 6.9. The point at which the tail drops abruptly to zero could not be modeled linearly and it is suspected that a nonlinear breakdown process, such as the leader exiting the aircraft, was involved.

6.3 Flight 80-019 (Figure 6.4)

For this record nose attachment was again involved. This time there is no long tail, so no significant charging was taking place, indicating that an established lightning channel was probably already present. The integral of the waveform implies a net decrease in electric field, meaning negative charge was flowing onto the plane. These observations are characteristic of a negatively charged dart leader. The large positive spike in

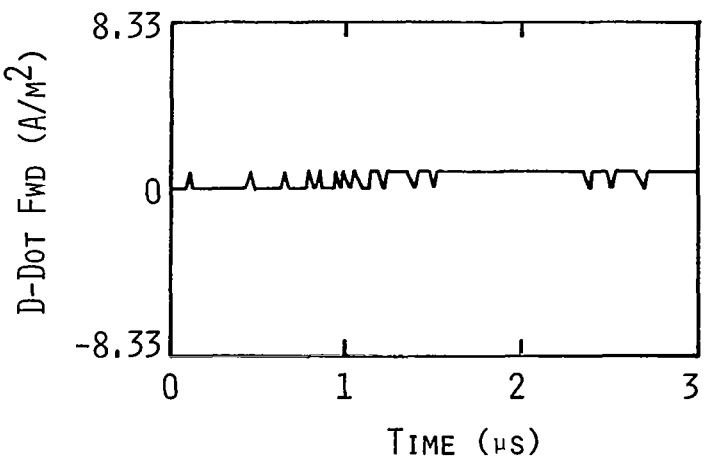

Figure 6.2 D-Dot Record Showing No Significant Structure (Flight 80-029)

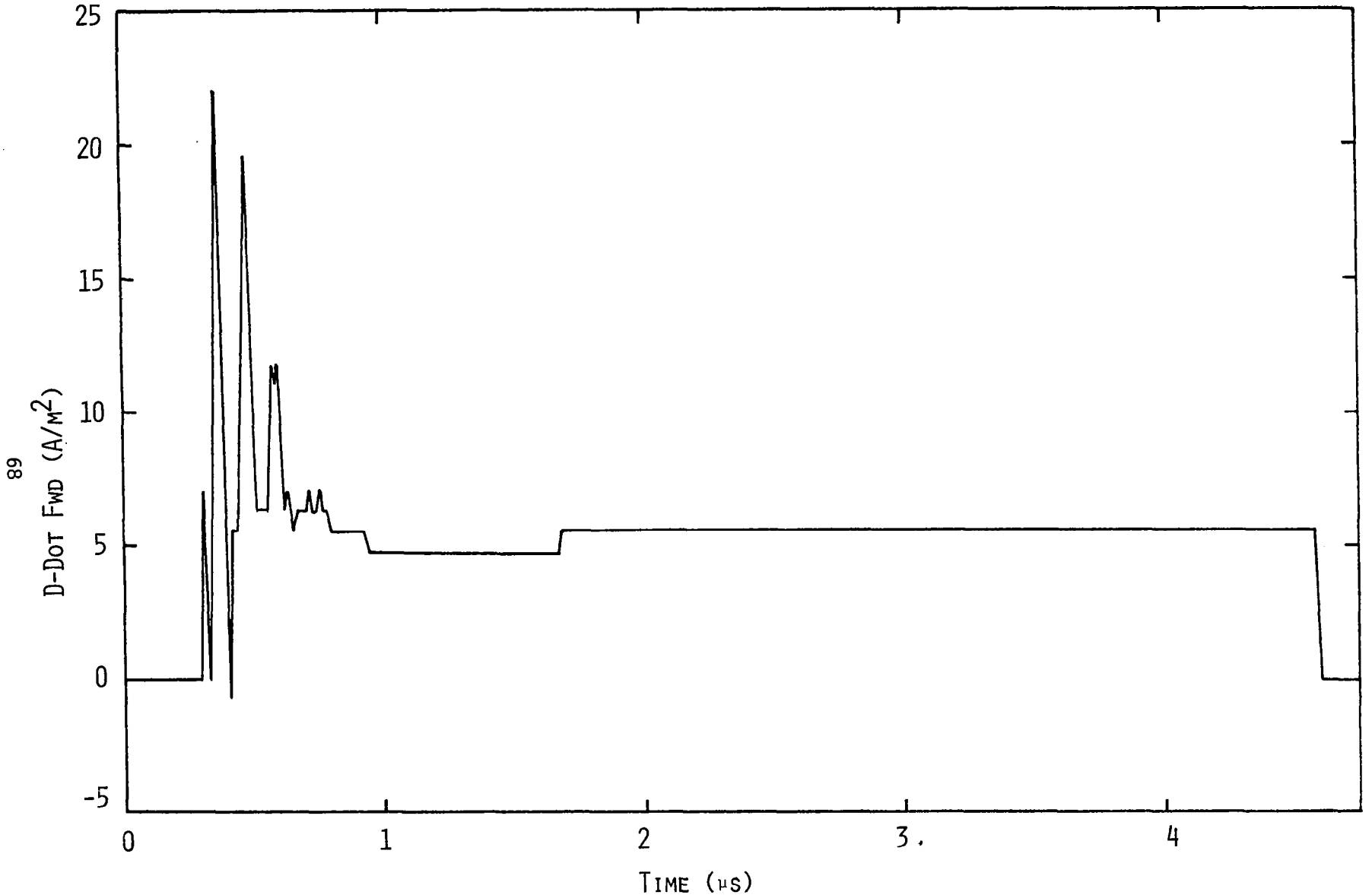

Figure 6.3 D-Dot Record from Flight 80-018

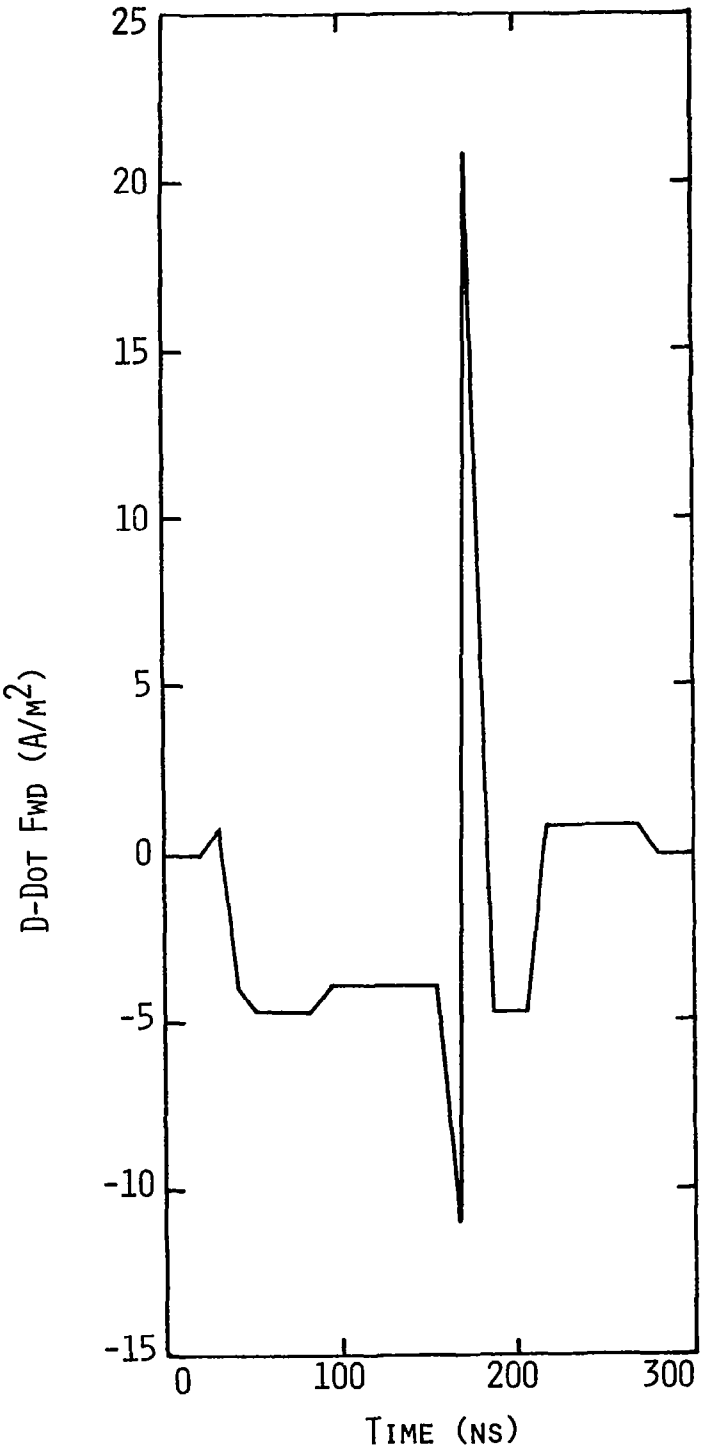

FIGURE 6.4 D-DOT RECORD FROM FLIGHT 80-019

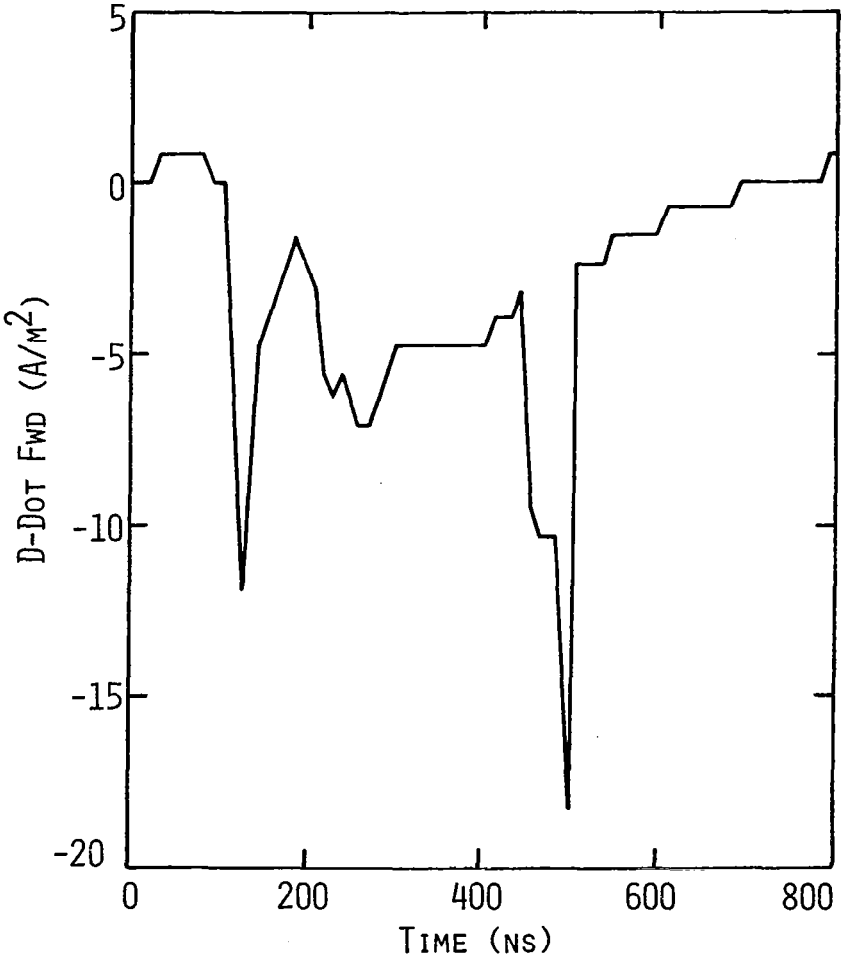

FIGURE 6.5 D-DOT RECORD FROM FLIGHT 80-036

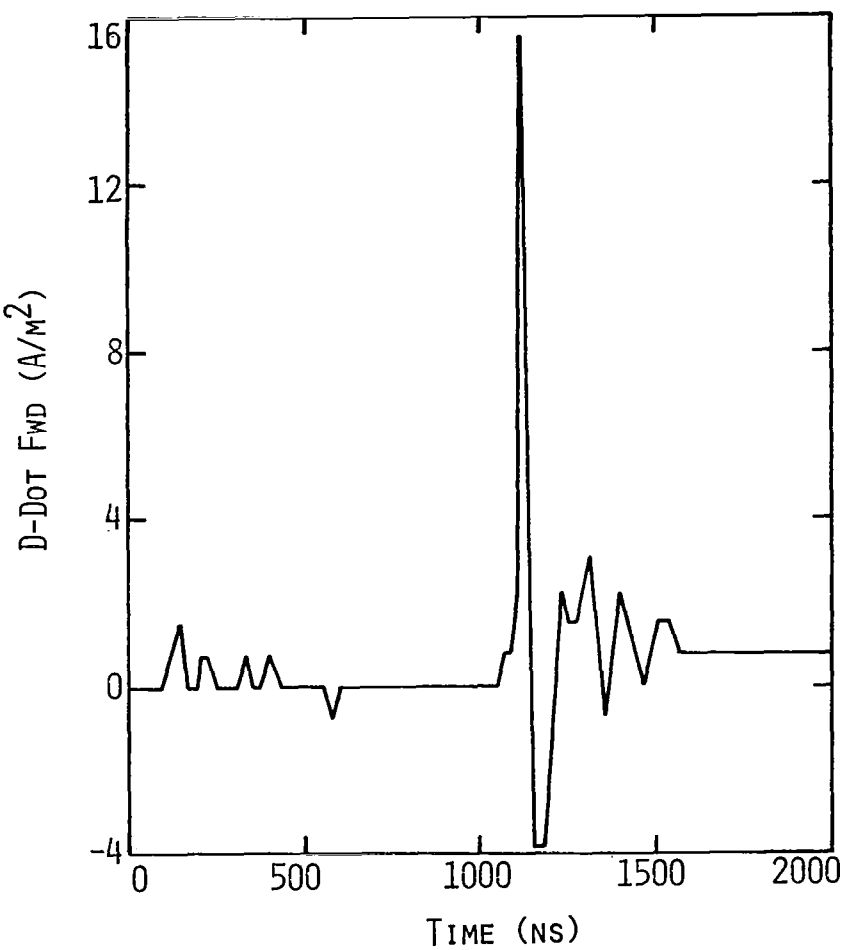

Figure 6.6 D-Dot Record From Flight 80-038 (Run 6)

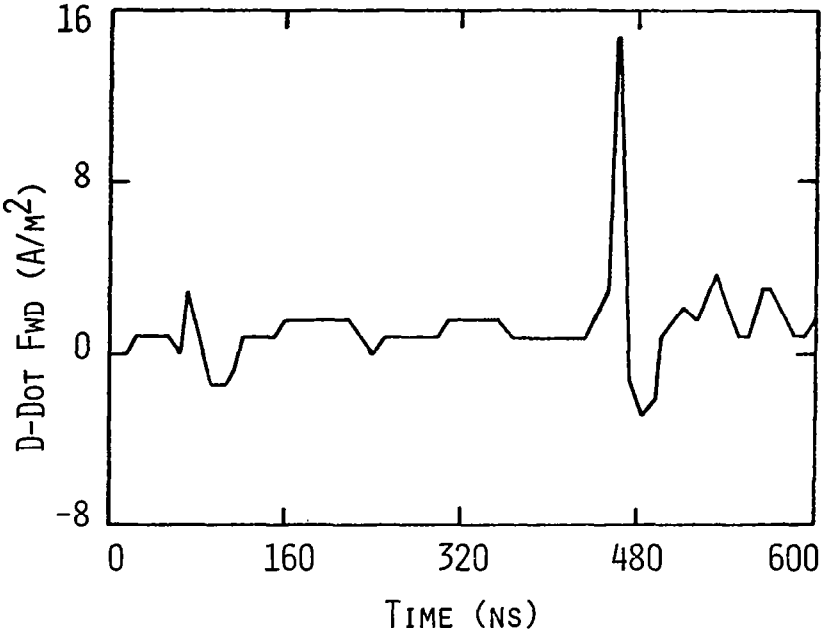

Figure 6.7 D-Dot Record from Flight 80-038 (Run 4)

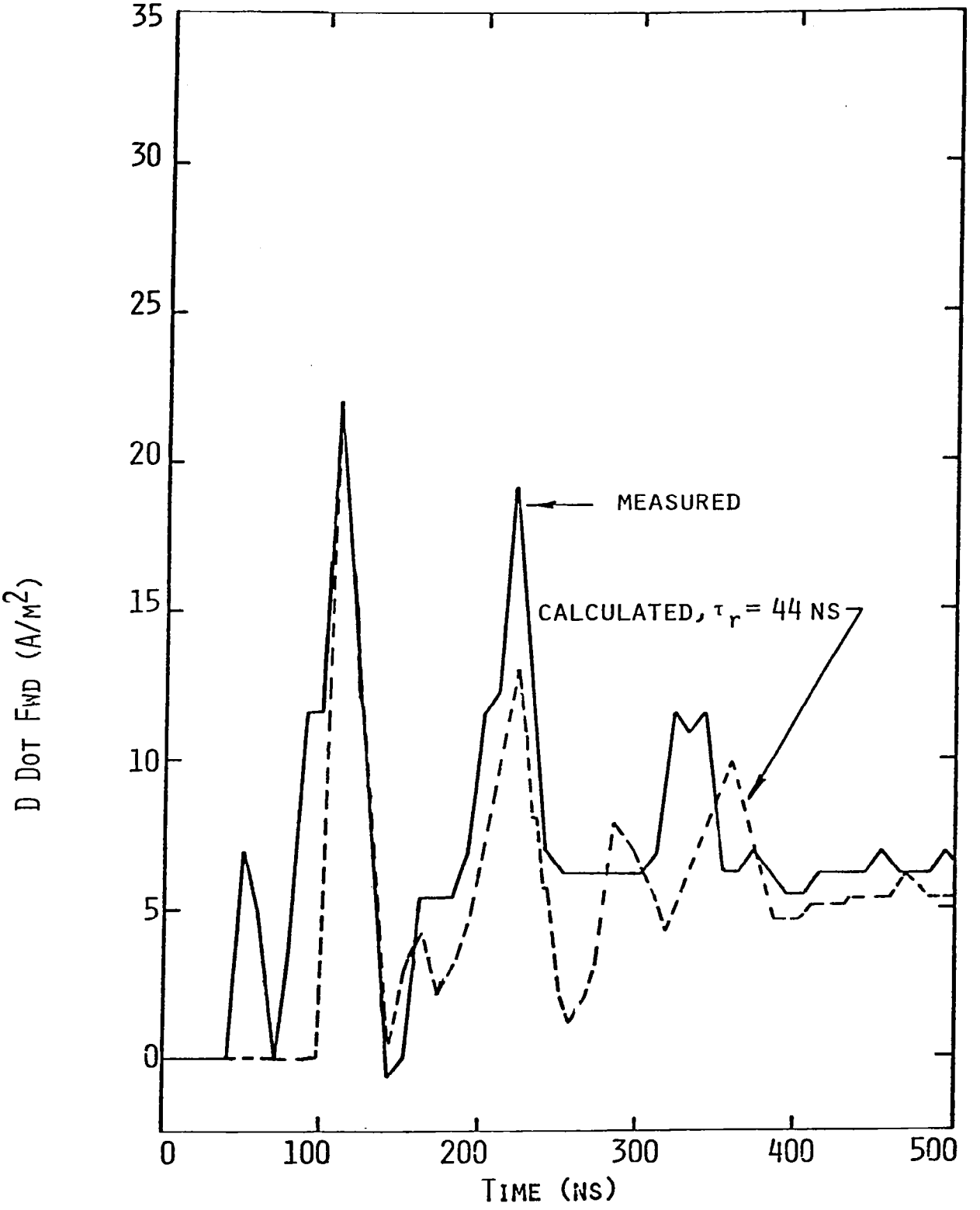

FIGURE 6.8 OVERLAY OF FIGURE 6.3 AND NUMERICAL RESPONSE (FLIGHT 80-018)

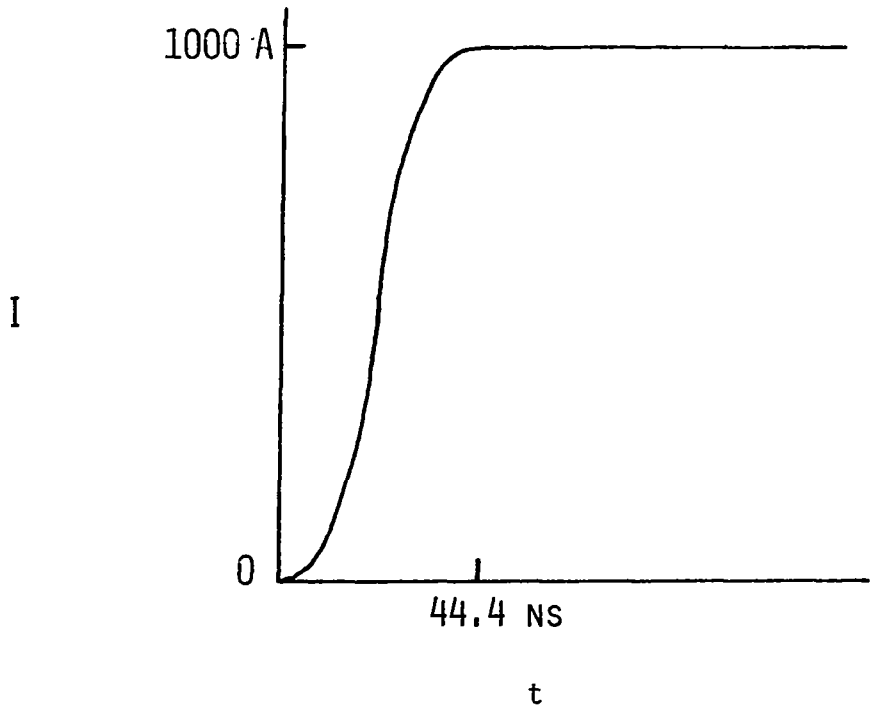

FIGURE 6.9 INJECTED CURRENT WAVEFORM FOR PREDICTION OF FIGURE 6.7

the waveform was of initial concern but it was readily reproduced in the analysis. Figure 6.4 was numerically duplicated by injecting a negative current pulse at the nose and allowing it to flow off the plane from a point at the base of the tail. Figure 6.10 shows an overlay of the predicted and measured responses, and Figure 6.11 is the injected current.

6.4 Flight 80-036 (Figure 6.5)

This is an example of a case in which a linear model can be made, and the current response found, but the derived injected current is such that a different model may be more satisfying. The measured response shows a decreasing electric field, probably meaning negative charge accumulating near the sensor. The response was duplicated, as shown in Figure 6.12, by injecting at the nose the current shown in Figure 6.13. The injected current tends to stretch the limits of believability somewhat, so it may be reasonable to look elsewhere for the proper lightning source. The place to look may well be in the nonlinear regime, as described in Chapter 2, where Figure 6.5 is used as an example of the type of waveform that might result from the approach of a negatively charged stepped leader approaching the plane from the rear.

6.5 Flight 80-038, Run 6 (Figure 6.6)

This is a fairly common type of D-dot response, showing an initial bipolar pulse and a small amount of subsequent ringing which settles down very quickly. The simplicity of the record makes it difficult to analyze, because it can be produced in so many ways. There is not enough information available in the record to cull out most of the mathematically possible sources. An overlay of predicted and measured response is offered in Figure 6.14 with a possible current source in Figure 6.15. This positive current was injected at the nose with an exit point at the base of the tail.

6.6 Flight 80-038, Run 4, (Figure 6.7)

This D-dot response is similar to that discussed in Section 6.5. The same comments apply to it. Figure 6.16 is the overlay of measured and predicted response, and Figure 6.17 is the injected current.

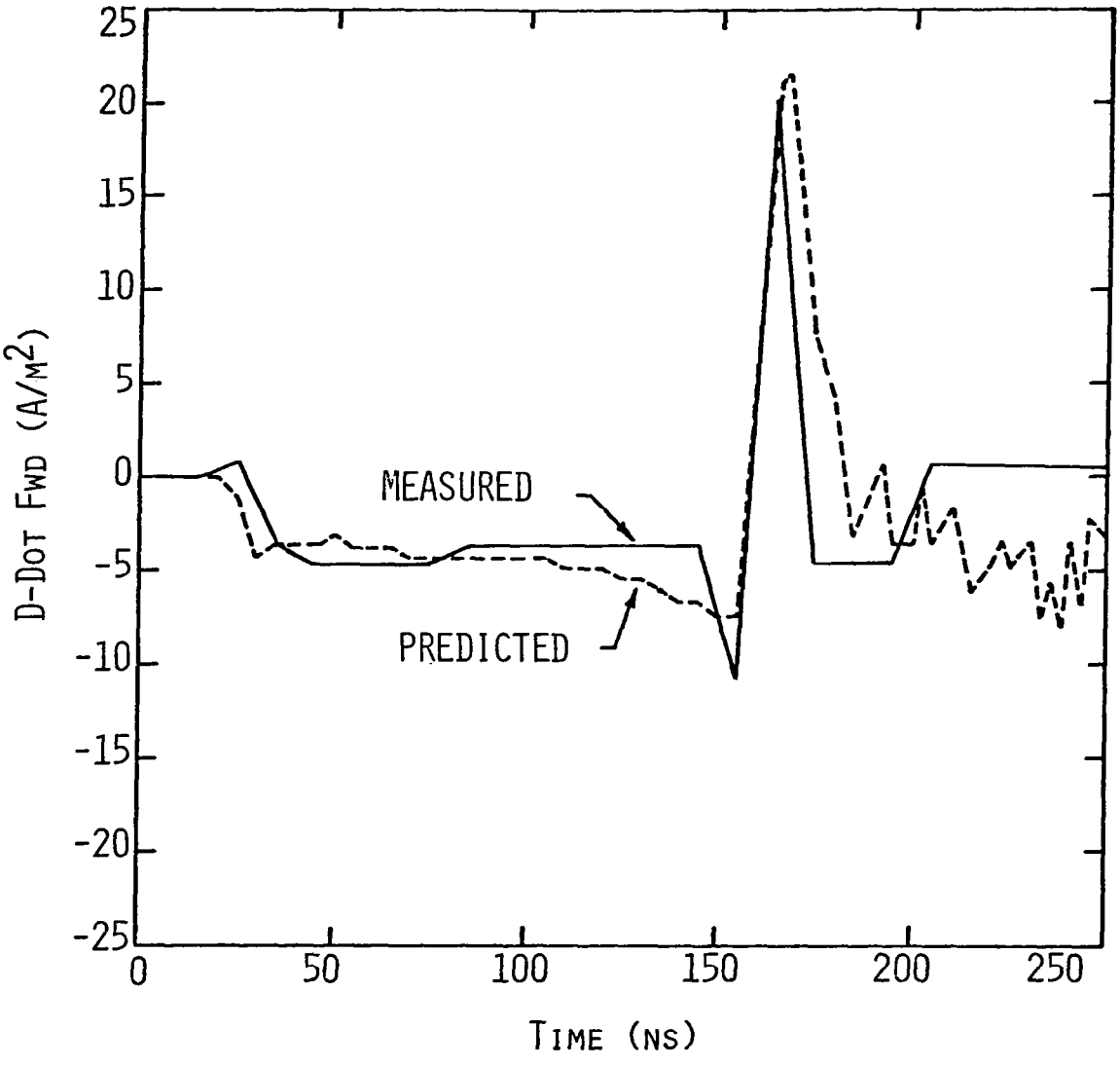

Figure 6.10 Overlay of Figure 6.4 and Numerical Prediction (Flight 80-019)

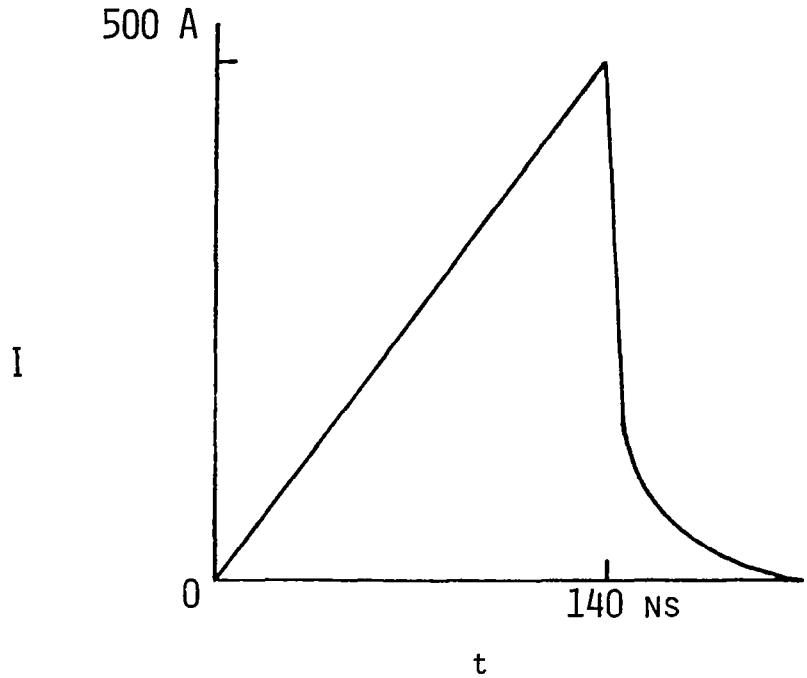

FIGURE 6.11 INJECTED CURRENT WAVEFORM FOR PREDICTION OF FIGURE 6.10

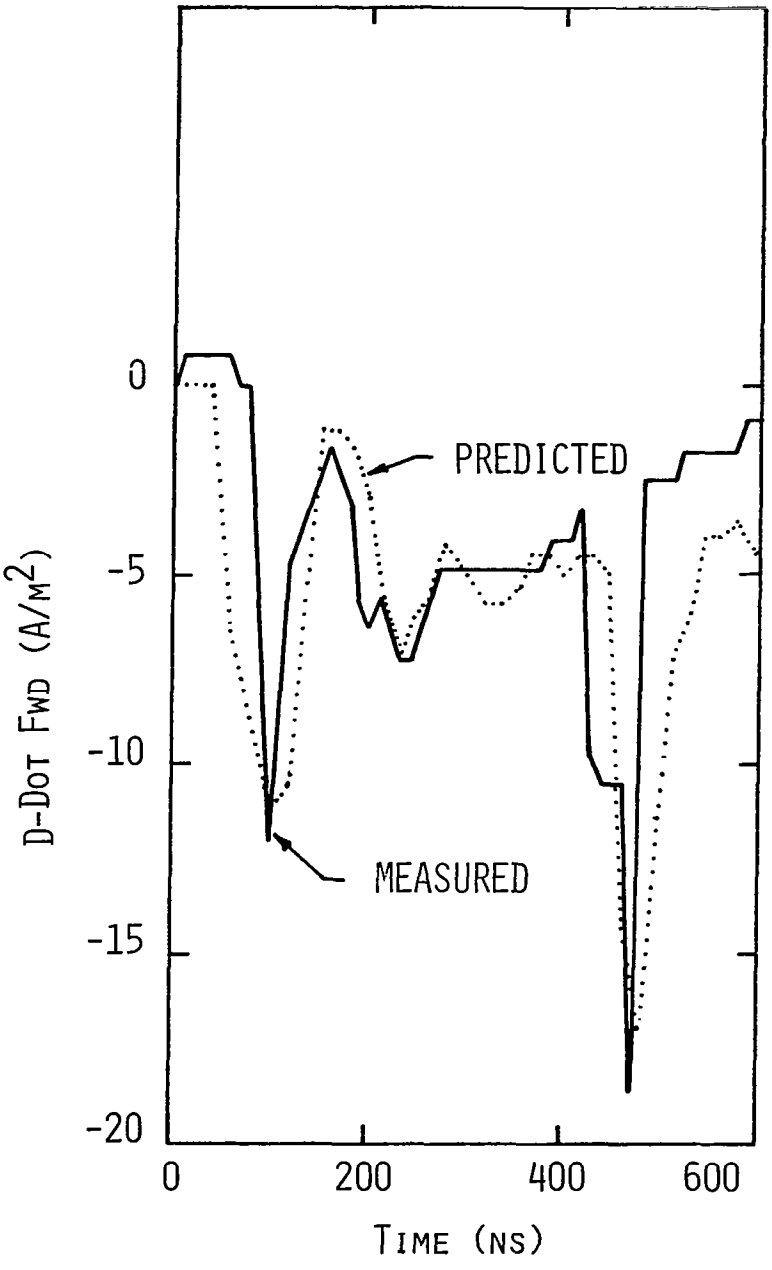

FIGURE 6.12 OVERLAY OF FIGURE 6.5 AND NUMERICAL PREDICTION (FLIGHT 80-036)

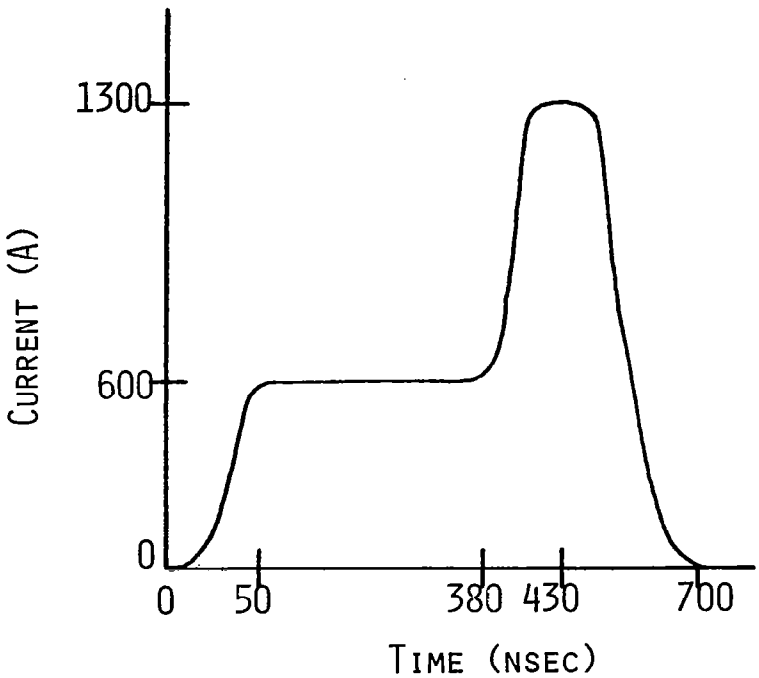

FIGURE 6.13 INJECTED CURRENT WAVEFORM FOR PREDICTION OF FIGURE 6.12

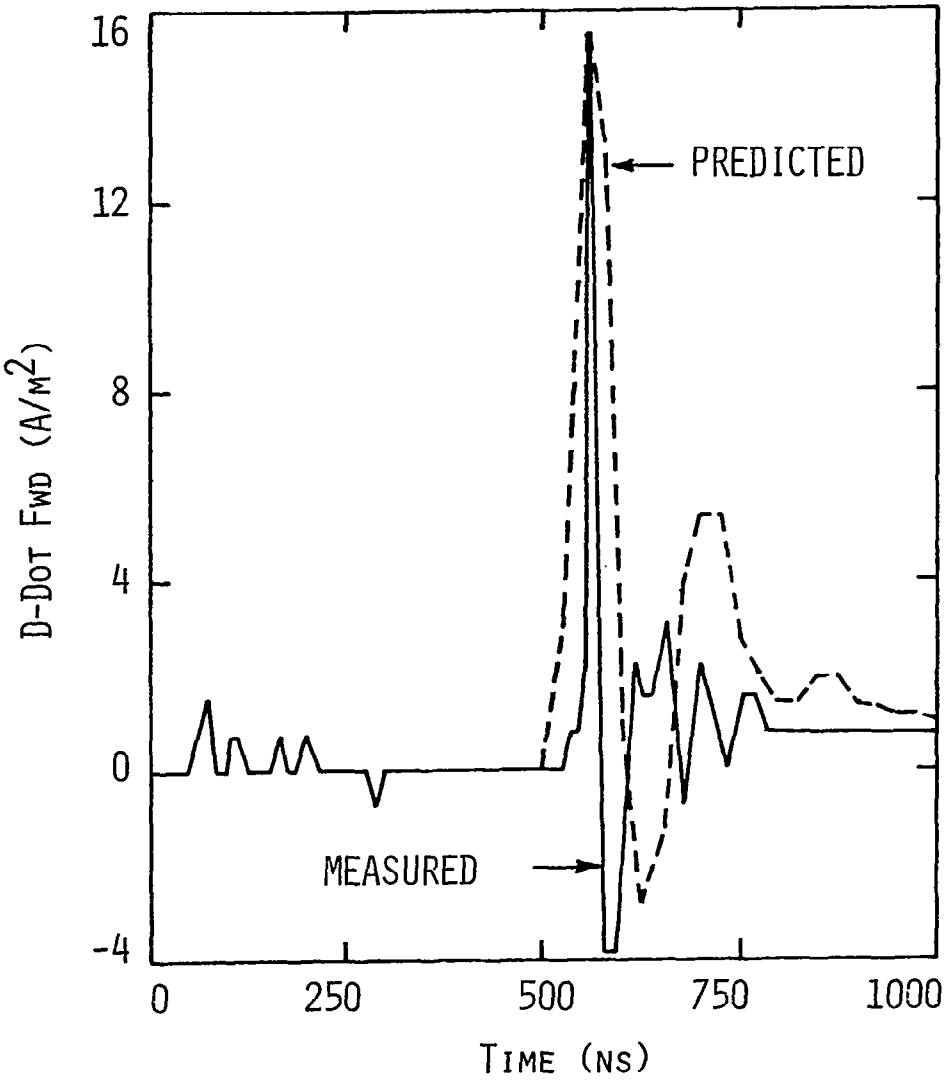

Figure 6.14 Overlay of Figure 6.6 and Numerical Prediction (Flight 80-038)

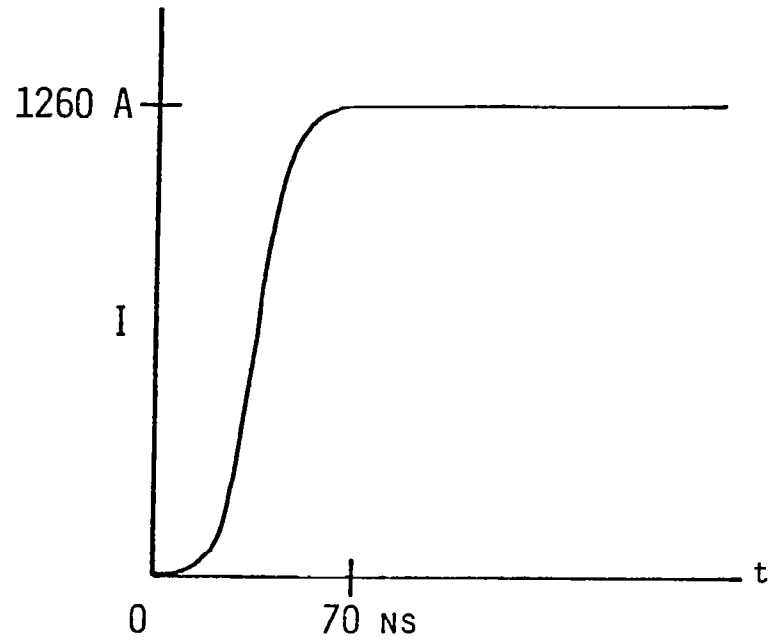

FIGURE 6.15 INJECTED CURRENT WAVEFORM FOR PREDICTION OF FIGURE 6.14

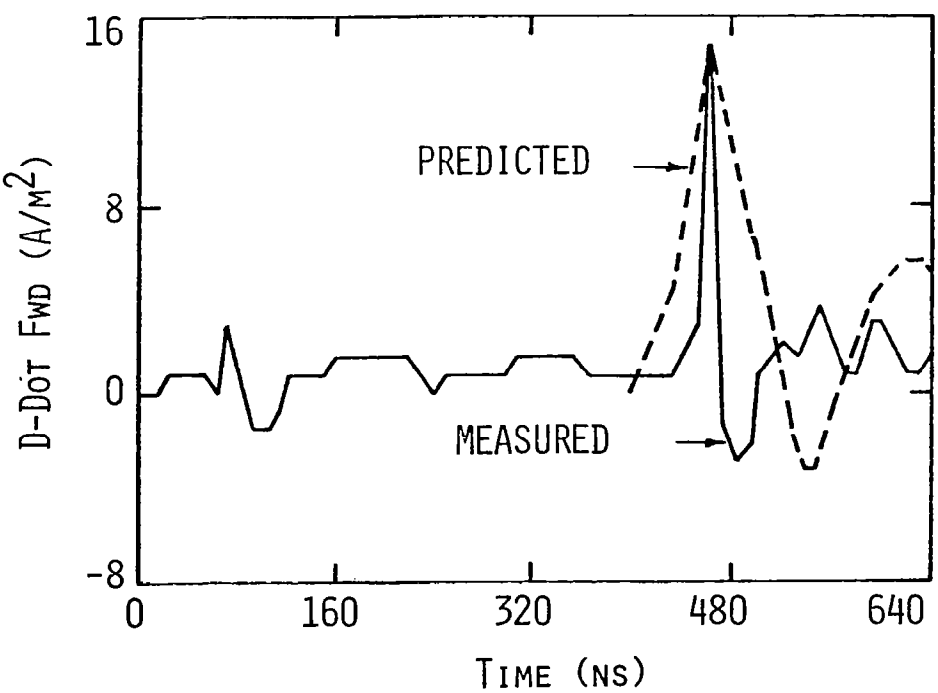

FIGURE 6.16 OVERLAY OF FIGURE 6.7 AND NUMERICAL PREDICTION (FLIGHT 80-038)

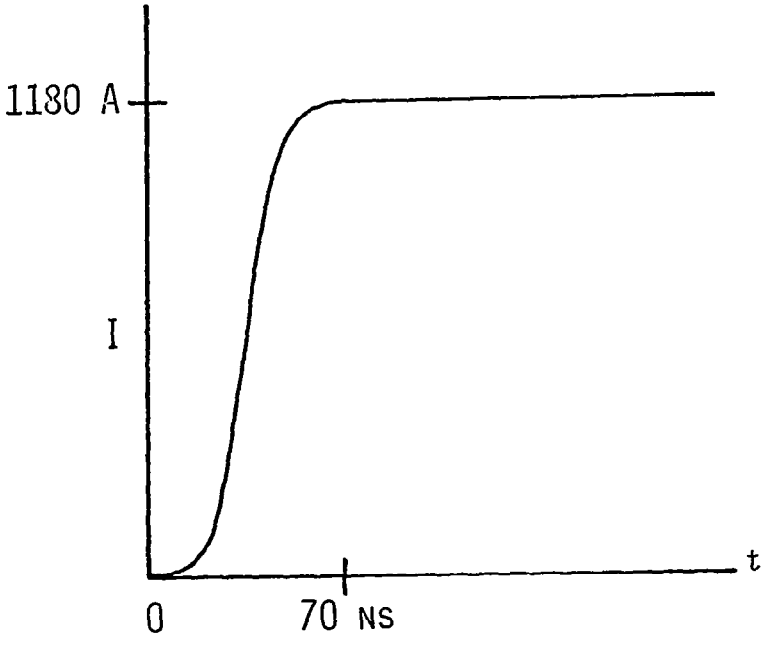

FIGURE 6.17 INJECTED CURRENT WAVEFORM FOR PREDICTION OF FIGURE 6.16

6.7 Discussion of Other Waveforms

Some of the measured D-dot waveforms show a long nonzero tail which most likely indicates a continually growing (in magnitude) electric field at the sensor point. This implies that a charge is building up on the aircraft. There are at least two possible explanations for this phenomenon. First consider the approach of a stepped leader toward the aircraft. It is a continuous nonlinear process because the air is ionized by the leader charge, increasing the conductivity and allowing the leader to step ahead. The air breakdown process requires a minimum electric field to be present which in turn requires a minimum leader charge density. As the leader charge flows onto the aircraft it finds very little resistance to its motion, and so it diffuses across the aircraft skin. This decreases the charge density (electric field) at any given point probably below the minimum field necessary for air breakdown. So the leader cannot exit from the plane until more charge has flowed in and the field at some point has grown large enough to continue the air breakdown process. When this occurs one would expect to see the charging abruptly stop, as it does, for example, in Figure 6.3.

The second possible explanation is related to the first in that it also involves a diffusing of charge over the surface of the aircraft. For this case assume the plane is already part of an established lightning channel, along which a current impulse is propagating. It enters the nose of the plane and immediately begins diffusing across the surface. Now the question of what is necessary to force the current to flow off the plane along the exit channel needs to be answered. The requirement is the same as that needed to cause current to flow along a wire. There must be a potential difference built up across the plane in the same way a potential difference exists between the two ends of a wire. The potential at any point on the plane is directly proportional to the charge density at that point, so as the charge diffuses, the charge density and the potential decrease on the plane. Therefore there will be a large potential difference between the entering lightning channel and the plane. This will cause current to readily flow onto the plane. Now concerning the exit channel, the low charge density on the aircraft does not provide a sufficient

potential difference between it and the exit channel to force off much current. In a sense the charge needs some incentive to leave through the exit channel. This incentive has to be provided by a charge buildup on the plane in order to provide the necessary potential difference. Eventually, because charge continues to flow onto the plane, the potential does get large enough, and the current leaves the plane. The T3DFD code predicts that for the F106 the delay time for the current to begin exiting the plane is of the order of 500 nanoseconds.

To test this theory numerically a study was done of current injection onto conducting bodies. Three cases were investigated. These were the injection of current onto the end of a uniform rectangular cylinder, a rectangular cylinder with some widening to simulate a fuselage, and a rectangular cylinder with widening and extensions to simulate a fuselage with wings. For the uniform cylinder the injected current all arrived at the other end delayed only by a speed of light transit time. This was to be expected as the uniform cylinder case is equivalent to a single uniform wire. For the cylinder with widening, the current was delayed by more than the speed of light transit time and significantly more for the cylinder with wings. The study proves that the time for the current to cross an aircraft is dependent on its geometric shape. The charging process seen in the lightning data records can be explained as the building up of electric potential across the plane which is necessary to force the exiting current to leave through the exit channel. This process is likely to not show an abrupt drop to zero at the end of a long tail, however, as happens in Figure 6.3. Also the tails would not be as long as is seen in that figure, because the current transit time across the aircraft appears to be dependent entirely on its shape, and is less than the several microseconds of charging seen there.

CHAPTER 7

NONLINEAR EFFECTS

7.1 Background

While much of the modeling of the lightning aircraft interaction can be done in a linear fashion, there are aspects that demand a nonlinear treatment. Even simple models of the lightning interaction process clearly indicate that the aircraft undergoes corona and streamering. The processes of initial leader attachment to and eventual exit from the aircraft are strongly dependent on air breakdown phenomena which must be modeled nonlinearly. In addition, the presence of corona around the aircraft could significantly alter its response to direct and nearby lightning. In this chapter a corona model will be described which was developed for use in nuclear electromagnetic pulse (NEMP) problems and its applicability to the lightning regime will be examined. The model will be applied to a simple physical situation and its limitations will be defined and improvements suggested.

It should be emphasized that virtually all of the physical processes involved in the interaction of lightning with an aircraft are nonlinear or are in some way dependent on nonlinear effects. For example, the dart leader's interaction has been treated linearly throughout this study. Yet the entry and exit points of the lightning channel on the aircraft along which the leader propagates were established by a nonlinear process. Hence the dart leader interaction can be treated linearly only after the nonlinear effects have been defined, in this case by physically examining the aircraft for entry and exit points. The same reasoning applies to K-changes which also propagate along previously established lightning channels.

In addition some of these nominally linear processes can enter a nonlinear regime if they are large enough. As another example, if the fields produced by a large K-change interacting with the aircraft become intense enough to produce corona, a nonlinear treatment is necessary. For the actual measurements taken to date, this may not have occurred very

often, because only small strikes are represented in the data (except for the 15 kA from strike in 1981). However, it should be kept in mind that a small strike cannot simply be scaled up to determine the effect of a large strike. The response of the aircraft to high intensity strikes is likely to require a full nonlinear treatment.

Because only small strikes are involved in the 1980 data, the question may arise as to whether any nonlinear modeling is necessary to interpret that data. This questions was touched on in Chapter 2 and will be addressed again here. For the case of small strikes only, it reduces to another question, that of whether there are any records of stepped leaders in the data. Small K-changes and dart leaders can probably be modeled linearly, but the stepped leader interaction cannot. The linear T3DFD finite difference code does not presently model the air breakdown associated with corona and the approach of the stepped leader. It presently does not realistically model streamer formation from the aircraft out toward the stepped leader, nor the attachment of the streamer to the leader charge, nor the leader's subsequent exit from the aircraft. So if there are stepped leader records in the data, they can be interpreted only by a nonlinear code. It is probable that stepped leader records do exist in the data, and that Figure 7.1, showing a D-dot response on flight 80-038, is an example. This record will require a nonlinear code to explain it in a satisfactory manner.

7.2 Air Conductivity Modeling

The inclusion of nonlinearities in the T3DFD code is done by introducing a spatially and temporally varing air conductivity σ. This air conductivity is a nonlinear function of the electric field and is often calculated using a three species approximation. This is the version that will now be described. The three species involved are electrons, positively charged ions, and negatively charged ions. The densities of each of these species is calculated assuming detailed balancing and local neutrality. The air conductivity σ is then found from the densities and electron and ion mobilities. The pertinent equations are:

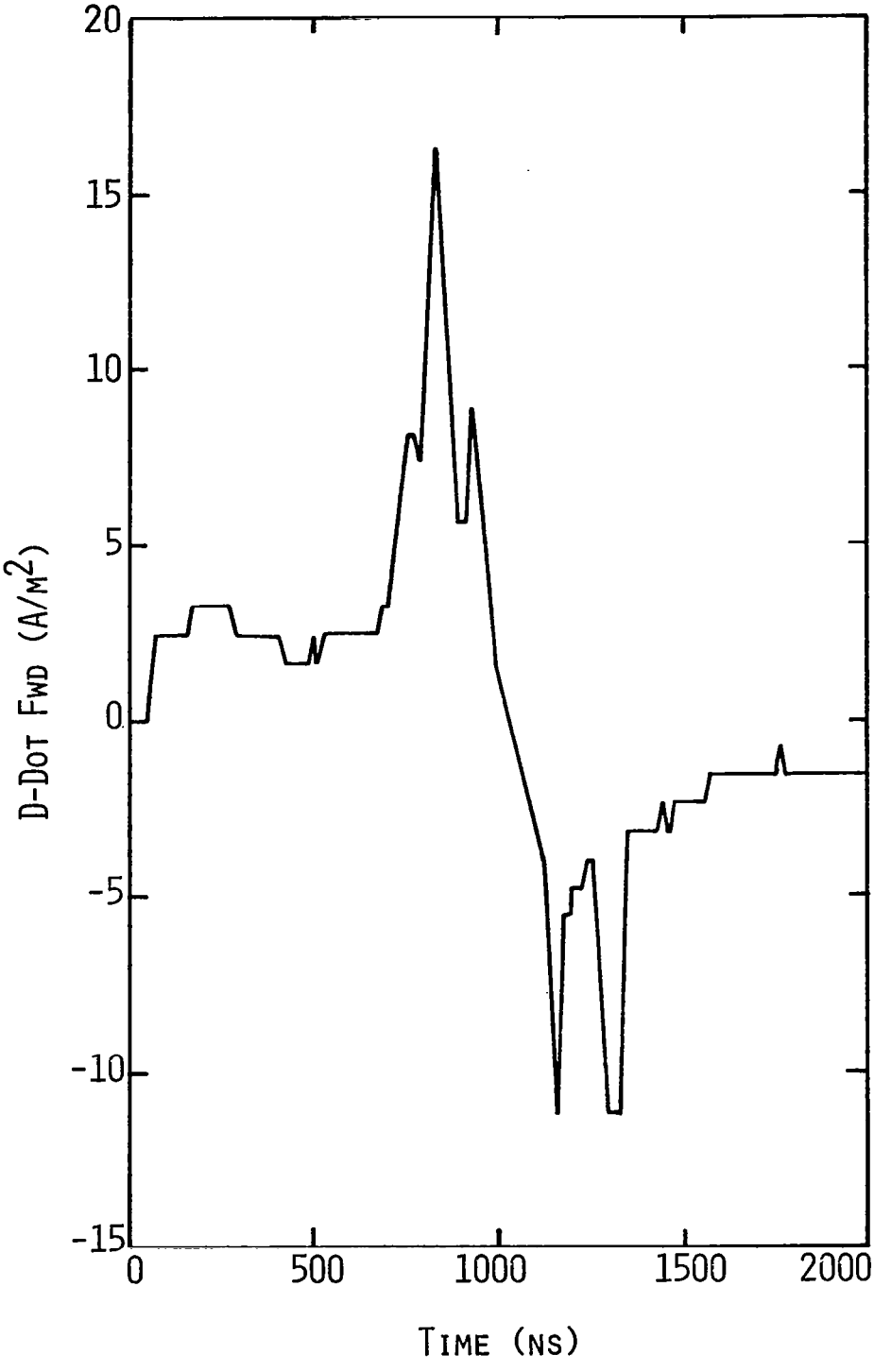

Figure 7.1 D-Dot Data Record Showing Possible Initial Leader Attachment to Nose of the Aircraft (Flight 80-038)

$$\sigma = q(n_e\mu_e + (n_- + n_+)\,\mu_i) \quad . \tag{7.1}$$

Here q is the charge on one electron 1.6×10^{-19} coulombs,
n_e is the number density of secondary electrons [m^{-3}],
n_- and n_+ are the number densities of negative and positive ions [m^{-3}], and
μ_e and μ_i are the electron and ion mobilities in [$m^2/(volt\ sec)$].

The electron and ion densities are computed from the ionization rate and local neutrality:

$$\frac{\partial n_e}{\partial t} + [\beta n_+ + \alpha_e - G]\, n_e = \dot{Q}(t) \tag{7.2}$$

$$\frac{\partial n_-}{\partial t} + [\delta n_+]\, n_- = \alpha_e n_e \tag{7.3}$$

$$n_+ = n_e + n_- \tag{7.4}$$

Here α_e is the electron attachment rate (sec^{-1}),
G is the electron avalanche rate (sec^{-1}),
β is the electron-ion recombination coefficient ($m^3\cdot sec^{-1}$), and
δ is the negative-positive ion recombination coefficient ($m^3\cdot sec^{-1}$),
$\dot{Q}$ is a cosmic ray source function ($\sim 10^7$ electrons/$m^3\cdot$sec).

The rate coefficients and mobilities are found from air chemistry formulas and are given in Table 7.1 [18].

7.3 Application of the Air Conductivity Model

This model for the air conductivity has been used in the area of nuclear electromagnetic pulse analysis [18-22]. In order to check its applicability to corona formation it was implemented in a two-dimensional finite difference model of an experiment performed by Collins and Meek [23]. In this experiment a rod-plane gap arrangement was used as shown in

Table 7.1 Air Chemistry Coefficient Formulas [18]

Calculation of Erel:

$$Erel = \frac{E}{\rho_r} / (1+2.457P^{0.834}) \quad \text{for } \frac{E}{\rho_r} < 0.07853(1+2.457P^{0.834})$$

$$Erel = \frac{E}{\rho_r} - 1.195P^{0.834} \quad \text{for } \frac{E}{\rho_r} > 3.015+1.195P^{0.834}$$

$$Erel = \sqrt{\frac{E}{\rho_r} + \left(\frac{0.6884P^{0.834}}{2}\right)^2} - \frac{0.6884P^{0.834}}{2}\Bigg)^2 \quad \text{for all other } \frac{E}{\rho_r}$$

Where P is the percent water vapor and ρ_r is relative air density. Note: E is in esu, where Eesu = Emks/3x10^4.

Calculation of Electron Attachment Rate α_e:

$$\alpha_e = \frac{100-P}{100}(\alpha_3(1+0.344P)+\alpha_2)$$

$$\alpha_2 = 1.22x10^8\rho_r e^{-21.15/Erel}$$

$$\alpha_3 = \rho_r^2 (6.2x10^7+8.x10^{10}Erel^2)/(1+10^3Erel^2(Erel(1+0.03Erel^2))^{1/3})$$

Calculation of Avalanche Rate, G:

$$G = 5.7x10^8\rho_r Y^5/(1+0.3Y^{2.5}); \quad Y = \frac{Erel}{100}$$

Calculation of Electron-Ion Recombination Coefficient , and Ion-ion Neutralization Coefficient, :

$$\delta = 2x10^{-13} + \rho_r 2.1x10^{-12} \ (m^3/sec)$$

$$\beta = 2x10^{-13} + 2.8x10^{-12}(P)^{1/3} \ (m^3/sec)$$

Calculation of Electron Mobility, μ_e:

$$\mu_e = \frac{100\mu_a}{100-P+PxR}; \quad R = 1.55+210/(1+11.8Erel+7.2Erel^2) \ \frac{m/sec}{volts/meter}$$

$$\mu_a = (((16.8+Erel)/(0.63+26.7Erel))^{0.6})/(3.x\rho_r)$$

Calculation of Ion Mobility, μ_i:

$$\mu_i = \frac{2.5x10^{-4}}{\rho_r} \ \frac{m/sec}{volts/m}$$

Figure 7.2. A voltage impulse was then applied to the rod and the resulting fields measured. The onset of corona could be seen in the measurements as a sharp increase in the field levels at the plane, and a sharp reduction in field levels at the rod. A typical field plot from the experiment is shown in Figure 7.3 for an impulse voltage of 64 kV.

The prediction of the nonlinear finite difference code for the electric field at the tip of the rod is shown in Figure 7.4. Note that the onset of corona appears to be accurately modeled, but the field behavior after this point deviates from the experimentally measured value. The drop in the field seen in the experiment is significantly larger than the finite difference code predicts. The difference between code and experiment is even more dramatic when the electric field at the lower plane is considered, as shown in Figure 7.5. It is clear from this figure that the code is simply predicting the geometric field at the plane. No information about corona formation at the rod is evident at the plane. The experiment shows that the corona region propagates toward the plane, but this is not accurately predicted by the code. The problem is in one of the assumptions made to calculate the air conductivity, given in Equation (7.4), which required that $n_+ = n_e + n_-$ at all points in space (the local neutrality condition). This condition is restrictive in that it does not allow a space charge region to form. Positively and negatively charged particles are allowed to form, but after they are formed they cannot go anywhere. They are forced to stay together to maintain neutrality at each point. This, of course, is not the real physical situation. If an electron is stripped from an atom to produce a negative particle and a positive particle, the two particles will move apart due to the opposite force exerted on them by the electric field. This drifting apart produces a net space charge which tries to neutralize the field which created it. The net result is a balance between the applied electric field and that caused by the space charge. The local neutrality assumption, by not allowing the space charge to form, does not permit the corona to expand properly. Hence the code predicts spatially small corona regions which have little effect on the electric field at the lower plane in the experiment.

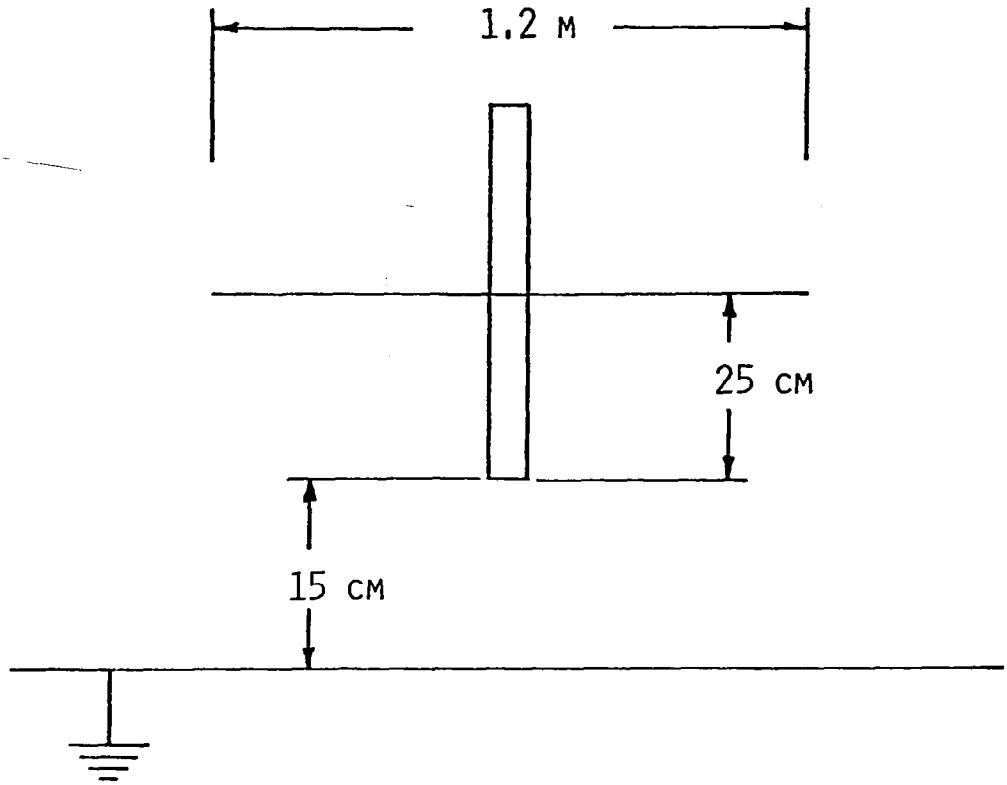

FIGURE 7.2 ROD-PLANE GAP ARRANGEMENT FOR EXPERIMENT OF COLLINS AND MEEK [23]

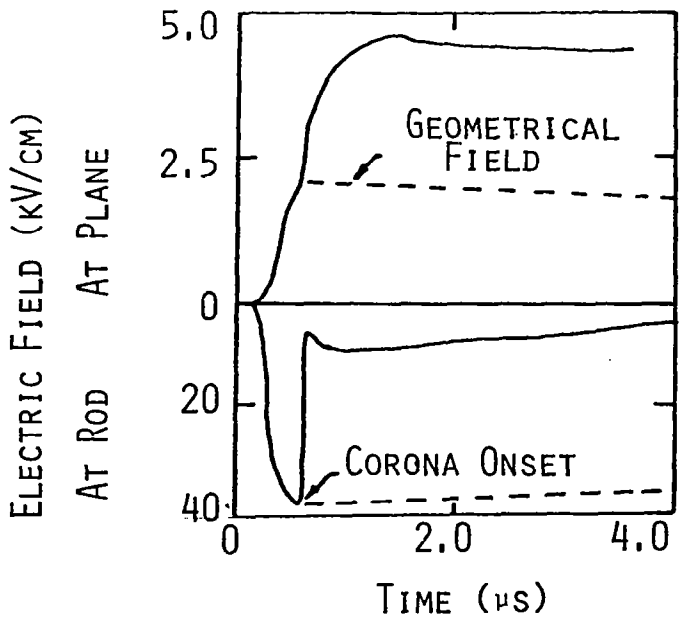

FIGURE 7.3 FIELD VARIATION AT ROD AND PLANE

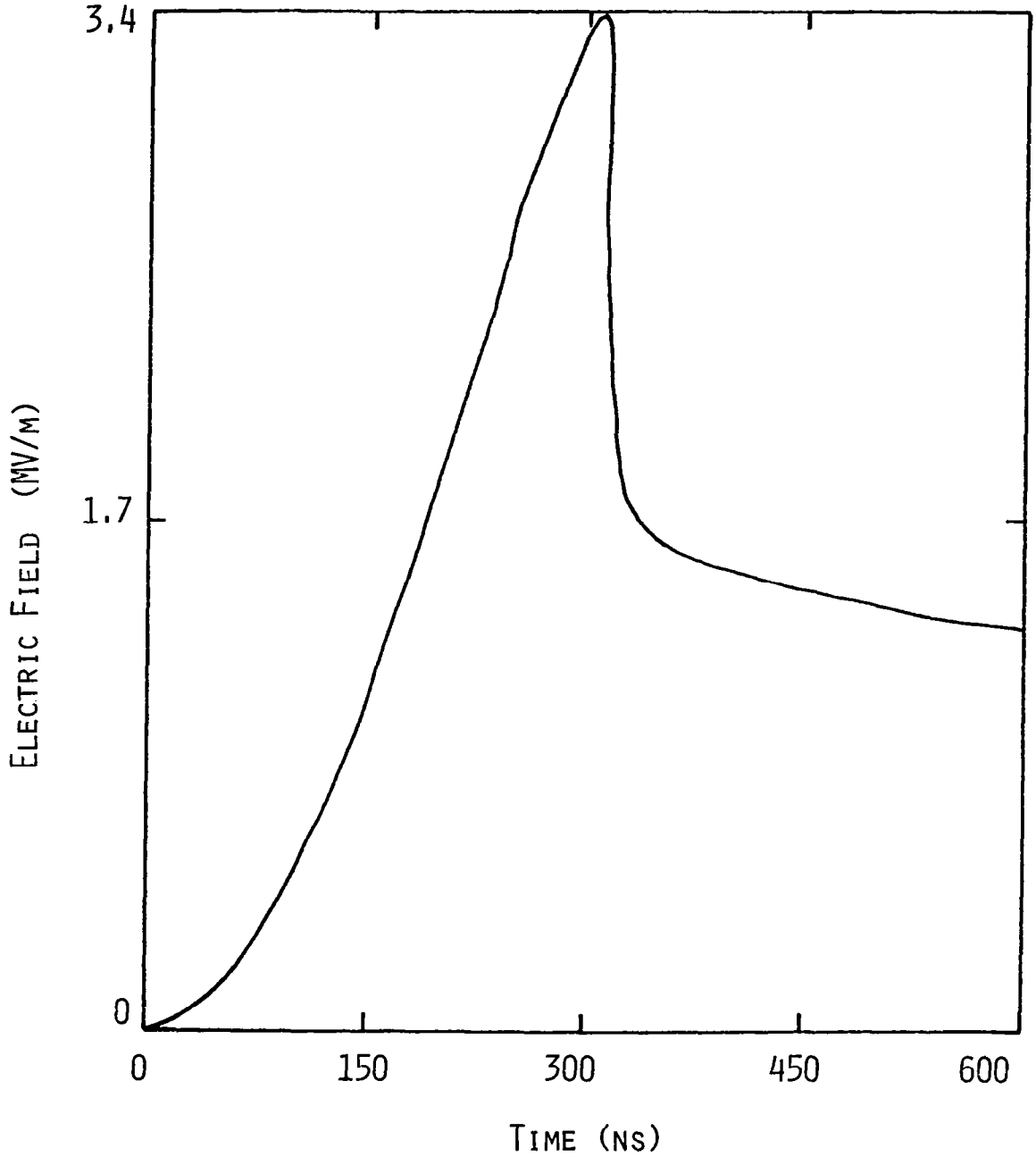

FIGURE 7.4 PREDICTED FIELD VARIATION AT ROD

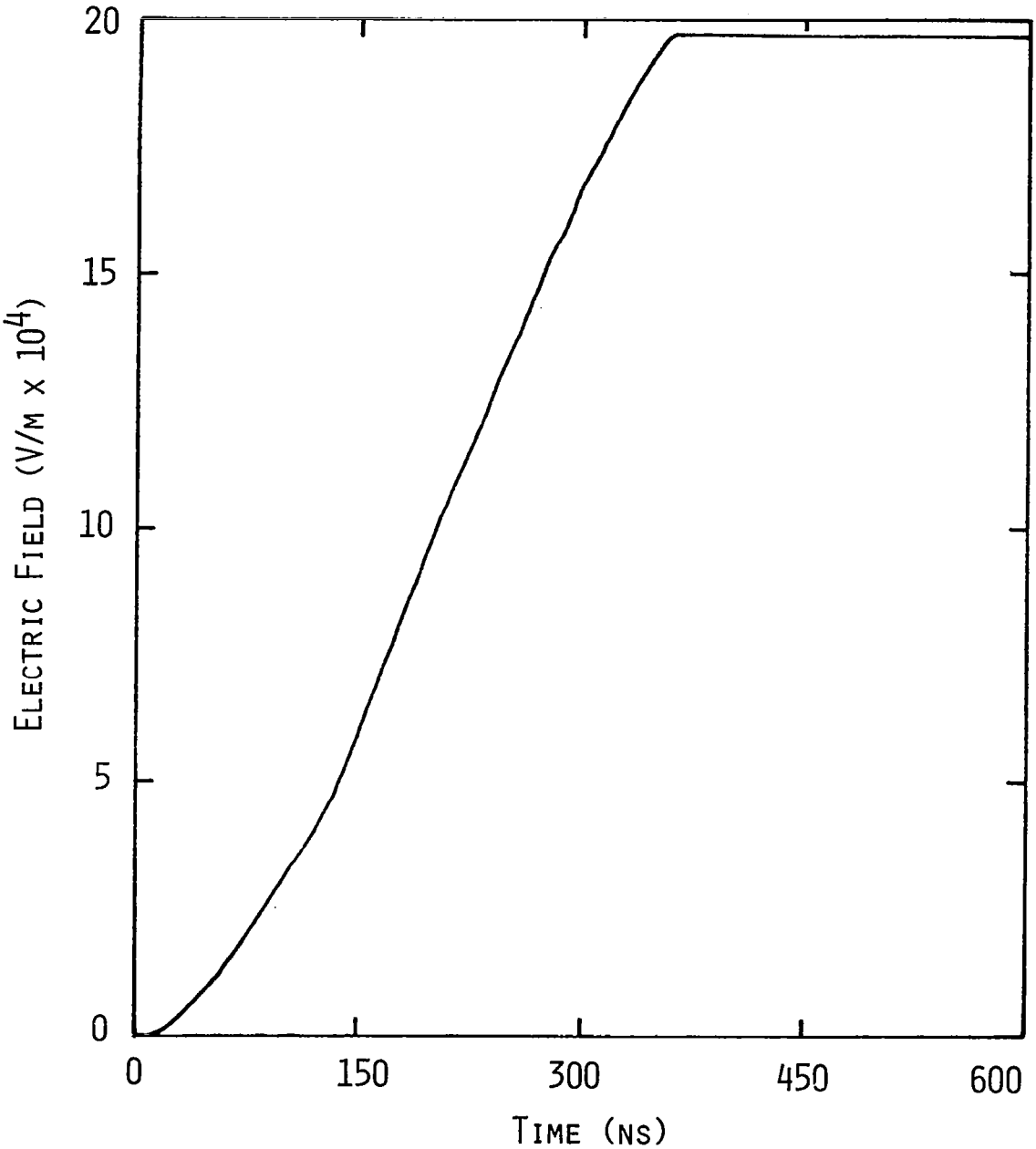

Figure 7.5 Predicted Field Variation at Plate

7.4 Improvements in Air Conductivity Modeling

The problem arises how to replace the neutrality condition, Equation 7.4. Another equation is necessary to determine the three number densities n_e, n_+, and n_-. The solution is not to add one more equation, but four. The important one is the continuity of charge equation

$$\frac{\partial \rho}{\partial t} + \nabla \cdot \vec{J} = 0. \tag{7.5}$$

Here $\vec{J}$ is the vector current density (Amp/m^2) and ρ is the charge density ($coul/m^3$). When definitions for $\vec{J}$ and ρ are inserted into Equation (7.5) one gets the following:

$$\frac{\partial}{\partial t}(n_+ - n_- - n_e) + \nabla \cdot (n_+ \vec{V}_+ - n_-\vec{V}_- - n_e\vec{V}_e) = 0. \tag{7.6}$$

In Equation (7.6) the $\vec{V}$'s introduced are the velocities associated with each of the three species. This is the reason that four equations are needed to replace the neutrality condition, rather than one. The $\vec{V}$'s must be determined from force equations which can in general be written as below.

$$\begin{aligned}
\frac{d}{dt}\vec{V}_e &= -\frac{e}{m_e}(\vec{E} + \vec{V}_e \times \vec{B}) - \upsilon\vec{V}_e, \\
\frac{d}{dt}\vec{V}_- &= -\frac{e}{m_-}(\vec{E} + \vec{V}_- \times \vec{B}) - \upsilon\vec{V}_-, \\
\frac{d}{dt}\vec{V}_+ &= \frac{-e}{m_+}(\vec{E} + \vec{V}_+ \times \vec{B}) - \upsilon\vec{V}_+.
\end{aligned} \tag{7.7}$$

In Equation (7.7) the masses of the individual species have been introduced, υ is an approximate collision frequency and $\frac{d}{dt}$ represents the convective derivative, $\frac{d}{dt} \equiv \frac{\partial}{\partial t} + \vec{V} \cdot \nabla$. Note that the assumption has been made that all ions are singly charged.

It is now necessary to make some simplifications of the force equations, because they are complex in the complete form. First the magnetic force term is omitted because it is in general much smaller than the electric force. This reduces the force equations to a balance between the electric force and a term caused by collisions. By redefining the $\vec{V}$'s as an average drift velocity one is able to make use of the electron and

ion mobilities, which are derived from the balance between the electric and collision terms. The corona region is thus assumed to be a collision dominated plasma. Hence the force equations reduce to a simple definition of the velocities, as below.

$$\begin{aligned} \vec{V}_e &= -\mu_e \vec{E}, \\ \vec{V}_- &= -\mu_i \vec{E}, \\ \vec{V}_+ &= \mu_i \vec{E}. \end{aligned} \tag{7.8}$$

Another level of approximation can be made at this point. That is to assume that the ions, being much heavier than the electrons, are immobile. Then $\vec{V}_- = \vec{V}_+ = 0$ and one is left with only the first of Equations (7.8).

The last question to ask here is under what condition will $\vec{V}_e = -\mu_e \vec{E}$ be valid ? Clearly it cannot be right in all situations, because if there are no collisions, $\upsilon = 0$, and $\vec{V}_e$ grows without bound. Of course no average drift velocity can be defined for this case. Therefore there must be a minimum threshold for υ above which the mobilities can be used and below which they cannot. There are two conditions for the above equation to hold.

The first condition is that the actual velocity of the electron, not its drift velocity, must be much less than the speed of light at all times. That is, if an electron suffers a collision, then begins accelerating in an electric field, its velocity must not approach c in the time before it suffers another collision. This is a condition on the size of the collision frequency, and reduces to,

$$\upsilon >> \frac{eE}{m_e c} . \tag{7.9}$$

For electrons and a worst case field of 3×10^6 Volts/m, this becomes $\upsilon >> 1.76 \times 10^9 \text{ sec}^{-1}$.

The second condition is related to finite difference approximations and is a requirement that the average drift velocity of the electron defined

previously be a well defined quantity in the discrete mesh of a computer code. The requirement is that the mean free path of an electron between collisions must be much smaller than the cell dimension of the mesh. Again this reduces to a condition on υ,

$$\upsilon >> \sqrt{\frac{e\,E}{2m_e\,\Delta x}}, \tag{7.10}$$

where Δx is the cell dimension. For the worst case field of 3×10^6 volts/m this becomes $\upsilon >> 5.13 \times 10^8\ (\Delta x)^{-1/2}$. The condition is more restrictive for finely spaced grids than coarse ones, and for finite difference codes such as that for the F106, this condition is weaker than the first. An estimated collision frequency at one atmosphere is about 10^{10} sec^{-1}, so one is justified in using the mobility approximation.

The addition of the charge continuity equation to the air conductivity formulation will give more accurate results for lightning studies than the method of requiring local neutrality. The new method will allow streamers to form, because charges are allowed to separate. This was not possible with the old formulation. The corona size is also likely to increase over the size with the old method. This may be significant in terms of how the aircraft will respond to a lightning event.

CHAPTER 8

UNIQUENESS

The subject of uniqueness has arisen several times in this report. In this chapter it will be illustrated why the measured lightning data to date cannot uniquely determine lightning sources, and what is needed to ensure uniqueness or at least to increase confidence in the results. The discussion will be informal, because many of the conclusions to be drawn do not yet have a rigorous mathematical backing.

The mathematical theory of partial differential equations states that given a driving source, initial conditions, and boundary conditions, the solution to a given differential equation is unique. When applied to Maxwell's equations, this means that the electromagnetic fields at all points in space and time are uniquely determined by the driving source and boundary conditions. The source is defined here in a general way. It is a function both of time and space and can be a current, an electric or magnetic field, or a charge distribution. For this study of lightning excitation of the F106, sources have been restricted to currents and plane wave illumination. The boundary condition is the presence of the metallic aircraft which requires that all fields spatially inside the aircraft be zero. The choice of a source then fulfills the requirements for a uniqueness solution to Maxwell's equations, and the finite difference code T3DFD can compute that solution. That is, T3DFD calculates the response of the F106 to a given lightning source, and that response is unique.

Now consider the analysis task undertaken in the present study. It is, in essence, to determine the source given the boundary conditions and the response at a single point. This is the inverse problem to what was discussed above, and to which mathematical uniqueness theorems apply. If the boundary conditions and the single response are the only information known, there are an infinite number of possible sources which solve the problem. For example, with LEMP any direction of illumination will work if there is complete freedom in waveform, polarization, and amplitude.

For direct strikes any entry point for the lightning current will suffice if the current waveform is unrestrained. In reality matters are not this bad, at least not for direct strikes. Usually the point of entry of a lightning current can be determined from examination of the aircraft. This pins down the location of the source and leaves its waveform free.

In a case such as the one above, in which the current entry point is known, it might be expected that a unique source could be found, but there are still some complications. It is true that a derived source will be unique in the linear case, but if the problem is nonlinear, involving air breakdown somewhere near the aircraft with the subsequent exit of current, the solution is again not unique. The source found in the linear problem may no longer be correct, because there are now more free parameters, involving exit point, time of air breakdown, and exit current waveform. Again there are likely to be an infinite number of possible sources which give the desired response, when the definition of source is expanded to include the exiting current. Also it is possible that there could be multiple exit and entry points, all active at different times. In summary this leaves one with a complicated tangle of possible sources, all of which can produce the same measured response.

The question then naturally arises as to how the situation can be resolved. To be mathematically rigorous it is probably necessary to measure the responses at every point in space at all times in order to uniquely determine the source. However, physically the situation is not this pessimistic because one has some prior knowledge of the source. For direct strikes the location is generally known, and from previous lightning studies some limits can be put on the waveform. Also one can often differentiate between linear and nonlinear cases by the form of the response. That is, one can determine if the response looks like that of a stepped leader as described in Chapter 2, for which nonlinearity is definitely necessary, or if it looks more like a dart leader, which can be treated linearly. By limiting oneself to only physically possible lightning waveforms, taking advantage of known entry and exit points, and choosing between linearity and nonlinearity on the basis of general characteristics of response waveforms, the total number of possible sources can probably be

cut down to just a few. But the problem of which of these few is the correct source still remains.

The question then arises if there is a way to take the last step and decide among the few remaining possible sources. The recording of truly simultaneous aircraft responses will allow this to be done with a large degree of confidence. Even just two sensors on the plane which are known to have triggered simultaneously would give much more confidence in the derived lightning source. The 1980 and 1981 data include records which may be simultaneous, but the best correlation is within 500 microseconds. Until the instrumentation channels are forced to trigger simultaneously there can be no real certainty.

In conclusion, lightning sources which are determined from a single measured response have some room for error, and these sources should be considered as only possible. These sources will give the correct response at the measuring point but may be drastically in error elsewhere. The forcing of simultaneous recordings from different sensor locations should alleviate this difficulty, and coupled with the other physical knowledge about the lightning event, allow truly unique lightning sources to be determined. In addition, high resolution recording of the boom current for boom studies should leave little doubt regarding the injected current.

CHAPTER 9

PRELIMINARY INTERPRETATION METHODOLOGY

9.1 Background

An issue that has not been addressed in the previous chapters is that of how the actual data interpretation is done. That is, the procedures used in attempting to determine a lightning source function given a response of the aircraft have not yet been defined. It should be understood that this is the inverse problem to what is normally done. The usual problem is to determine the response of the aircraft given a source function. This latter problem is what the finite difference code T3DFD is tailored to do.

9.2 Approach

For a given source T3DFD will compute the unique aircraft response. It cannot calculate a unique source given the aircraft response. This means that operator intervention becomes necessary to interpret the data using T3DFD. Determining the source that produced a given data record is, at least initially, a trial and error process. A source is fed into T3DFD and the response calculated. The source is then adjusted by the operator to correct for differences between the calculated and measured responses. In this fashion the operator iterates toward a source which could have produced the given record. The words "could have" are used here, because there is no guarantee that the source found in the iteration process is the only possible one which gives the measured response, as was discussed in Chapter 8. Hence operator intervention again becomes necessary at this point. The operator must ask whether the source found is reasonable, or is too convoluted to describe a real lightning pulse. This issue of physical realizability is important as long as one is dealing with the measured aircraft response at a single point only. It would become less important if truly simultaneous responses from different parts of the aircraft were available, because this would drastically reduce the range of possible sources. Physical realizability would still be required, of course, but

there would be fewer unrealizable sources which give the proper response.

The trial and error procedure described above seems at first glance to be very inelegant and time consuming. This has been found to be true in the initial phase of data interpretation. However, as an operator gains experience, much of the trial and error can be eliminated. It is possible with experience to scan a measured waveform and pick out general features which allow the proper source to be constructed quickly and accurately.

As an example of the way the operator can interpret a waveform consider Figure 9.1. This is a D-dot response from flight 80-018 and was discussed in Chapter 6. The entry point of the strike is the nose of the aircraft as determined by pilot comments. This defines the location of the source, and leaves the operator with two free parameters, the waveform of the injected current and its amplitude. Normally a simple waveform is chosen, such as a step function with a sine-squared leading edge. Then the free parameter of the current waveform is reduced to the leading edge's rise time.

As discussed in Chapter 6, no exit point was allowed for the injected current, so a late-time charging must take place. This forces the long tail on the response waveform, and its amplitude can be matched by varying the amplitude of the injected current. Hence one free parameter is fixed by the amplitude of the response's tail.

The other free parameter, the rise time of the pulse, can then be varied in the effort to match the early time behavior of the response. A fast rise time will drive aircraft resonances and result in several oscillations about the late time constant level. A slow rise time will not drive the aircraft resonances and will simply show a smooth rise to the late time level. The operator then can try a number of possible rise times and choose the one which best matches the measured data. Figure 9.2 is an overlay of the data with three numerical predictions. The predictions correspond to different rise times in the injected current pulse and give some indication of the way in which the operator chooses between these rise times.

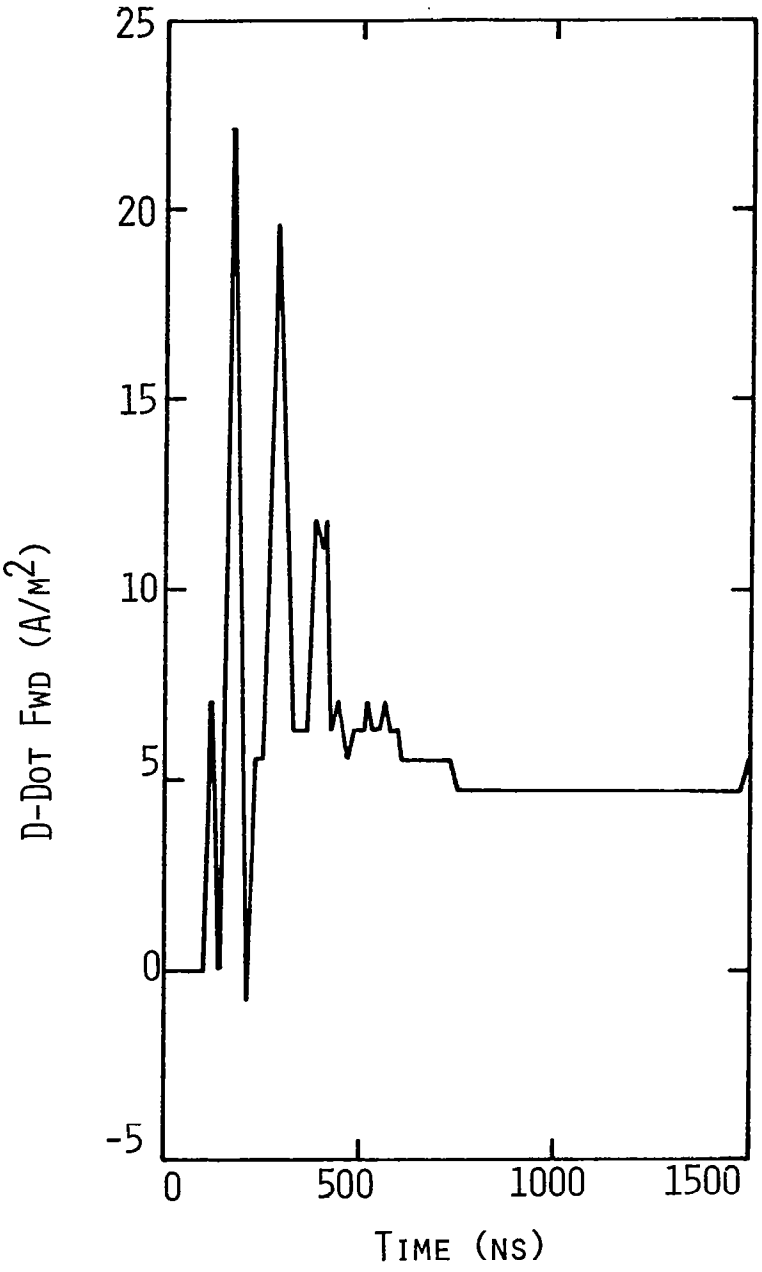

Figure 9.1 D-Dot Record From Flight 80-018

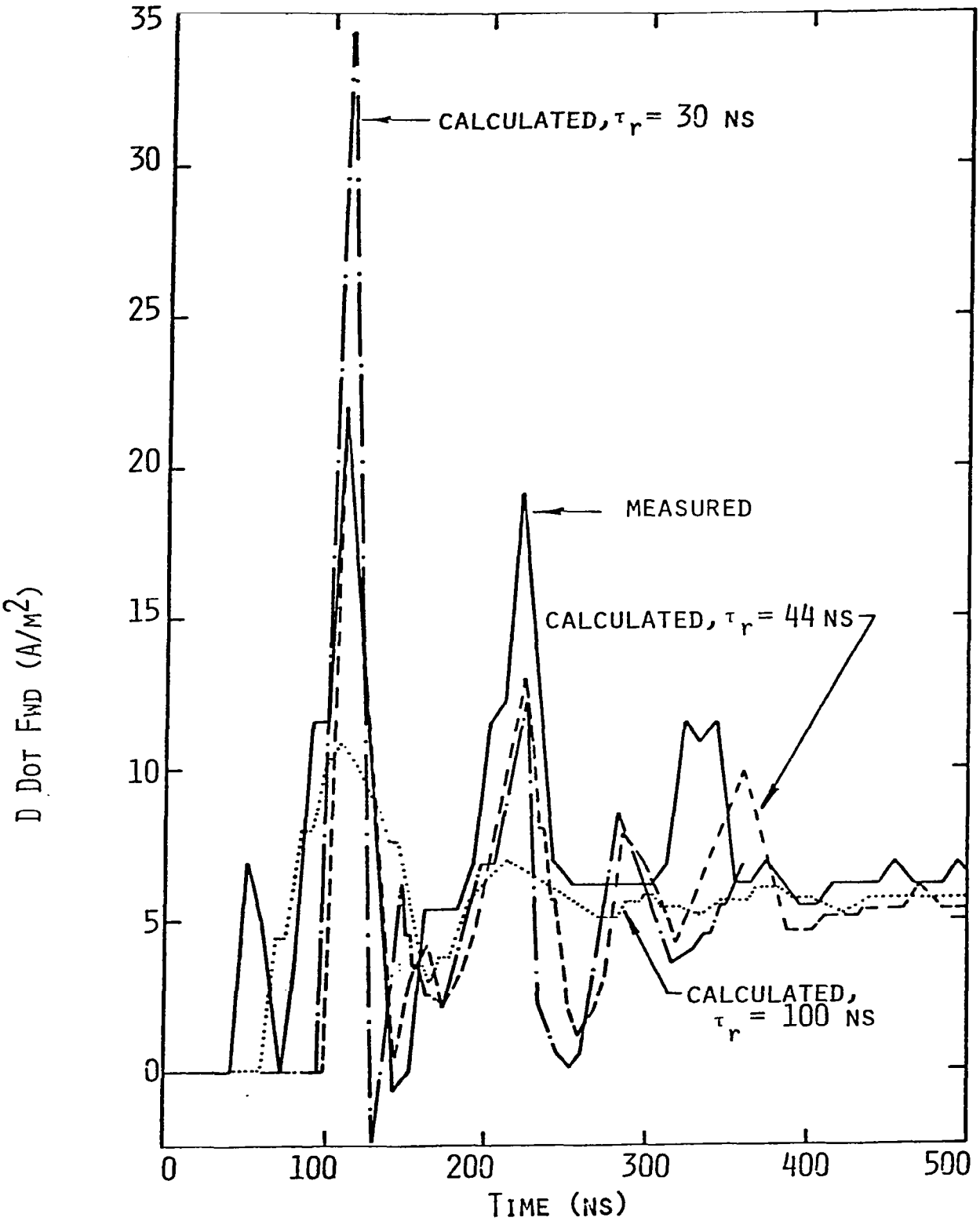

FIGURE 9.2 EFFECT OF RISETIME ON PREDICTED RESPONSE (FLIGHT 80-018)

There are two issues which this interpretation methodology cannot resolve as yet. The first comes back again to the uniqueness of the derived source. The operator can weed out physically impossible sources, but cannot with confidence choose between two or more reasonable ones. The resolution of this difficulty awaits the availability of simultaneous measurements.

The second issue is that of nonlinearity, and whether this is necessary to explain any of the data. This is related to the uniqueness issue in a sense. That is, any given data record can usually be explained by one or more driving sources in a linear fashion. If a nonlinear version of T3DFD also predicts the measured response, one is back to the problem of which is correct, the linear or the nonlinear. Physical realizability of the source is again the only decision tool available, at present. Of course one must remember that the as yet undeveloped nonlinear T3DFD code will be much more general than the present code, and will be able to handle both linear and nonlinear processes. The nonlinear code will allow the detailed examination of the aircraft response in both the linear and nonlinear regimes, which may result in a resolution of whether nonlinearities are necessary to interpret the data.

The application of the lightning information gleaned from the F106 study to other aircraft is really simple to accomplish. The T3DFD code incorporates the F106 as boundary conditions on the electric field. Given the sources derived from the F106 measurements, the response of any other aircraft to the same sources can be computed simply by changing the boundary conditions to conform to the new aircraft. The calculated responses will have none of the uniqueness difficulties associated with the F106 data, and will be obtainable without the intervention of a skilled operator.

In summary, the interpretation procedure is to use the T3DFD finite difference code to derive lightning sources in a refined trial and error fashion. This can be done for both the linear and nonlinear versions of the code. After these sources are found, their application to other aircraft and the calculation of aircraft response is a relatively trivial matter.

CHAPTER 10

SUGGESTIONS FOR THE IN-FLIGHT TEST PROGRAM

10.1 Background

In the course of analyzing the direct and nearby strike data, several possible improvements to the aircraft instrumentation system became apparent. These improvements would make the interpretation task easier, and the derived results more precise and complete. The suggestions made should not all be considered as vital to the success of the program, because it is realized that compromises must be made between what is desired and what can be achieved. The discussion will try to indicate which changes are most necessary.

Below is a list of changes which could improve the in-flight test program:

1) more sensor points,
2) truly simultaneous measurements,
3) actual field (in addition to the time derivative) measurements,
4) more variety in flight altitudes,
5) faster sampling rate for the I-dot channel,
6) addition of a wing or tail boom.

Each of these suggestions will now be discussed separately.

10.2 More Sensor Points

The 1980 and 1981 test flights recorded data from only three sensor locations, I-dot on the nose boom, D-dot forward and underneath the fuselage, and B-dot on the fuselage above the right wing. The addition of more sensor points would aid the analysis in two ways. First, it would alleviate the uniqueness problem discussed in Chapter 8. Second, the increased field resolution over the aircraft would help to pinpoint entry and exit points for direct strikes. This is because one would expect a larger response for a sensor near the entry than for one far away, for the simple

reason that the entering current has diffused over the plane by the time it reaches the distant sensor, reducing the response. This analytic determination of entry and exit points would be a useful confirmation of the methods now used, which involves a physical examination of the aircraft.

10.3 Truly Simultaneous Measurements

Simultaneous measurements (within a few nanoseconds) is the most important suggestion that can be made. The determination of a unique lightning source which caused a given response is dependent upon this. It is vitally important to the analyst that the response of the aircraft be measured at several points at the same time. The 1980 and 1981 data records contain several instances for which simultaneous measurements may have been taken at two separate sensors, but without accurate knowledge there is no way to be sure. The analyst must be sure that multiple sensor responses are caused by the same source. It is hoped that this problem will be largely solved by the addition of a significantly enlarged digital recorder to be on line for the 1982 season.

10.4 Actual Field Measurements

The measurement of actual fields on the aircraft (in addition to derivative measurements) would aid in interpreting lightning phenomena which are ambiguous from the time derivative measurements. For example, consider the two plots of electric field versus time in Figure 10.1. The time derivative of each gives the same result, but different physical events would have to be involved to produce the field plots.

The first plot is characteristic of a K-change in which the aircraft starts out negatively charged and end up with much less net negative charge. The record could be caused by a positively charged leader which deposits a net positive charge on the plane. Field measurements could unambiguously decide between these two events.

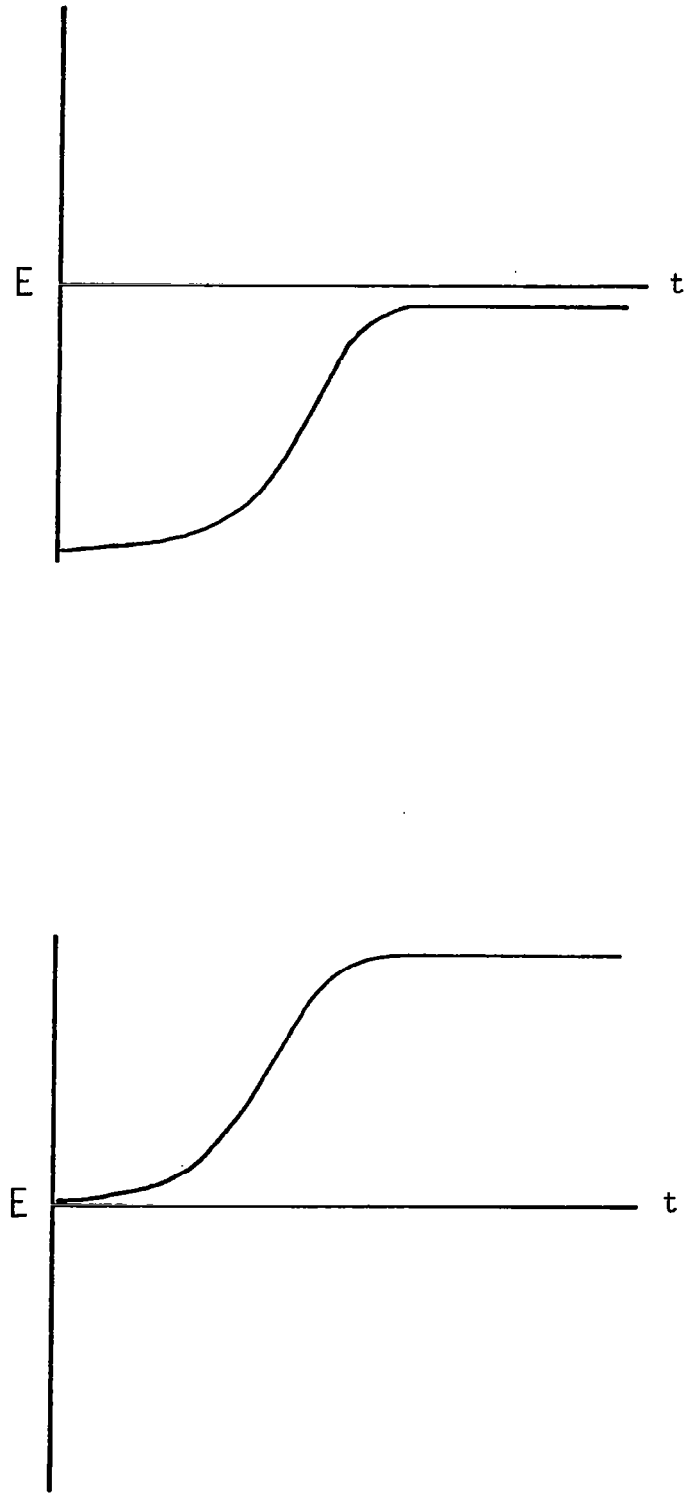

FIGURE 10.1 FIELD WAVEFORMS WHICH WILL GIVE IDENTICAL DERIVATIVE RESPONSES

10.5 Variety in Flight Altitudes

The test flights to date have only encountered strikes of small amplitude, most likely intracloud discharges. If larger amplitudes are desired it will be of interest to fly at lower altitudes, where cloud to ground discharges are more likely to be intercepted, although the frequency of being struck would be greatly reduced. It is possible that these large amplitude discharges have very different characteristics than the small ones measured so far. Because the ultimate goal of the program is the protection of future aircraft from lightning, it would be advisable to study the large discharges in some detail.

10.6 Faster Sampling Rate for I-Dot Sensors

The I-dot sensor in the nose boom would give much more useful information if it had a faster sampling rate. I-dot records are significantly affected by the 6 MHz bandwidth and require numerically inaccurate enhancement to pull out the actual currents on the boom. The records must be "unfiltered" to improve the response, which is an inaccurate process. A faster sampling rate would remove this difficulty. Again, it is understood this problem will be corrected by the improved instrumentation system to be on line in 1982.

10.7 Addition of a Wing or Tail Boom

The purpose of adding a wing or tail boom would be to provide a known exit point for the direct strike current. For a nose entry, the exit would almost certainly be at the sharp point of another available boom. This would make analysis easier, because exits would not move from point to point for different strikes. Also if currents on the entry and exit booms were simultaneously measured, a measure of the time delay between entry and exit of a lightning current could be made. This could then be compared with both linear and nonlinear analytical predictions for this time delay.

CHAPTER 11

CONCLUSION AND SUMMARY

In this report it has been shown that it is possible to invert the lightning data to determine lightning channel currents. A preliminary methodology for doing this has been developed.

The method involves the use of the finite difference computer code T3DFD, which has been shown to be accurate, and experienced operator intervention. The uniqueness of the derived currents requires more investigation.

The LEMP measured data has been found to require pulse rise times of less than 100 nanoseconds. It should be remembered, however, that the instrumentation system will naturally select pulses having a fast rise time. The direct strike data can also be explained by current rise times of less than 100 nanoseconds, and amplitudes on the order of one kiloamp. This is consistent with the relatively weak currents expected in cloud flashes. Nonlinear phenomena, such as initial leader attachment to the aircraft, are undoubtedly present in the data and will require the nonlinear version of T3DFD for satisfactory interpretation.

CHAPTER 12

REFERENCES

1. Uman, M.A.; and Krider, E.P.: "Lightning Environment Modeling," Volume I of "Atmospheric Electricity Hazards Analytical Model Development and Application," Electro Magnetic Applications EMA 081-R-21, and AFWAL-TR-81-3084, August 1981.
2. Baum, C.E., et al.: "Measurement of Electromagnetic Properties of Lightning with 10 Nanosecond Resolution." NASA CP-2128, FAA-RD-80-30, Lightning Technology, April 22, 1980.
3. Clifford, Don W.; Krider, Philip E.; and Uman, Martin A.: A Case for Submicrosecond Rise Time Lightning Current Pulses for Use in Aircraft Induced Coupling Studies. 1979 IEEE International Symposium on Electromagnetic Compatibility. San Diego, Calif., Oct. 9-11, 1979, pp. 143-149.
4. Cianos, N.; and Pierce, E.T.: "A Ground-Lightning Environment for Engineering Usage." Stanford Research Institute Technical Report No. 1, Project 1834 (August 1972).
5. Thomas, Robert M., Jr.: Expanded Interleaved Solid-State Memory for a Wide Bandwidth Transient Waveform Recorder, Lightning Technology. NASA CP-2128, 1980, pp. 119-129.
6. Pitts, F.L., et al.: In-Flight Lightning Characteristics Measurements System. Federal Aviation Administration - Florida Institute of Technology Workshop on Grounding and Lightning Technology, FAA-RD-79-6, March 1979, pp. 105-111.
7. Pitts, Felix L.; and Thomas, Mitchell E.: Initial Direct Strike Lightning Data. NASA TM-81867, 1980.
8. Pitts, Felix L.: "Electromagnetic Measurement of Lightning Strikes to Aircraft," presented at AIAA 19th Aerospace Sciences Meeting, St. Louis, Missouri, January 12-15, 1981.
9. Pitts, Felix L.; and Thomas, Mitchell E.: 1980 Direct Strike Lightning Data. NASA TM-81946, 1981.
10. Pitts, Felix L.; and Thomas Mitchell E.: 1980 Direct Strike Lightning Data. NASA TM-83273, 1982.
11. Harrington, R.F.: Time Harmonic Electromagnetic Fields. McGraw-Hill, New York, 1971, p.34.
12. Yee, K.S.: "Numerical Solution of Initial Boundary Value Problems Involving Maxwell's Equations in Isotropic Media," IEEE Transactions Ant. & Propagat., AP-14, May 1966, pp. 302-307.
13. Merewether, D.E., and Fisher, R.: "Finite Difference Solution of Maxwell's Equation for EMP Applications." Report EMA-79-R-4 (Revised), Electro Magnetic Applications, Inc. (EMA), P.O.Box 8482, Albuquerque, NM 87198, 22 April 1980.

14. Mur, Gerrit: "Absorbing Boundary Conditions for the Finite-Difference Approximation of the Time-Domain Electromagnetic Field Equations." IEEE Trans. EMC, EMC-23, Number 4, November 1981, pp. 377-382.

15. Trost, T.F.; and Turner, C. D.: "Transient Electromagnetic Fields on a Delta Wing Aircraft Model with Injected Currents." Proceedings of the International Aerospace Conference in Lightning and Static Electricity, St. Catherines College, Oxford, 28 March 1982.

16. Weeks, W.J.: Electromagnetic Theory for Engineering Applications. Wiley, New York, 1964.

17. Fisher, Bruce D.; Keyser, Gerald L.; and Deal, Perry L.: "Lightning Attachment Patterns and Flight Conditions Experienced During Storm Hazards '80." NASA TP-2087, 1982.

18. Radasky, William A.: "An Examination of the Adequacy of the Three Species Air Chemistry Treatment for the Prediction of Surface Burst EMP." DNA 3880T, December 1975.

19. Merewether, D.E.: "A Numerical Solution for the Response of a Strip Transmission Line over a Broad Plane Excited by Ionizing Radiation." IEEE Transactions on Nuclear Science, Vol. NS-18, No.5, August 1971.

20. Perala, R.A.; and Cook, R. B.: "Transient Nonlinear Circuit Models of Scattering Antennas with Corona." IEEE Transactions on Nuclear Science, Vol. NS-28, No.1, December 1981.

21. Perala, R.A.; and Cook, R. B.: "The Effects of Air Breakdown on Antenna Response." EMA-79-R-1, October 27, 1978.

22. Perala, R.A.; and Cook, R. B.: "The Effects of Corona on the EMP Response of Insulated Cables Lying on the Surface of the Earth," IEEE Transactions on Nuclear Science, Vol. NS-27, No.6, December 1980.

23. Collins, M.M.C.; and Meek, J.M.: "Measurement of Field Changes Preceding Impulse Breakdown of Rod-Plane Gaps," Proceedings of the Seventh International Conference on Phenomena in Ionized Bases, August 22-27, Gradevinska Kujiga Publishing House, Belgrade, 22-27 August 1965.

A P P E N D I X A

COMPENDIUM OF THE RESULTS FOR THE PARAMETER STUDY OF LEMP INTERACTION WITH THE F106B

This appendix gives the results of the parameter study for LEMP interaction with the F106B. The plane wave consists of a step function with $[\text{Sin}\ (\alpha t)]^2$ leading edge. The parameter variation includes:

1. 6 orthogonal angles of incidence: front, back, top, bottom, left side, and right side.
2. 2 orthogonal polarization angles for each angle of incidence.
3. Risetimes of 20, 40, 100, and 200 nsec.

Because the numerical D-dot sensor could not be placed on the symmetry line of the aircraft underneath the fuselage, there are four cases which predict a D-dot and electric field response when there should be none from symmetry considerations (see Page 43). These are:

1. Bottom Illumination, E_{inc} Toward Left (Port)
   Figures A.17 - A.20
2. Top Illumination, E_{inc} Toward Left (Port)
   Figures A.21 - A.24
3. Front Illumination, E_{inc} Toward Left(Port)
   Figures A.33 - A.36
4. Rear Illumination, E_{inc} Toward Left (Port)
   Figures A.37 - A.40

A.1 - A.4 Right Side Illumination, E_{inc} Vertical

A.1 - A.4 Right Side Illumination, E_{inc} Vertical

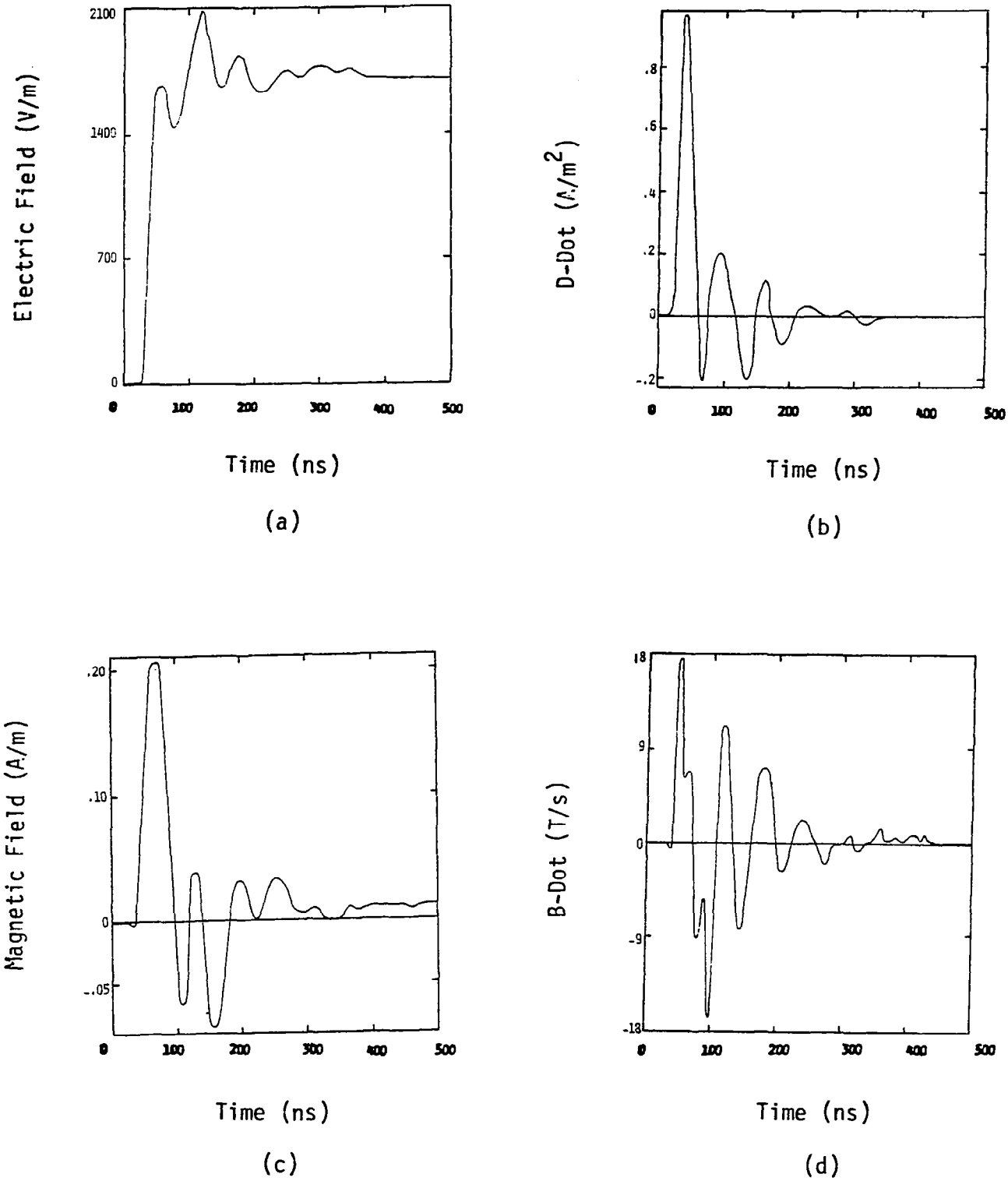

FIGURE A.1 20 NSEC RISE TIME

A.1 - A.4 Right Side Illumination, E_{inc} Vertical

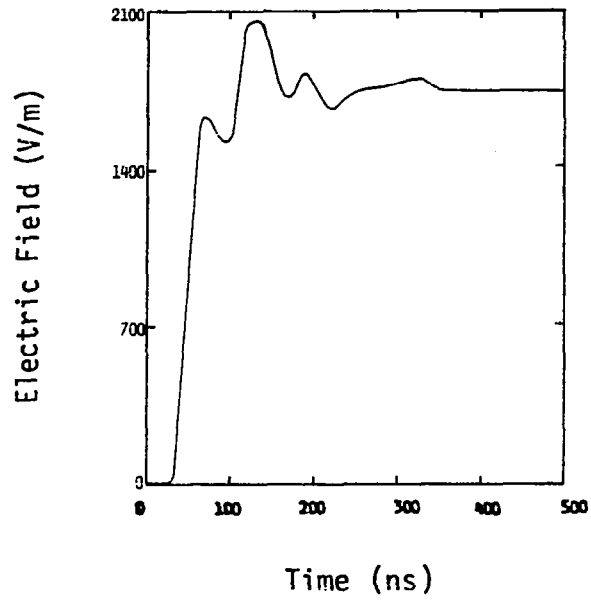

(a)

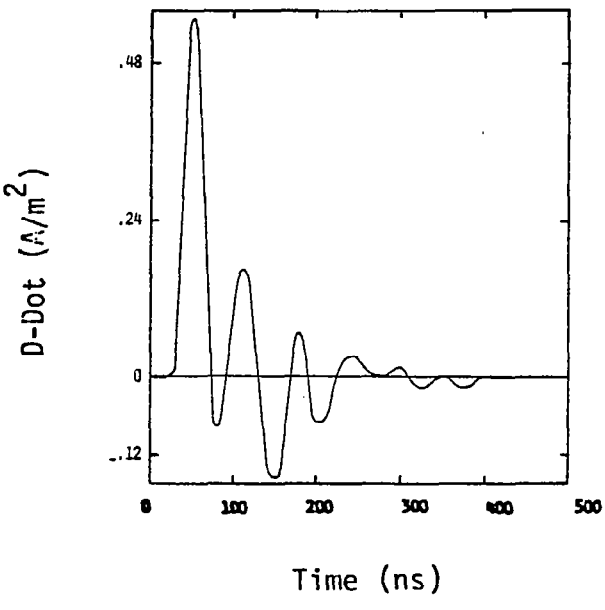

(b)

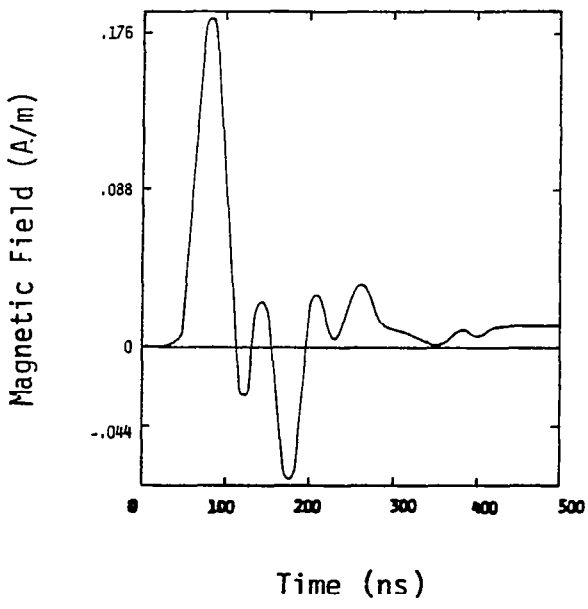

(c)

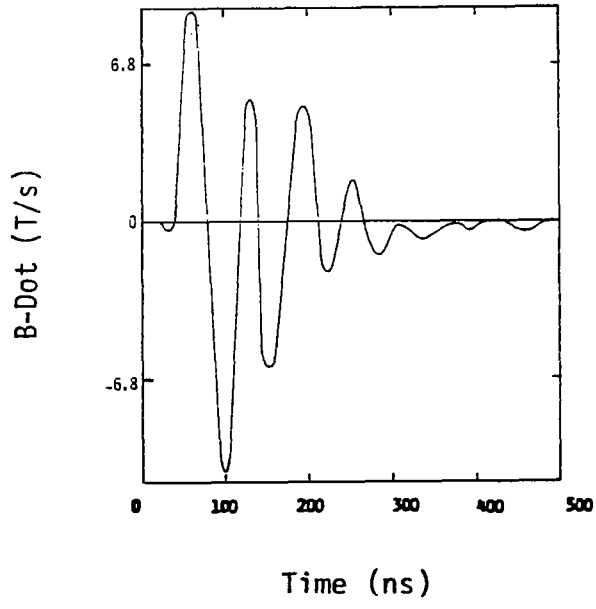

(d)

FIGURE A.2 40 NSEC RISE TIME

A.1 - A.4 Right Side Illumination, E_{inc} Vertical

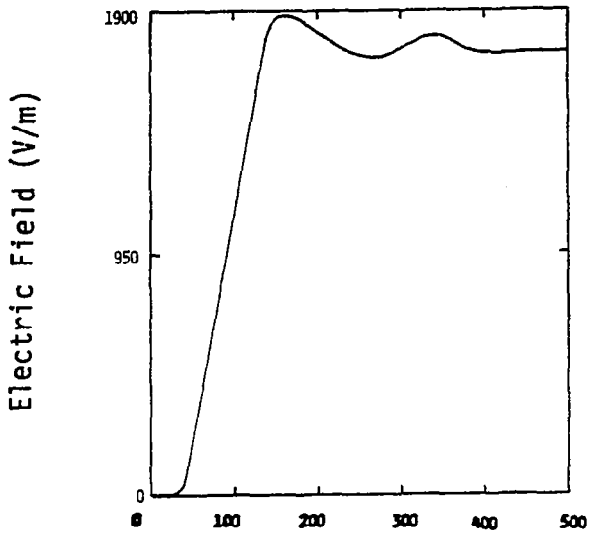

(a)

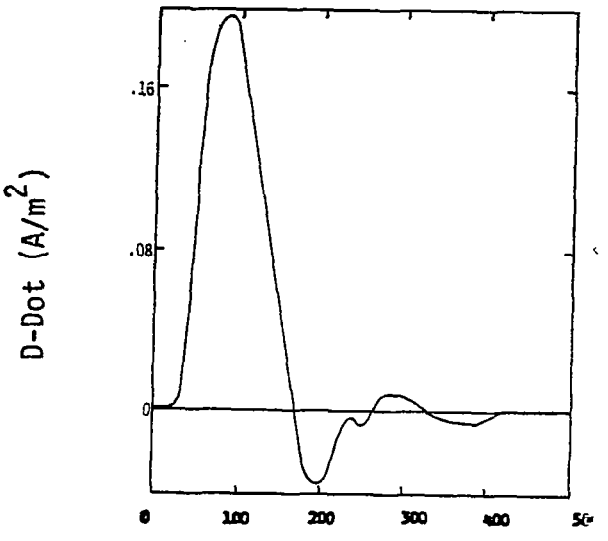

(b)

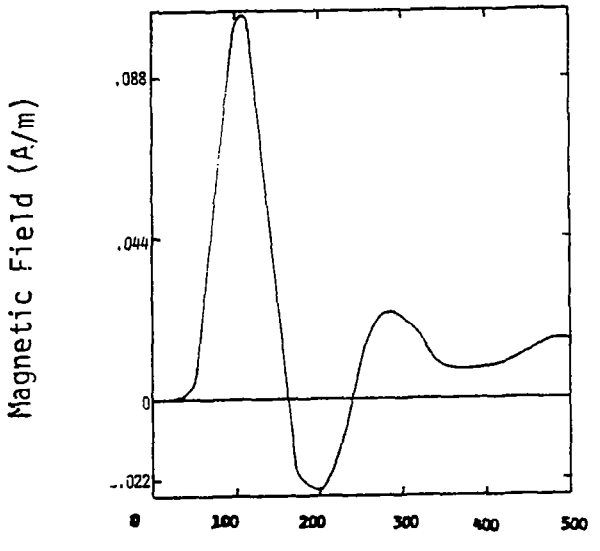

(c)

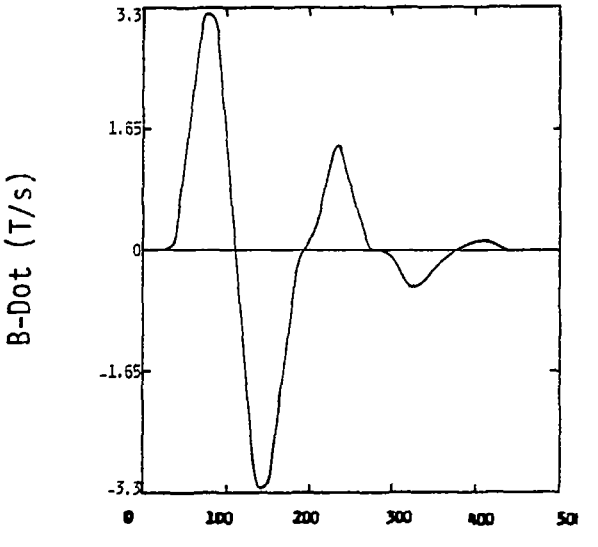

(d)

FIGURE A.3 100 NSEC RISE TIME

A.1 - A.4 Right Side Illumination, E_{inc} Vertical

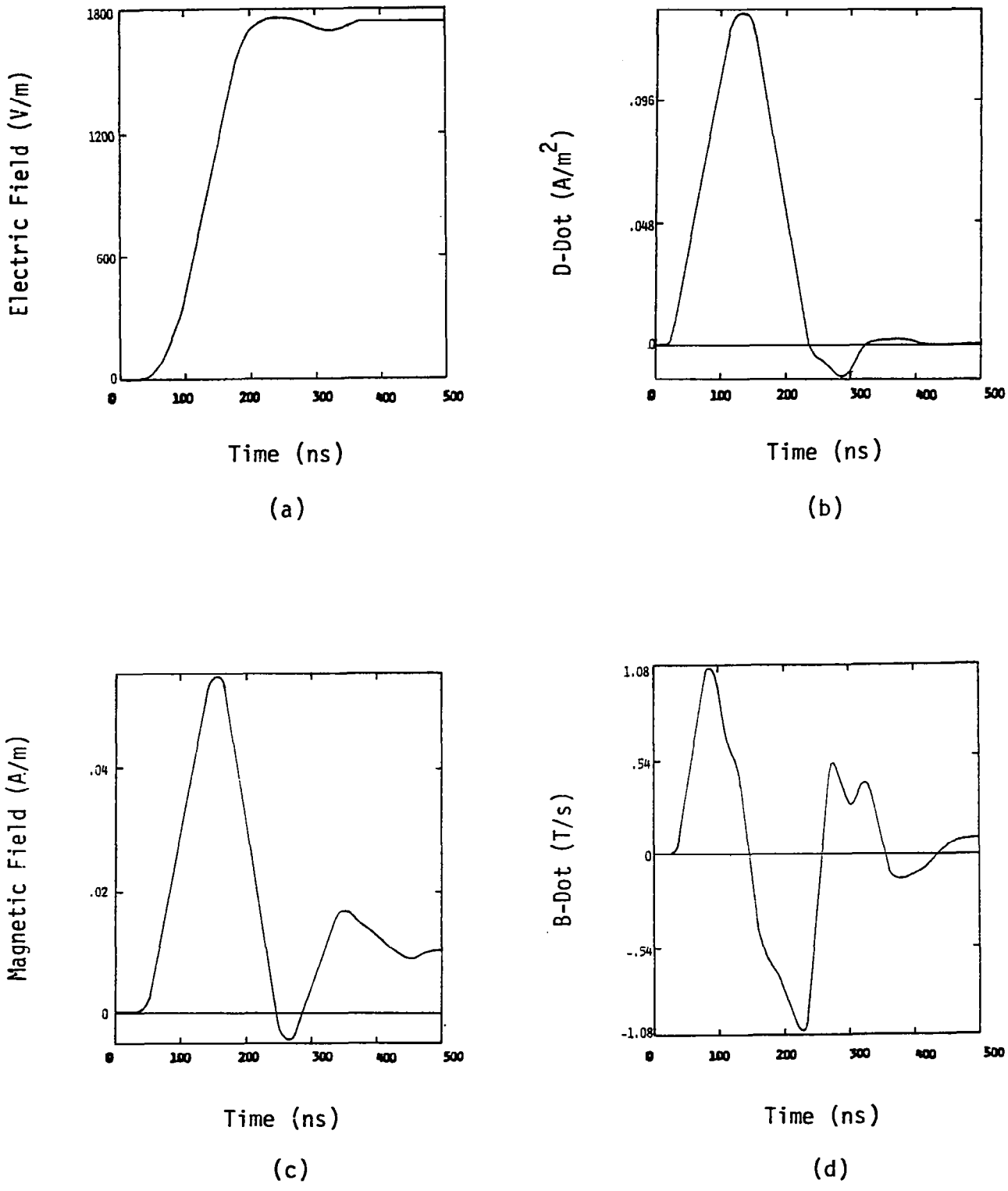

FIGURE A.4 200 NSEC RISE TIME

A.5 - A.8 Left Side Illumination, E_{inc} Vertical

A.5 - A.8 Left Side Illumination, E_{inc} Vertical

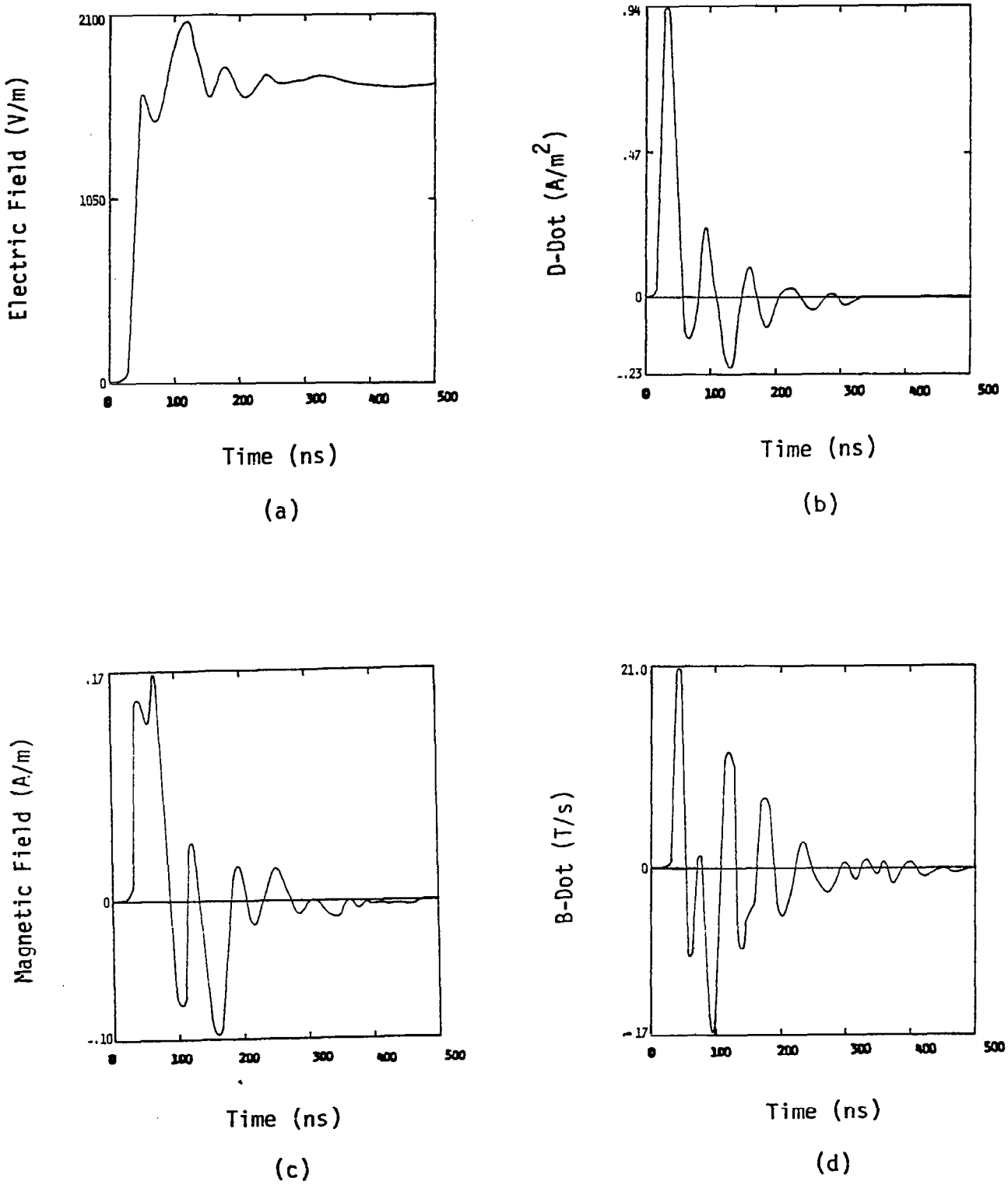

FIGURE A.5 20 NSEC RISE TIME

A.5 - A.8 Left Side Illumination, E_{inc} Vertical

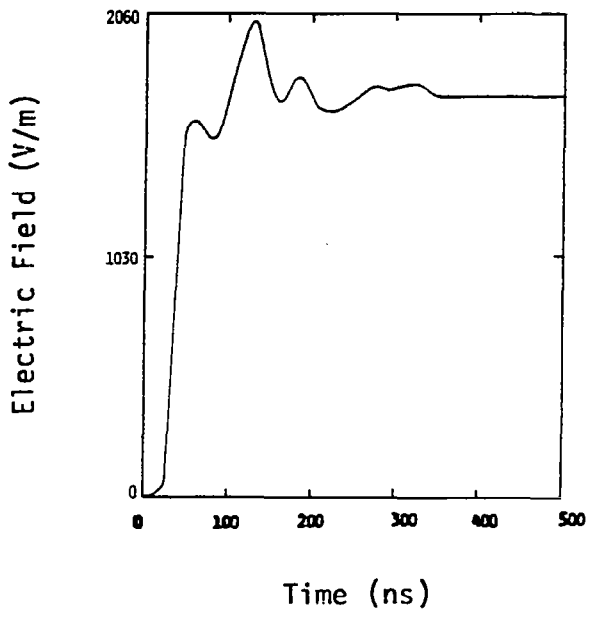

(a)

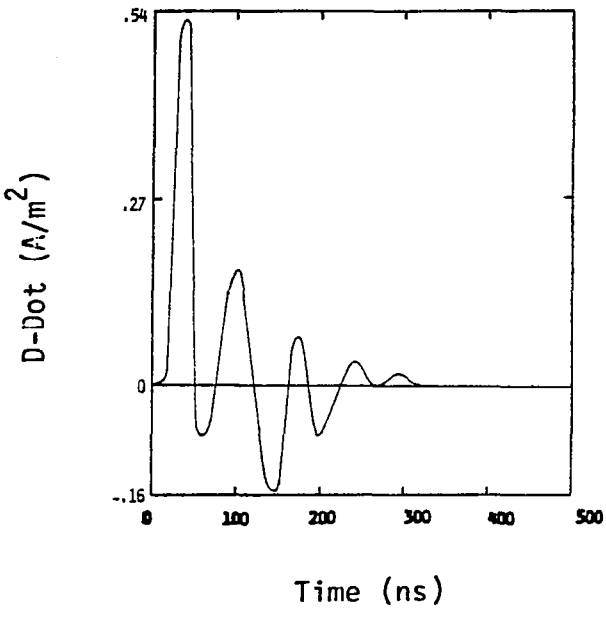

(b)

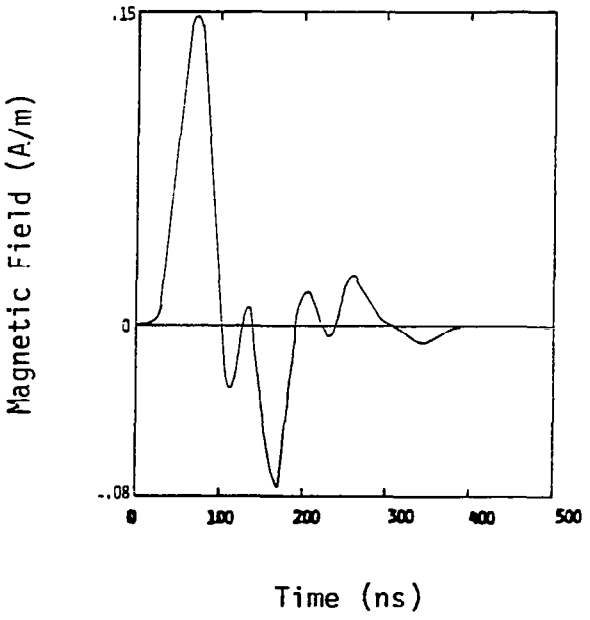

(c)

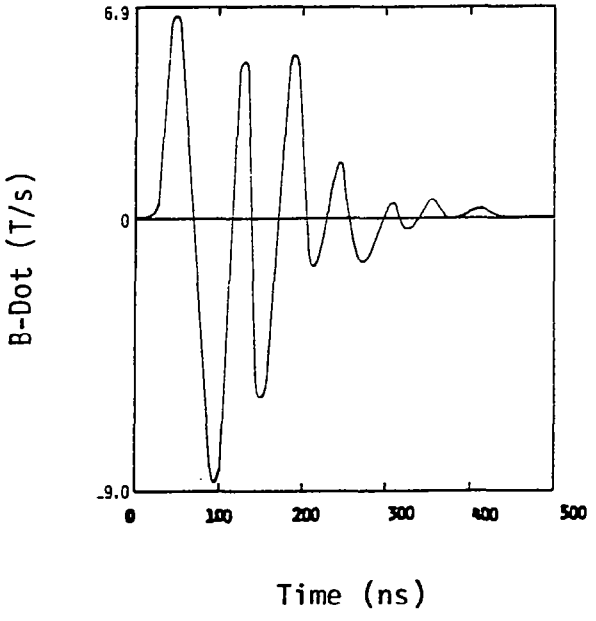

(d)

FIGURE A.6 40 NSEC RISE TIME

A.5 - A.8 Left Side Illumination, E_{inc} Vertical

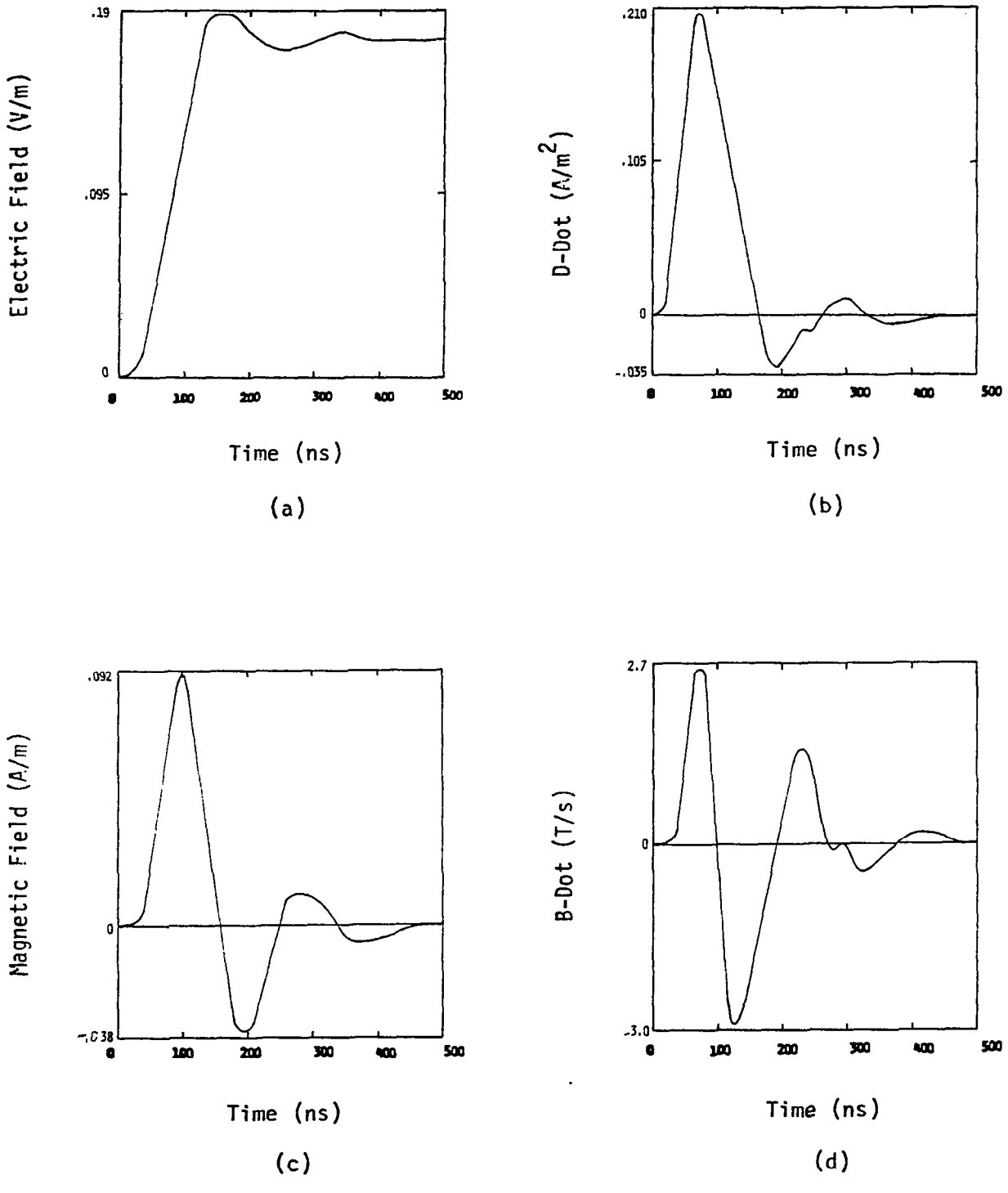

FIGURE A.7 100 NSEC RISE TIME

A.5 - A.8 Left Side Illumination, E_{inc} Vertical

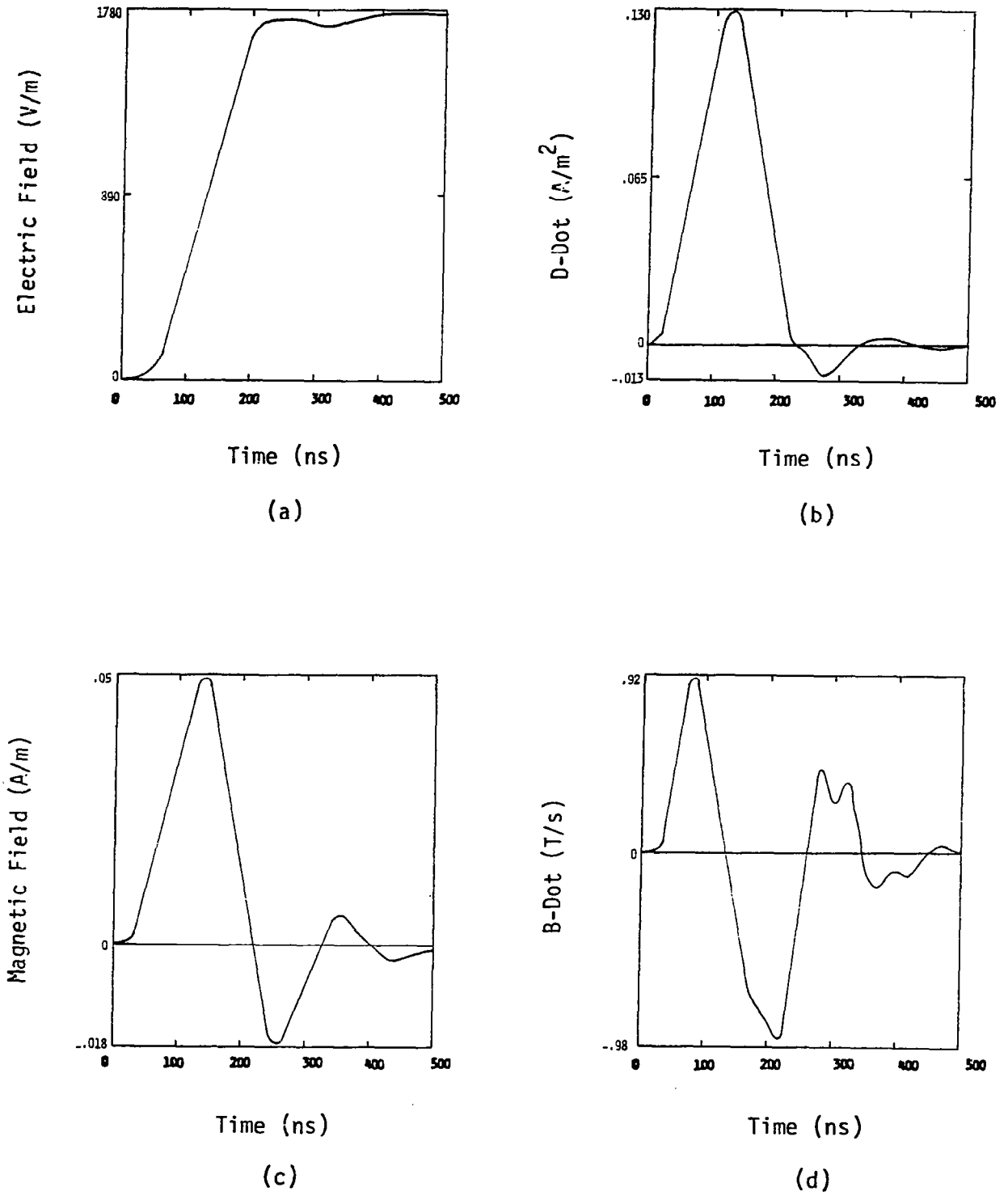

FIGURE A.8 200 NSEC RISE TIME

A.9 - A.12 Right Side Illumination, E_{inc} Toward Rear

A.9 - A.12 Right Side Illumination, E_{inc} Toward Rear

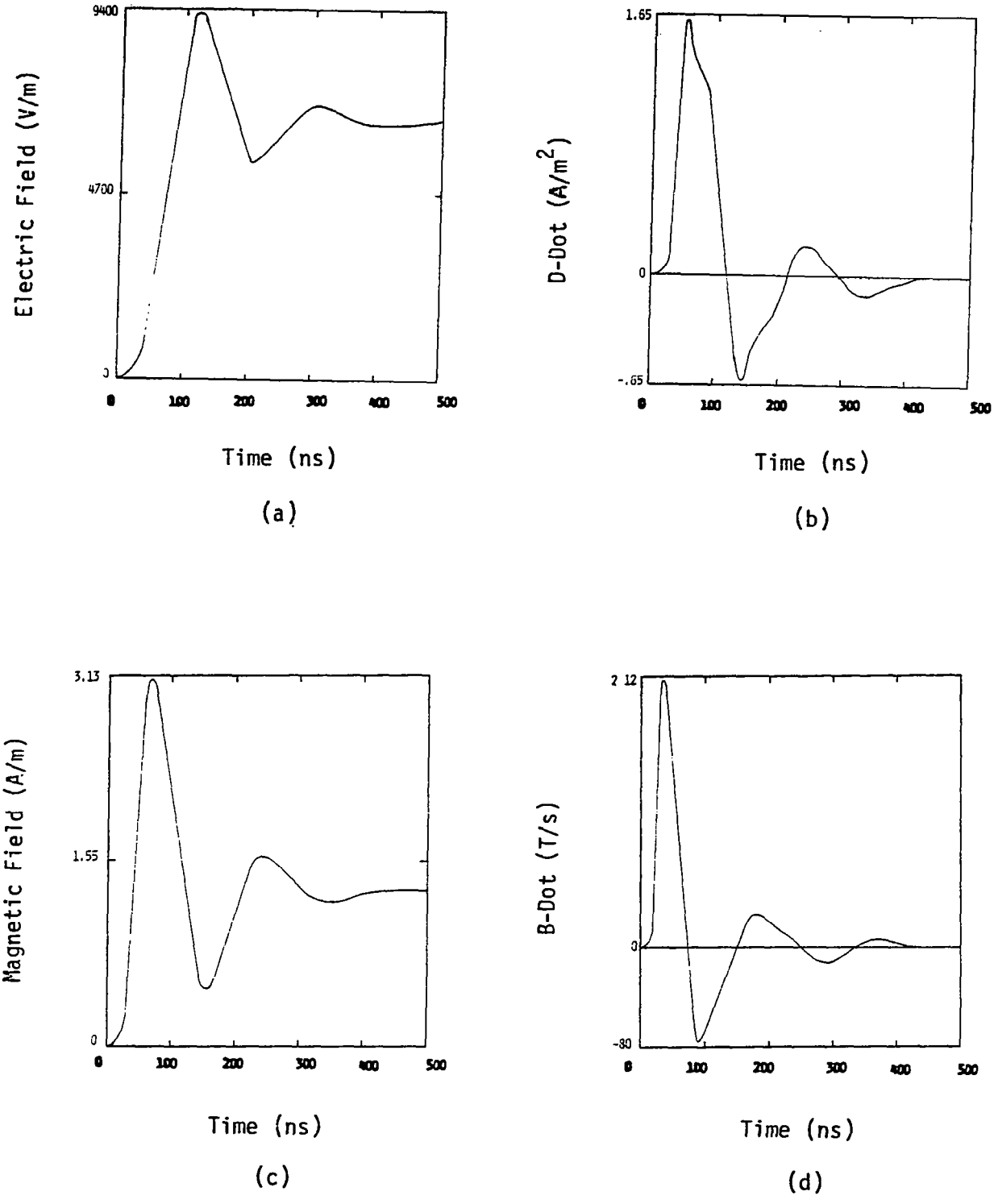

FIGURE A.9 20 NSEC RISE TIME

A.9 - A.12 Right Side Illumination, E_{inc} Toward Rear

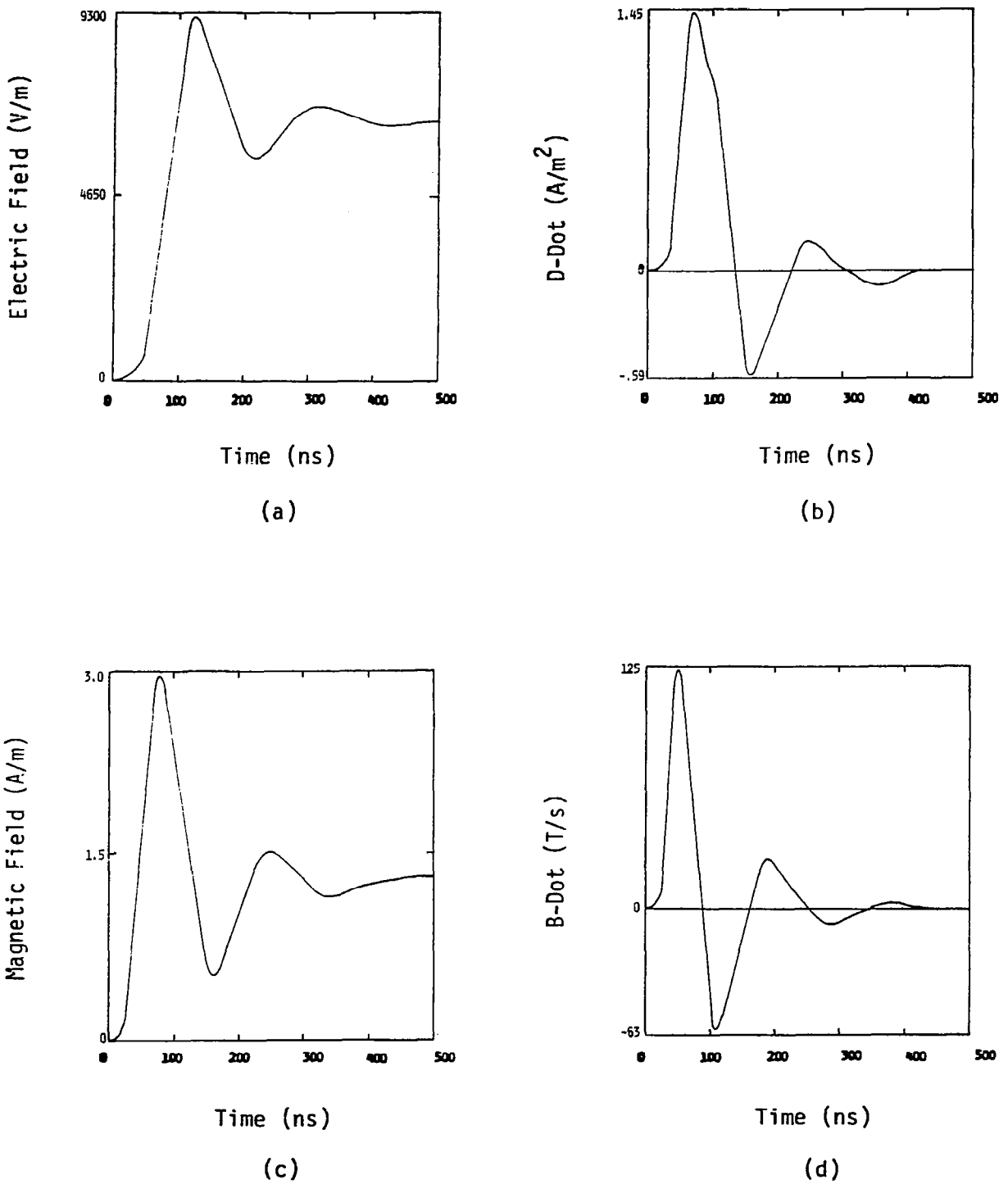

FIGURE A.10 40 NSEC RISE TIME

A.9 - A.12 Right Side Illumination, E_{inc} Toward Rear

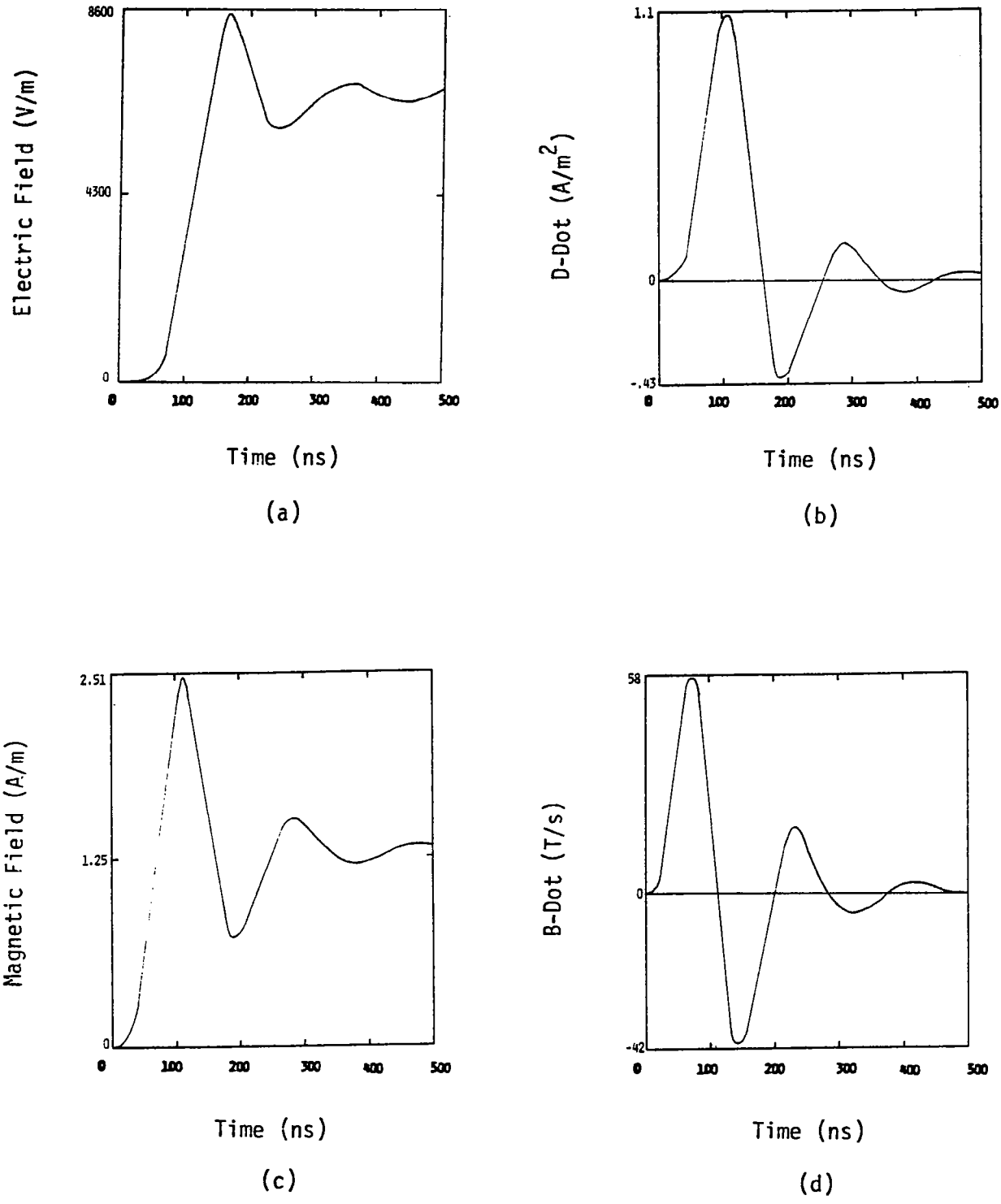

FIGURE A.11 100 NSEC RISE TIME

A.9 - A.12 Right Side Illumination, E_{inc} Toward Rear

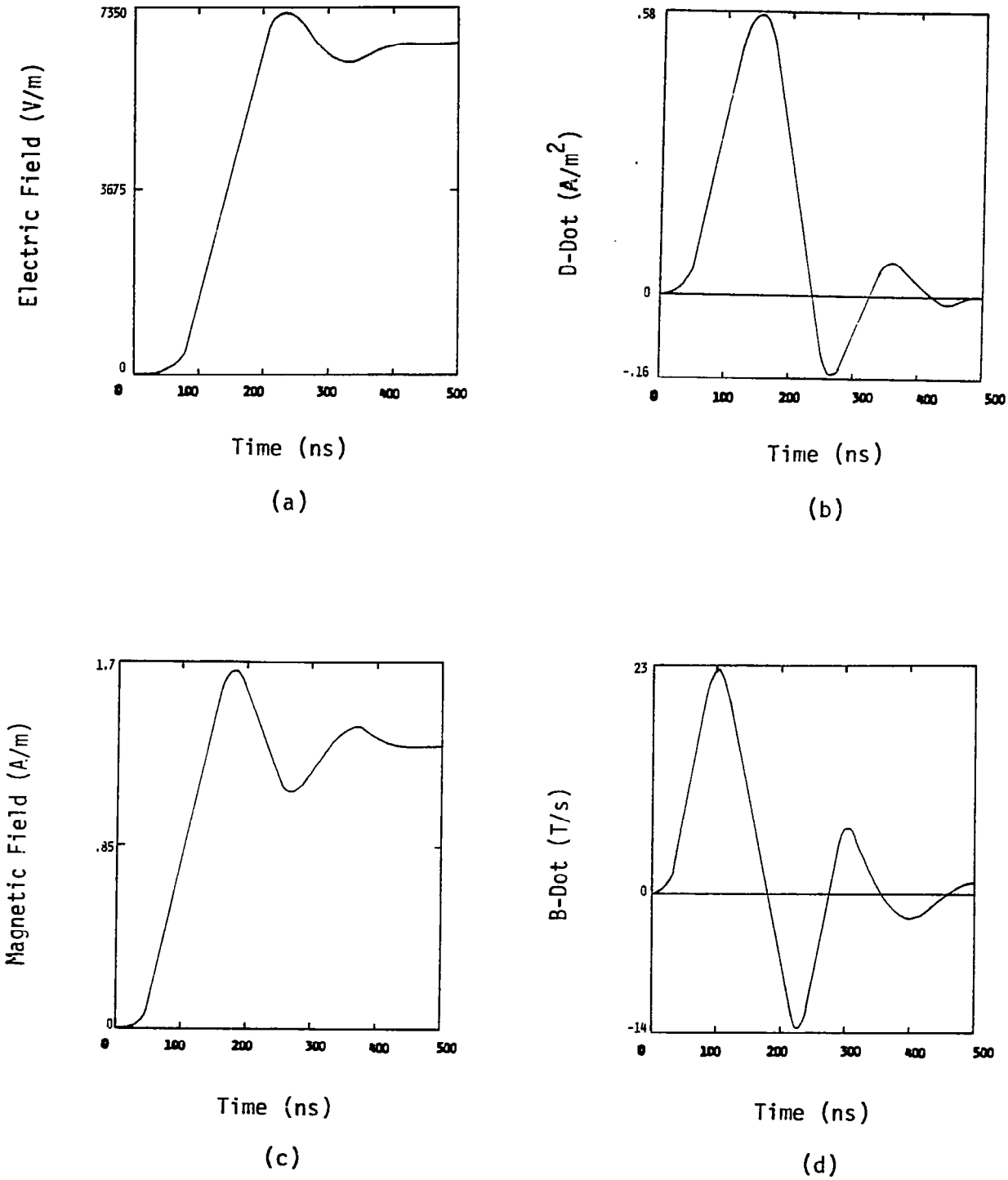

FIGURE A.12 200 NSEC RISE TIME

A.13 - A.16 Left Side Illumination, E_{inc} Toward Rear

A.13 - A.16 Left Side Illumination, E_{inc} Toward Rear

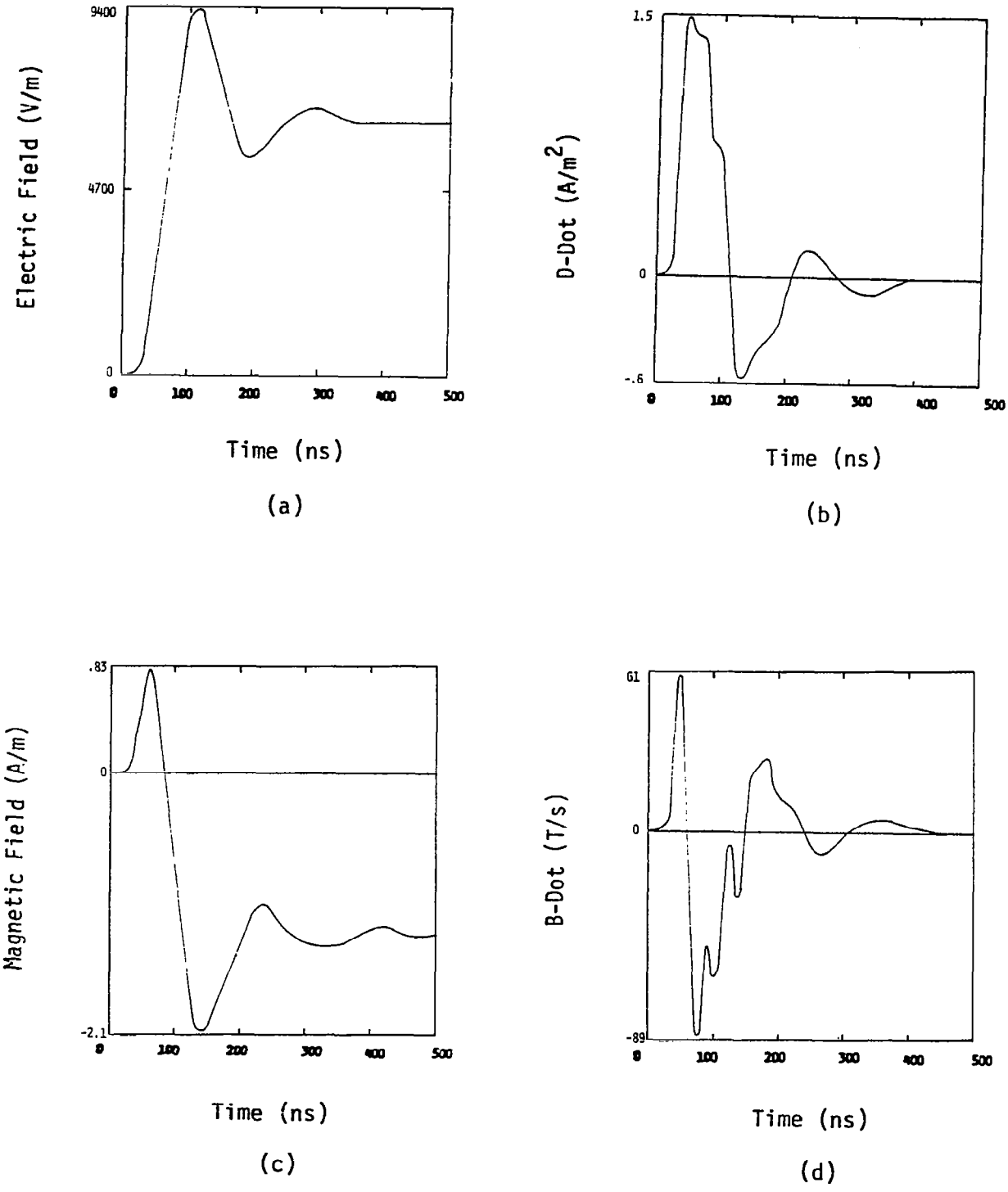

FIGURE A.13 20 NSEC RISE TIME

A.13 - A.16 Left Side Illumination, E_{inc} Toward Rear

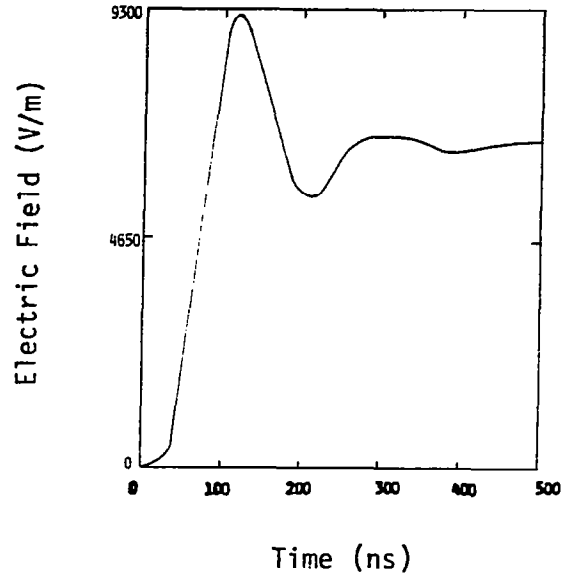

(a)

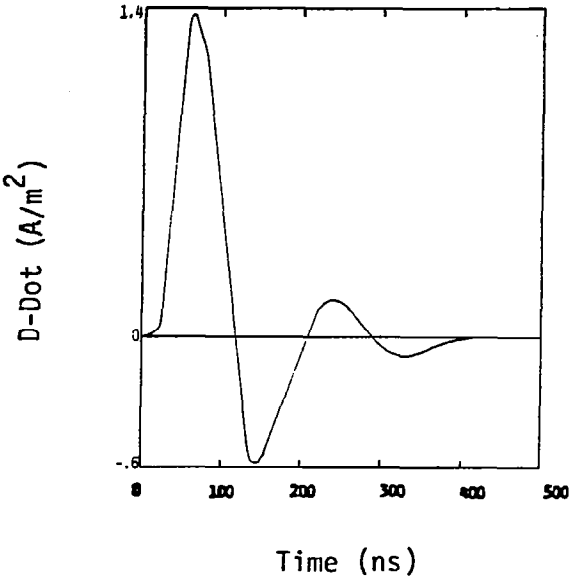

(b)

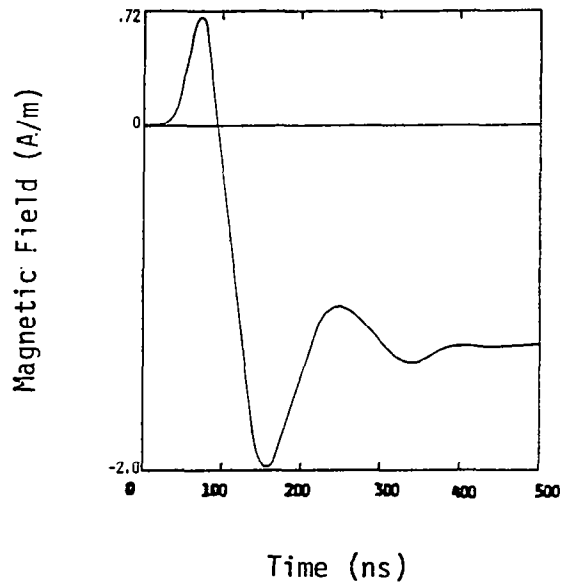

(c)

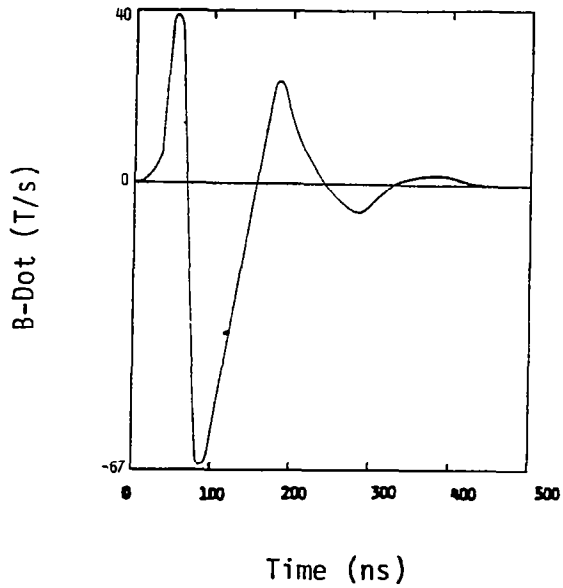

(d)

FIGURE A.14 40 NSEC RISE TIME

A.13 - A.16 Left Side Illumination, E_{inc} Toward Rear

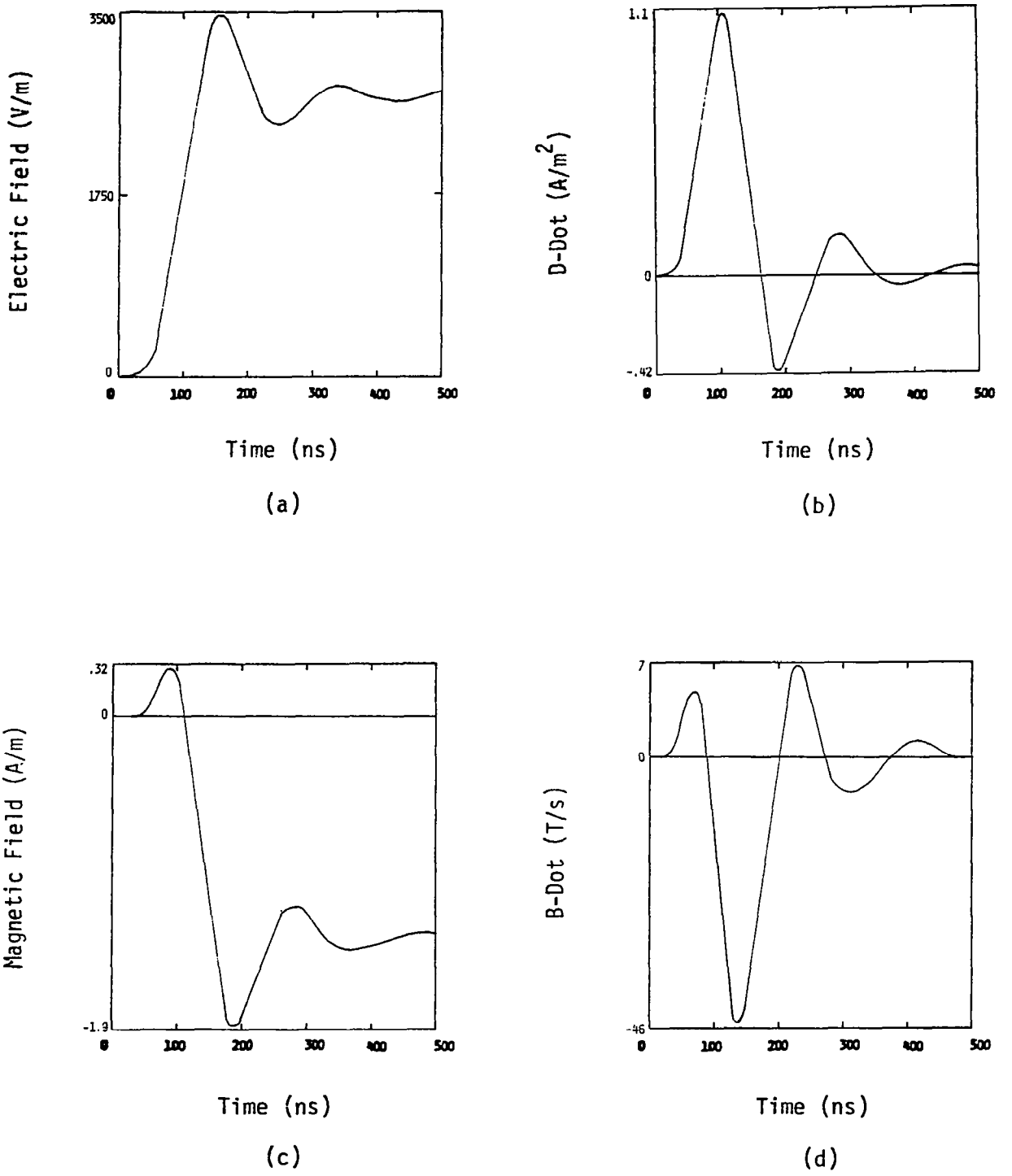

FIGURE A.15 100 NSEC RISE TIME

A.13 - A.16 Left Side Illumination, E_{inc} Toward Rear

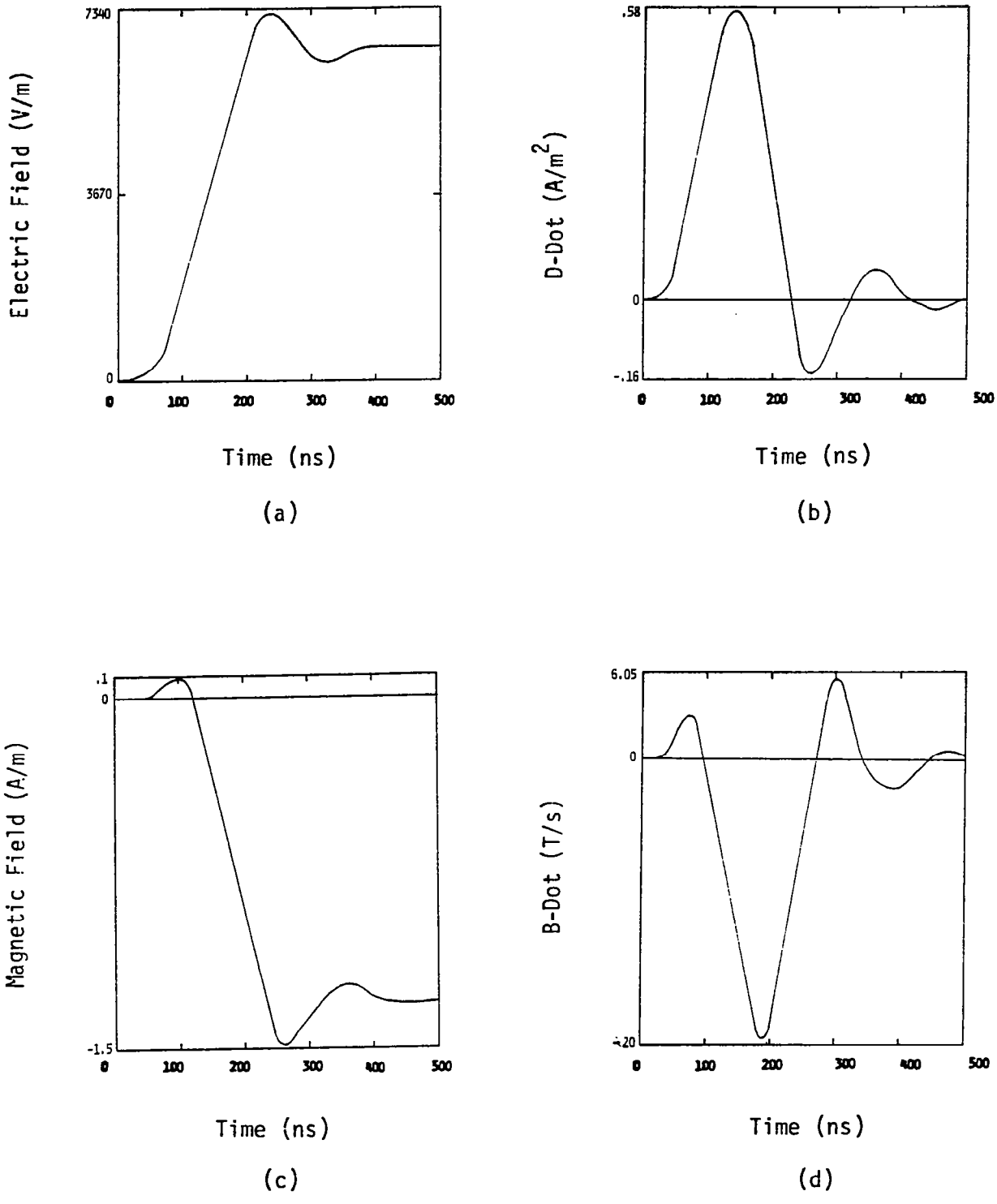

FIGURE A.16 200 NSEC RISE TIME

A.17 - A.20 Bottom Illumination, E_{inc} Toward Left (Port)

A.17 - A.20 Bottom Illumination, E_{inc} Toward Left (Port)

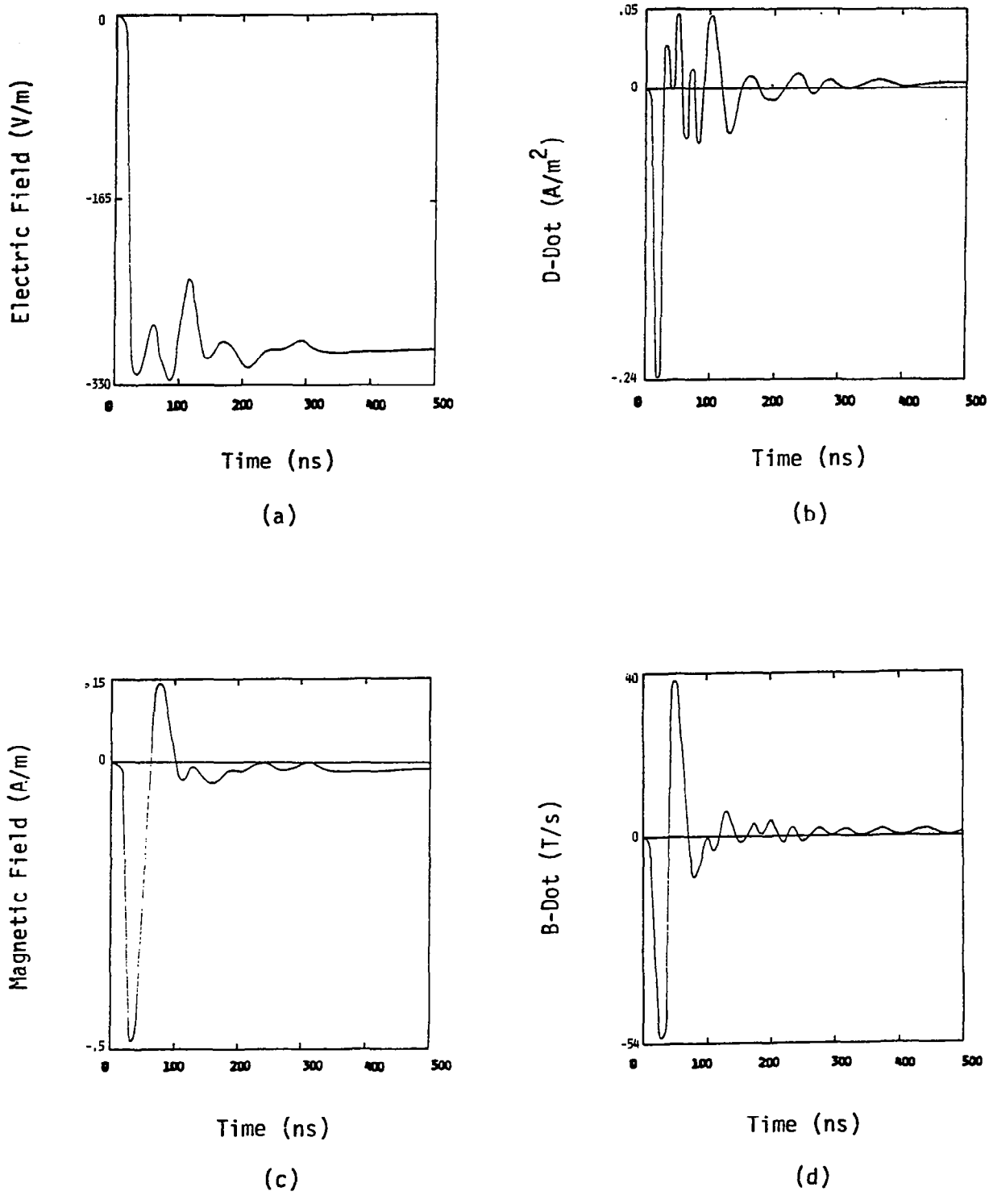

FIGURE A.17 20 NSEC RISE TIME

A.17 - A.20 Bottom Illumination, E_{inc} Toward Left (Port)

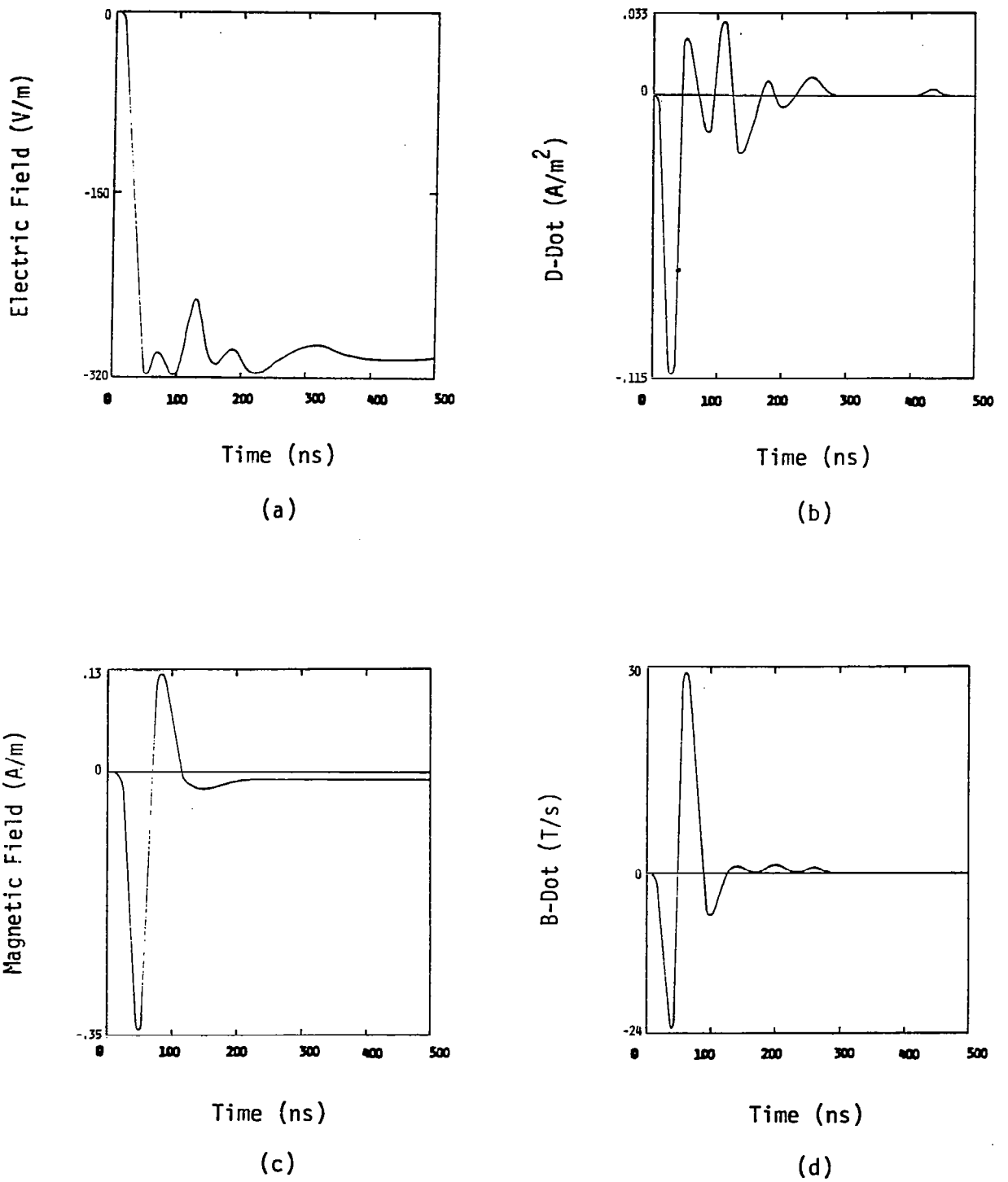

FIGURE A.18 40 NSEC RISE TIME

A.17 - A.20 Bottom Illumination, E_{inc} Toward Left (Port)

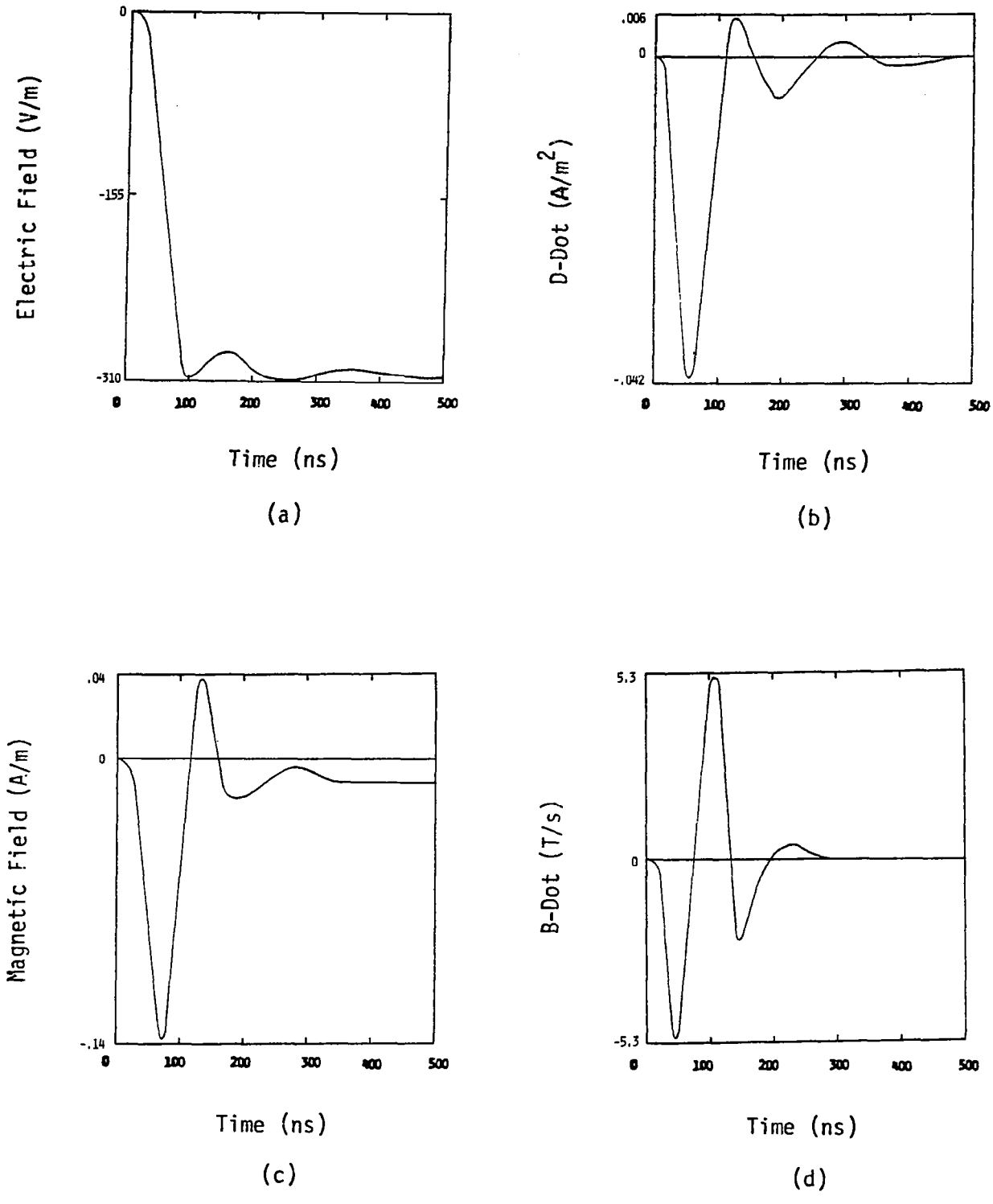

FIGURE A.19 100 NSEC RISE TIME

A.17 - A.20 Bottom Illumination, E_{inc} Toward Left (Port)

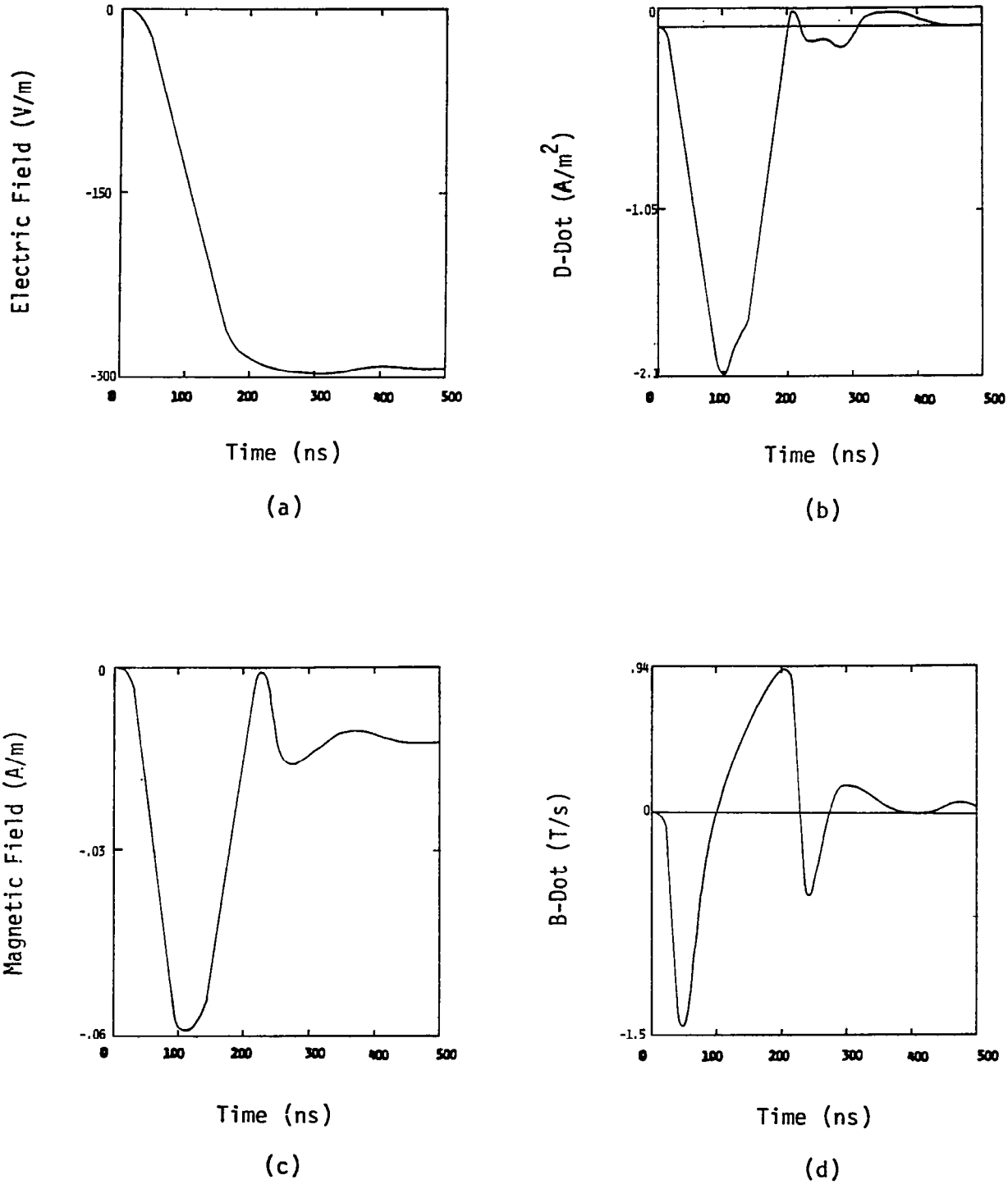

FIGURE A.20 200 NSEC RISE TIME

A.21 - A.24 Top Illumination, E_{inc} Toward Left (Port)

A.21 - A.24 Top Illumination, E_{inc} Toward Left (Port)

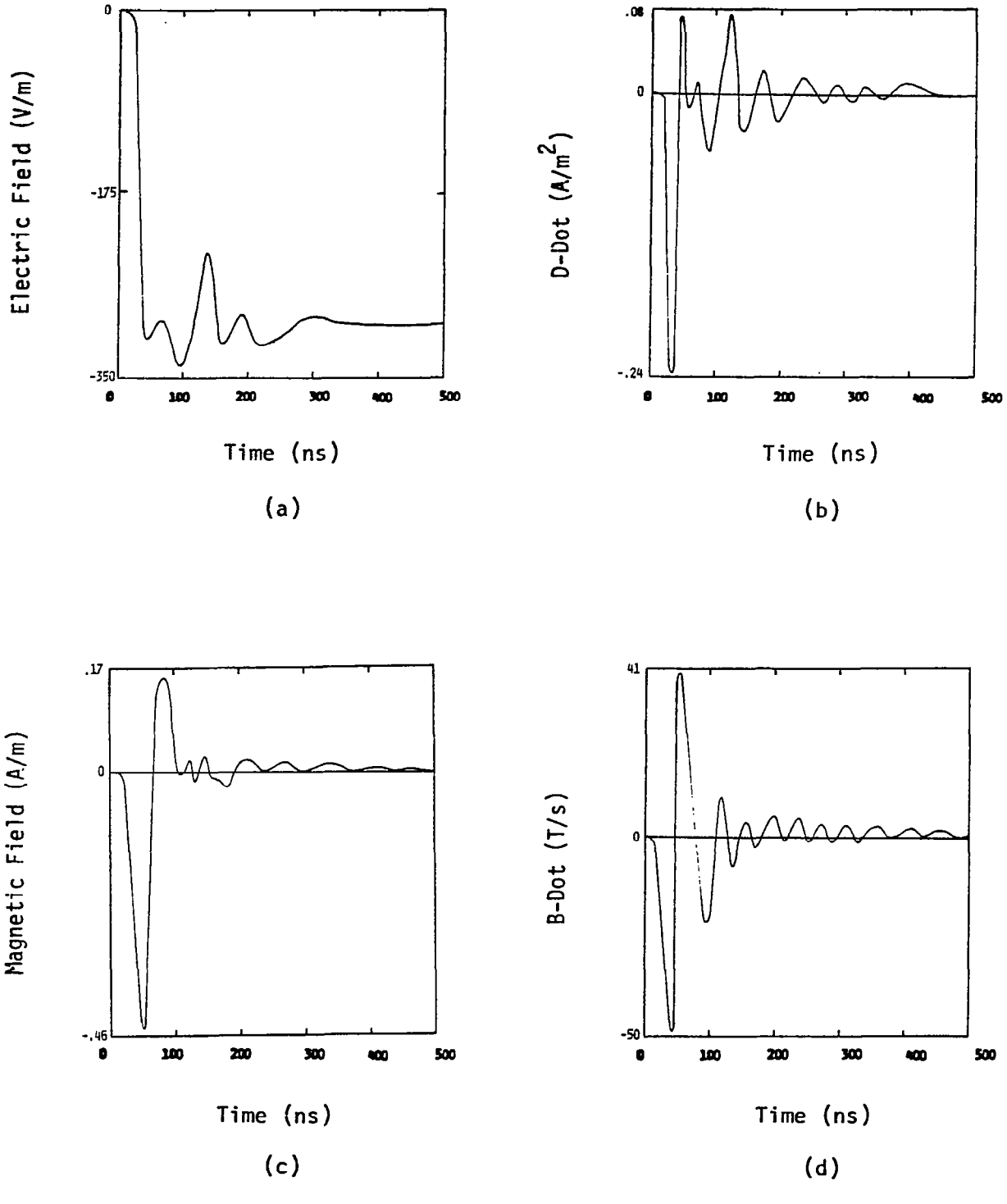

FIGURE A.21 20 NSEC RISE TIME

A.21 - A.24 Top Illumination, E_{inc} Toward Left (Port)

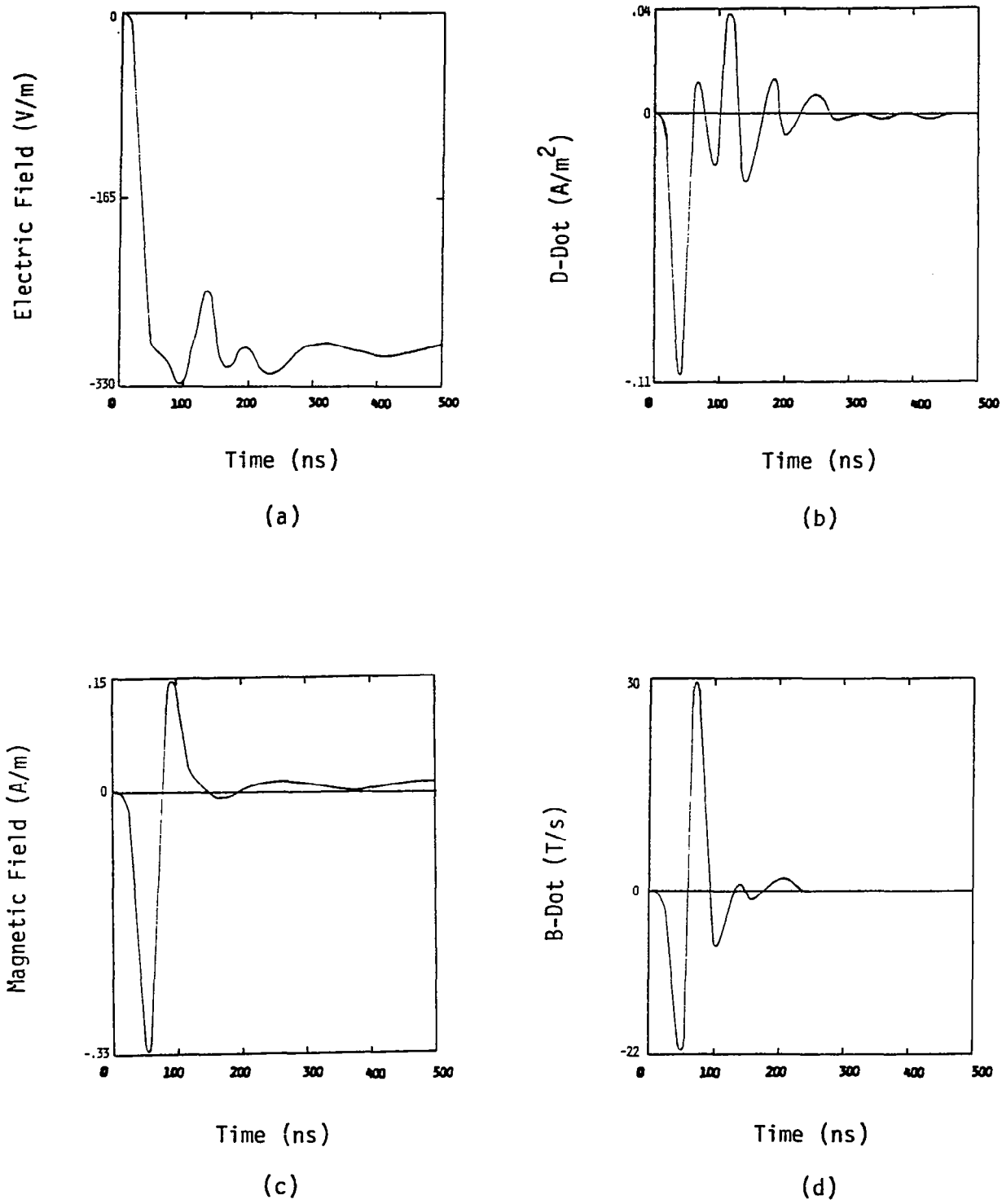

FIGURE A.22 40 NSEC RISE TIME

A.21 - A.24 Top Illumination, E_{inc} Toward Left (Port)

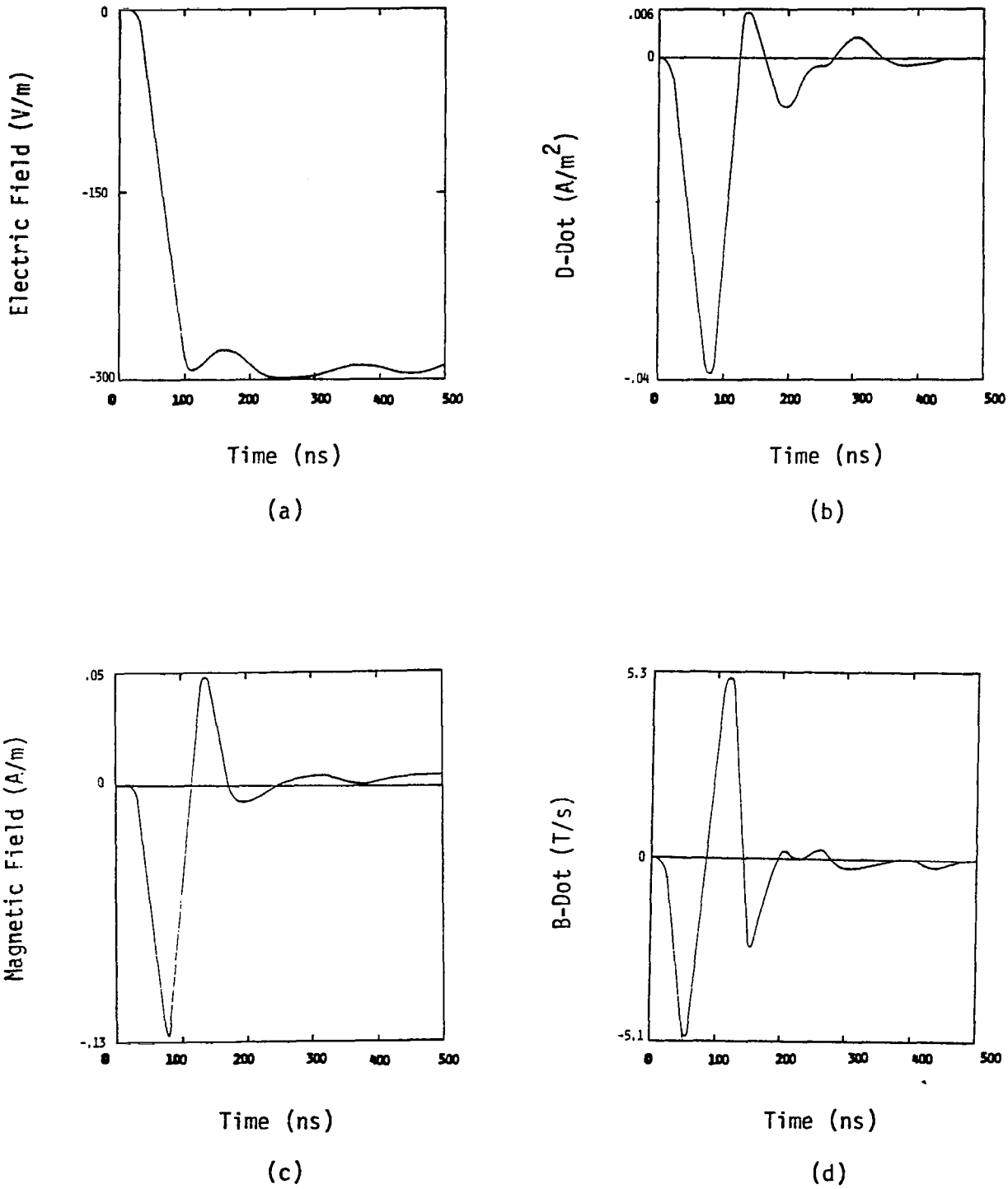

FIGURE A.23 100 NSEC RISE TIME

A.21 - A.24 Top Illumination, E_{inc} Toward Left (Port)

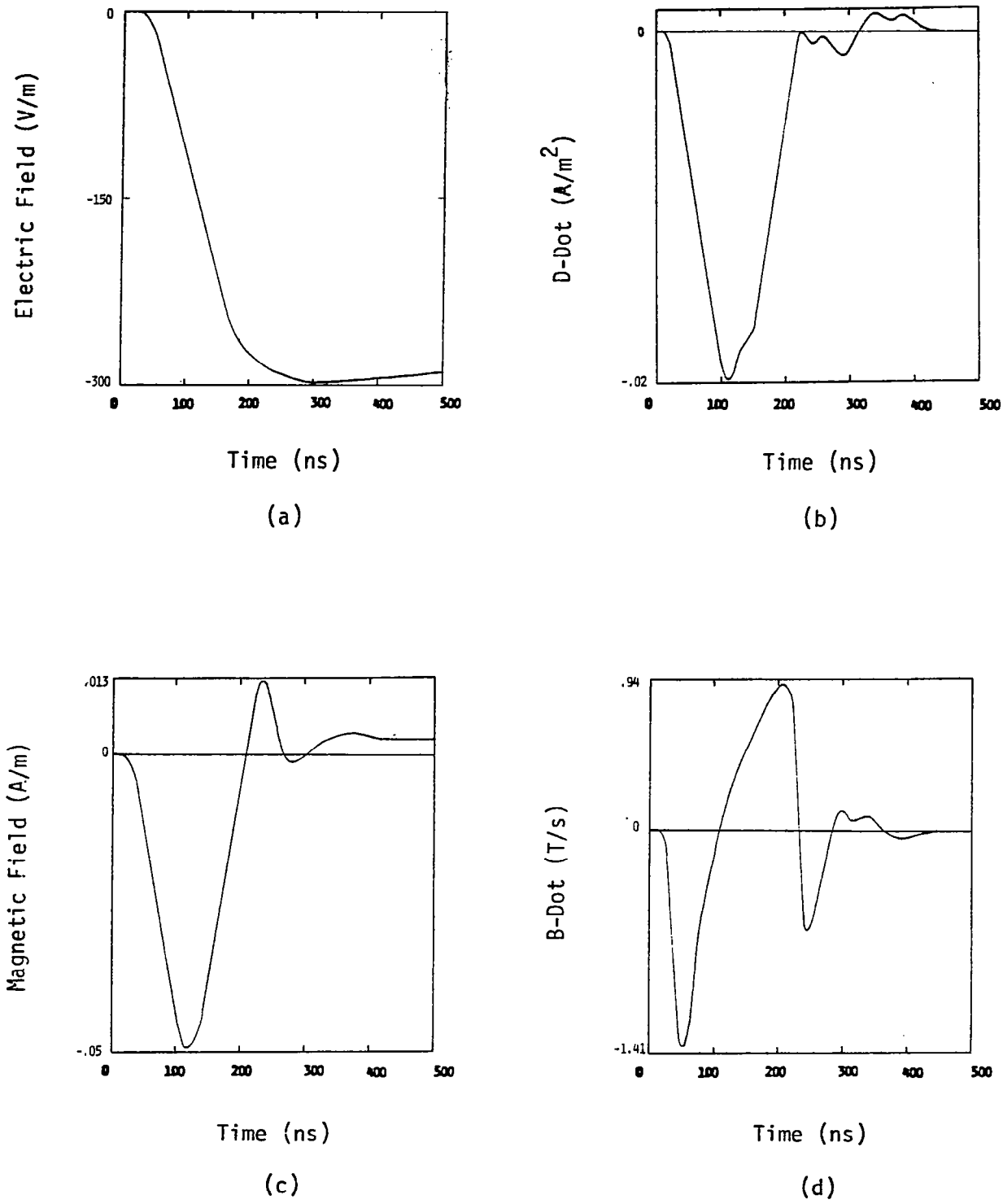

FIGURE A.24 200 NSEC RISE TIME

A.25 - A.28 Bottom Illumination, E_{inc} Toward Rear

A.25 - A.28 Bottom Illumination, E_{inc} Toward Rear

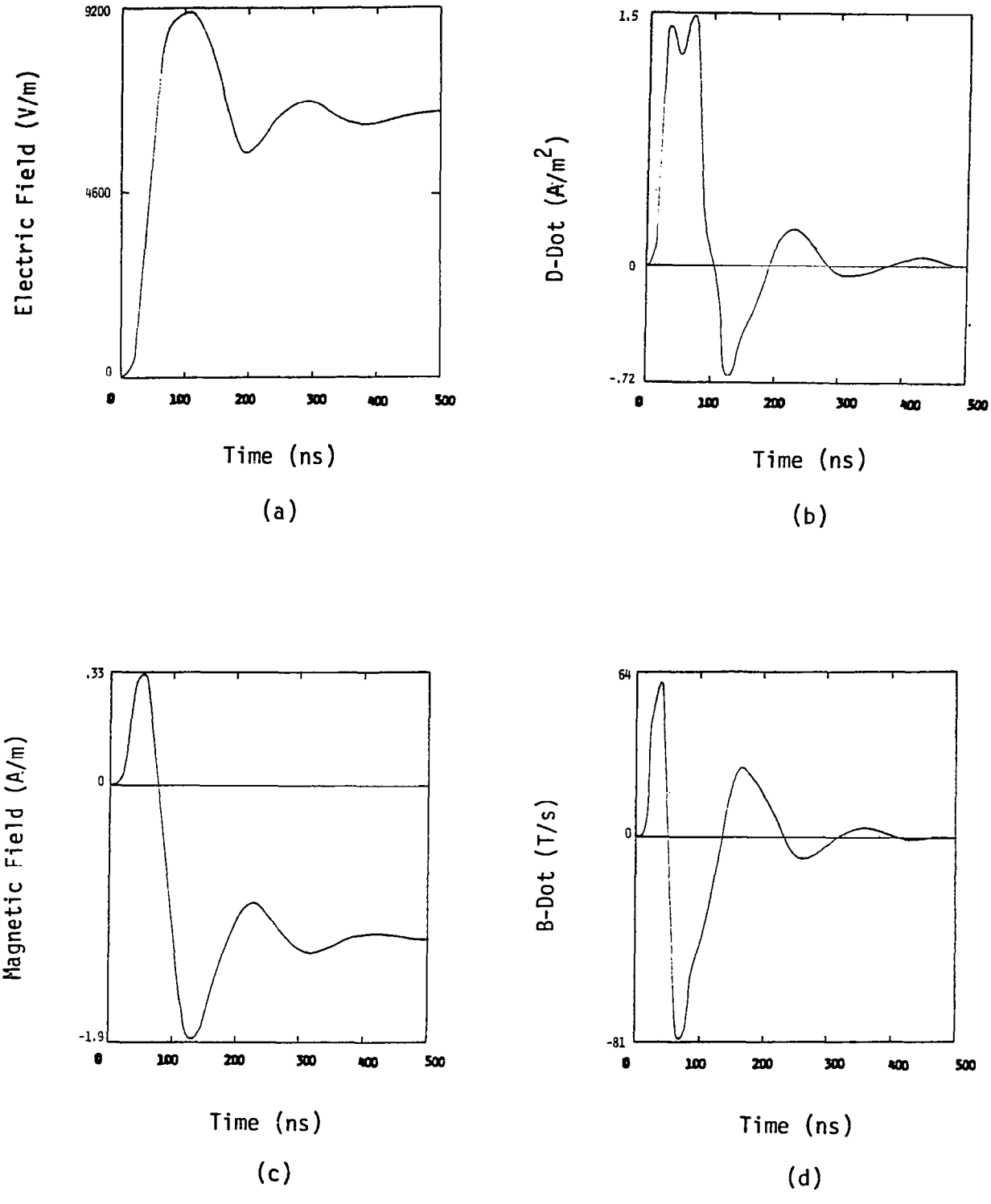

FIGURE A.25 20 NSEC RISE TIME

A.25 - A.28 Bottom Illumination, E_{inc} Toward Rear

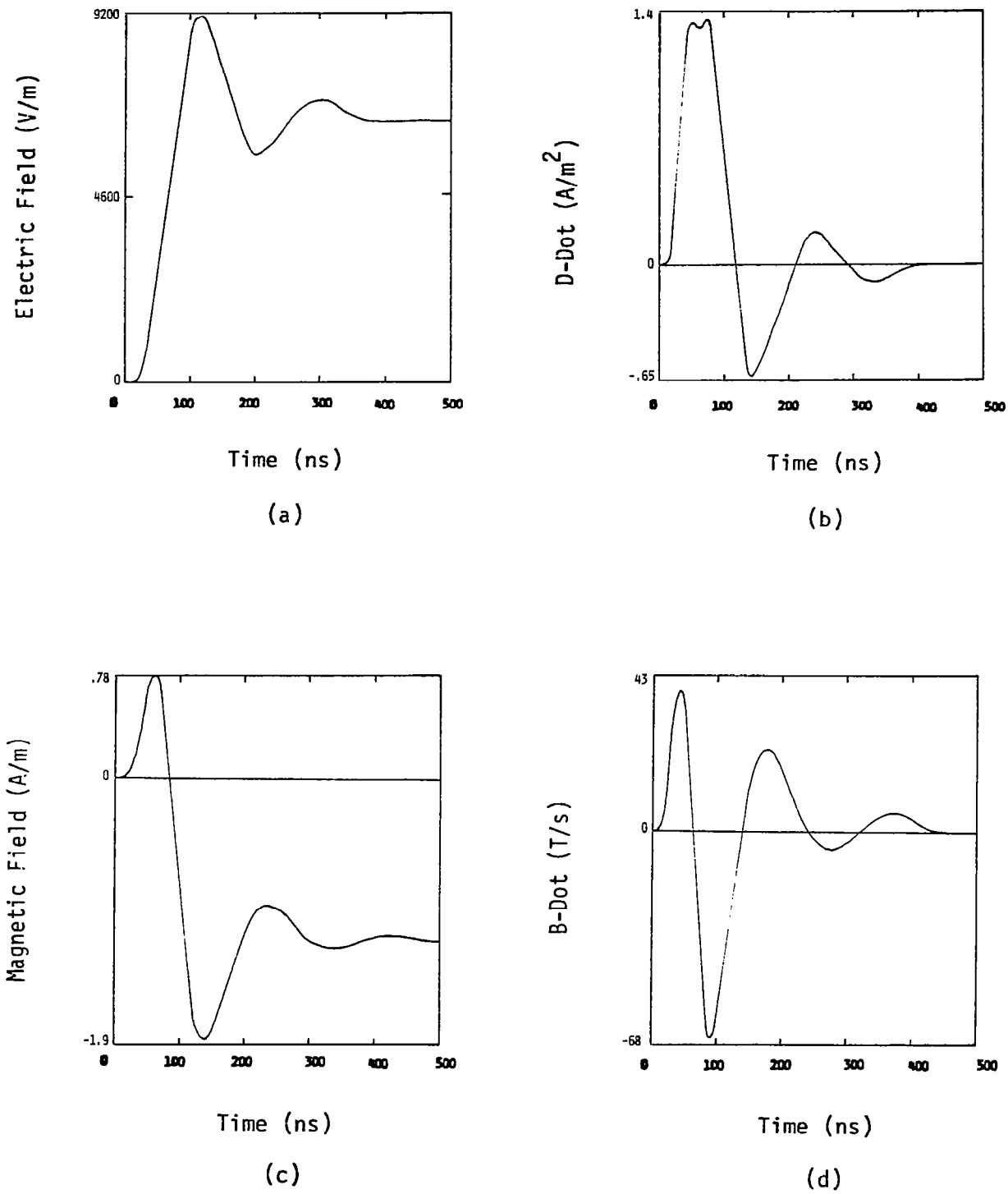

FIGURE A.26 40 NSEC RISE TIME

A.25 - A.28 Bottom Illumination, E_{inc} Toward Rear

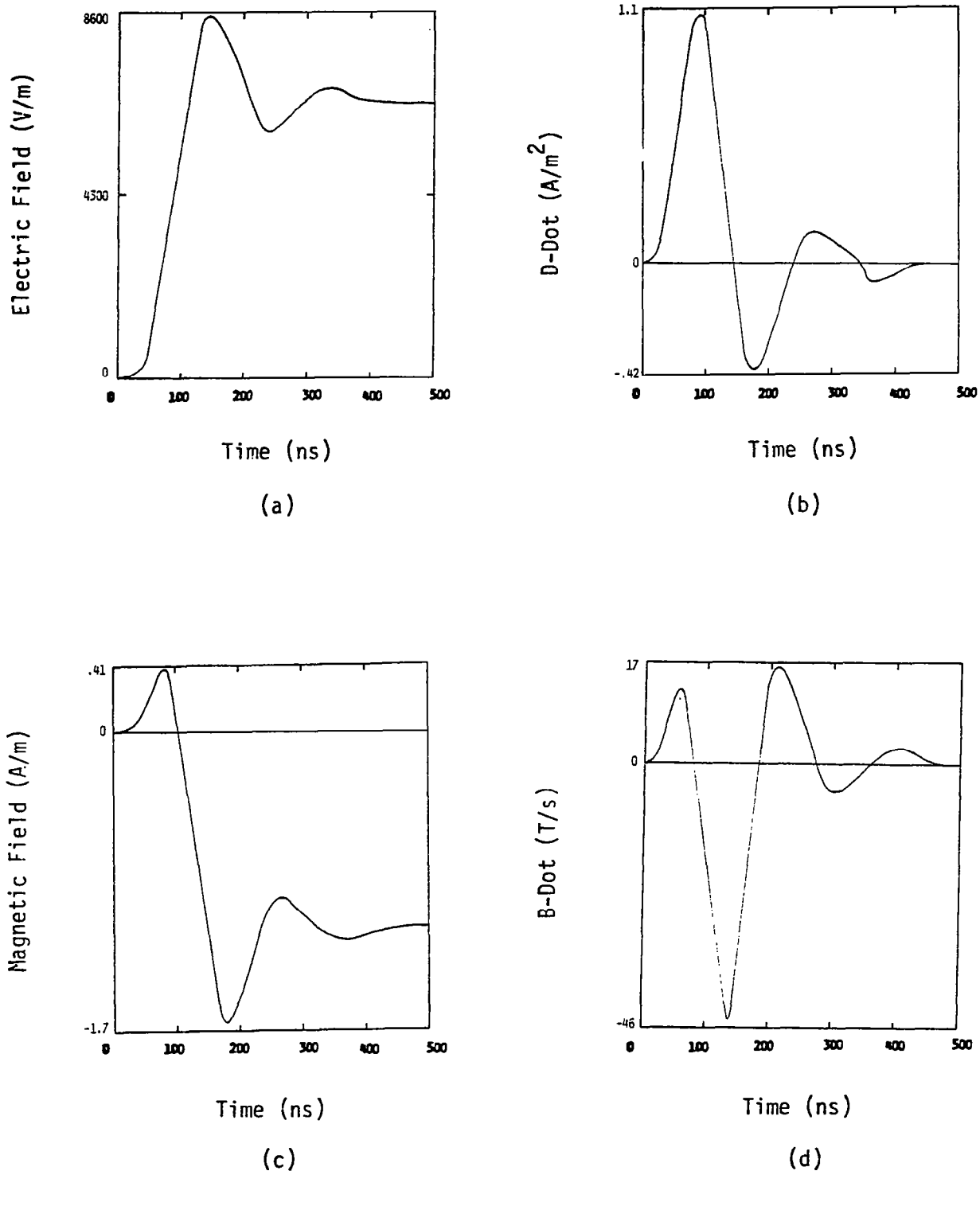

FIGURE A.27 100 NSEC RISE TIME

A.25 - A.28 Bottom Illumination, E_{inc} Toward Rear

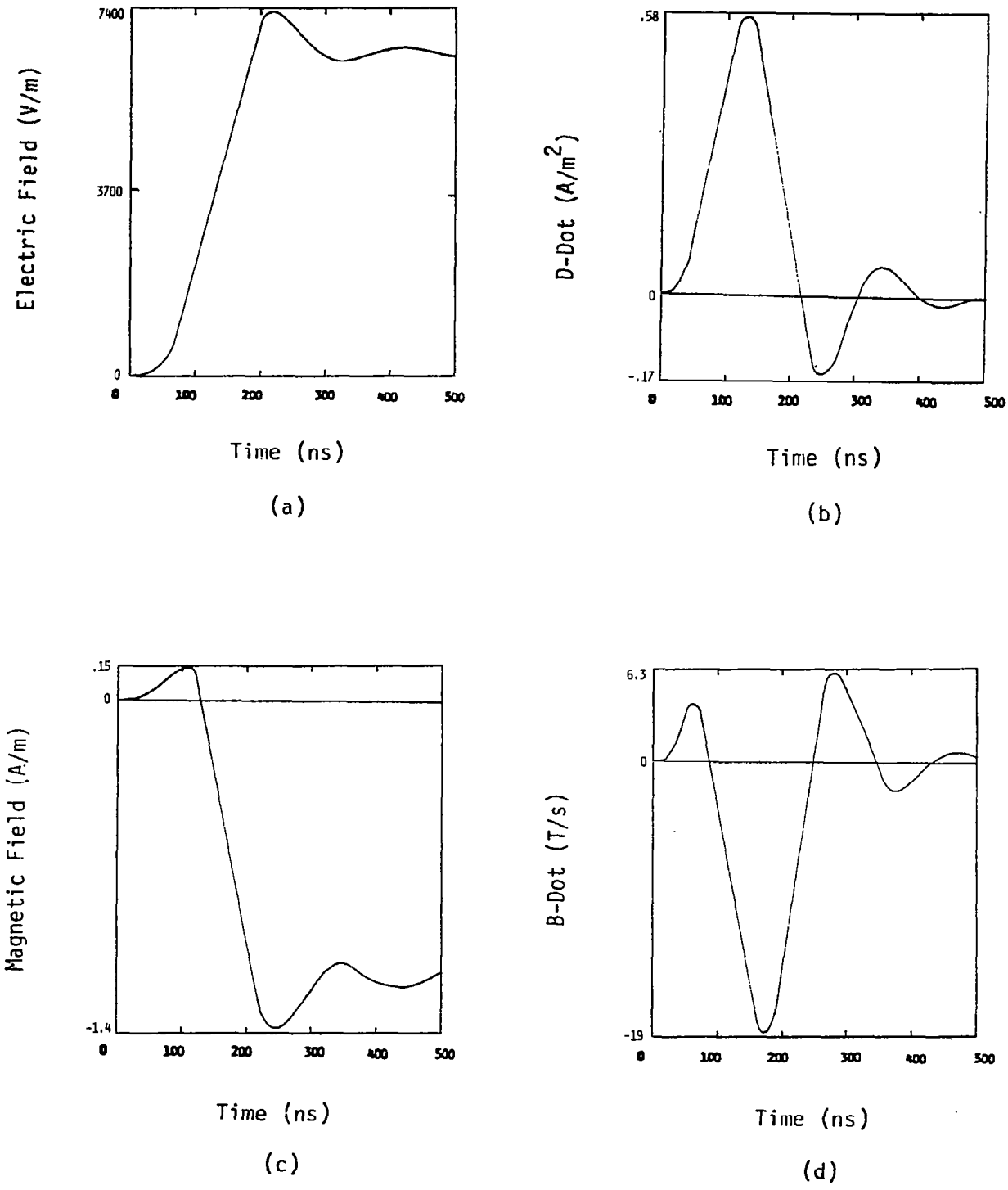

FIGURE A.28 200 NSEC RISE TIME

A.29 - A.32 Top Illumination, E_{inc} Toward Rear

A.29 - A.32 Top Illumination, E_{inc} Toward Rear

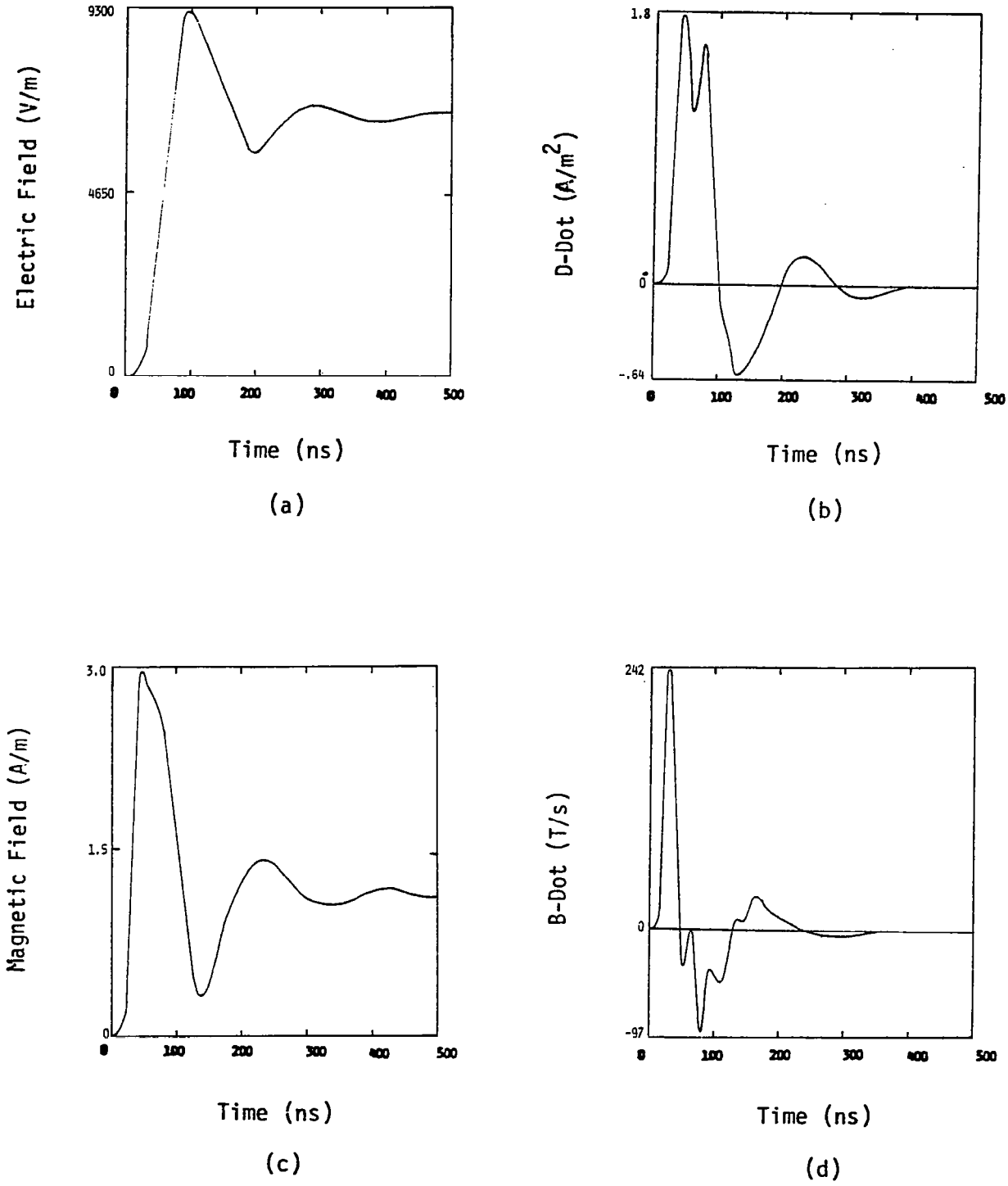

FIGURE A.29 20 NSEC RISE TIME

A.29 - A.32 Top Illumination, E_{inc} Toward Rear

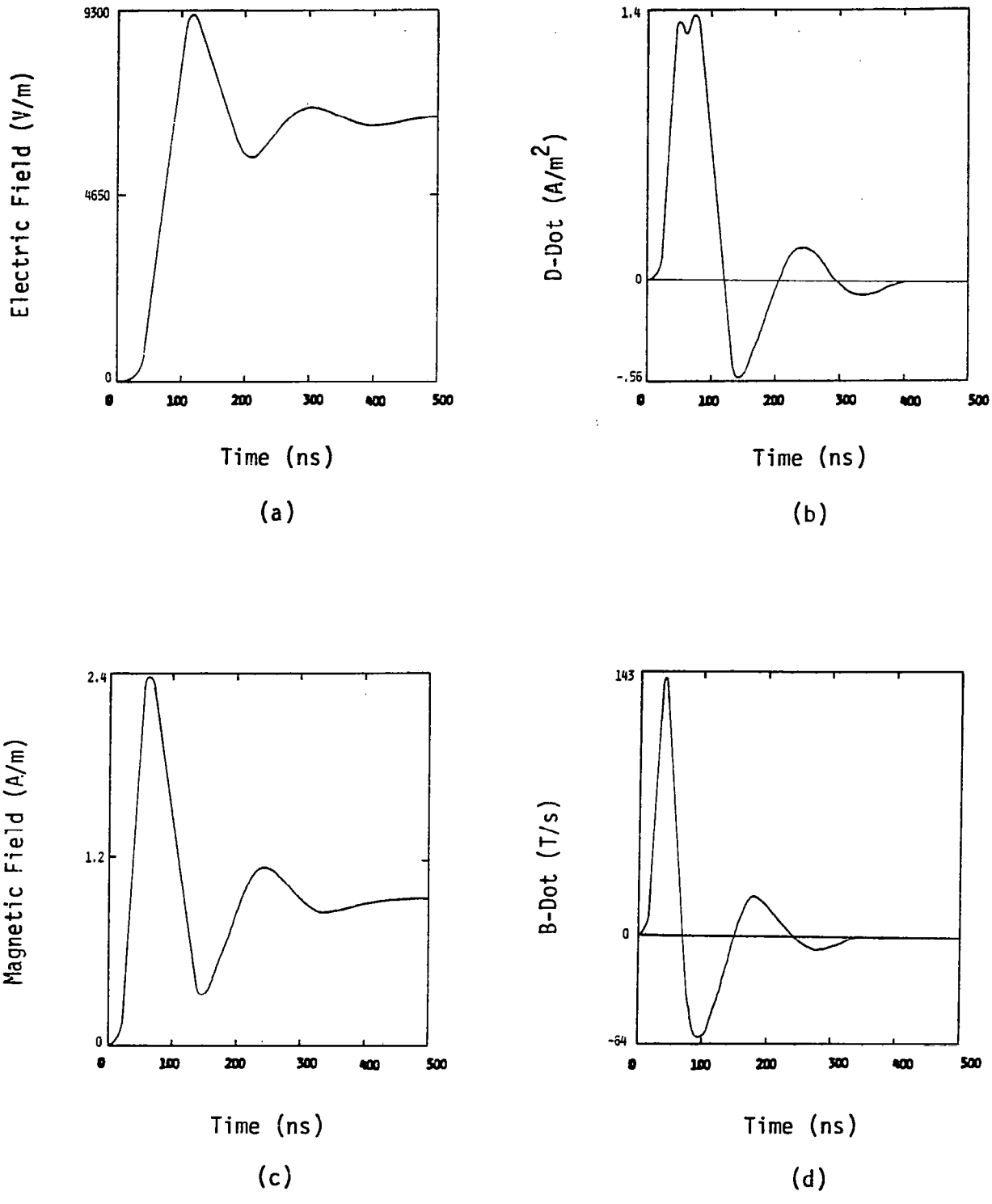

FIGURE A.30 40 NSEC RISE TIME

A.29 - A.32 Top Illumination, E_{inc} Toward Rear

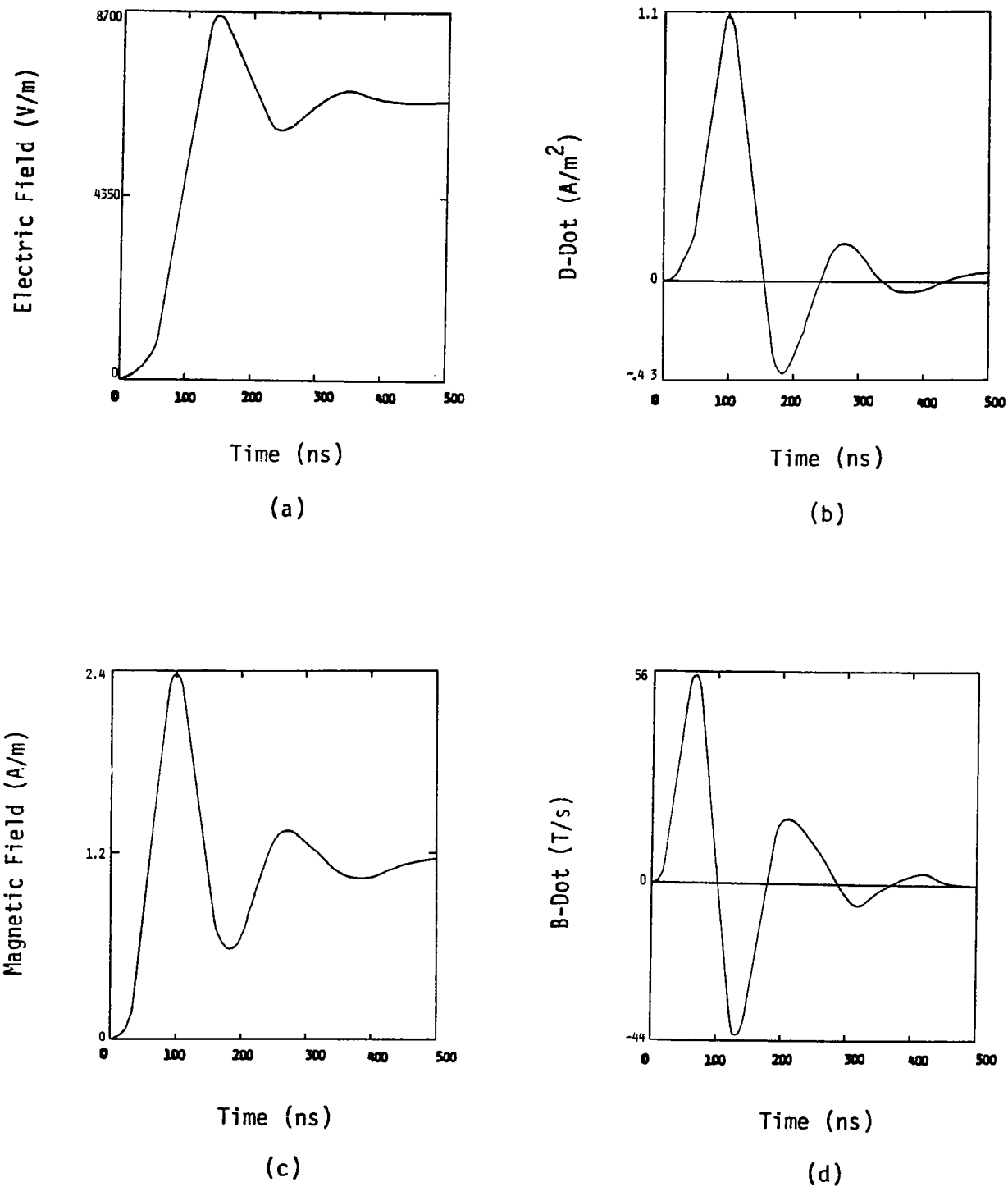

FIGURE A.31 100 NSEC RISE TIME

A.29 - A.32 Top Illumination, E_{inc} Toward Rear

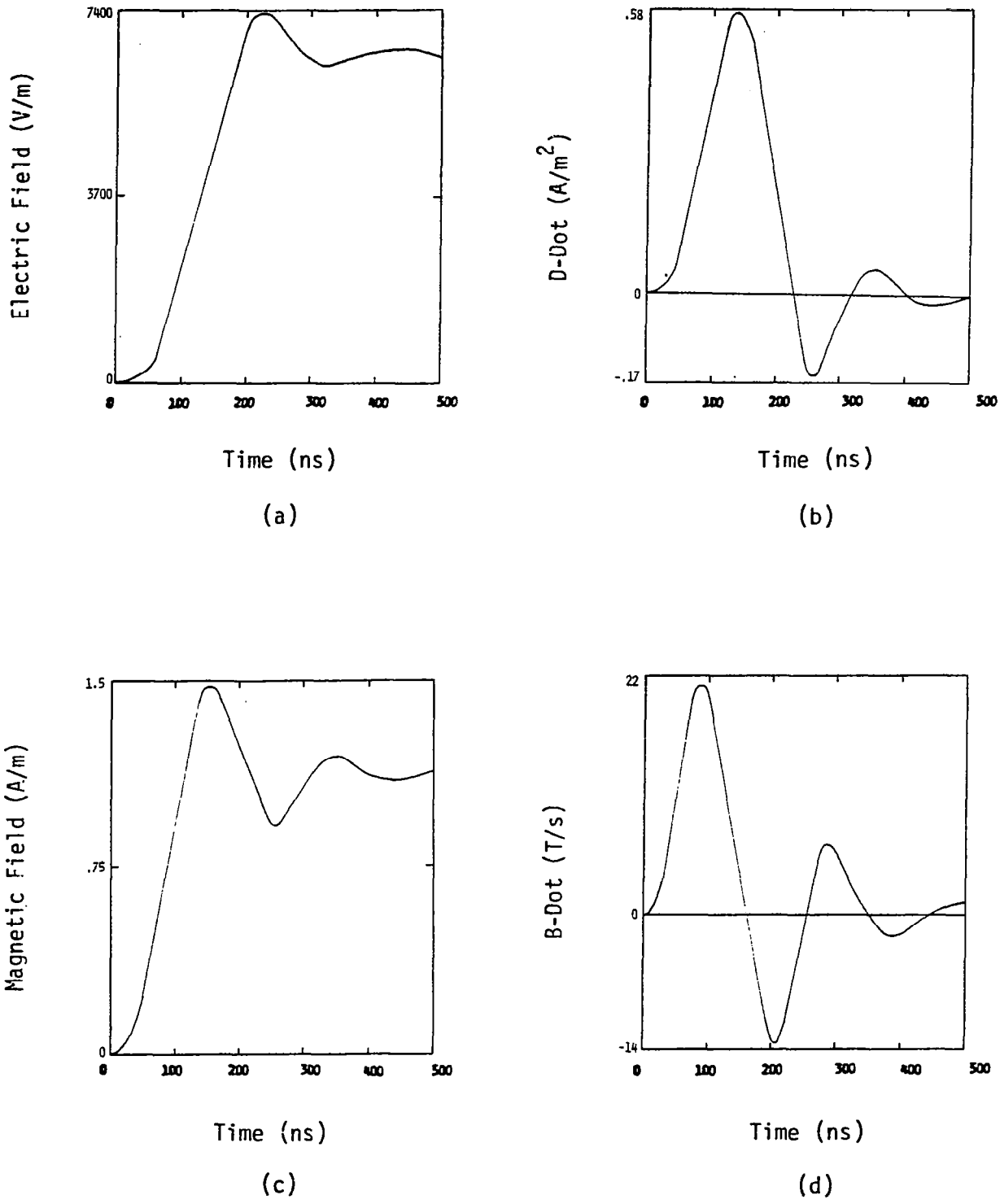

FIGURE A.32 200 NSEC RISE TIME

A.33 - A.36 Front Illumination, E_{inc} Toward Left (Port)

A.33 - A.36 Front Illumination, E_{inc} Toward Left (Port)

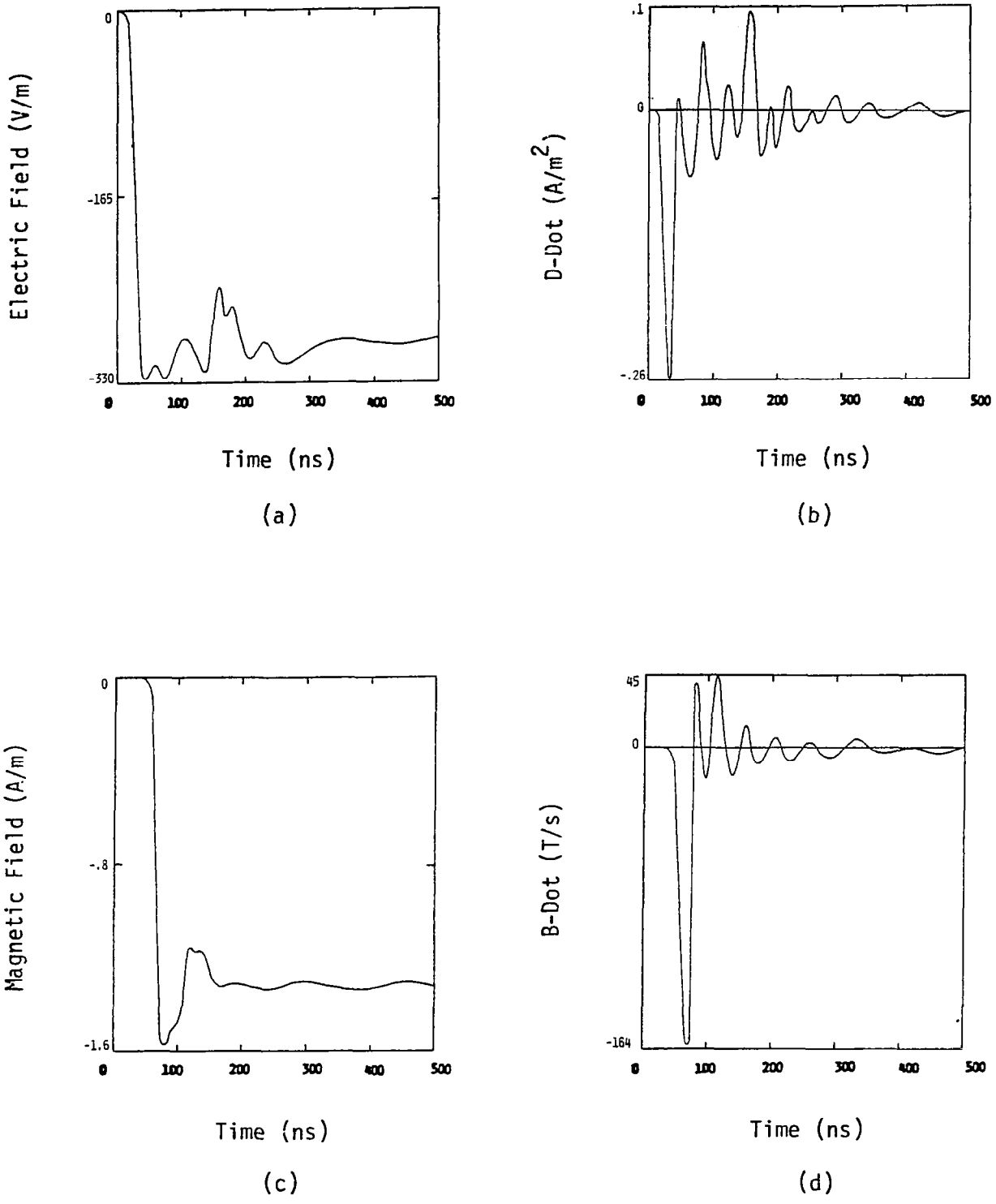

FIGURE A.33 20 NSEC RISE TIME

A.33 - A.36 Front Illumination, E_{inc} Toward Left (Port)

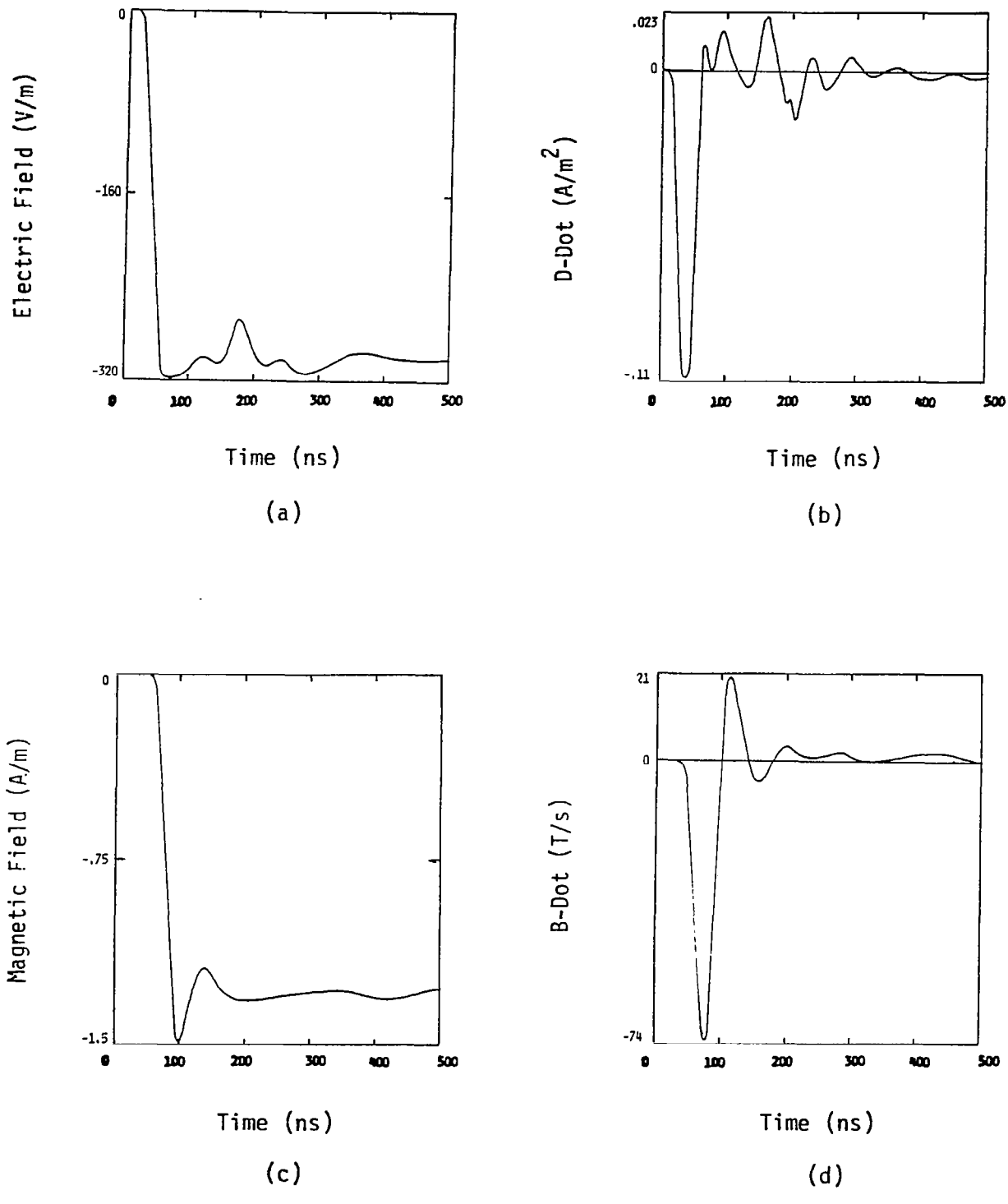

FIGURE A.34 40 NSEC RISE TIME

A.33 - A.36 Front Illumination, E_{inc} Toward Left (Port)

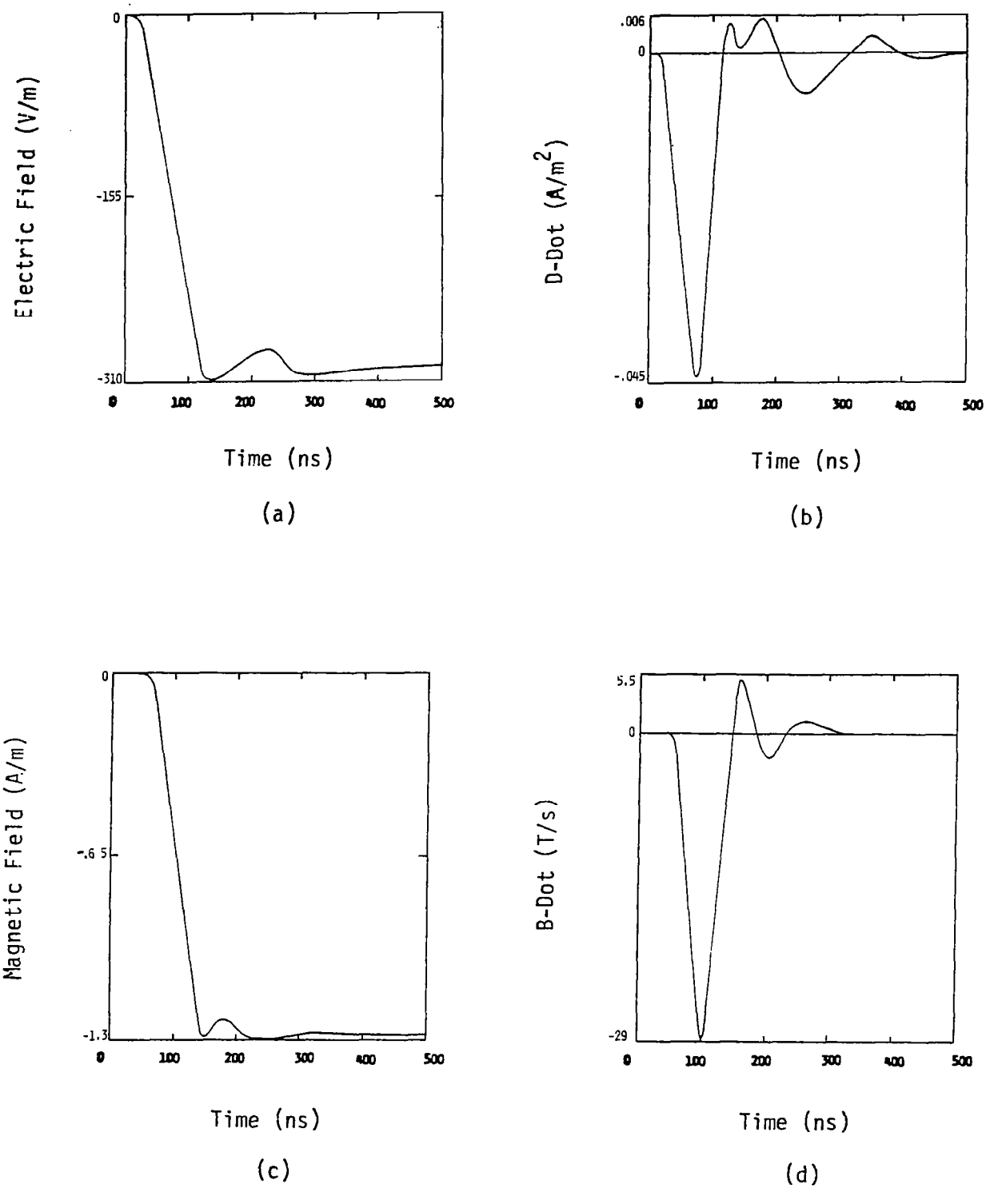

FIGURE A.35 100 NSEC RISE TIME

A.33 - A.36 Front Illumination, E_{inc} Toward Left (Port)

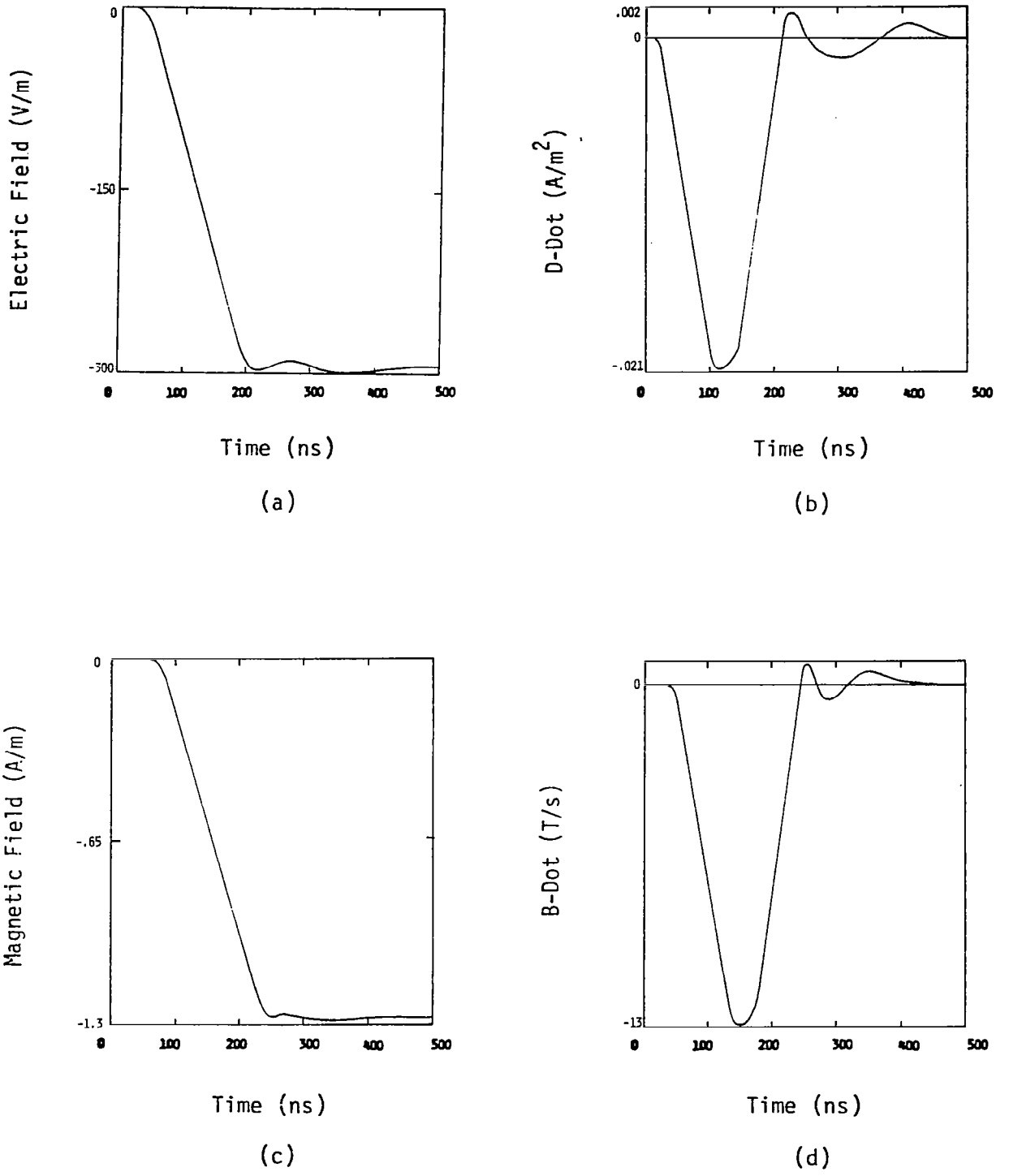

FIGURE A.36 200 NSEC RISE TIME

A.37 - A.40 Rear Illumination, E_{inc} Toward Left (Port)

A.37 - A.40 Rear Illumination, E_{inc} Toward Left (Port)

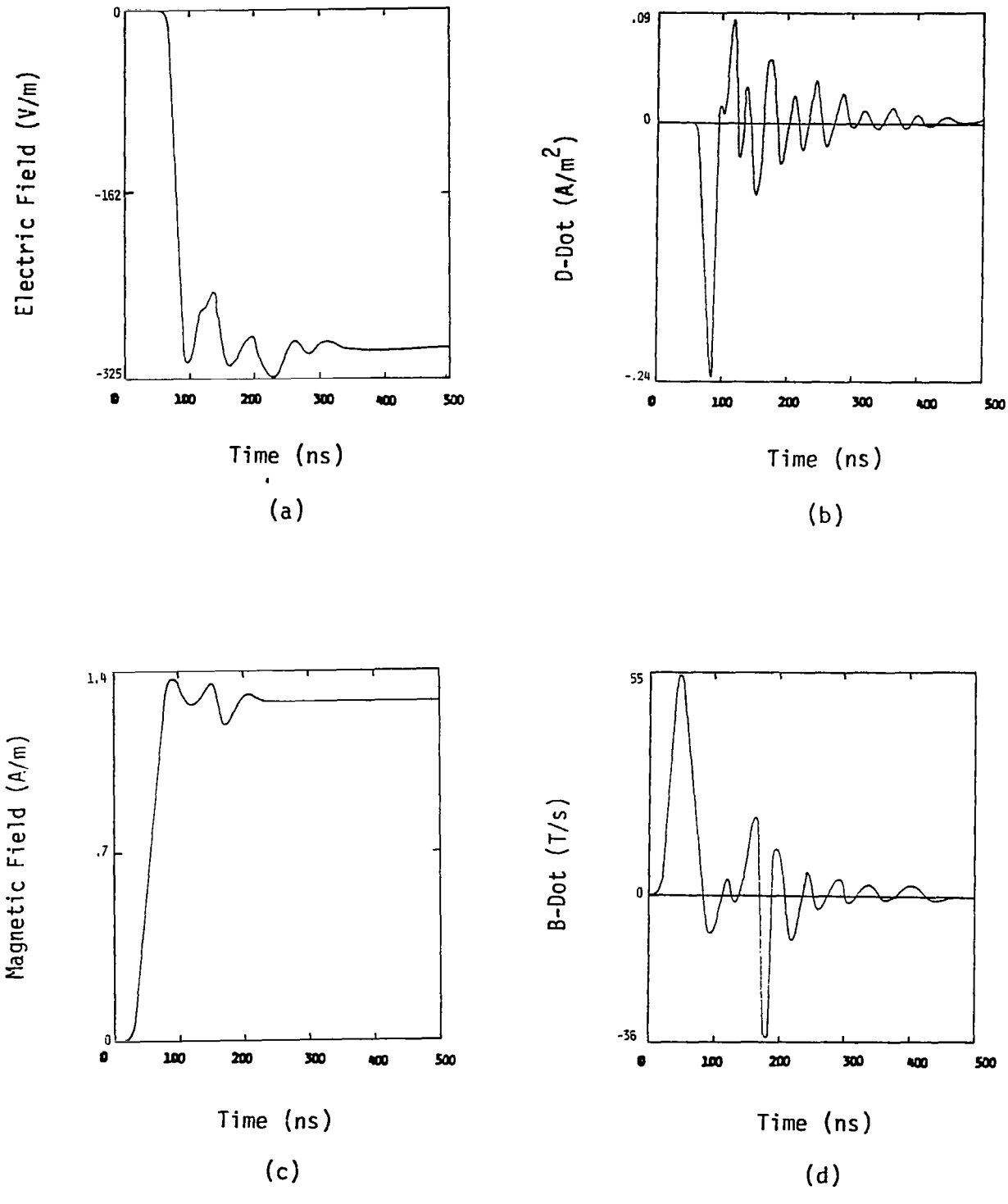

FIGURE A.37 20 NSEC RISE TIME

A.37 - A.40 Rear Illumination, E_{inc} Toward Left (Port)

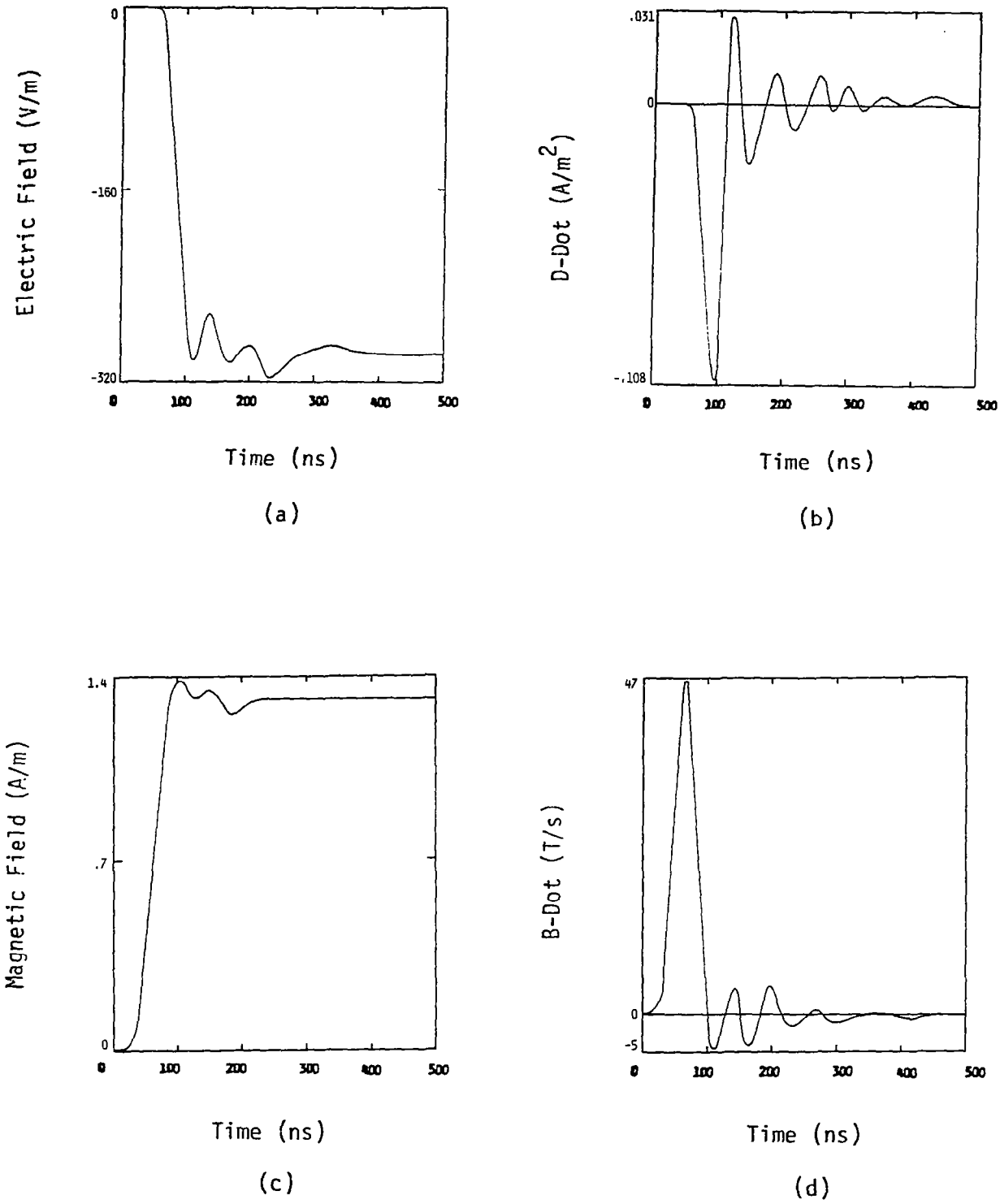

FIGURE A.38. 40 NSEC RISE TIME

A.37 - A.40 Rear Illumination, E_{inc} Toward Left (Port)

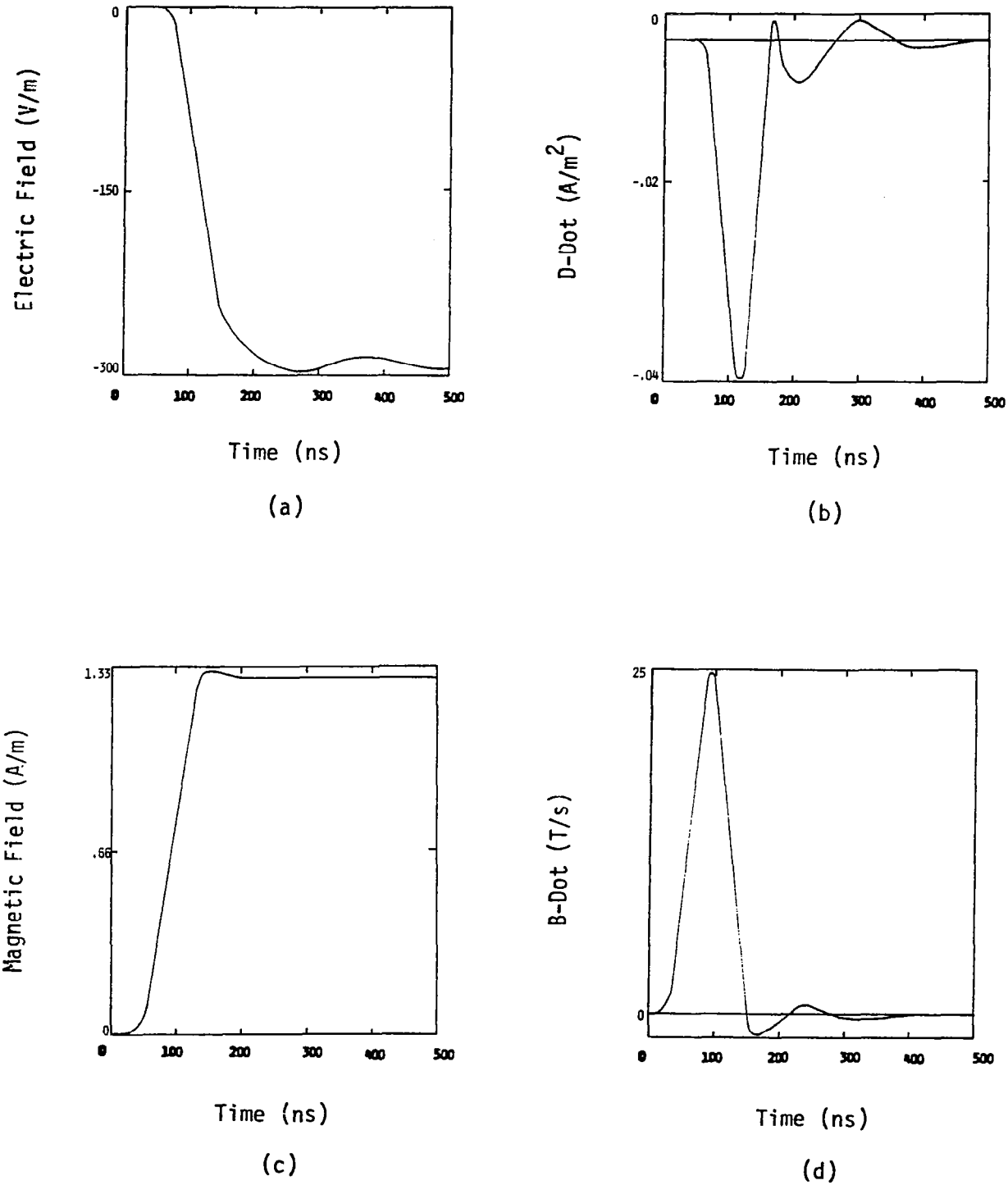

FIGURE A.39 100 NSEC RISE TIME

A.37 - A.40 Rear Illumination, E_{inc} Toward Left (Port)

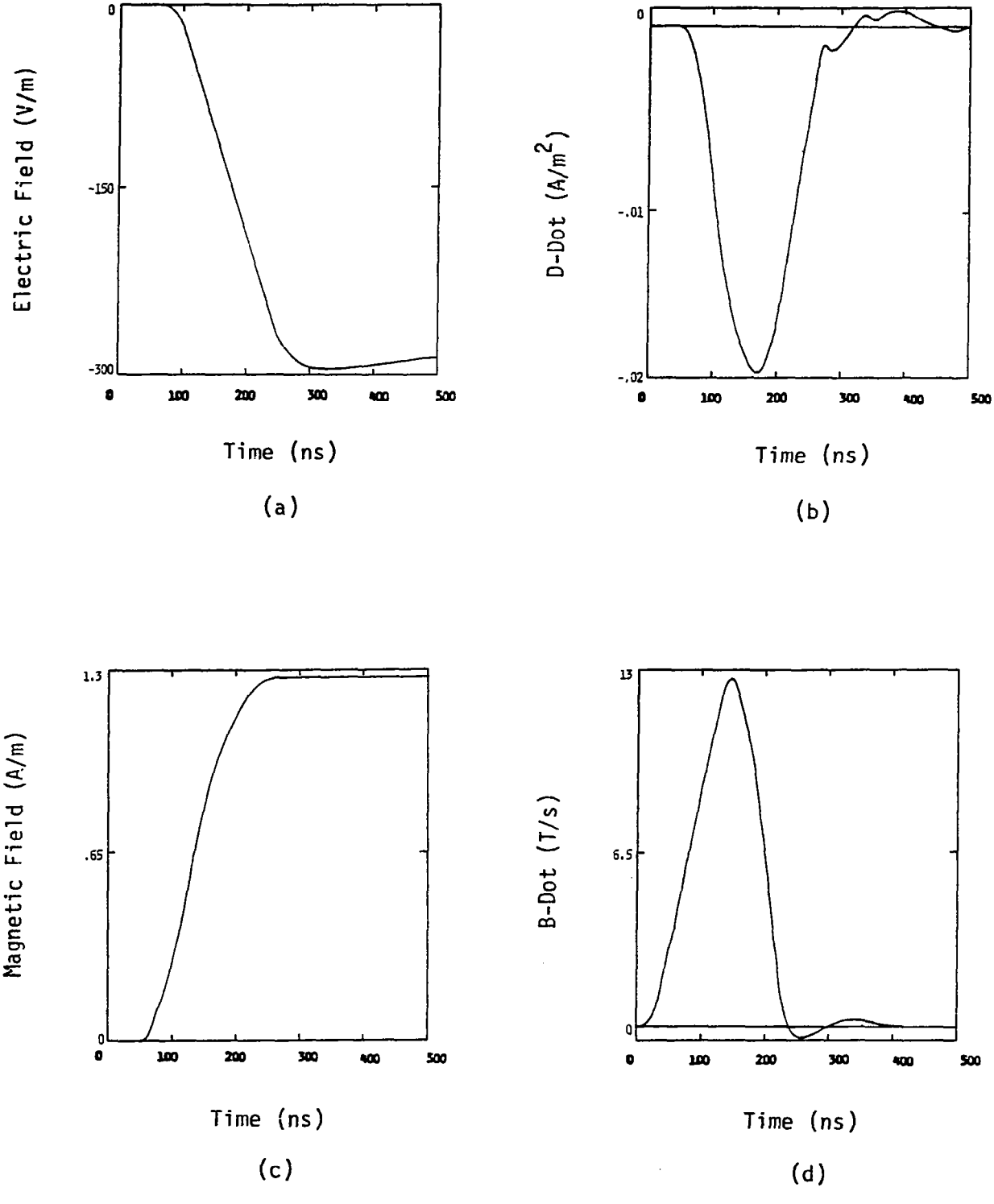

FIGURE A.40 200 NSEC RISE TIME

A.41 - A.44 Front Illumination, E_{inc} Vertical

A.41 - A.44 Front Illumination, E_{inc} Vertical

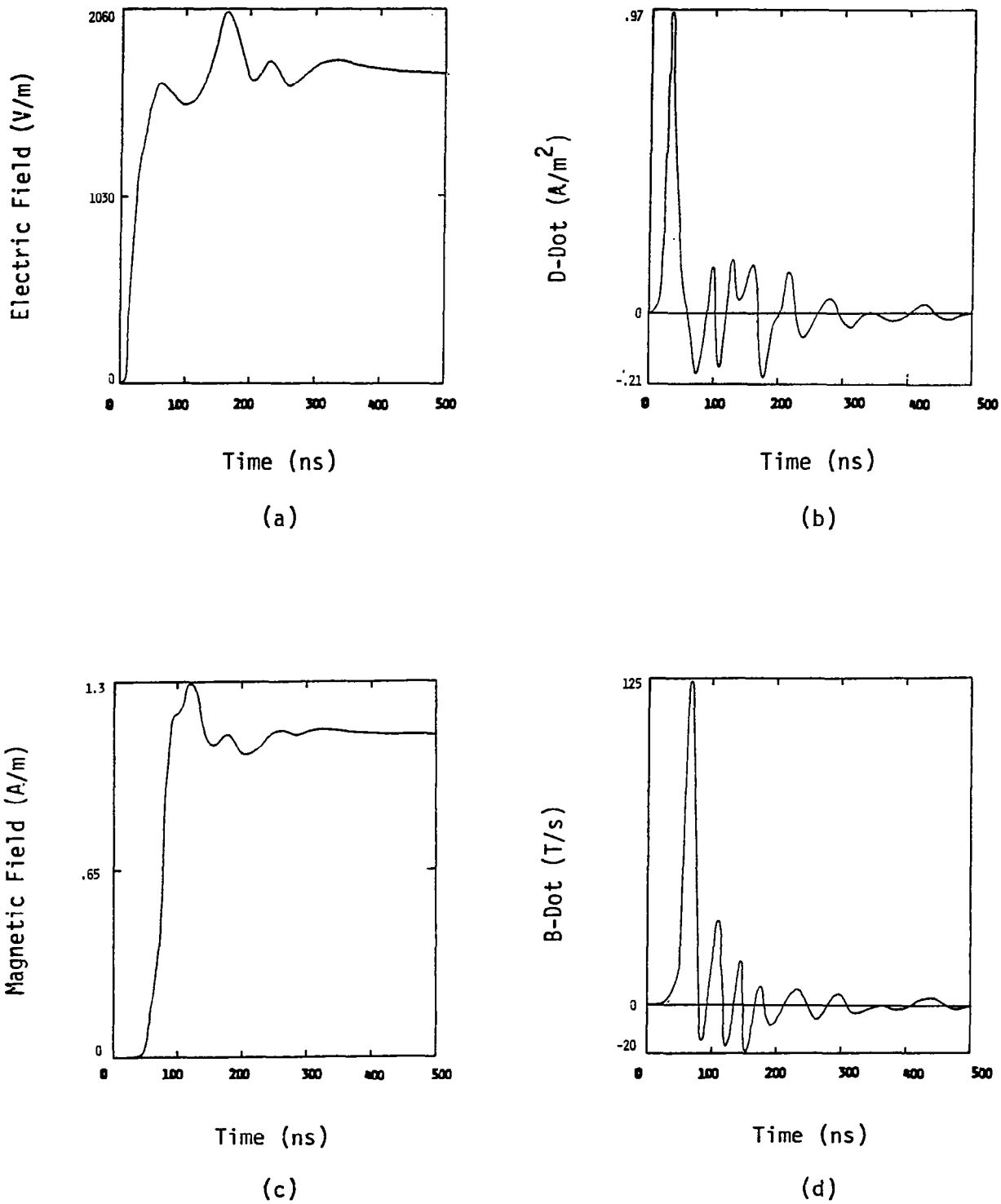

FIGURE A.41 20 NSEC RISE TIME

A.41 - A.44 Front Illumination, E_{inc} Vertical

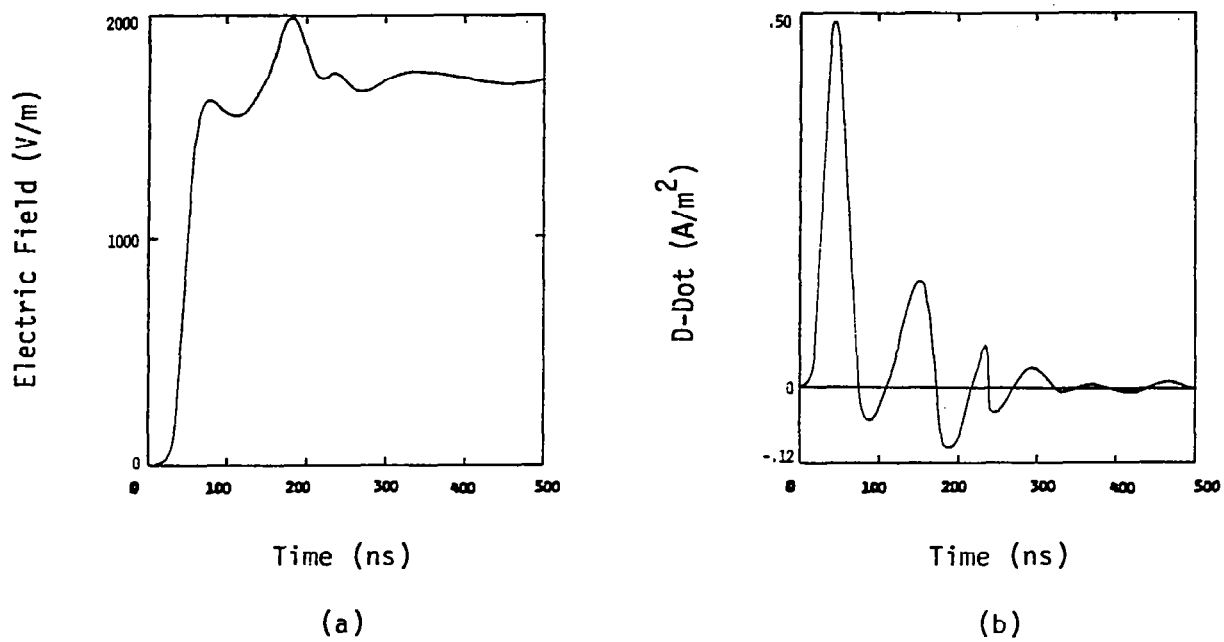

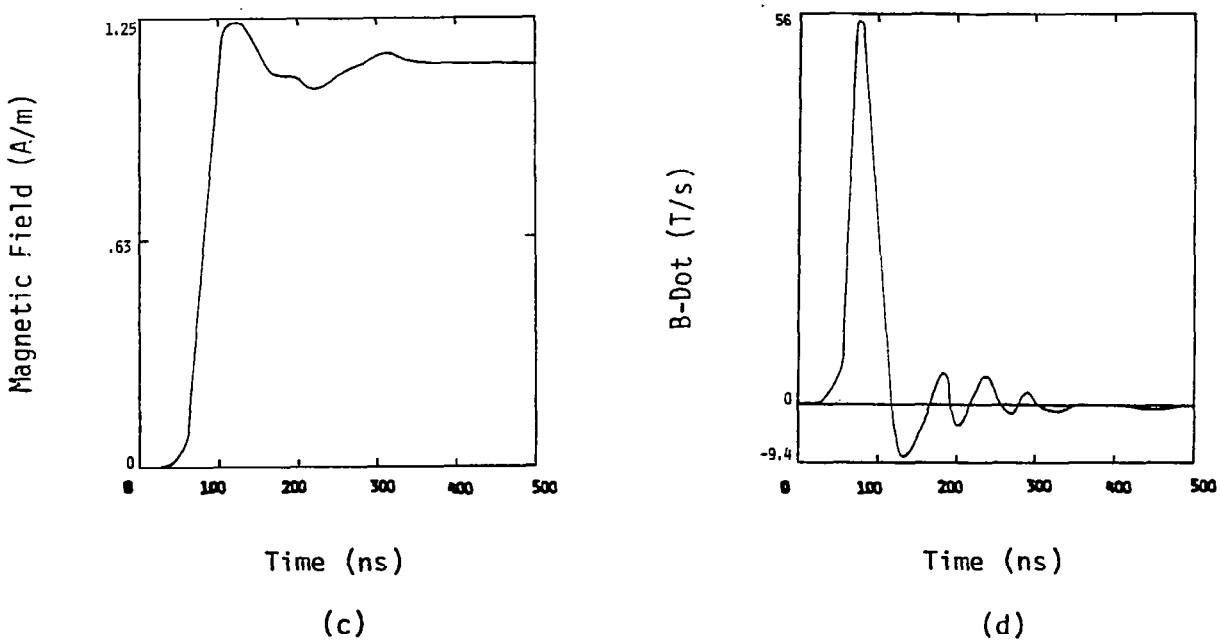

FIGURE A.42 40 NSEC RISE TIME

A.41 - A.44 Front Illumination, E_{inc} Vertical

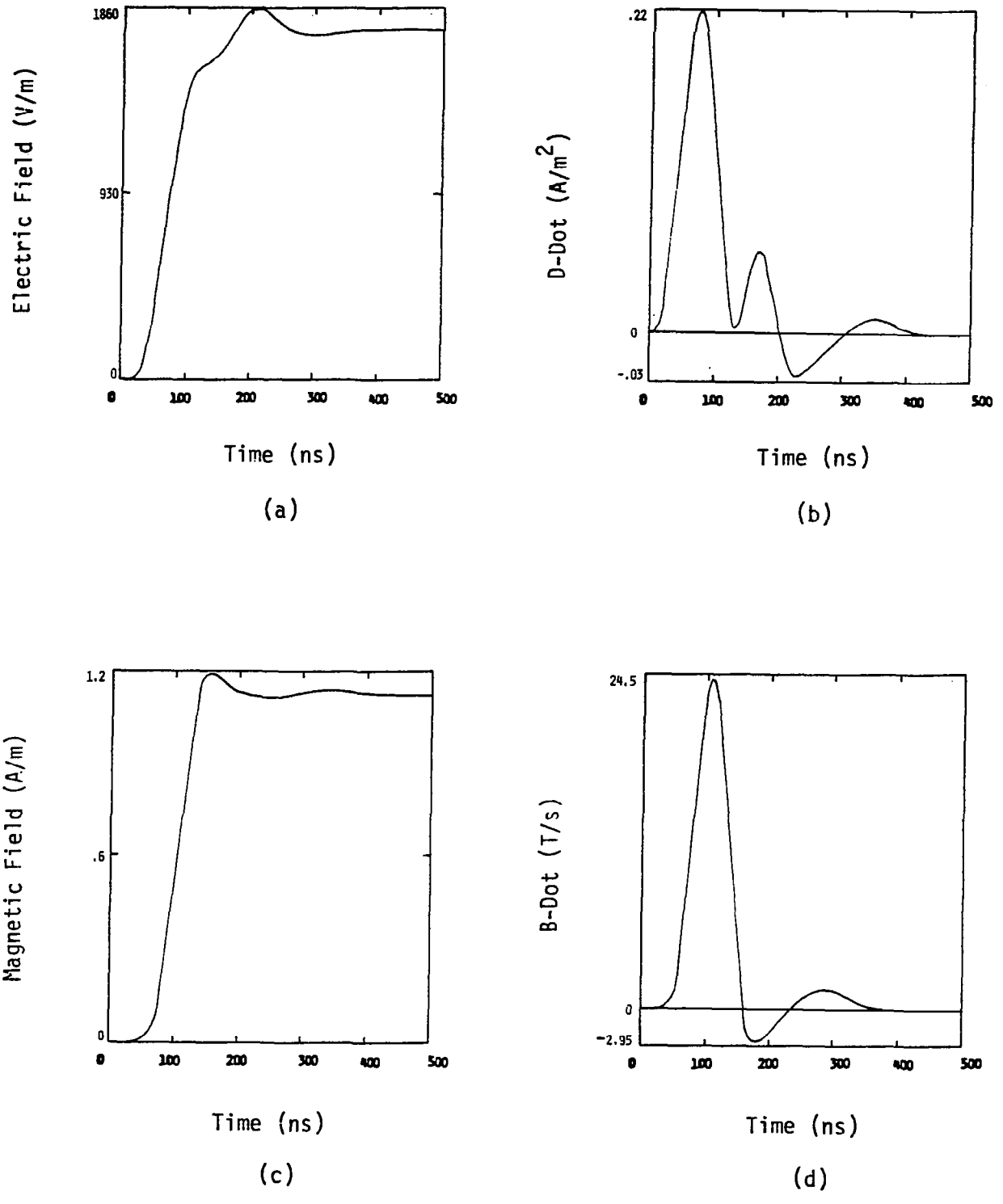

FIGURE A.43 100 NSEC RISE TIME

A.41 - A.44 Front Illumination, E_{inc} Vertical

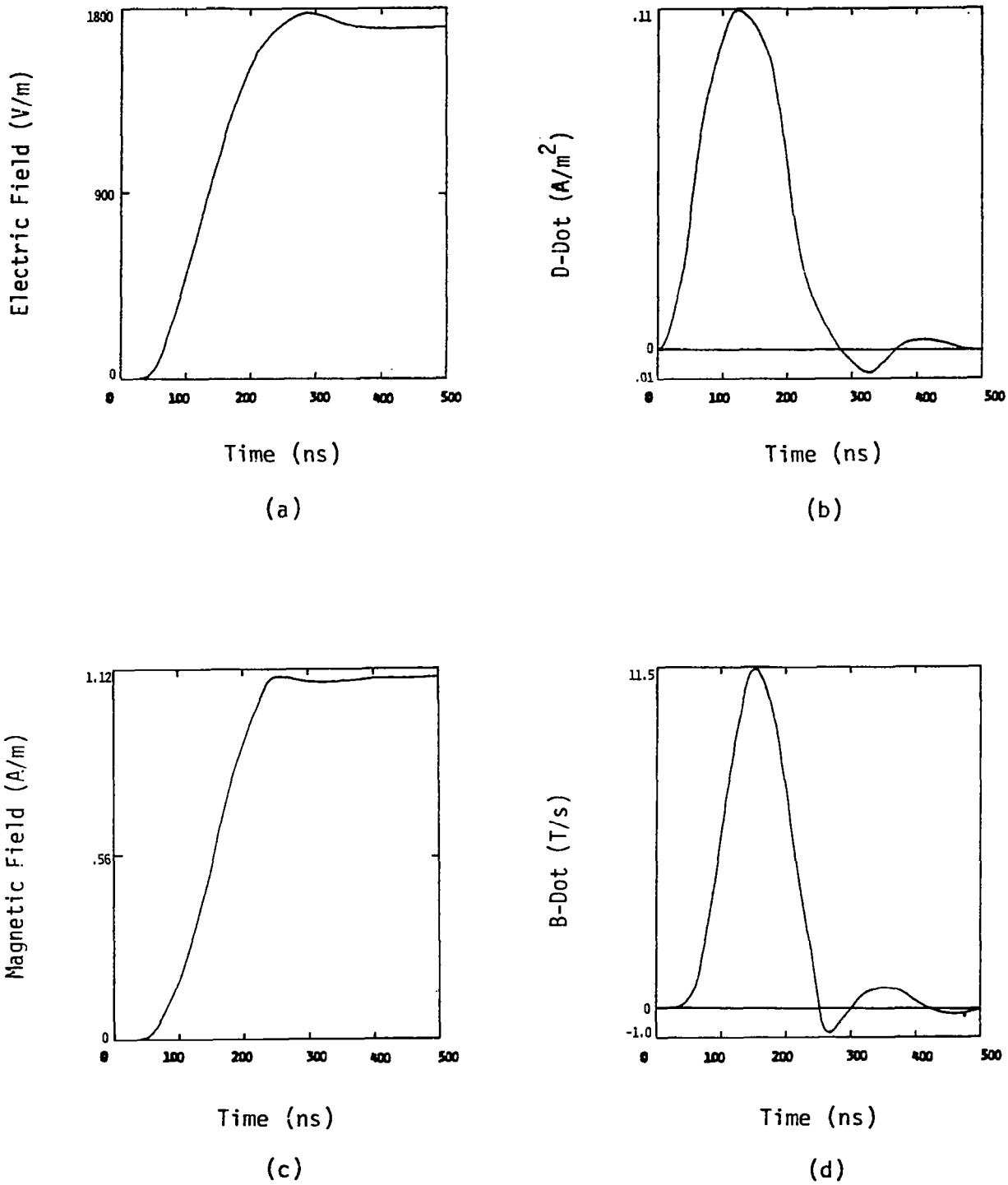

FIGURE A.44 200 NSEC RISE TIME

A.45 - A.48 Rear Illumination, E_{inc} Vertical

A.45 - A.48 Rear Illumination, E_{inc} Vertical

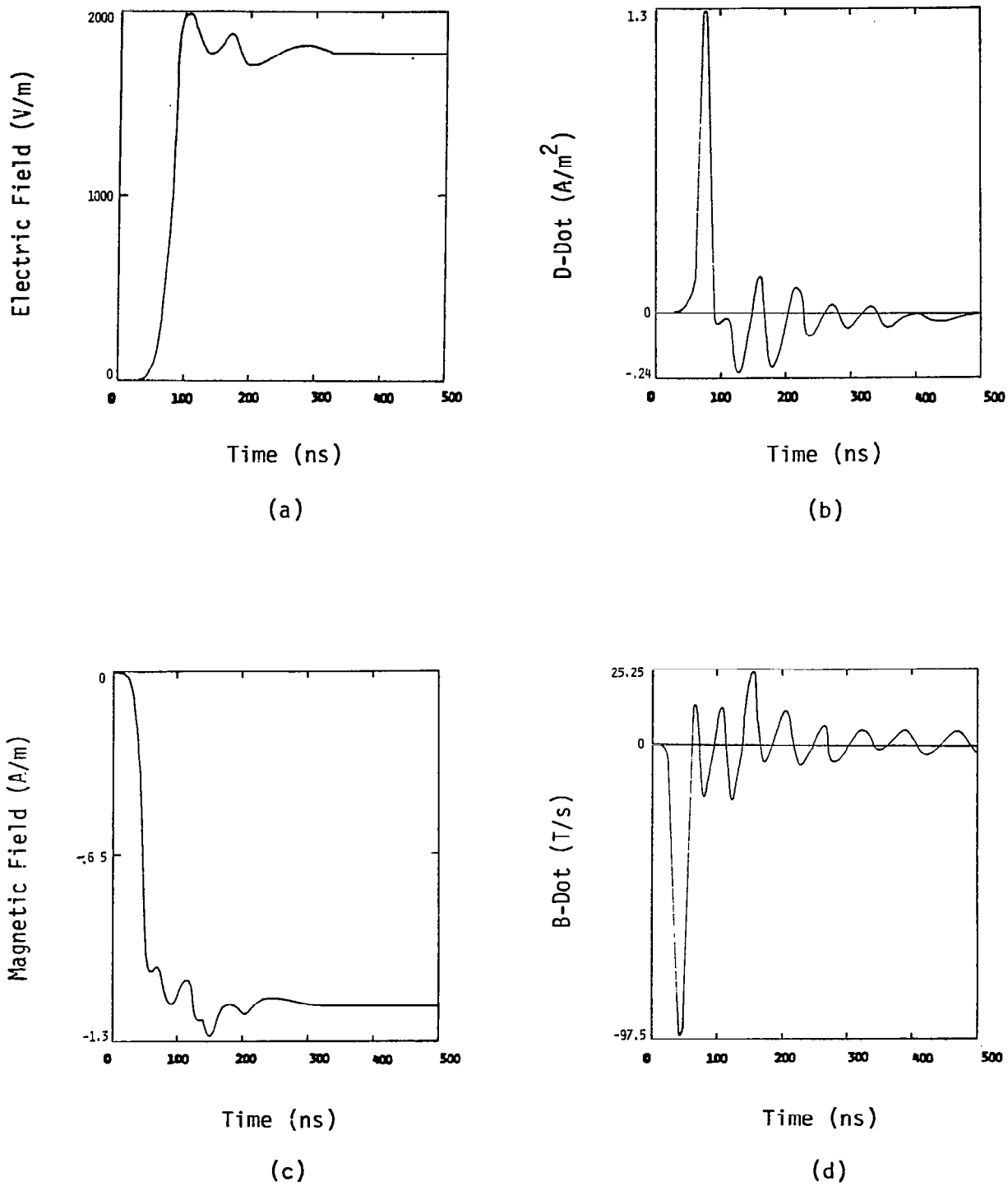

FIGURE A.45 20 NSEC RISE TIME

A.45 - A.48 Rear Illumination, E_{inc} Vertical

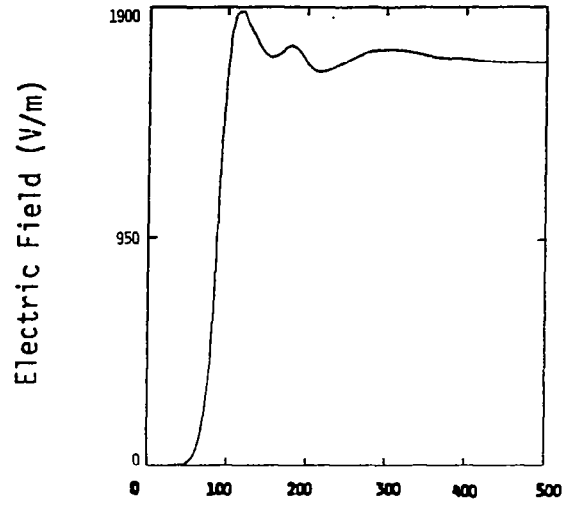

(a)

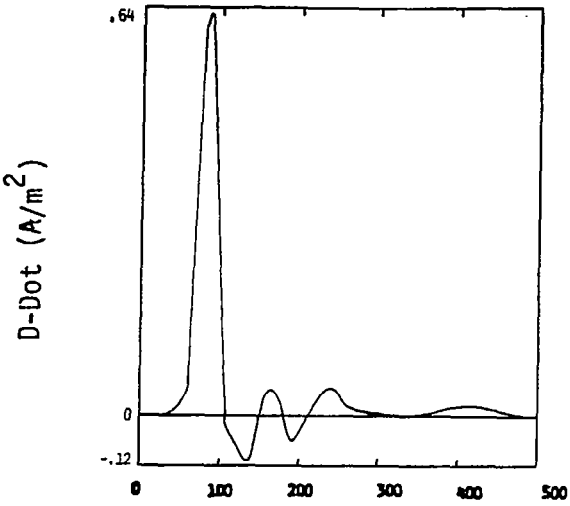

(b)

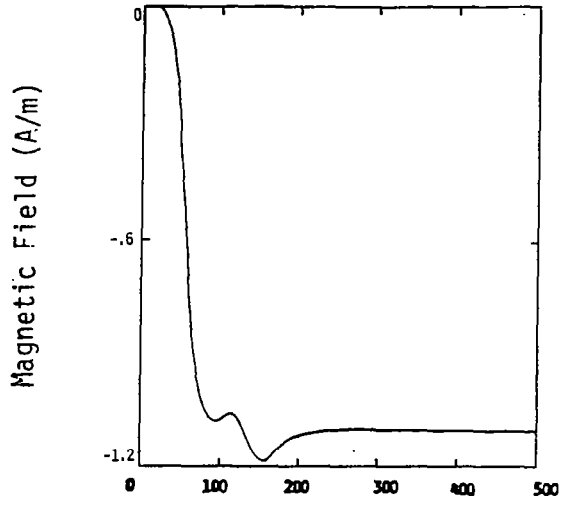

(c)

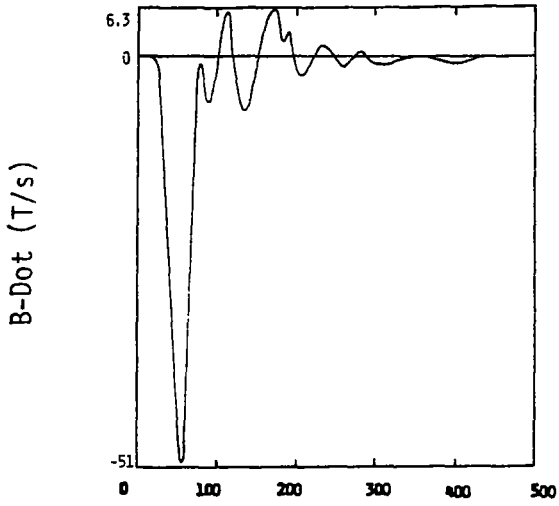

(d)

FIGURE A.46 40 NSEC RISE TIME

A.45 - A.48 Rear Illumination, E_{inc} Vertical

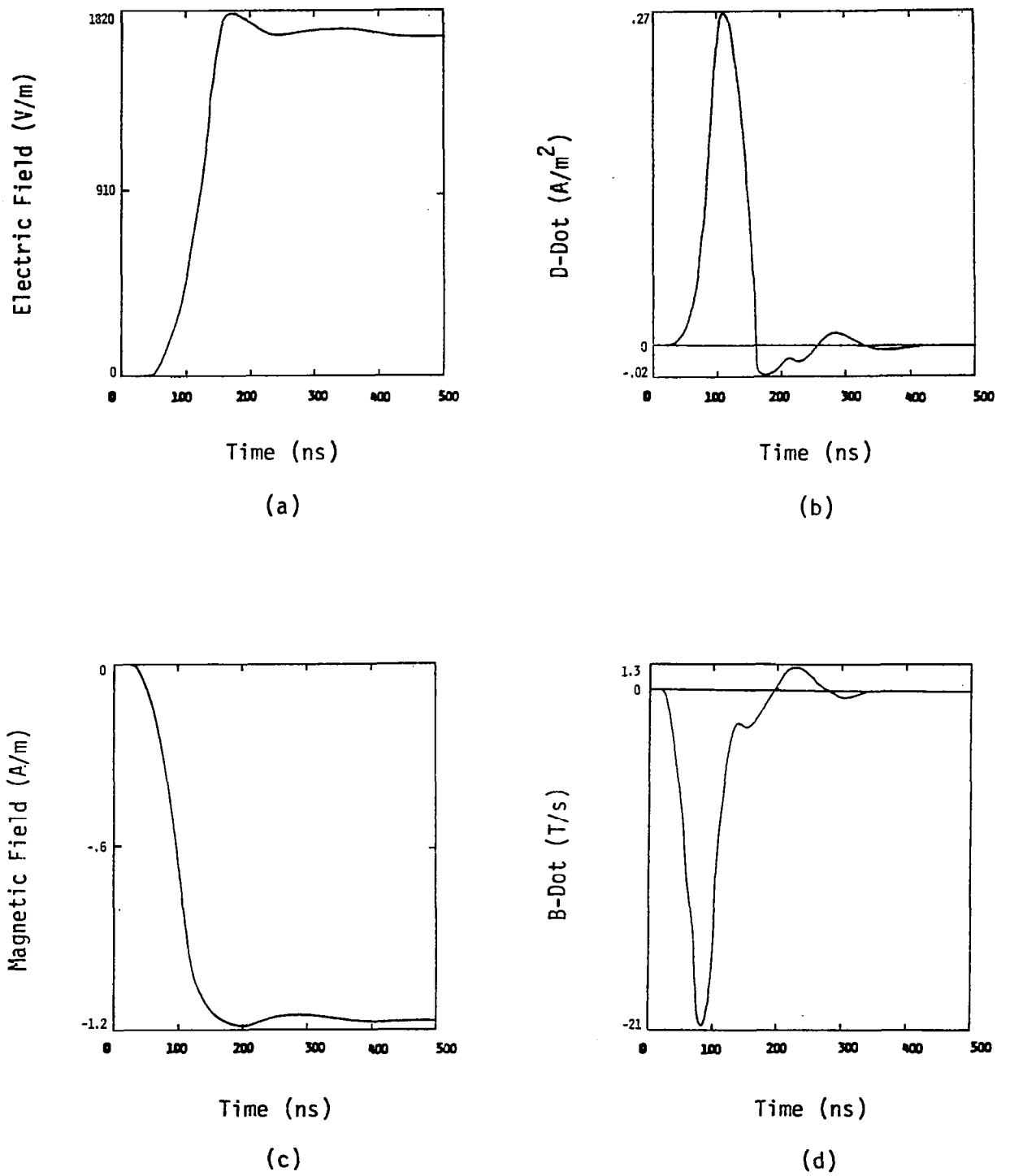

FIGURE A.47 100 NSEC RISE TIME

A.45 - A.48 Rear Illumination, E_{inc} Vertical

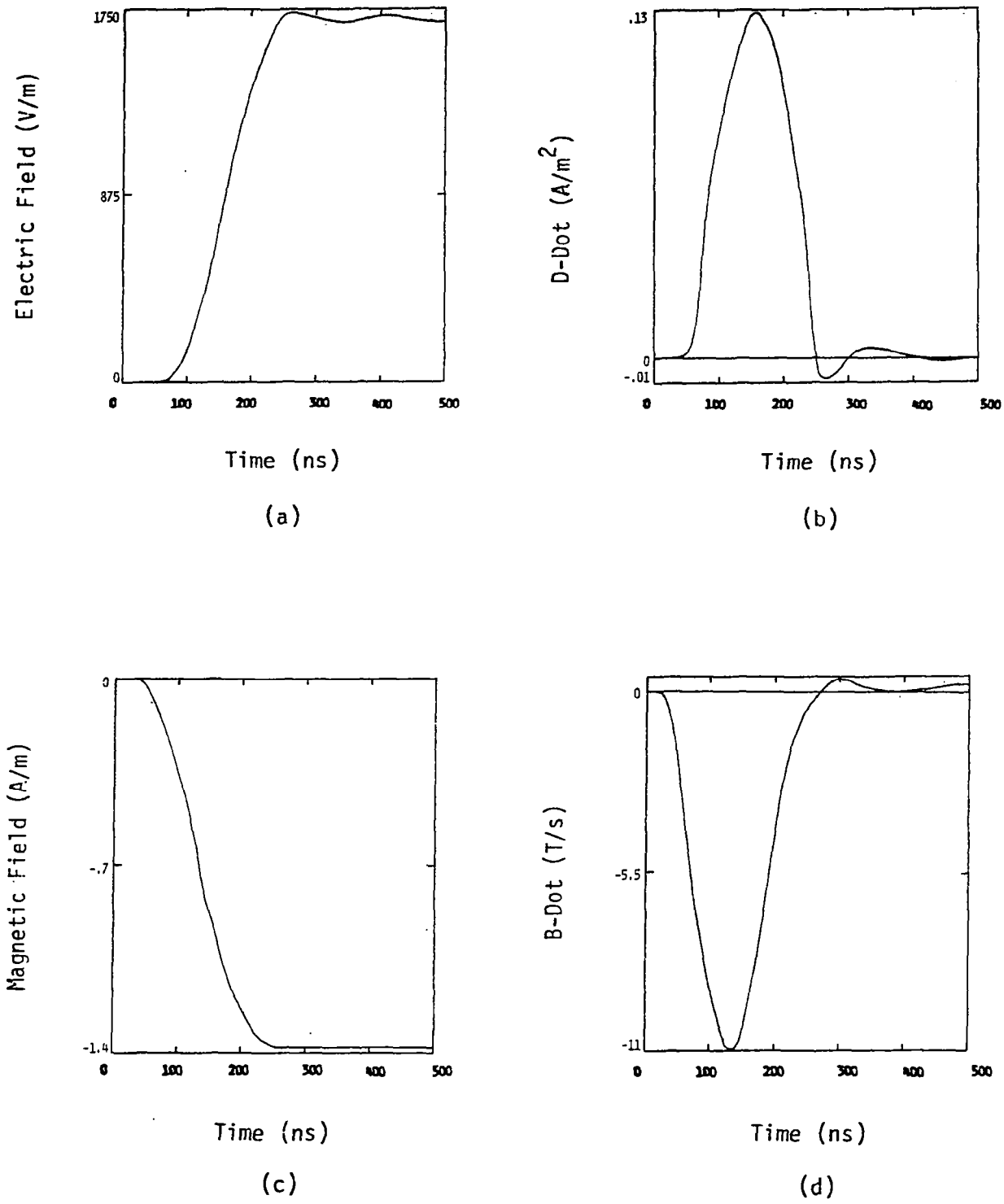

FIGURE A.48 200 NSEC RISE TIME

1. Report No.	2. Government Accession No.	3. Recipient's Catalog No.
NASA CR-3590		

4. Title and Subtitle	5. Report Date
INTERPRETATION METHODOLOGY AND ANALYSIS OF IN-FLIGHT LIGHTNING DATA	October 1982
	6. Performing Organization Code
7. Author(s)	8. Performing Organization Report No.
Terence Rudolph and Rodney A. Perala	EMA 82-R-21
	10. Work Unit No.
9. Performing Organization Name and Address	
Research Triangle Institute P. O. Box 12194, Building 5 Research Triangle Park, North Carolina 27709	11. Contract or Grant No. NAS1-16489
	13. Type of Report and Period Covered Contractor Report
12. Sponsoring Agency Name and Address	
National Aeronautics and Space Administration Washington, DC 20546	14. Sponsoring Agency Code

15. Supplementary Notes

Langley Technical Monitor: Felix L. Pitts

Terence Rudolph and Rodney A. Perala: Electro Magnetic Applications, Inc., Denver, Colorado. Prepared under Subcontract 1-43U-2094.

16. Abstract

The objective of the work described here is to develop a methodology whereby electromagnetic measurements of inflight lightning stroke data can be understood and extended to other aircraft. Recent measurements made on the NASA F106B aircraft indicate that sophisticated numerical techniques and new developments in corona modeling are required to fully understand the data. Thus the problem is nontrivial and successful interpretation can lead to a significant understanding of the lightning/aircraft interaction event. This is of particular importance because of the problem of lightning induced transient upset of new technology low level microcircuitry which is being used in increasing quantities in modern and future avionics. Inflight lightning data is analyzed and lightning environments incident upon the F106B are determined.

17. Key Words (Suggested by Author(s))	18. Distribution Statement
Lightning, Inflight Data, Finite Difference, Interpretation, LEMP, Attached Strokes, F-106	Unclassified - Unlimited Subject Category 47

19. Security Classif. (of this report)	20. Security Classif. (of this page)	21. No. of Pages	22. Price*
Unclassified	Unclassified		

* For sale by the National Technical Information Service, Springfield, Virginia 22161

NASA-Langley, 1982